Title
Molecular Imaging Approaches to Understanding the Roles of Hydrogen Peroxide Biology in Stress and Development

Author
Dickinson, Bryan Craig

Publication Date
2010

Peer reviewed|Thesis/dissertation

Molecular Imaging Approaches to Understanding the Roles of Hydrogen Peroxide Biology in Stress and Development

By

Bryan Craig Dickinson

A dissertation submitted in partial satisfaction of the

requirements for the degree of

Doctor of Philosophy

in

Chemistry

in the

Graduate Division

of the

University of California, Berkeley

Committee in charge:

Professor Christopher J. Chang, Chair
Professor Michelle C.Y. Chang
Professor David V. Schaffer

Fall 2010

Molecular Imaging Approaches to Understanding the Roles of Hydrogen Peroxide Biology in Stress and Development

by Bryan Craig Dickinson

Abstract

Molecular Imaging Approaches to Understanding the Roles of Hydrogen Peroxide Biology in Stress and Development

by

Bryan Craig Dickinson

Doctor of Philosophy in Chemistry

University of California, Berkeley

Professor Christopher J. Chang, Chair

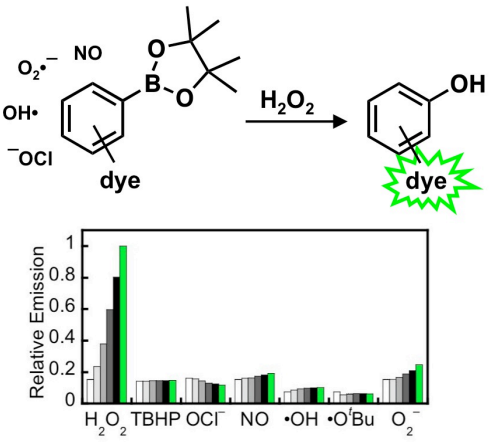

The production of hydrogen peroxide (H_2O_2) in biological systems is associated with a variety of pathologies including neurodegenerative diseases, cancer, and the general process of aging. However, a growing body of evidence suggests that the reactivity of this particular reactive oxygen species (ROS) is also harnessed for physiological processes. Molecular imaging using fluorescence microscopy offers a valuable approach for deciphering the multifaceted roles of H_2O_2 in biological processes. The use of aryl boronates for the selective detection of H_2O_2 in biological systems is a validated approach to the development of H_2O_2-responsive fluorophores. This dissertation describes the design, synthesis, and characterization of an assortment of new boronate-based fluorescent probes for H_2O_2, as well as their application toward uncovering new roles for H_2O_2 in stress and development. Peroxyfluor-2, Peroxyfluor-3, Peroxy Yellow 1, and Peroxy Orange 1 are turn-on fluorescent probes that can detect physiological levels of H_2O_2 produced for cell signaling, as well as monitor multiple ROS simultaneously in single cells. Mitochondria Peroxy Yellow 1 is a bifunctional probe featuring a triphenylphosphonium group for mitochondrial targeting and a single boronate for H_2O_2 detection that allows for the detection of mitochondrial H_2O_2 associated with a Parkinson's diseases model. Nuclear Peroxy Emerald 1 is a nuclear-targeted probe that reveals Sirtuin-dependent changes in nuclear H_2O_2 metabolism in *C. Elegans*. Peroxyfluor-6 (PF6) is a bifunctional probe featuring acetoxymethylester-protected phenol and carboxylic acid functionalities for enhanced cellular uptake and retention. PF6 reveals endogenous H_2O_2 production within neural stem cells and molecular biological experiments expose a new role for H_2O_2 in growth signaling within this critical brain cell population *in vitro* and *in vivo*. Finally, Peroxy Yellow 1 Methyl-Ester, a probe designed for analysis by flow cytometry, reveals that Aquaporins 3 and 8, but not Aquaporin 1, can mediate H_2O_2 uptake across the plasma membrane of mammalian cells, and that Aquaporin 3 can facilitate the uptake of endogenous H_2O_2 relevant to cell signaling.

For my parents.

Table of Contents

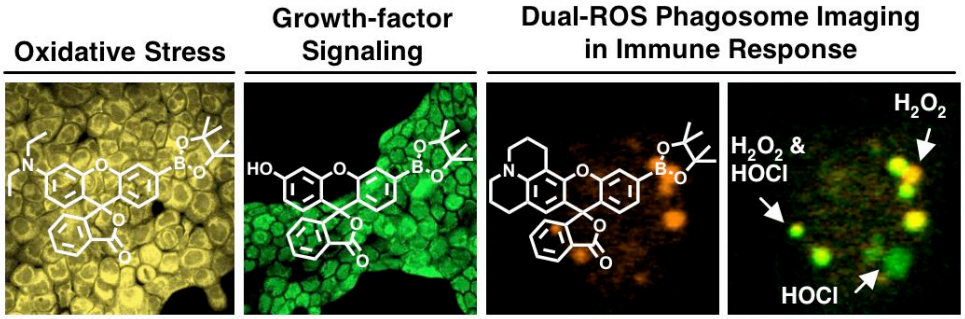

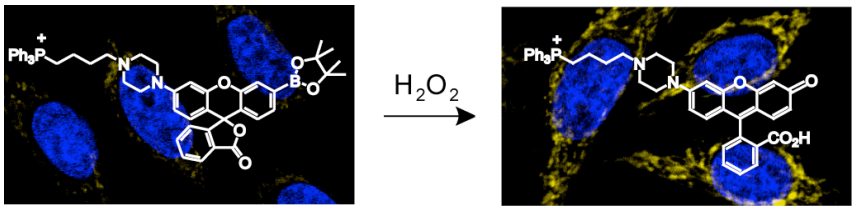

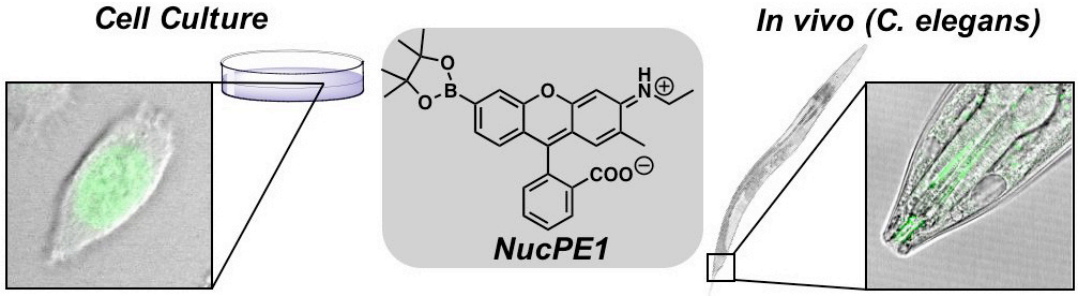

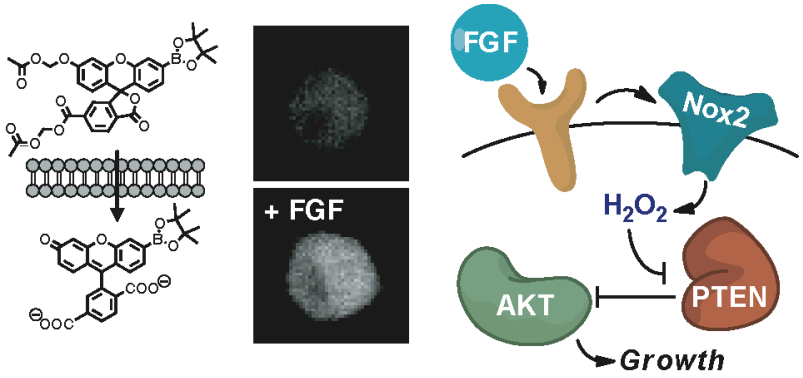

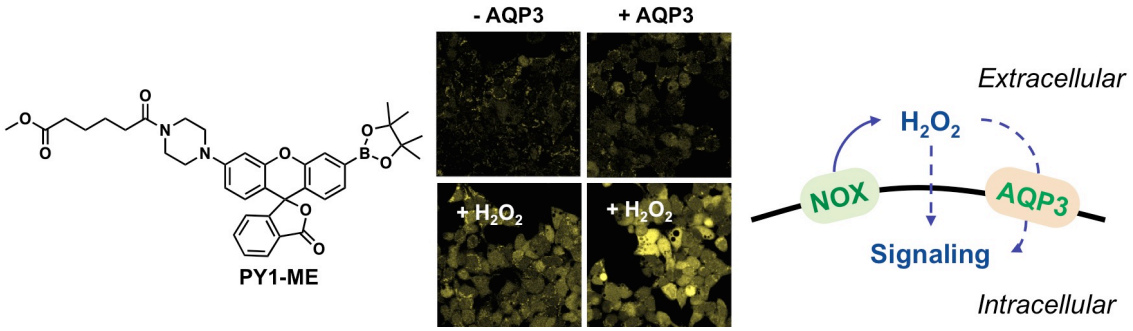

Acknowledgements

I am grateful to Chris Chang for all of his support and guidance during the course of my graduate career. Chris provided critical intellectual advice, great ideas, and the tools to carry them out. His frank and bluecollar approach to science has served as a mold for the type of researcher I hope to be. Graduate school is not easy, and it should not be, but I can honestly say that my time in Chris's lab was both formative and enjoyable.

The members of the Chang Lab also deserve very heartfelt thanks. It is they who made even the most stressful and overwhelming days bearable. The original members of the lab, expecially Evan Miller and Emily Que, were especially influential to my development as a scientist. Evan and Emily embody what it means to be a well-rounded researcher, and I feel honored to call them both mentors and friends. Calvin Huynh was a fantastically talented undergraduate that worked with me for a significant portion of my graduate work, especially that contained within Chapter 1 of this thesis.

I am also indebted to the Chemical Biology Graduate Program at Berkeley. It was at a Chemical Biology seminar at the end of my first year that I first met Dave Schaffer. We set-up a collaboration immediately after meeting to investigate redox signaling in neural stem cells, a project that eventually became Chapter 4 of this thesis and the cornerstone of my graduate career. I am also therefore thankful that Dave Schaffer was so welcoming and supportive of our collaboration, offering both resources as well as invaluable scientific guidance.

My undergraduate advisor, David Fushman, invited me into his lab despite my lack of experience, and allowed me to pursue independent research under the guidance of a fantastic scientist, Ranjani Varadan. Ranjani and David's pure love of science and supportiveness were what inspired me and gave me the confidence to pursue a graduate degree in chemistry. My time at Maryland was very special, largely due to my work in David's lab.

My wife, Maura, the love of my life, was brave enough to take an adventure to California with me. Our Sunday's together hiking, eating, wine tasting, camping, and generally enjoying each other's company were an invaluable refresher every week. When hiking Half Dome at Yosemite with Maura, I got a scared half way up the cables and thought about turning back. She looked at me with fire in her eyes and said, "We've made it this far, and we are getting to the top!" This represents her general approach toward life, which inspires me to be the best person and scientist I can be.

My little sister, Lindsey, made the trek out to California frequently during my graduate years. Lindsey's adventuresome spirit and insouciant approach to life have always provided perspective to my own life. Lindsey is a great little sister, and though being apart from her has been tough I look forward to living on the same coast again soon.

Finally, my parents, to whom this thesis is dedicated to, deserve the most recognition for my accomplishments. From my early youth they encouraged me to develop my independence and creativity, two assets that were crucial to suceeding in my graduate work. My mom's persistent optimisim and my dad's motivated work ethic also both served as beneficial models as I navigated through graduate school. In addition to various forms of material support, they provided me with guidance and great conversation on the phone during my mile-long walk into work everyday. Most importantly, they always taught me that being happy was the most important thing I could be, a lesson I have always kept close to my heart. All in all, this has been one heck of a life so far. Thanks Mom and Dad!

Chapter 1:

A Palette of Fluorescent Probes with Varying Emission Colors for Imaging Hydrogen Peroxide Signaling in Living Cells

Portions of this work were published in the following scientific journal:

Dickinson, B. C.; Huynh, C.; Chang, C. J. "A palette of fluorescent probes with varying emission colors for imaging hydrogen peroxide signaling in living cells." *Journal of the American Chemical Society* **2010**, *132*, 5906–5915.

Portions of this work were performed in collaboration with the following persons:

Spectroscopic characterizations and synthesis were assisted by Calvin Huynh.

Abstract

We present a new family of fluorescent probes with varying emission colors for selectively imaging hydrogen peroxide (H_2O_2) generated at physiological cell signaling levels. This structurally homologous series of fluorescein- and rhodol-based reporters relies on a chemospecific boronate-to-phenol switch to respond to H_2O_2 over a panel of biologically relevant reactive oxygen species (ROS) with tunable excitation and emission maxima and sensitivity to endogenously produced H_2O_2 signals, as shown by studies in RAW264.7 macrophages during the phagocytic respiratory burst and A431 cells in response to EGF stimulation. We further demonstrate the utility of these reagents in multicolor imaging experiments by using one of the new H_2O_2-specific probes, Peroxy Orange 1 (PO1), in conjunction with the green-fluorescent highly reactive oxygen species (hROS) probe, APF. This dual-probe approach allows for selective discrimination between changes in H_2O_2 and hypochlorous acid (HOCl) levels in live RAW264.7 macrophages. Moreover, when macrophages labeled with both PO1 and APF were stimulated to induce an immune response, we discovered three distinct types of phagosomes: those that generated mainly hROS, those that produced mainly H_2O_2, and those that possessed both types of ROS. The ability to monitor multiple ROS fluxes simultaneously using a palette of different colored fluorescent probes opens new opporunities to disentangle the complex contributions of oxidation biology to living systems by molecular imaging.

Introduction

The production of reactive oxygen species (ROS) molecules by biological systems is an inevitable consequence of aerobic life.[1,2] The mismanagement and accumulation of ROS in mammals leads to a condition broadly referred to as oxidative stress, in which the production and destruction of the various cellular oxidants no longer maintains a healthy equilibrium.[3] Oxidative stress is linked to aging and a host of diseases where age is a risk factor, including cancer[4-6] and neurodegenerative Alzheimer's and Parkinson's diseases.[6-8] However, whereas ROS can be damaging when uncontrolled, they also have the potential to be used for beneficial biological activities ranging from immune response to cell signaling.[9-20] At the cellular level, the delicate balance between oxidative stress and signaling is influenced by the chemistry of a particular ROS or set of ROS, as they are not generated in isolation of one another and can often interconvert and undergo further reactions to produce other ROS metabolites.[3,18,21,22] In other words, at any given time a cell is producing a variety of ROS, where each type exerts specific downstream biological effects. As the lifetimes and reactivities of individual classes of ROS can greatly vary,[18] studying multiple ROS simultaneously in a single cell is critical to understanding their discrete roles in complex environments.

Fluorescent probes are well suited to study the generation of specific types of ROS in biological systems, as optical microscopy allows for the use of multiple probes simultaneously in a single specimen as long as spectral overlap is sufficiently minimized.[23-29] In this regard, several new types of indicators have been reported for the detection of nitric oxide (NO),[15,30-36] peroxynitrite,[37,38] and nitrative stress,[39] as well as superoxide,[40-43] singlet oxygen,[44,45] ozone,[46] H_2O_2,[16,47-65] hypochlorous acid,[66,67] highly reactive oxygen species (hROS),[68-70] and general redox events.[71-84] In terms of H_2O_2 detection, we previously described the design, synthesis, and characterization of Peroxyfluor-1 (PF1, Scheme 1-1),[51] a novel probe for H_2O_2 in which two H_2O_2-mediated boronate deprotections yield the highly fluorescent dye molecule fluorescein. Owing to its chemospecific deprotection mechanism, PF1 and related bisboronate derivatives

exhibit high selectivity for H_2O_2 over other ROS and can respond to changes in H_2O_2 fluxes at oxidative stress levels.[53,58,62] To maintain H_2O_2 specificity while increasing sensitivity to image H_2O_2 produced at low signaling levels, we devised the single boronate caged probes Peroxy Green 1 (PG1, Scheme 1-1) and Peroxy Crimson 1 (PC1, Scheme 1-1).[16] Green-fluorescent PG1 was capable of visualizing endogenous H_2O_2 generation in both A431 cells and primary neurons upon epidermal growth factor (EGF) stimulation, but red-fluorescent PC1 was not responsive enough detect peroxide bursts at these basal levels. Because the most common types of fluorescent reporters utilize GFP, fluorescein, or related green-colored fluorophores that overlap and are thus incompatible with PG1 for multicolor imaging experiments, we sought to address this shortcoming by expanding the available palette of colors for chemospecific peroxide imaging at low cell signaling levels. We now report a new series of monoboronate probes that responds to H_2O_2 over a range of rationally tunable visible excitation and emission wavelengths (Scheme 1-1). Three of these derivatives, Peroxyfluor-3 (PF3), Peroxy Yellow 1 (PY1), and Peroxy Orange 1 (PO1), are sensitive enough to image H_2O_2 signals produced in RAW264.7 macrophages and A431 cells during immune response and growth factor stimulation, respectively. Moreover, dual-color imaging experiments using PO1 along with the green-fluorescent highly reactive oxygen species (hROS) probe APF allows for selective discrimination between changes in H_2O_2 and hypochlorous acid (HOCl) levels in macrophages, as well as identification of phagosomes that produce H_2O_2 and/or hROS during an endogenous immune response.

Results and Discussion

Design and Synthesis of a Palette of Monoboronate Fluorescent Probes for Hydrogen Peroxide Based on Fluorescein and Rhodol Scaffolds. The original Tokyo Green fluorophore scaffold utilized for PG1, although functional in many ways, is limited to green emission profiles. We therefore turned our attention to fluorescein and rhodol dyes that allow us to rationally expand the palette of excitation and emission colors throughout the visible region by altering oxygen or nitrogen substituents on the 2' position of the xanthene core (Scheme 1-1). Schemes 1-2 and 1-3 outline synthetic routes to a family of five new monoboronate probes for chemoselective H_2O_2 detection. Two of these probes are based on green methoxyfluorescein (Peroxyfluor-2, PF2) and fluorescein (Peroxyfluor-3, PF3) platforms, whereas the other three reporters feature rhodol derivatives made from aminophenol (Peroxy Emerald 1, PE1), diethylaminophenol (Peroxy Yellow 1, PY1), and julolidine (Peroxy Orange 1, PO1) building blocks. Briefly, treatment of the parent dyes with *N*-phenyl bis(trifluoromethanesulfonamide) affords the corresponding triflate derivatives, and palladium-mediated coupling with bis(pinacolato)diboron furnishes the final boronate-protected products. PF3 was then acetylated with acetic anhydride to yield PF3-Ac to increase cell permeability, where the acetyl functionality should be removed by nonspecific esterases once inside the cytoplasm to reveal PF3. We anticipate that this modular synthetic strategy should be applicable to a wide variety of scaffolds and note complementary synthetic methods for C-N and C-O bond formation that have been reported in the recent literature,[85-92] as well as a triphenylphosphonium-capped piperazine rhodol for mitochondrial targeting.[61]

Spectroscopic Properties and Responses to Hydrogen Peroxide. We evaluated the spectral properties and H_2O_2 responses of the new monoboronate dyes in aqueous media buffered to physiological pH (20 mM HEPES buffer, pH 7); data are provided in Table 1-1. The

methoxy and boronate groups on PF2 force it to adopt a closed lactone form that is nonfluorescent and displays no absorption features in the visible region. The other four dyes each feature one prominent absorbance band in the visible region with weak but measurable fluorescence. The addition of H_2O_2 triggers a marked increase in fluorescence intensity for all five probes (Figure 1-1 and 1-8) with available emission colors spanning from green to yellow to orange. As expected because of their common boronate switch, the fluorescein and rhodol reporters respond with good selectivity to H_2O_2 over a variety of biologically relevant ROS, including superoxide, NO, hypochlorite, and *tert*-butyl hydroperoxide, as well as hydroxyl and *tert*-butoxy radicals (Figure 1-2). Kinetics measurements of the H_2O_2-mediated boronate deprotections were performed under pseudo-first-order conditions (5 μM dye, 10 mM H_2O_2), giving observed rate constants ranging from k = 3.7(1) to 8.1(1) x 10^{-3} s^{-1}. These data provide further evidence that H_2O_2-triggered conversion of boronates to phenols is a robust and versatile methodology for reaction-based H_2O_2 detection.

Fluorescence Detection of H_2O_2 in Living Cells in Situations of Oxidative Stress. With data establishing that all five monoboronate reporters selectively respond to H_2O_2 in aqueous solution, we turned our attention to assessing their performance in live-cell imaging assays. Incubation of live A431 cells with 10 μM PF2, 5 μM PF3-Ac, 5 μM PY1, or 5 μM PO1 for 40 min at 37 °C results in low levels of intracellular fluorescence as determined by scanning confocal microscopy measurements (Figure 1-3, a,d,g, and j), and addition of 100 μM H_2O_2 to these dye-loaded cells for 20 min at 37 °C triggers increases in green, yellow, or orange intracellular fluorescence (Figure 1-3, b,e,h, and k). PE1 does not show a turn-on response to H_2O_2 in cells under similar conditions owing to high background staining. Further brightfield transmission and nuclear staining experiments confirm that the cells are viable throughout the imaging assays (Figures 1-9 and 1-10). These experiments demonstrate that four of the probes, PF2, PF3-Ac, PY1, and PO1, are cell-permeable and nontoxic as well as capable of detecting elevations in H_2O_2 levels under oxidative stress conditions. The excitation wavelengths of this series of reagents align well with the 488 nm (PF2, PF3-Ac), 514 nm (PY1), and 543 nm (PO1) laser lines commonly used for light microscopy.

Fluorescence Detection of H_2O_2 at Signaling Levels upon Immune or Growth Factor Stimulation. We next tested whether the monoboronate probes were sensitive enough to detect H_2O_2 produced at low signaling levels upon physiological stimulation. Initial experiments focused on macrophages, which fight off infections by engulfing pathogens and using NADPH oxidase (Nox) and associated proteins to produce H_2O_2 and other ROS to alleviate the threat.[12,18] We utilized RAW264.7 macrophages, which are estimated to produce low micromolar levels of H_2O_2 upon stimulation with phorbol myristate acetate (PMA),[93-95] as a cell line model for H_2O_2-mediated immune response. RAW264.7 cells loaded with 10 μM PF2, 5 μM PF3-Ac, 5 μM PY1, or 5 μM PO1 for 60 min at 37 °C show low levels of intracellular fluorescence (Figure 1-4, a,e,i, and m). Upon stimulation of probe-loaded cells with PMA for 40 min at 37 °C to induce an immune response, we observe bright, punctate fluorescent patterns corresponding to phagocytic vesicles (Figure 1-4, b,f,j, and n), showing that these reporters can visualize endogenous production of H_2O_2 under conditions of immune signaling. We confirmed cell viability during live-cell imaging using a combination of brightfield transmission and nuclear staining experiments (Figures 1-11 and 1-12).

We then sought to expand the utility of these fluorescent indicators to image H_2O_2 signaling in nonphagocytic systems. In particular, mounting data reveal that Nox proteins used in

phagocytic ROS killing are also expressed in a wide variety of nonphagocytic cell types throughout the body and that these enzyme complexes can be activated by ligands such as growth factors and cytokines. We previously showed that A431 cells, which express high levels of epidermal growth factor receptor (EGFr), respond to epidermal growth factor (EGF) stimulation by producing H_2O_2 via a Nox/PI3K pathway.[16] Along these lines, A431 cells loaded with 5 μM PF3-Ac, 5 μM PY1, or 5 μM PO1 for 60 min at 37 °C display modest intracellular fluorescence (Figure 1-5, a,d, and g). Treatment of the dye-loaded cells with 500 ng/mL EGF ligand for 40 min at 37 °C triggers a modest turn-on enhancement in bright green, yellow, or orange intracellular fluorescence compared to unstimulated cells (Figure 1-5, b,e, and h) via Nox-generated H_2O_2. Brightfield transmission and nuclear staining measurements confirm that the cells are viable throughout the imaging experiments (Figures 1-13 and 1-14). Taken together, PF3-Ac, PY1, and PO1 offer a set of green, yellow, and orange dyes that are capable of detecting endogenous bursts of H_2O_2 produced for physiological signaling purposes.

Simultaneous, Dual-Color Imaging of H_2O_2 and hROS in Living Cells with Complementary Chemoselective Fluorescent Probes. Our next goal was to exploit the utility of the newly developed H_2O_2-specific fluorescent indicators with varying emission profiles to image multiple analytes/processes in living cells. In particular, because a given ROS can undergo an array of primary and secondary reactions to produce other classes of ROS molecules, we envisioned using a dual-probe approach to simultaneously visualize H_2O_2 and an additional important downstream product of cellular H_2O_2 chemistry. We focused on macrophages as a cell model system, as H_2O_2 produced by Nox complexes in these cell types can be converted to HOCl by reaction with heme-dependent myeloperoxidase enzymes.[96-99] For dual-color imaging experiments, we selected APF,[68] a 4-aminophenyl-fluorescein reporter developed by Nagano and co-workers that responds selectively to HOCl and other highly reactive oxygen species (hROS) by an increase in green fluorescence (488 nm excitation, 520 nm emission), along with the H_2O_2-selective probe PO1 that responds in a complementary orange optical window (543 nm excitation, 565 nm emission).

Initial experiments sought to test the ROS specificities of these dyes in a dual-probe/dual-color imaging mode. To this end, RAW264.7 macrophages loaded simultaneously with 5 μM APF and 5 μM PO1 for 50 min at 37 °C display low levels of both green and orange fluorescence (Figure 1-6, a and b). In contrast, APF- and PO1-stained cells incubated with 50 μM H_2O_2 for 20 min exhibit a selective increase in intracellular orange fluorescence from PO1 without any change in green emission from the APF probe (Figure 1-6, c and d). Moreover, APF- and PO1-loaded cells incubated with 100 μM HOCl for 20 min give a selective turn-on increase in intracellular green fluorescence from APF without any change in orange emission from the PO1 dye (Figure 1-6, e and f). In all cases, brightfield transmission and nuclear staining measurements confirm reasonable cell viability through the duration of the imaging assays (Figure 1-15), however the exogenous ROS treatments can cause some toxicity. This set of experiments establishes not only that fluorescence signals arising from green APF and orange PO1 probes can be distinguished by optical microscopy but also that each reporter maintains its chemical selectivity in the presence of one another in living systems.

We then moved on to study endogenously produced ROS bursts using this dual-probe imaging approach. APF- and PO1-loaded macrophages stimulated with 1 μg/mL PMA for 20 min display bright, punctate patterns of green and/or orange fluorescence localized to phagosomes, where ROS are generated in response to immune insult (Figures 1-6, g and h, and 1-15). As shown in Figure 1-7 and 1-16, we discovered three classes of phagosomes that are characterized

by different relative ratios of H_2O_2 and hROS fluxes. Specifically, some phagosomes display only PO1-derived orange fluorescence, indicating that H_2O_2 production dominates (Figure 1-7, a,b,c, and d), whereas other phagosomes show only APF-derived green fluorescence, indicating that most of the phagocytic burst results in formation of hROS (Figure 1-7, e,f,g, and h). A third distinct class of phagosomes possesses both green and orange fluorescence signals (Figure 1-7, i,j,k, and l) resulting from a combination of phagocytic increases in both H_2O_2 and hROS. These data establish that the dual-probe approach can reveal chemical differences through simultaneous imaging of discrete classes of ROS molecules.

Concluding Remarks

To close, we have described the synthesis, properties, and biological applications of a new class of monoboronate fluorescent probes for imaging H_2O_2 produced at low signaling levels with a range of varying excitation and emission colors. By rationally tuning substitutents on a homologous xanthene core, we have developed boronate-caged fluorescein and rhodol derivatives for H_2O_2 detection with excitation profiles that match well with common 488, 514, and 543 nm lines used for light microscopy. All five probes in this series give a selective turn-on fluorescence response to H_2O_2 in aqueous solution buffered to physiological pH with minimal interference from other biologically relevant ROS. Moreover, PF2, PF3-Ac, PY1, and PO1 are capable of visualizing changes in H_2O_2 levels in living cells in situations of oxidative stress, and PF3-Ac, PY1, and PO1 can be used to image low levels of H_2O_2 produced for signaling purposes upon phagocytic immune or nonphagocytic growth factor stimulation in live samples. Owing to the expanded color palette of H_2O_2-selective probes with sensitivity to low cell signaling levels, we were able to combine one of our newly synthesized H_2O_2 probes, PO1, with a complementary green-fluorescent reporter for hROS, APF, for selective discrimination between changes in H_2O_2 and HOCl levels in live RAW264.7 macrophages by a dual-probe/dual-color imaging approach. Further, we observed that PMA-stimulated macrophages were shown to respond with three discrete types of phagosomes via PO1/APF imaging: those that produced primarily hROS and selectively turned on APF during the phagocytic burst, those that primarily generated H_2O_2 and caused an increase in PO1 fluorescence, and those that deprotected both PO1 and APF probes and, therefore, possessed an elevated mixture of both H_2O_2 and hROS during immune signaling. By establishing selective H_2O_2-responsive probes with varying emission colors that can be used at low signaling levels, this work greatly expands our ability to study peroxide biology, particularly in conjunction with other reporters for cellular analytes and reaction processes. We are currently pursuing such opportunities in a variety of physiological and disease models, with particular interest in brain and immune systems.

Experimental Section

Synthetic Materials and Methods. All reactions were carried out under a dry nitrogen atmosphere. 2-(4-Diethylamino-2-hydroxybenzoyl)benzoic acid,[100] 8-Hydroxy-9-o-carboxybenzoyljulolidine,[101] rhodol,[102] and methoxyfluorescein[103] were synthesized according to literature methods. Silica gel P60 (SiliCycle) was used for column chromatography. Analytical thin layer chromatography was performed using SiliCycle 60 F254 silica gel (precoated sheets, 0.25 mm thick). All chemicals were purchased from Sigma-Aldrich (St. Louis, MO) and used as received. ^{1}H NMR, ^{13}C NMR, and ^{31}P NMR spectra were collected in $CDCl_3$, $(CD_3)_2O$, or 9:1 $CDCl_3/CD_3OD$ (Cambridge Isotope Laboratories, Cambridge, MA) at 25 ºC on a Bruker AV-

300, AVQ-400, or DRX-500 spectrometer at the College of Chemistry NMR Facility at the University of California, Berkeley. All chemical shifts are reported in the standard δ notation of parts per million using the peak of residual solvent proton signals as an internal reference. High-resolution mass spectral analyses were carried out at the College of Chemistry Mass Spectrometry Facility at the University of California, Berkeley. Low-resolution mass spectral analyses were carried out on an Agilent 6130 LC/MS system (Santa Clara, CA). Microwave reactions were performed using a CEM Intelligent Explorer/Discover (Matthews, NC).

Methoxyfluorescein Triflate (1). Methoxyfluorescein (500 mg, 1.45 mmol) and *N*-phenyl bis(trifluoromethanesulfonamide) (2.06 g, 5.78 mmol) were added to a vial and dissolved in 10 mL of dimethylformamide. Diisopropylethylamine (1.22 mL, 7.37 mmol) was then added, and the reaction stirred for 120 min at room temperature. The reaction was then extracted into dichloromethane, washed three times with water, and dried under reduced pressure. Purification by column chromatography (2:1 hexanes/ethyl acetate) yielded **1** as a white solid (440 mg, 63%). ^{1}H NMR ($(CD_3)_2O$, 400 MHz): δ 8.0 (1H, d, *J* = 7.6 Hz), 7.84 (1H, dt, *J* = 1.2, 7.2 Hz), 7.78 (1H, dt, *J* = 1.2, 7.2 Hz), 7.54 (1H, D, *J* = 2.4 Hz), 7.38 (1H, d, *J* = 7.6 Hz), 7.25 (1H, dd, *J* = 2.4, 8.8 Hz), 7.13 (1H, d, *J* = 8.8 Hz), 7.94 (1H, d, *J* = 2.4 Hz), 6.82 (1H, d, *J* = 8.8 Hz), 6.78 (1H, dd, *J* = 2.4, 8.8 Hz), 3.89 (3H, s). ^{13}C NMR ($(CD_3)_2O$, 100 MHz): δ 169.2, 162.9, 153.6, 152.9, 152.8, 151.1, 136.6, 131.6, 131.4, 130.1, 127.3, 125.9, 125.0, 121.5, 118.1, 113.6, 111.9, 111.5. 101.73, 56.24. ^{19}F NMR ($(CD_3)_2O$, 376.5 MHz): δ -73.25. HR-FABMS: calculated for [M^+] 479.0412, found 479.0426.

Peroxyfluor-2, PF2 (2). Compound **1** (150 mg, 0.31 mmol), bis(pinacolato)diboron (120 mg, 0.47 mmol), palladium acetate (63 mg, 0.10 mmol), and cyclo-hexyl JohnPhos (66 mg, 0.20 mmol) were added to a glass vial in an inert atmosphere glovebox and dissolved in 3 mL of dioxane. Diisopropylethamine (0.31 mL, 1.79 mmol) was then added the vial, and the contents were stirred at room temperature overnight. The contents were then brought out of the box and dried under reduced pressure. Purification by column chromatography (2:1 hexanes/ethyl acetate) afforded PF2 as a white solid (103 mg, 73%). ^{1}H NMR ($(CD_3)_2O$, 400 MHz): δ 8.02 (1H, d *J* =7.6 Hz), 7.79 (1H, t, *J* = 6.8 Hz), 7.74 (1H, t, *J* = 7.2 Hz), 7.66 (1H, s), 7.46 (1H, d, *J* = 8.0 Hz), 7.26 (1H, d, *J* = 7.6 Hz), 6.90 (1H, d, *J* = 4.0 Hz), 6.89 (1H, s), 6.78 (1H, d, *J* = 8.8 Hz), 6.72 (1H, dd, *J* = 2.4, 8.8 Hz), 3.86 (3H, s), 1.35 (12H, s). ^{13}C NMR ($(CD_3)_2O$, 100 MHz): δ 169.5, 162.6, 154.1, 153.2, 151.6, 136.3, 131.0, 130.4, 130.0, 128.3, 127.2, 125.7, 124.9, 123.8, 123.1, 112.8, 112.1, 106.7, 85.1, 82.7, 56.1, 25.5. HR-FABMS: calculated for [M^+] 457.1822, found 457.1831.

Fluorescein Monotriflate (3). Fluorescein (2.0 g, 5.8 mmol) and *N*-phenyl bis(trifluoromethanesulfonamide) (2.1 g, 5.8 mmol) were added to a dry Schlenk flask and flushed with nitrogen. The reaction contents were dissolved in 15 mL of DMF and diisopropylethylamine (3.8 mL, 23.1 mmol) was added. After 48 h of stirring of the contents at room temperature, the reaction mixture was acidified with hydrochloric acid, extracted into ethyl acetate, and evaporated under reduced pressure. Purification by column chromatography (1:1 hexanes/ethyl acetate) afforded **3** as a pale yellow solid (1.7 g, 63%). ^{1}H NMR ($(CD_3)_2O$, 400 MHz): δ 8.01 (1H, d, *J* = 8.0 Hz), 7.81 (1H, dt, *J* = 1.2, 7.6 Hz), 7.75 (1H, dt, *J* = 1.2, 7.6 Hz), 7.50 (1H, d, *J* = 2.4 Hz). 7.36 (1H, d, *J* = 7.6 Hz), 7.21 (1H, dd, *J* = 2.4, 8.8 Hz), 7.09 (1H, d, *J* = 8.8 Hz), 6.81 (1H, d *J* = 2.4 Hz), 6.72 (1H, d, *J* = 8.8 Hz), 6.68 (1H, dd, *J* = 2.4, 8.8 Hz). ^{13}C NMR ($(CD_3)_2O$, 100 MHz): δ 168.2, 159.7, 152.6, 152.0, 151.8, 150.0, 135.5, 130.5, 130.3,

129.3, 126.3, 124.8, 124.0, 120.5, 117.0, 113.2, 110.4, 110.0, 102.5, 81.1. ^{19}F NMR ($(CD_3)_2O$, 376.5 MHz): δ -73.21. HR-FABMS: calculated for [M^+] 465.0256, found 465.0243.

Peroxyfluor-3, PF3 (4). Compound **3** (200 mg, 0.43 mmol), bis(pinacolato)diboron (111 mg, 0.430 mmol), Pd (dppf) Cl_2•CH_2Cl_2 (106 mg, 0.130 mmol), potassium acetate (127 mg, 1.29 mmol), and 10 mL of toluene were added to a dry pressure tube in an inert atmosphere glovebox. The pressure tube was then brought out of the box and microwave-heated for 2 h at 110 °C. After the reaction mixture was cooled to room temperature, the contents of the pressure flask were washed into a round-bottom flask with dichloromethane and evaporated to dryness. Purification by column chromatography (1:1 hexanes/ethyl acetate) delivered **4** as a yellow solid (105 mg, 55%). ^{1}H NMR ($(CD_3)_2O$, 400 MHz): δ 8.00 (1H, d, *J* = 7.6 Hz), 7.76 (1H, t, *J* = 6.8 Hz), 7.70 (1H, t, *J* = 6.8 Hz), 7.64 (1H, s), 7.43 (1H, d, *J* = 7.6 Hz), 7.24 (1H, d, *J* = 7.6 Hz), 6.86 (1H, d, *J* = 8.0 Hz), 6.80 (1H, d, *J* = 2.0 Hz), 6.69 (1H, d, *J* = 8.4 Hz), 6.64 (1H, dd, *J* = 2.0, 8.4 Hz), 1.32 (12H, s). ^{13}C NMR ($(CD_3)_2O$, 100 MHz): δ 168.7, 159.7, 153.2, 152.2, 151.4, 150.7, 135.3, 130.0, 129.3, 129.1, 127.4, 126.3, 124.7, 123.9, 122.9, 122.2, 112.7, 110.1, 102.6, 84.1, 82.1, 24.3. HR-FABMS: calculated for [M^+] 443.1676, found 443.1666.

Peroxyfluor-3 Acetate, PF3-Ac (5). Compound **4** (33 mg, 0.080 mmol) and cesium carbonate (121 mg, 0.370 mmol) were added to a dry Schlenk tube and dissolved in 3 mL of dry acetonitrile. Acetic anhydride (14 uL, 0.15 mmol) was added, and the reaction stirred at room temperature for 30 min. The contents of the reaction were evaporated under reduced pressure. Purification by column chromatography (3:1 hexanes/ethyl acetate) afforded **5** as a clear film (16 mg, 43%). ^{1}H NMR ($CDCl_3$/10% CD_3OD, 400 MHz): 8.04 (1H, d, *J* = 6.8 Hz), 7.75 (1H, s), 6.64 (2H, quintet, *J* = 7.2 Hz), 4.45 (1H, d, *J* = 7.6 Hz), 7.14 (1H, d, *J* = 7.2 Hz), 7.08 (1H, d, *J* = 2.0 Hz), 6.82 – 6.88 (2H, m), 6.80 (1H, dd, *J* = 2.0, 8.4 Hz), 2.32 (1H, s), 1.35 (12H, s). HR-FABMS: calculated for [M^+] 485.1772, found 485.1780.

Aniline Rhodol Triflate (6). Rhodol (150 mg, 0.46 mmol) and *N*-phenyl bis(trifluoromethanesulfonamide) (250 mg, 0.69 mmol) were added to a glass vial and dissolved in 10 mL of acetonitrile. Diisopropylethylamine (0.23 mL, 1.4 mmol) was added, and the reaction stirred at room temperature for 72 h. The product was then extracted into ethyl acetate, washed once with water, and dried under reduced pressure. Purification by column chromatography (1:1 hexanes/ethyl acetate) yielded **6** as a white solid (49 mg, 23%). ^{1}H NMR ($(CD_3)_2O$, 400 MHz): δ 7.99 (1H, d, *J* = 7.6 Hz), 7.80 (1H, t, *J* = 7.6 Hz), 7.73 (1H, t, *J* = 7.2 Hz), 7.46 (1H, d, *J* = 2.0 Hz), 7.33 (1H, d, *J* = 7.6 Hz), 7.17 (1H, dd, *J* = 2.0, 8.8 Hz), 7.04 (1H, d, *J* = 8.8 Hz), 6.60 (1H, s), 6.52 (1H, d, *J* = 8.8 Hz), 6.48 (1H, d, *J* = 8.4 Hz). ^{13}C NMR ($(CD_3)_2O$, 100 MHz): δ 168.4, 152.6, 152.2, 152.0, 149.9, 135.4, 130.4, 130.1, 128.7, 126.7, 124.6, 124.0, 120.8, 118.7 (q, *J* = 318 Hz), 116.6, 112.0, 110.3, 106.1, 99.8, 81.9. ^{19}F NMR (Acetone, 376.5 MHz): δ -73.217. Low-res MS: 464.1.

Peroxy Emerald 1, PE1 (7). 6 (49 mg, 0.11 mmol), bis(pinacolato)diboron (27 mg, 0.11 mmol), Pd (dppf) Cl_2•CH_2Cl_2 (26 mg, 0.03 mmol), potassium acetate (31 mg, 0.32 mmol), and 3 mL of toluene were added to a dry pressure tube in an inert atmosphere glovebox. The pressure tube was then brought out of the box and microwave-heated for 4 h at 110 ºC. After the reaction cooled to room temperature, the reaction contents were washed into a round-bottom flask with dichloromethane and methanol and dried under reduced pressure. Purification by column chromatography (1:1 hexanes/ethyl acetate) yielded PE1 as a light orange solid (7.0 mg, 15%). ^{1}H NMR (Acetone, 400 MHz): δ 7.99 (1H, d, *J* = 7.6 Hz), 7.78 (1H, t, *J* = 7.6 Hz), 7.72 (1H, t, *J*

= 7.6 Hz), 7.62 (1H, s), 7.41 (1H, d, *J* = 7.6 Hz), 7.26 (1H, d, *J* = 7.6 Hz), 6.83 (1H, d, *J* = 7.6 Hz), 6.60 (1H, d, *J* = 2.0 Hz), 6.52 (1H, d, *J* = 8.8 Hz), 6.45 (1H, dd, *J* = 2.0, 8.8 Hz), 1.34 (12H, s). ^{13}C NMR (Acetone, 100 MHz): δ 169.6, 154.2, 153.3, 152.1, 151.9, 136.1, 130.8, 129.9, 129.6, 128.3, 127.7, 125.4, 124.9, 123.8, 123.4, 112.4, 107.4, 100.9, 85.0, 83.7, 74.9, 25.2. HR-FABMS: calculated for [M^+] 442.1831, found 442.1820.

Diethylamino Rhodol (8). Synthesis adopted from literature.[101] 2-(4-Diethylamino-2-hydroxybenzoyl)benzoic acid (1.26 g, 4.00 mmol) and resorcinol (443 g, 4.0 mmol) were added to a heavy-walled pressure flask and dissolved in 15 mL of trifluoroacetic acid. The reaction contents were heated to 90 °C for 12 h, then cooled to room temperature, and evaporated to dryness. Purification by column chromatography (4.5:4.5:1 dichloromethane/ethyl acetate/methanol) delivered **8** as a red-brown solid (1.2 g, 77% yield). ^{1}H NMR ($CDCl_3$ /10% CD_3OD, 400 MHz): δ 8.19 (1H, d, *J* = 7.2 Hz), 7.59 (2H, quartet, *J* = 7.2 Hz), 7.11 (1H, d, *J* = 7.2 Hz), 6.86-6.95 (3H, m), 6.68 (2H, dd, *J* = 2.0, 9.2 Hz), 6.64 (1H, d, *J* = 2.0 Hz), 3.44 (4H, q, *J* = 7.2 Hz), 1.16 (6H, t, *J* = 7.2 Hz). ^{13}C NMR ($CDCl_3$ /10% CD_3OD, 100 MHz): δ 163.5, 153.4, 152.4, 150.9, 128.9, 127.3, 126.7, 126.2, 126.0, 124.4, 113.2, 110.0, 109.7, 108.7, 98.6, 92.3, 41.8, 8.3. HR-FABMS: calculated for [M^+] 388.1549, found 388.1546.

Diethylamino Rhodol Triflate (9). Compound **8** (500 mg, 1.39 mmol) and *N*-phenyl bis(trifluoromethanesulfonamide) (745 mg, 2.09 mmol) were added to a vial and flushed with nitrogen. The reaction contents were dissolved in 5 mL of DMF, and diisopropylethylamine (691 uL, 4.18 mmol) was added. After 10 min of stirring at room temperature, the product was extracted into ethyl acetate, washed three times with water, and evaporated under reduced pressure. Purification by column chromatography (3:1 hexanes/ethyl acetate) afforded **9** as a light pink solid (440 mg, 61%). ^{1}H NMR ($CDCl_3$/10% CD_3OD, 400 MHz): δ 7.99 (1H, d, *J* = 7.6 Hz), 7.65 (1H, t, *J* = 7.2 Hz), 7.60 (1H, t, *J* = 7.2 Hz), 7.20 (1H, d, *J* = 2.4 Hz), 7.17 (1H, d, *J* = 7.6 Hz), 6.90 (1H, dd, *J* = 2.4, 8.8 Hz), 6.84 (1H, d, *J* = 8.8 Hz), 6.54 (1H, d, *J* = 9.2 Hz), 6.44 (1H, d, *J* = 2.4 Hz), 6.36 (1H, dd, *J* = 2.4, 8.8 Hz), 3.31 (4 H, q, *J* = 7.2 Hz), 1.11 (6H, t, *J* = 7.2 Hz). ^{13}C NMR ($CDCl_3$ /10% CD_3OD, 100 MHz): δ 169.5, 152.5, 152.4, 152.4, 149.8, 149.8, 135.3, 130.0, 129.2, 128.7, 126.7, 125.0, 124.0, 123.4, 120.2, 116.1, 113.8, 110.3, 109.0, 104.1, 97.4, 83.1, 44.4, 12.3. ^{19}F NMR ($CDCl_3$ /10% CD_3OD, 376.5 MHz): δ -72.05. HR-FABMS: calculated for [M^+] 520.1042, found 520.1036.

Peroxy Yellow 1, PY1 (10). Compound **9** (200 mg, 0.38 mmol), bis(pinacolato)diboron (94 mg, 0.38 mmol), Pd (dppf) Cl_2•CH_2Cl_2 (94 mg, 0.12 mmol), potassium acetate (113 mg, 1.16 mmol), and 3 mL of toluene were added to a dry pressure tube in an inert atmosphere glovebox. The pressure tube was then brought out of the box and microwave-heated for 2 h at 110 ºC. After cooling the reaction mixture to room temperature, the contents of the pressure flask were washed into a round-bottom flask with dichloromethane and evaporated to dryness. Purification by column chromatography (4:1 hexanes/ethyl acetate) delivered PY1 as a light tan solid (41 mg, 22%). ^{1}H NMR ($CDCl_3$ /10% CD_3OD, 400 MHz): δ 7.98 (1H, d, *J* = 7.6 Hz), 7.69 (1H, s), 7.62 (1H, t, *J* = 7.2 Hz), 7.58 (1H, t, *J* = 7.2 Hz), 7.35 (1H, d, *J* = 7.6 Hz), 7.13 (1H, d, *J* = 7.2 Hz), 6.73 (1H, d, *J* = 8.0 Hz), 6.55 (1H, d, *J* = 9.2 Hz), 6.433 (1H, s), 6.34 (1H, d, *J* = 8.8 Hz) 3.33 (4H, q, *J* = 7.2 Hz), 1.31 (12H, s), 1.14 (6H, t, *J* = 7.2 Hz). ^{13}C NMR ($CDCl_3$ /10% CD_3OD, 100 MHz): δ 170.1, 153.2, 152.8, 151.1, 134.9, 129.6, 128.8, 128.8, 127.2, 126.7, 124.9, 124.0, 123.9, 121.8, 84.2, 44.5, 12.4. HR-FABMS: calculated for [M^+] 498.2452, found 498.2441.

Julolidine Rhodol (11). Synthesis adopted from literature.[101] 8-Hydroxy-9-o-carboxybenzoyljulolidine (3.23 g, 9.56 mmol) and resorcinol (1.05 g, 9.56 mmol) were added to a heavy-walled pressure flask and dissolved in 20 mL of methane sulfonic acid. The reaction contents were heated to 90 °C for 3 h, then cooled to room temperature, and basified with aqueous sodium hydroxide. The mixture was then extrated into ethyl acetate and evaporated under reduced pressure. Purification by column chromatography (4.5:4.5:2 dichloromethane/ethyl acetate/methanol) delivered **11** as a maroon solid (2.5 g, 63% yield). ^{1}H NMR ($CDCl_3$ /10% CD_3OD, 400 MHz): δ 8.01 (1H, d, *J* = 7.2 Hz), 7.46 (2H, quartet, *J* = 8.8 Hz), 7.02 (1H, d, *J* = 7.2 Hz), 6.92 (1H, d, *J* = 9.2 Hz), 6.64 (1H, s), 6.58 (1H, s), 6.49 (1H, d, *J* = 7.6 Hz), 3.33 (4H, quintet, *J* = 6.0 Hz), 2.86 (2H, d, *J* = 6.4 Hz), 2.50 - 2.58 (2H, m), 1.72 - 1.99 (4H, m). ^{13}C NMR ($CDCl_3$ /10% CD_3OD, 100 MHz): δ 174.6, 167.8, 153.9, 148.1, 146.4, 134.0, 126.9, 125.9, 125.8, 125.3, 125.0, 122.9, 118.5, 117.4, 109.7, 108.7, 100.9, 99.0, 46.7, 46.2, 23.4, 16.7, 15.8. HR-FABMS: calculated for [M^+] 412.1549, found 412.1555.

Julolidine Rhodol Triflate (12). Compound **11** (500 mg, 1.2 mmol) and *N*-phenyl bis(trifluoromethanesulfonamide) (868 mg, 2.4 mmol) were added to a vial and flushed with nitrogen. The reaction contents were dissolved in 5 mL of DMF, and diisopropylethylamine (805 uL, 4.9 mmol) was added. After 20 min of stirring at room temperature, the product was extracted into ethyl acetate, washed three times with water, and evaporated under reduced pressure. Purification by column chromatography (1:1 hexanes/ethyl acetate) afforded **12** as a light red solid (224 mg, 34%). ^{1}H NMR ($(CD_3)_2O$, 400 MHz): δ 7.98 (1H, d, *J* = 7.6 Hz), 7.79 (1H, t, *J* = 7.2 Hz), 7.73 (1H, t , *J* = 7.6 Hz), 7.52 (1H, d, *J* = 2.8 Hz), 7.31 (1H, d, *J* = 7.6 Hz), 7.15 (1H dd, *J* = 2.4, 8.8 Hz), 7.00 (1H, d, *J* = 8.8 Hz), 6.19 (1H, s), 3.20 (2H, t, *J* = 6.0 Hz), 3.15 (2H, t, *J* = 6.0 Hz), 2.91 (2H, t, *J* = 6.8 Hz), 2.41-2.59 (2H, m), 1.92-2.00 (2H, m), 1.76-1.86 (2H, m). ^{13}C NMR ($(CD_3)_2O$ /10% CD_3OD, 100 MHz): δ 168.3, 152.5, 152.4, 149.9, 147.3, 144.7, 135.2, 130.3, 130.0, 126.9, 124.6, 124.5, 124.1, 120.7, 118.5, 116.3, 110.4, 106.8, 104.5, 82.6, 49.4, 48.9, 21.4, 20.8, 20.7, 19.9. ^{19}F NMR ($(CD_3)_2O$, 376.5 MHz): δ -73.284. HR-FABMS: calculated for [M^+] 544.1042, found 544.1036.

Peroxy Orange 1, PO1 (13). Compound **12** (100 mg, 0.18 mmol), bis(pinacolato)diboron (47 mg, 0.18 mmol), Pd (dppf) Cl_2•CH_2Cl_2 (45 mg, 0.05 mmol), potassium acetate (55 mg, 0.55 mmol), and 5 mL of toluene were added to a dry pressure tube in an inert atmosphere glovebox. The pressure tube was then brought out of the box and microwave-heated for 2 h at 110 ºC. After cooling the reaction mixture to room temperature, the contents of the pressure flask were washed into a round bottom flask with dichloromethane and evaporated to dryness. Purification by column chromatography (4.5:4.5:1 dichloromethane/ethyl acetate/methanol) delivered PO1 as light red solid (36 mg, 38%). ^{1}H NMR ($CDCl_3$ /10% CD_3OD, 400 MHz): δ 7.95 (1H, d, *J* = 7.2 Hz), 7.40 (1H, s), 7.58 (1H, t, *J* = 7.2 Hz), 7.54 (1H, t, *J* = 7.2 Hz), 7.33 (1H, d, *J* = 8.0 Hz), 7.11 (1H, d, *J* = 7.6 Hz), 6.69 (1H, d, *J* = 7.6 Hz), 6.10 (1H, s), 3.10 (2H, t, *J* = 5.2 Hz), 3.06 (2H, t, *J* = 5.2 Hz), 2.87 (2H, t, *J* = 6.4 Hz), 2.37-2.54 (2H, m), 1.91-1.99 (2H, m), 1.79 (2H, t, *J* = 5.2 Hz), 1.28 (12H, s). ^{13}C NMR ($CDCl_3$ /10% CD_3OD, 100 MHz): δ 170.1, 153.2, 151.1, 147.8, 144.7, 134.9, 129.5, 128.6, 127.1, 126.8, 124.8, 124.6, 124.0, 123.5, 121.6, 117.8, 107.2, 104.5, 85.1, 84.1, 74.9, 49.7, 49.3, 27.3, 24.8, 21.6, 21.1, 20.9. HR-FABMS: calculated for [M^+] 522.2456, found 522.2452.

Spectroscopic Materials and Methods. Millipore water was used to prepare all aqueous solutions. All spectroscopic measurements were performed in 20 mM HEPES buffer, pH 7. Absorption spectra were recorded on a Varian Cary 50 spectrophotometer (Walnut Creek, CA),

and fluorescence spectra were recorded on a Photon Technology International Quanta Master 4 L-format scanning spectrofluorometer (Lawrenceville, NJ) equipped with an LPS-220B 75-W xenon lamp and power supply, A-1010B lamp housing with integrated igniter, switchable 814 photon-counting/analog photomultiplier detection unit, and MD5020 motor driver. Samples for absorption and emission measurements were contained in 1-cm x 1-cm quartz cuvettes (1.5-mL volume, Starna, Atascadero, CA). Fluorescence quantum yields were determined by reference to fluorescein in 0.1M NaOH ($\Phi = 0.94$) or rhodamine B in water ($\Phi = 0.31$).

Preparation and Staining of Cell Cultures. RAW264.7 macrophages were cultured in Dulbecco's Modified Eagle Medium (DMEM) containing high glucose with GlutaMAX (Invitrogen, Carlsbad, CA) and supplemented with 10% Fetal Bovine Serum (FBS, Hyclone). A431 cells were cultured in DMEM plus GlutaMAX™ supplemented with 10% FBS. Cells were split 1/30 twice a week. Two days before imaging, cells were passed and plated on 18- mm glass coverslips coated with poly-L-lysine (50 μg/mL, Sigma, St. Louis, MO). 18 hours before imaging, A431 cells that were to be used for EGF stimulation experiments were serum-starved in DMEM alone. For all experiments, solutions of dyes (from 5 mM stocks in DMSO) were made in DPBS with calcium chloride and magnesium chloride (Sigma). H_2O_2 (100 mM stock solution in Millipore water), HOCl (100 mM stock solution in Millipore water), phorbol myristate acetate (PMA, 1 mg/mL stock solution in DMSO), or EGF (100 μg/mL stock in Millipore water) was added by bath application to the cell culture media. The cells were then kept in an incubator (37 °C, 5% CO_2) during the course of all experiments.

Fluorescence Imaging Experiments. Confocal fluorescence imaging studies were performed with a Zeiss LSM510 NLO Axiovert 200 laser scanning microscope and a 40x or 63x Achroplan IR water-immersion objective lens. Excitation of PF2 and PF3-loaded cells at 488 nm was carried out with an Ar laser and emission was collected using a META detector between 495 and 581 nm. Excitation of PY1-loaded cells at 514 nm was carried out with an Ar laser and emission was collected using a META detector between 516 and 581 nm. Excitation of PO1-loaded cells at 543 nm was carried out with a HeNe laser and emission was collected using a META detector between 548 and 613 nm. Excitation of Hoechst 33342 was carried out using a MaiTai two-photon laser at 780-nm pulses (mode-locked Ti:sapphire laser, Tsunami Spectra Physics) and emission was collected between 452 and 537 nm. Excitation of PO1 and APF-loaded cells at 488 and 543 nm was carried out with Ar and HeNe lasers, respectively, and emission was collected using a META detector between at 495-538 and 548-602 nm, respectively, using sequential scans. Image analysis was performed in Image J.

Figures and Schemes

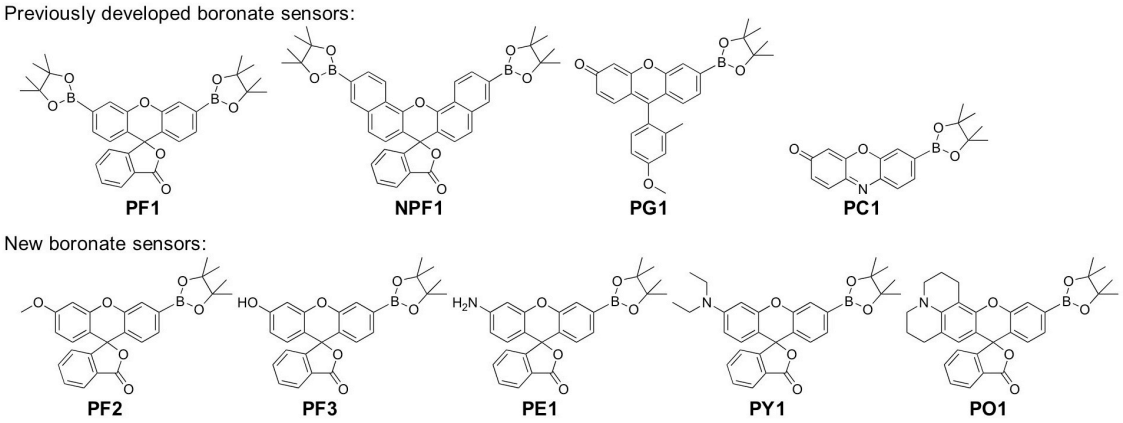

Scheme 1-1. Boronate-based H_2O_2-specific fluorescent indicators.

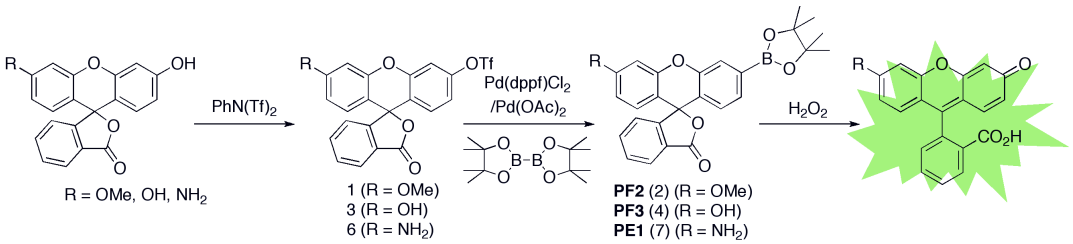

Scheme 1-2. Synthesis and activation of PF2, PF3, and PE1.

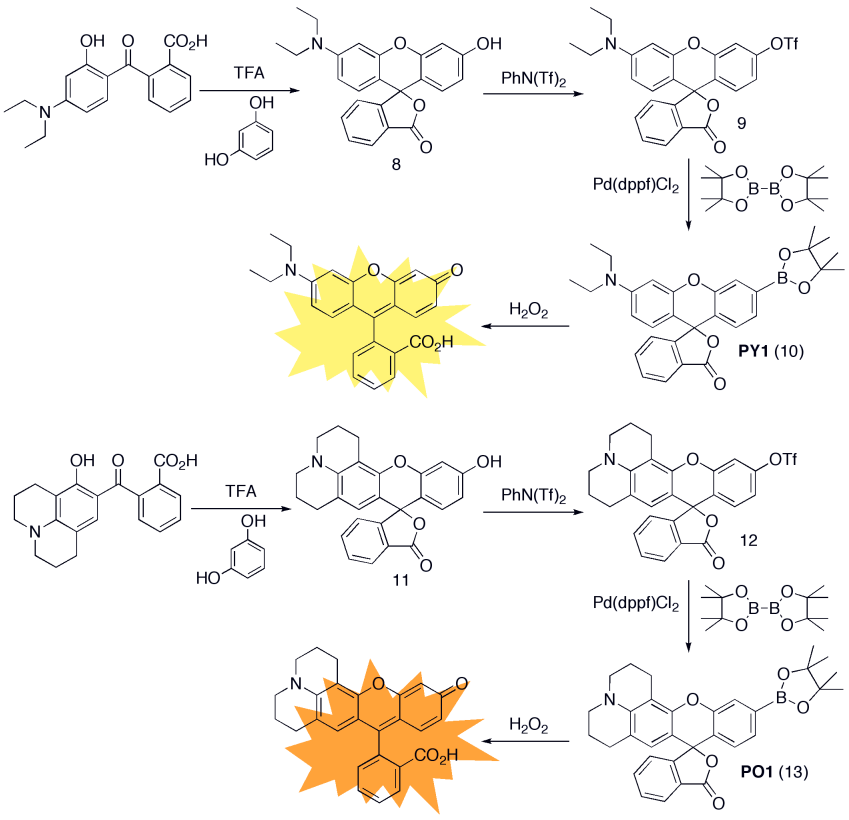

Scheme 1-3. Synthesis and activation of PY1 and PO1.

Table 1-1. Spectroscopic properties of PF2, PF3, PE1, PY1, and PO1 acquired at 25 ºC in 20 mM HEPES, pH 7. Fluorescein reported in 0.1 M NaOH.[104]

	Boronate-form				**Phenol-form**				
	λ_{abs} (nm)	ε ($M^{-1}cm^{-1}$)	λ_{em} (nm)	ϕ	λ_{abs} (nm)	ε ($M^{-1}cm^{-1}$)	λ_{em} (nm)	ϕ	k (x 10^{-3} s-1)
PF2	n/a	n/a	n/a	n/a	475	28600	511	0.27	4.7 (1)
PF3	454	24000	521	0.10	492	88000	515	0.94	3.8 (1)
PE1	480	16400	519	0.30	491	51200	514	0.93	8.1 (1)
PY1	494	16200	558	0.01	519	48900	548	0.12	3.7 (1)
PO1	507	13900	574	0.07	540	29300	565	0.46	5.2 (1)

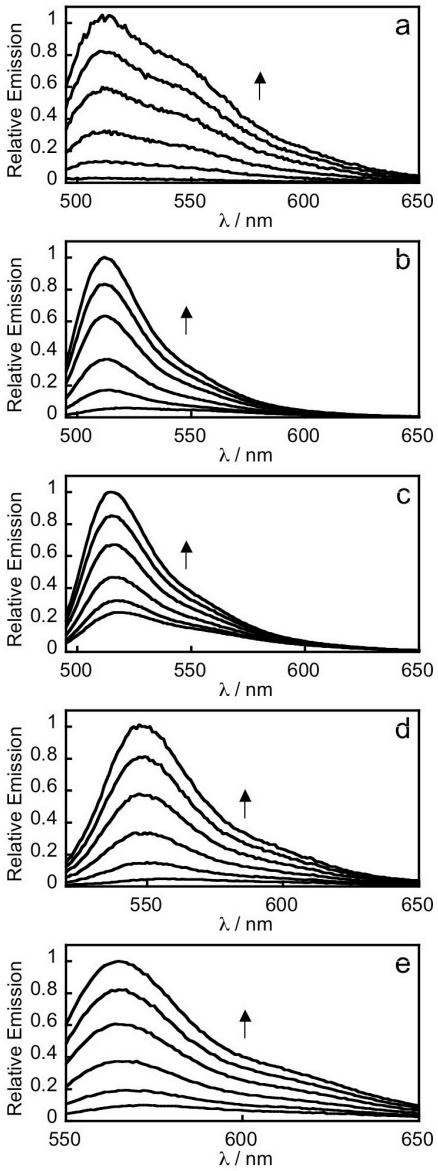

Figure 1-1. Fluorescence turn-on response of 5 μM PF2 (a), PF3 (b), PE1 (c), PY1 (d) or PO1 (e) to H_2O_2. Data were acquired at 25 ºC in 20 mM HEPES, pH 7, with excitation at λ = 488 nm for PF2 and PF3, λ = 490 nm for PE1, λ = 514 nm for PY1, and λ = 540 nm for PO1. Emission was collected between 493 and 750 nm for PF2 and PF3, 495 and 750 nm for PE1, 520 and 750 nm for PY1 and 545 and 750 nm for PO1. Time points represent 0, 5, 15, 30, 45, and 60 minutes after the addition of 100 μM H_2O_2. Reactions are not complete at these time points. Full turn-on response of each probe is shown in Fig. S1.

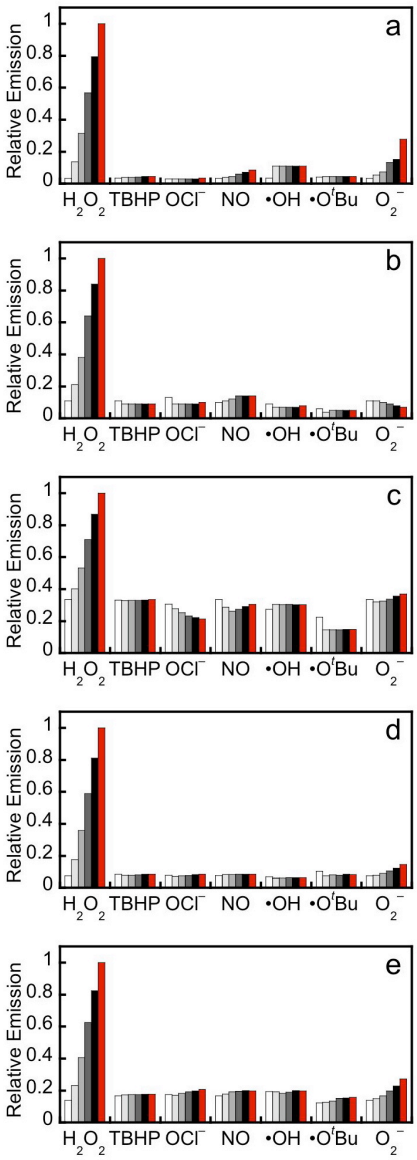

Figure 1-2. Fluorescence responses of 5 μM PF2 (a), PF3 (b), PE1 (c), PY1 (d) and PO1 (e) to various reactive oxygen species (ROS). Bars represent relative responses at 0, 5, 15, 30, 45, and 60 min after addition of each ROS. Data shown are for 200 μM NO and 100 μM for all other ROS. Data were acquired at 25 ºC in 20 mM HEPES, pH 7, with excitation at λ = 488 nm for PF2 and PF3, λ = 490 nm for PE1, λ = 514 nm for PY1, and λ = 540 nm for PO1. Emission was collected between 493 and 750 nm for PF2 and PF3, 495 and 750 nm for PE1, 520 and 750 nm for PY1 and 545 and 750 nm for PO1. Time points represent 0, 5, 15, 30, 45, and 60 minutes after the addition of 100 μM H_2O_2. Reactions are not complete at these time points.

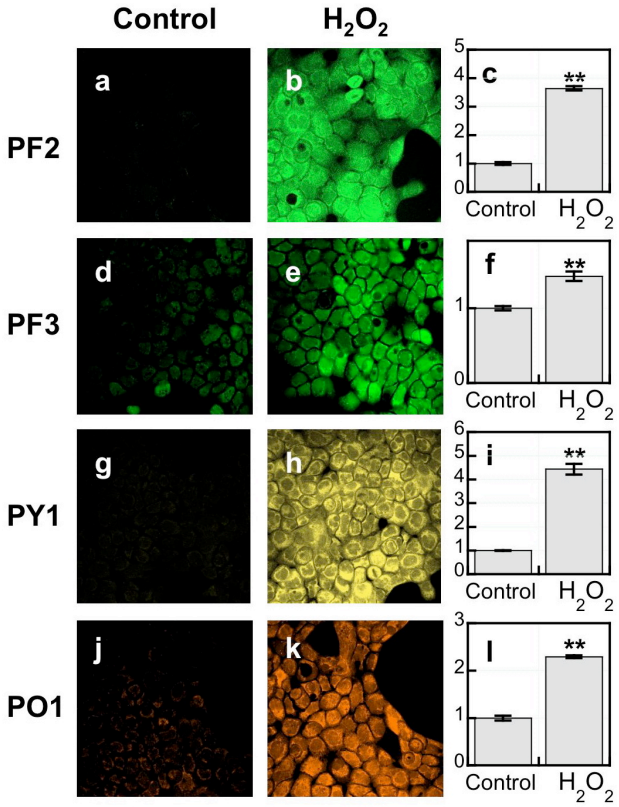

Figure 1-3. Confocal fluorescence images of H_2O_2 in live A431 cells under oxidative stress with PF2, PF3-Ac, PY1 and PO1. A431 cells incubated with 10 μM PF2 for 40 min at 37 ºC (a). A431 cells incubated with 10 μM PF2 for 40 min at 37 ºC with 100 μM H_2O_2 added for the final 20 min (b) and quantification (c). A431 cells incubated with 5 μM PF3-Ac for 40 min at 37 ºC (d). A431 cells incubated with 5 μM PF3-Ac for 40 min at 37 ºC with 100 μM H_2O_2 added for the final 20 min (e) and quantification (f). A431 cells incubated with 5 μM PY1 for 40 min at 37 ºC (g). A431 cells incubated with 5 μM PY1 for 40 min at 37 ºC with 100 μM H_2O_2 added for the final 20 min (h) and quantification (i). A431 cells incubated with 5 μM PO1 for 40 min at 37 ºC (j). A431 cells incubated with 5 μM PO1 for 40 min at 37 ºC with 100 μM H_2O_2 added for the final 20 min (k) and quantification (l). Data were normalized to controls and statistical analyses were performed with a two-tailed Student's *t*-test (n = 4). ***P* ≤ 0.005 and error bars are ± s.e.m.

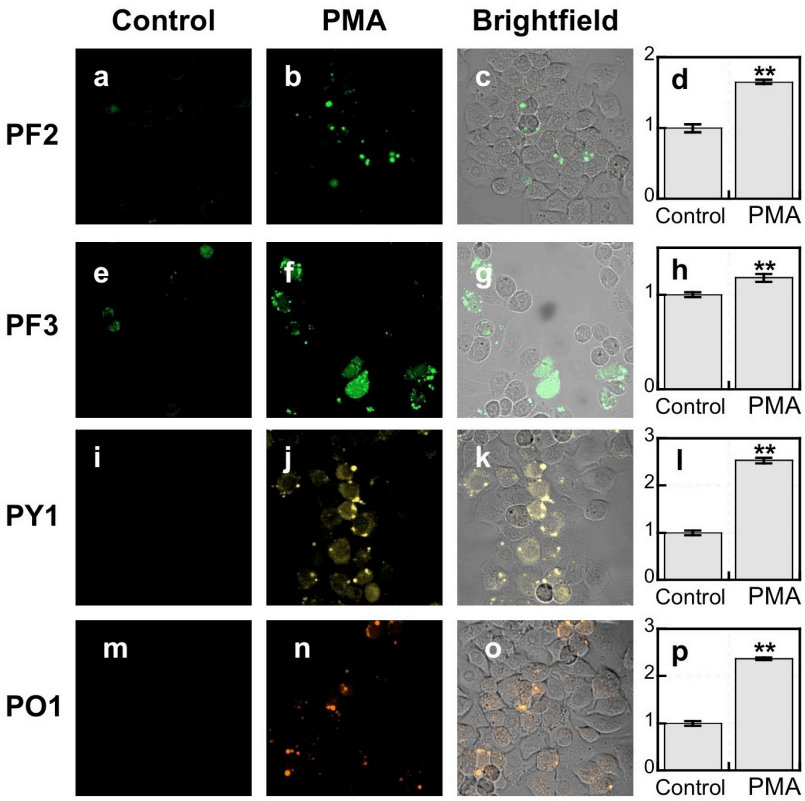

Figure 1-4. Confocal fluorescence images of PMA-induced H_2O_2 production in live RAW264.7 macrophages with PF2, PF3-Ac, PY1 and PO1. Macrophages incubated with 10 μM PF2 for 60 min at 37 ºC (a). Macrophages incubated with 10 μM PF2 for 60 min at 37 ºC with 1 μg/mL PMA added for the final 40 min (b) with a brightfield overlay (c) and quantification (d). Macrophages incubated with 5 μM PF3-Ac for 60 min at 37 ºC (e). Macrophages incubated with 5 μM PF3-Ac for 60 min at 37 ºC with 1 μg/mL PMA added for the final 40 min (f) with a brightfield overlay (g) and quantification (h). Macrophages incubated with 5 μM PY1 for 60 min at 37 ºC (i). Macrophages incubated with 5 μM PY1 for 60 min at 37 ºC with 1 μg/mL PMA added for the final 40 min (j) with a brightfield overlay (k) and quantification (l). Macrophages incubated with 5 μM PO1 for 60 min at 37 ºC (m). Macrophages incubated with 5 μM PO1 for 60 min at 37 ºC with 1 μg/mL PMA added for the final 40 min (n) with a brightfield overlay (o) and quantification (p). Data were normalized to controls and statistical analyses were performed with a two-tailed Student's *t*-test (n = 4). ***P* ≤ 0.005 and error bars are ± s.e.m.

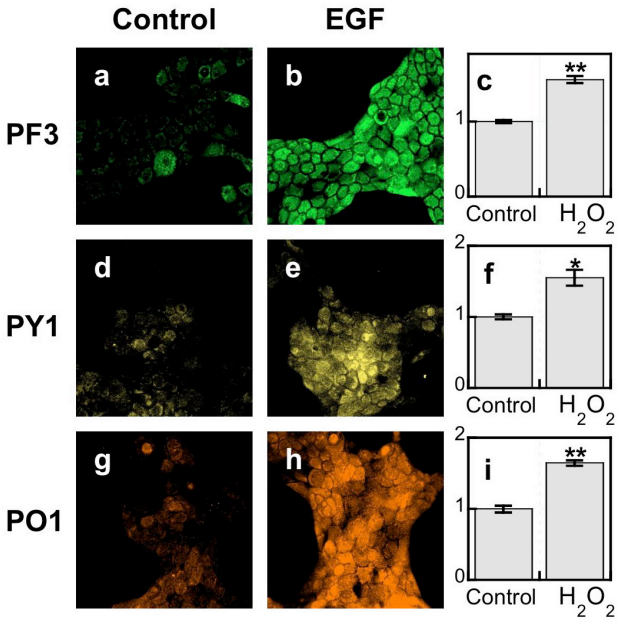

Figure 1-5. Confocal fluorescence images of EGF-induced H_2O_2 in live A431 cells with PF3-Ac, PY1 and PO1. A431 cells incubated with 5 μM PF3-Ac for 60 min at 37 ºC (a). A431 cells incubated with 5 μM PF3-Ac for 60 min at 37 ºC with 500 ng/mL EGF added for the final 40 min (b) and quantification (c). A431 cells incubated with 5 μM PY1 for 60 min at 37 ºC (d). A431 cells incubated with 5 μM PY1 for 60 min at 37 ºC with 500 ng/mL EGF added for the final 40 min (e) and quantification (f). A431 cells incubated with 5 μM PO1 for 60 min at 37 ºC (g). A431 cells incubated with 5 μM PO1 for 60 min at 37 ºC with 500 ng/mL EGF added for the final 20 min (h) and quantification (i). Data were normalized to controls and statistical analyses were performed with a two-tailed Student's *t*-test (n = 4). **P* ≤ 0.05, ***P* ≤ 0.005 and error bars are ± s.e.m.

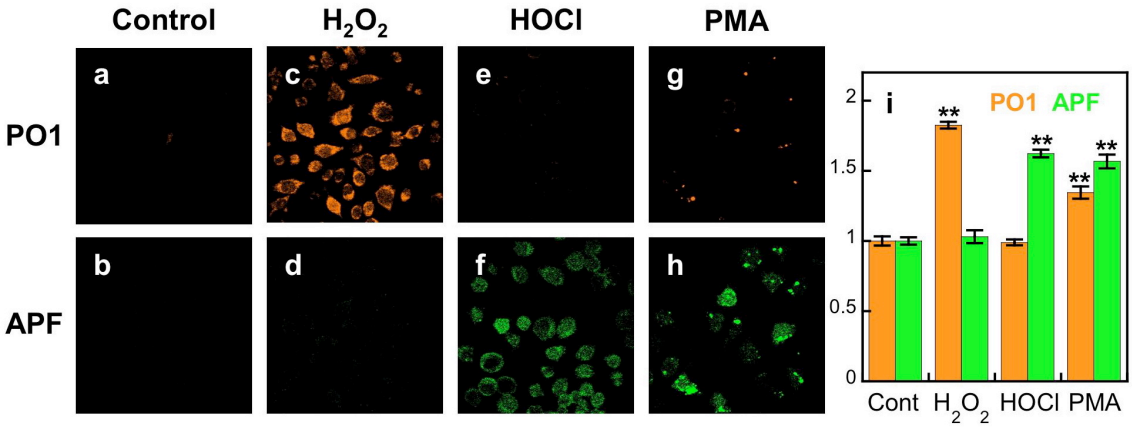

Figure 1-6. Confocal fluorescence images of PMA-induced ROS production in live RAW264.7 macrophages with PO1 and APF simultaneously. Macrophages incubated with 5 μM PO1 and 5 μM APF for 40 min at 37 ºC and imaged for PO1 (a) and APF (b). Macrophages incubated with 5 μM PO1 and 5 μM APF for 40 min at 37 ºC with 50 μM H_2O_2 added for the final 20 min and imaged for PO1 (c) and APF (d). Macrophages incubated with 5 μM PO1 and 5 μM APF for 40 min at 37 ºC with 100 μM HOCl added for the final 20 min and imaged for PO1 (e) and APF (f). Macrophages incubated with 5 μM PO1 and 5 μM APF for 40 min at 37 ºC with 1 μg/mL PMA added for the final 20 min and imaged for PO1 (g) and APF (h). Quantification of a-h (i). Data were normalized to controls and statistical analyses were performed with a two-tailed Student's *t*-test (n = 4). ***P* ≤ 0.005 and error bars are ± s.e.m.

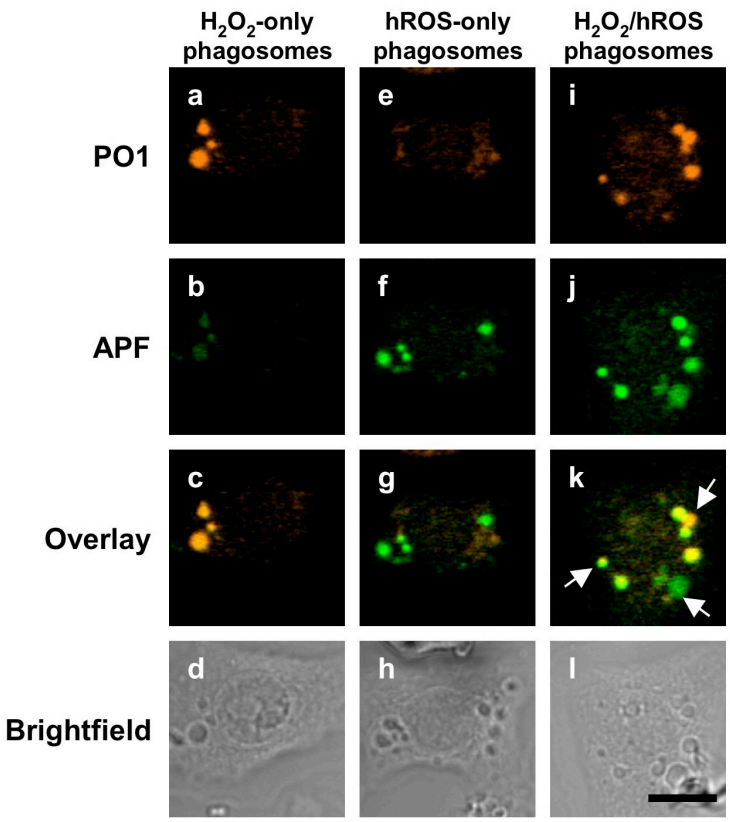

Figure 1-7. Confocal fluorescence images of different types of phagosomes in live RAW264.7 macrophages distinguished by PO1 and APF. A macrophage producing mostly H_2O_2 as shown by the PO1 signal (a), APF signal (b), overlay (c) and brightfield (d). A macrophage producing mostly hROS as shown by the PO1 signal (e), APF signal (f), overlay (g) and brightfield (h). A macrophage producing a mixture of H_2O_2 phagosomes, hROS phagosomes, and H_2O_2 and hROS phagosomes. as shown by the PO1 signal (i), APF signal (j), overlay (k) and brightfield (l). 10 μm scale bar shown.

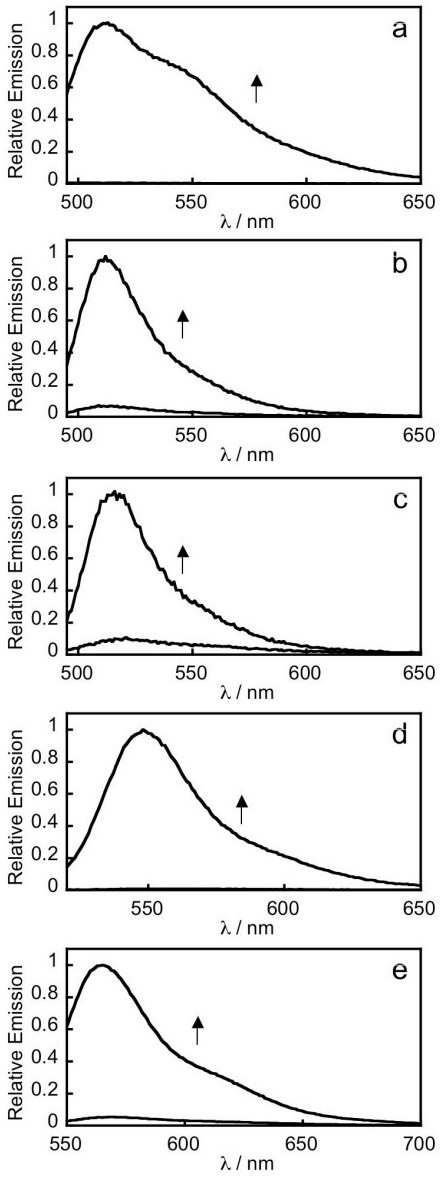

Figure 1-8. Complete fluorescence turn-on response of 5 μM PF2 (a), PF3 (b), PE1 (c), PY1 (d) or PO1 (e) to H_2O_2. Data were acquired at 25 ºC in 20 mM HEPES, pH 7, with excitation at λ = 488 nm for PF2 and PF3, λ = 490 nm for PE1, λ = 514 nm for PY1, and λ = 540 nm for PO1. Emission was collected between 493 and 750 nm for PF2 and PF3, 495 and 750 nm for PE1, 520 and 750 nm for PY1 and 545 and 750 nm for PO1. The emission spectra for the boronate-protected and deprotected forms of each dye are shown. In some cases, the boronate-protected form of the dye has an emission spectra that is not detectible in these plots.

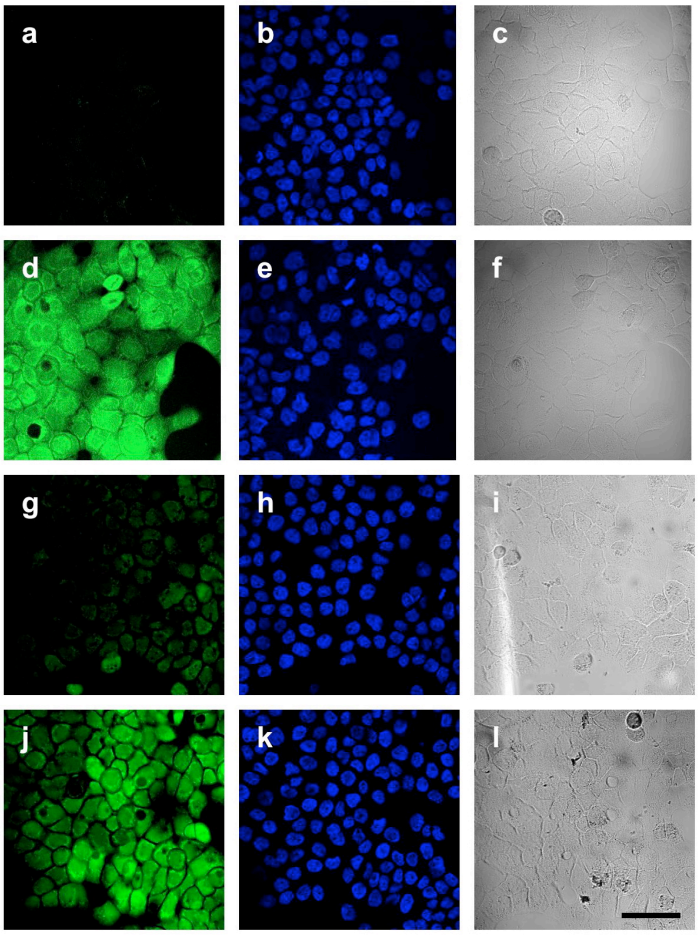

Figure 1-9. Confocal fluorescence images of H_2O_2 in live A431 cells under oxidative stress with PF2 and PF3-Ac with a nuclear stain and brightfields. A431 cells incubated with 10 μM PF2 for 40 min at 37 ºC and imaged for PF2 (a), Hoechst 33342 (b) and a brightfield (c). A431 cells incubated with 10 μM PF2 for 40 min at 37 ºC with 100 μM H_2O_2 added for the final 20 min and imaged for PF2 (d), Hoechst 33342 (e) and a brightfield (f). A431 cells incubated with 5 μM PF3-Ac for 40 min at 37 ºC and imaged for PF3-Ac (g), Hoechst 33342 (h) and a brightfield (i). A431 cells incubated with 5 μM PF3-Ac for 40 min at 37 ºC with 100 μM H_2O_2 added for the final 20 min and imaged for PF3-Ac (j), Hoechst 33342 (k) and a brightfield (l). 2 μM Hoechst 33342 added for the final 20 min of all experiments. 50 μm scale bare shown.

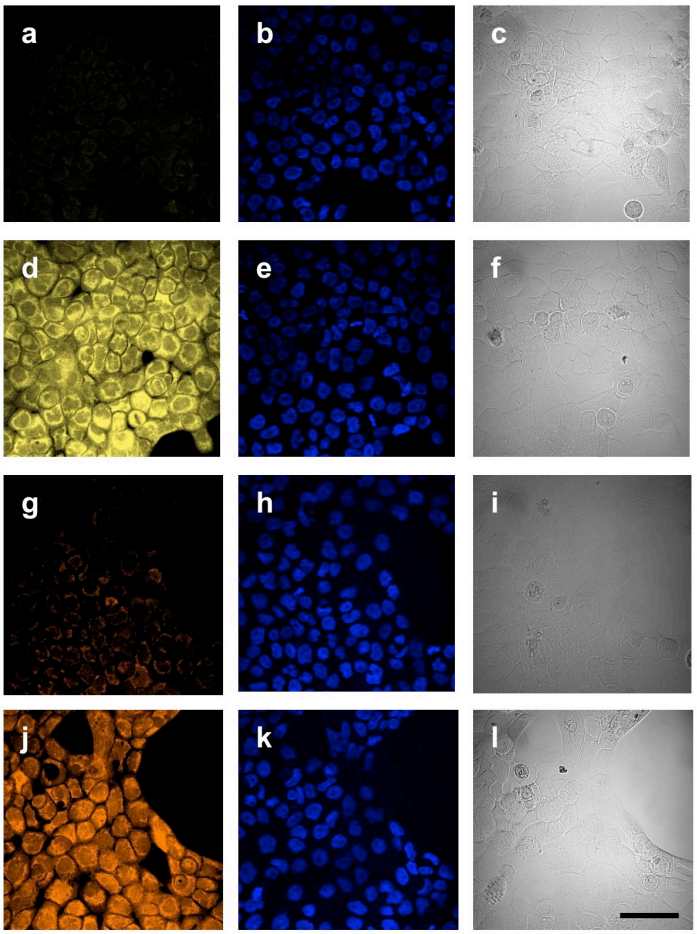

Figure 1-10. Confocal fluorescence images of H_2O_2 in live A431 cells under oxidative stress with PY1 and PO1 with a nuclear stain and brightfields. A431 cells incubated with 5 μM PY1 for 40 min at 37 ºC and imaged for PY1 (a), Hoechst 33342 (b) and a brightfield (c). A431 cells incubated with 5 μM PY1 for 40 min at 37 ºC with 100 μM H_2O_2 added for the final 20 min and imaged for PY1 (d), Hoechst 33342 (e) and a brightfield (f). A431 cells incubated with 5 μM PO1 for 40 min at 37 ºC and imaged for PO1 (g), Hoechst 33342 (h) and a brightfield (i). A431 cells incubated with 5 μM PO1 for 40 min at 37 ºC with 100 μM H_2O_2 added for the final 20 min and imaged for PO1 (j), Hoechst 33342 (k) and a brightfield (l). 2 μM Hoechst 33342 added for the final 20 min of all experiments. 50 μm scale bare shown.

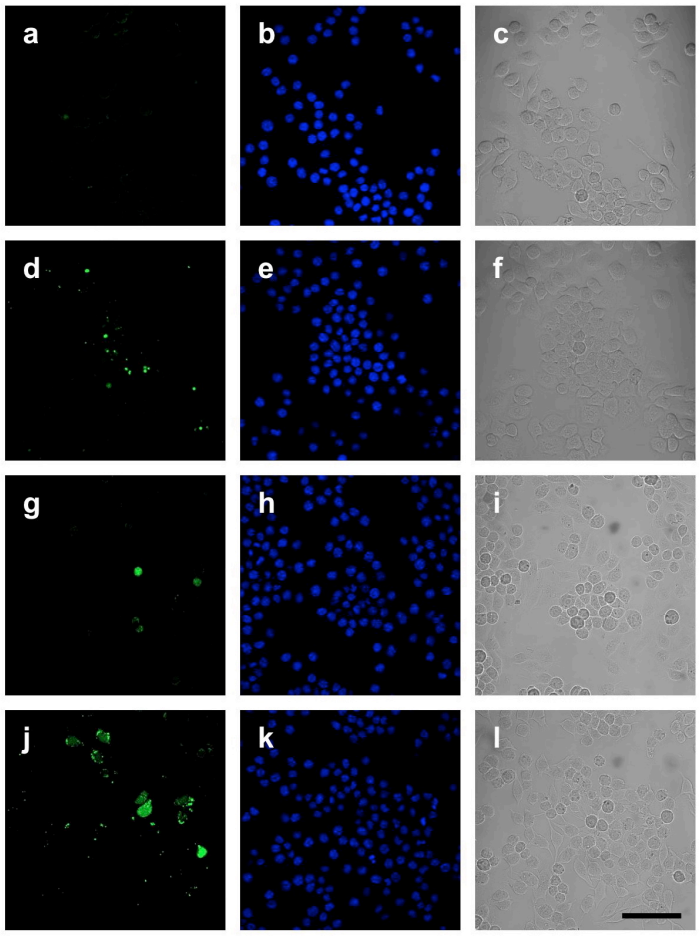

Figure 1-11. Confocal fluorescence images of PMA-induced H_2O_2 production in live RAW264.7 macrophages with PF2 and PF3-Ac with a nuclear stain and brightfield. Macrophages incubated with 10 μM PF2 for 60 min at 37 ºC and imaged for PF2 (a), Hoechst 33342 (b) and a brightfield (c). Macrophages incubated with 10 μM PF2 for 60 min at 37 ºC with 1 μg/mL PMA added for the final 40 min and imaged for PF2 (d), Hoechst 33342 (e) and a brightfield (f). Macrophages incubated with 5 μM PF3-Ac for 60 min at 37 ºC and imaged for PF3-Ac (g), Hoechst 33342 (h) and a brightfield (i). Macrophages incubated with 5 μM PF3-Ac for 60 min at 37 ºC with 1 μg/mL PMA added for the final 40 min and imaged for PF3-Ac (j), Hoechst 33342 (k) and a brightfield (l). 2 μM Hoechst 33342 added for the final 40 min of all experiments. 50 μm scale bare shown.

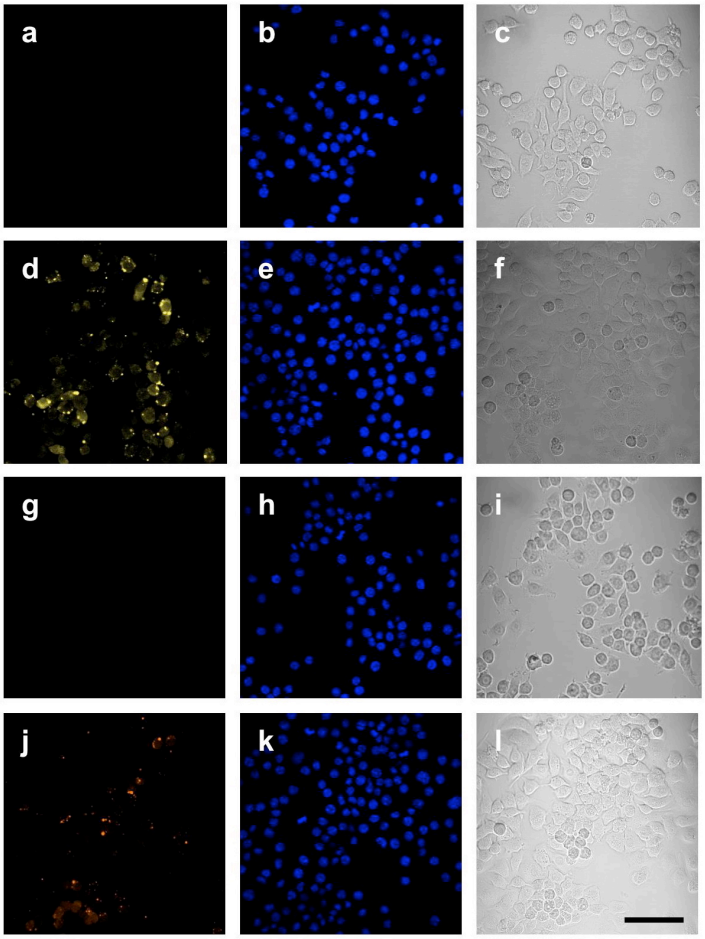

Figure 1-12. Confocal fluorescence images of PMA-induced H_2O_2 production in live RAW264.7 macrophages with PY1 and PO1 with a nuclear stain and brightfield. Macrophages incubated with 5 μM PY1 for 60 min at 37 ºC and imaged for PF2 (a), Hoechst 33342 (b) and a brightfield (c). Macrophages incubated with 10 μM PY1 for 60 min at 37 ºC with 1 μg/mL PMA added for the final 40 min and imaged for PY1 (d), Hoechst 33342 (e) and a brightfield (f). Macrophages incubated with 5 μM PO1 for 60 min at 37 ºC and imaged for PF3-Ac (g), Hoechst 33342 (h) and a brightfield (i). Macrophages incubated with 5 μM PO1 for 60 min at 37 ºC with 1 μg/mL PMA added for the final 40 min and imaged for PO1 (j), Hoechst 33342 (k) and a brightfield (l). 2 μM Hoechst 33342 added for the final 40 min of all experiments. 50 μm scale bare shown.

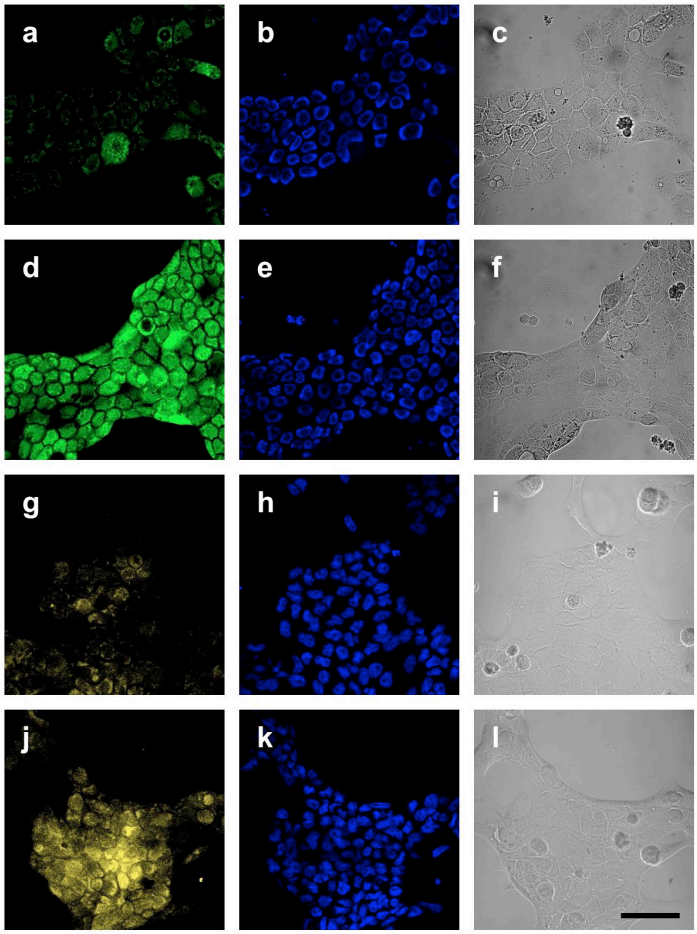

Figure 1-13. Confocal fluorescence images of EGF-induced H_2O_2 in live A431 cells with PF3-Ac and PY1 and a nuclear stain and brighfield. A431 cells incubated with 5 μM PF3-Ac for 60 min at 37 ºC and imaged for PF3-Ac (a), Hoechst 33342 (b) and a brightfield (c). A431 cells incubated with 5 μM PF3-Ac for 60 min at 37 ºC with 500 ng/mL EGF added for the final 40 min and imaged for PF3-Ac (d), Hoechst 33342 (e) and a brightfield (f). A431 cells incubated with 5 μM PY1 for 60 min at 37 ºC and imaged for PY1 (g), Hoechst 33342 (h) and a brightfield (i). A431 cells incubated with 5 μM PY1 for 60 min at 37 ºC with 500 ng/mL EGF added for the final 40 min and imaged for PY1 (j), Hoechst 33342 (k) and a brightfield (l). 2 μM Hoechst 33342 added for the final 40 min of all experiments. 50 μm scale bare shown.

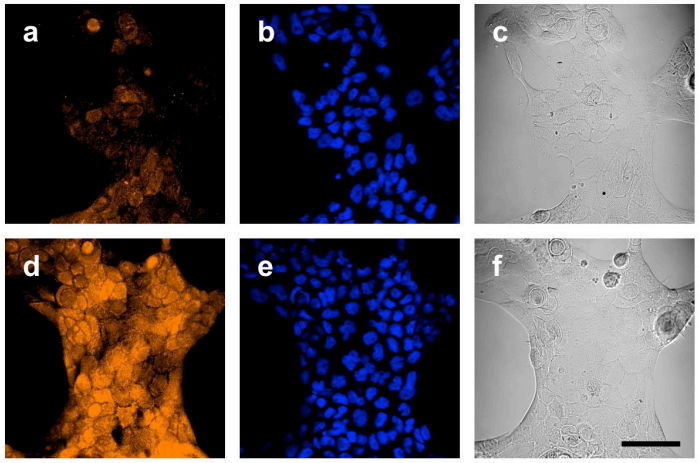

Figure 1-14. Confocal fluorescence images of EGF-induced H_2O_2 in live A431 cells with PO1 and a nuclear stain and brighfield. A431 cells incubated with 5 μM PO1 for 60 min at 37 ºC and imaged for PO1 (a), Hoechst 33342 (b) and a brightfield (c). A431 cells incubated with 5 μM PO1 for 60 min at 37 ºC with 500 ng/mL EGF added for the final 40 min and imaged for PO1 (d), Hoechst 33342 (e) and a brightfield (f).

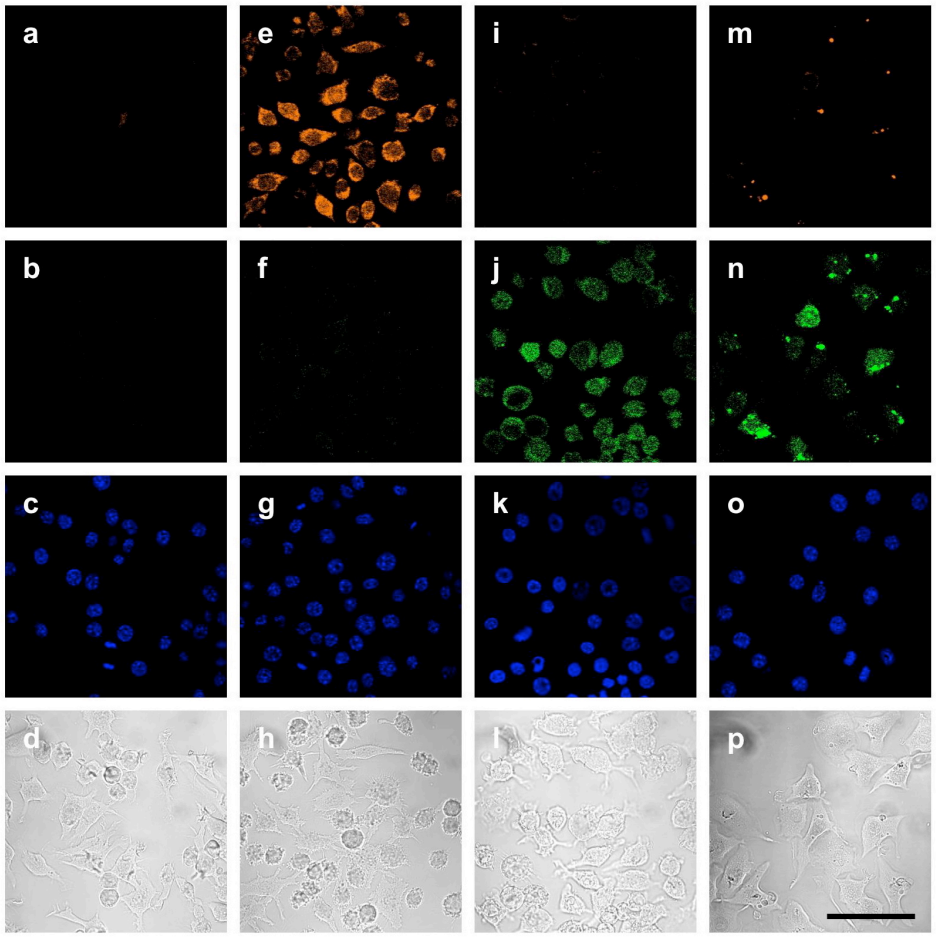

Figure 1-15. Confocal fluorescence images of PMA-induced ROS production in live RAW264.7 macrophages with PO1 and APF simultaneously with a nuclear stain and brightfield. Macrophages incubated with 5 μM PO1 and 5 μM APF for 40 min at 37 ºC and imaged for PO1 (a), APF (b), Hoechst 33342 (c), and a brightfield (d). Macrophages incubated with 5 μM PY1 and 5 μM APF for 40 min at 37 ºC with 50 μM H_2O_2 added for the final 20 min and imaged for PO1 (e), APF (f), Hoechst 33342 (g), and a brightfield (h). Macrophages incubated with 5 μM PO1 and 5 μM APF for 40 min at 37 ºC with 100 μM HOCl added for the final 20 min and imaged for PO1 (i), APF (j), Hoechst 33342 (k), and a brightfield (l). Macrophages incubated with 5 μM PO1 and 5 μM APF for 40 min at 37 ºC with 1 μg/mL PMA added for the final 20 min and imaged for PO1 (m), APF (n), Hoechst 33342 (o), and a brightfield (p). 2 μM Hoechst 33342 added for the final 20 min of all experiments. 50 μm scale bar shown.

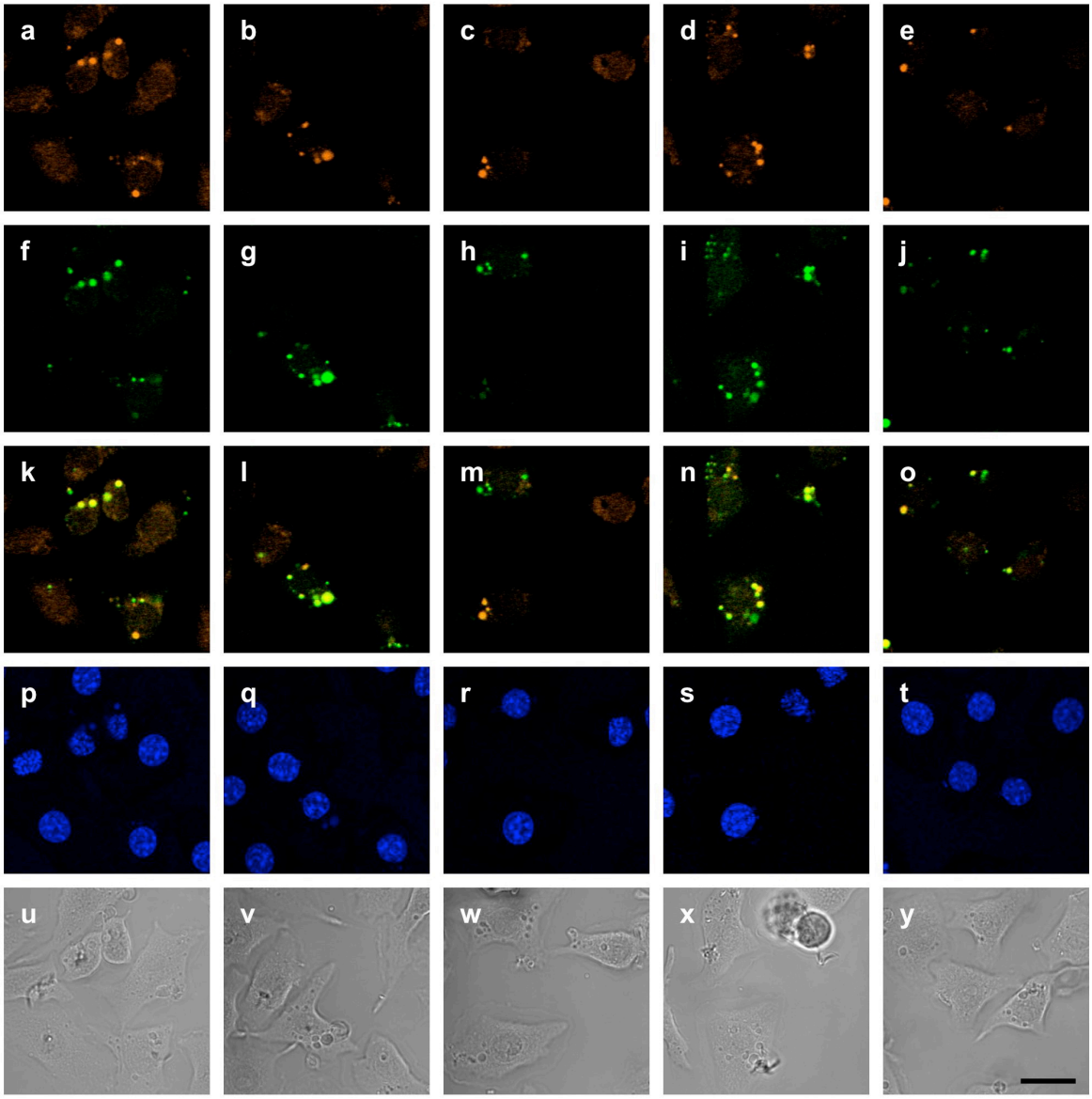

Figure 1-16. Confocal fluorescence images of PMA-induced ROS production in live RAW264.7 macrophages with PO1 and APF simultaneously with a nuclear stain and brightfield showing the various responses in ROS-production. Various regions of cells treated as in S6 showing signal from PO1 (a-e), APF (f-j), an overlay (k-o), Hoechst (p-t), and a brightfield (u-y). 20 μm scale bar shown.

References

1. Harman, D. The aging process. *Proc. Natl. Acad. Sci. USA* **1981**, *78*, 7124-7128.
2. Floyd, R. A. Oxidative damage to behavior during aging. *Science* **1991**, *254*, 1597.
3. Giorgio, M.; Trinei, M.; Migliaccio, E.; Pelicci, P. G. Hydrogen peroxide: a metabolic by-product or a common mediator of ageing signals? *Nat. Rev. Mol. Cell. Biol.* **2007**, *8*, 722-728.
4. Zhang, W.; Wang, T.; Qin, L.; Gao, H. M.; Wilson, B.; Ali, S. F.; Hong, J. S.; Liu, B. Neuroprotective effect of dextromethorphan in the MPTP Parkinson's disease model: role of NADPH oxidase. *FASEB J.* **2004**, *18*, 589-591.
5. Finkel, T.; Serrano, M.; Blasco, M. A. The common biology of cancer and ageing. *Nature* **2007**, *448*, 767-774.
6. Park, L.; Zhou, P.; Pitstick, R.; Capone, C.; Anrather, J.; Norris, E. H.; Younkin, L.; Younkin, S.; Carlson, G.; McEwen, B. S.; Iadecola, C. Nox2-derived radicals contribute to neurovascular and behavioral dysfunction in mice overexpressing the amyloid precursor protein. *Proc. Natl. Acad. Sci. USA* **2008**, *105*, 1347-1352.
7. Andersen, J. K. Oxidative stress in neurodegeneration: cause or consequence? *Nat. Rev. Neurosci.* **2004**, S18-25.
8. Barnham, K. J.; Masters, C. L.; Bush, A. I. Neurodegenerative diseases and oxidative stress. *Nat. Rev. Drug Discovery* **2004**, *3*, 205-214.
9. Sundaresan, M.; Yu, Z. X.; Ferrans, V. J.; Irani, K.; Finkel, T. Requirement for generation of H2O2 for platelet-derived growth factor signal transduction. *Science* **1995**, *270*, 296-299.
10. Bae, Y. S.; Kang, S. W.; Seo, M. S.; Baines, I. C.; Tekle, E.; Chock, P. B.; Rhee, S. G. Epidermal growth factor (EGF)-induced generation of hydrogen peroxide. Role in EGF receptor-mediated tyrosine phosphorylation. *J. Biol. Chem.* **1997**, *272*, 217-221.
11. Avshalumov, M. V.; Rice, M. E. Activation of ATP-sensitive K+ (KATP) channels by H2O2 underlies glutamate-dependent inhibition of striatal dopamine release. *Proc. Natl Acad. Sci. USA* **2003**, *100*, 11729-11734.
12. Lambeth, J. D. NOX enzymes and the biology of reactive oxygen. *Nat. Rev. Immunol.* **2004**, *4*, 181-189.
13. Rhee, S. G. H2O2, a necessary evil for cell signaling. *Science* **2006**, *312*, 1882-1883.
14. Stone, J. R.; Yang, S. Hydrogen peroxide: a signaling messenger. *Antioxid. Redox Signal.* **2006**, *8*, 243-270.
15. Miller, E. W.; Chang, C. J. Fluorescent probes for nitric oxide and hydrogen peroxide in cell signaling. *Curr. Opin. Chem. Biol.* **2007**, *11*, 620-625.
16. Miller, E. W.; Tulyathan, O.; Isacoff, E. Y.; Chang, C. J. Molecular imaging of hydrogen peroxide produced for cell signaling. *Nat. Chem. Biol.* **2007**, *3*, 263-267.
17. Veal, E. A.; Day, A. M.; Morgan, B. A. Hydrogen Peroxide Sensing and Signaling. *Mol. Cell* **2007**, *26*, 1-14.
18. Winterbourn, C. C. Reconciling the chemistry and biology of reactive oxygen species. *Nat. Chem. Biol.* **2008**, *4*, 278-286.
19. Poole, L. B.; Nelson, K. J. Discovering mechanisms of signaling-mediated cysteine oxidation. *Curr. Opin. Chem. Biol.* **2008**, *12*, 18-24.
20. Paulsen, C. E.; Carroll, K. S. Orchestrating Redox Signaling Networks through Regulatory Cysteine Switches. *ACS Chem. Biol.* **2010**, *5*, 47-62.

21. Murphy, M. P. How mitochondria produce reactive oxygen species. *Biochem. J.* **2009**, *417*, 1-13.
22. Dickinson, B. C.; Srikun, D.; Chang, C. J. Mitochondrial-targeted fluorescent probes for reactive oxygen species. *Curr. Opin. Chem. Biol.* **2010**, *14*, 50-56.
23. Shaner, N. C.; Steinbach, P. A.; Tsien, R. Y. A guide to choosing fluorescent proteins. *Nat. Meth.* **2005**, *2*, 905-909.
24. Giepmans, B. N. G.; Adams, S. R.; Ellisman, M. H.; Tsien, R. Y. The Fluorescent Toolbox for Assessing Protein Location and Function. *Science* **2006**, *312*, 217-224.
25. Soh, N. Recent advances in fluorescent probes for the detection of reactive oxygen species. *Anal. Bioanal. Chem.* **2006**, *386*, 532-543.
26. Domaille, D. W.; Que, E. L.; Chang, C. J. Synthetic fluorescent sensors for studying the cell biology of metals. *Nat. Chem. Biol.* **2008**, *4*, 168-175.
27. Terai, T.; Nagano, T. Fluorescent probes for bioimaging applications. *Curr. Opin. Chem. Biol.* **2008**, *12*, 515-521.
28. Lavis, L. D.; Raines, R. T. Bright ideas for chemical biology. *ACS Chem. Biol.* **2008**, *3*, 142-155.
29. Laughlin, S. T.; Bertozzi, C. R. Imaging the glycome. *Proc. Natl. Acad. Sci. USA* **2009**, *106*, 12-17.
30. Kojima, H.; Nakatsubo, N.; Kikuchi, K.; Kawahara, S.; Kirino, Y.; Nagoshi, H.; Hirata, Y.; Nagano, T. Detection and Imaging of Nitric Oxide with Novel Fluorescent Indicators: Diaminofluoresceins. *Anal. Chem.* **1998**, *70*, 2446-2453.
31. Kojima, H.; Hirotani, M.; Nakatsubo, N.; Kikuchi, K.; Urano, Y.; Higuchi, T.; Hirata, Y.; Nagano, T. Bioimaging of nitric oxide with fluorescent indicators based on the rhodamine chromophore. *Anal. Chem.* **2001**, *73*, 1967-1973.
32. Gabe, Y.; Urano, Y.; Kikuchi, K.; Kojima, H.; Nagano, T. Highly Sensitive Fluorescence Probes for Nitric Oxide Based on Boron Dipyrromethene ChromophoreRational Design of Potentially Useful Bioimaging Fluorescence Probe. *J. Am. Chem. Soc.* **2004**, *126*, 3357-3367.
33. Sasaki, E.; Kojima, H.; Nishimatsu, H.; Urano, Y.; Kikuchi, K.; Hirata, Y.; Nagano, T. Highly Sensitive Near-Infrared Fluorescent Probes for Nitric Oxide and Their Application to Isolated Organs. *J. Am. Chem. Soc.* **2005**, *127*, 3684-3685.
34. Lim, M. H.; Xu, D.; Lippard, S. J. Visualization of nitric oxide in living cells by a copper-based fluorescent probe. *Nat. Chem. Biol.* **2006**, *2*, 375-380.
35. Lim, M. H.; Lippard, S. J. Metal-based turn-on fluorescent probes for sensing nitric oxide. *Acc. Chem. Res.* **2007**, *40*, 41-51.
36. McQuade, L. E.; Lippard, S. J. Fluorescent probes to investigate nitric oxide and other reactive nitrogen species in biology (truncated form: fluorescent probes of reactive nitrogen species). *Curr. Opin. Chem. Biol.* **2010**, *14*, 43-49.
37. Yang, D.; Wang, H. L.; Sun, Z. N.; Chung, N. W.; Shen, J. G. A highly selective fluorescent probe for the detection and imaging of peroxynitrite in living cells. *J. Am. Chem. Soc.* **2006**, *128*, 6004-6005.
38. Sun, Z. N.; Wang, H. L.; Liu, F. Q.; Chen, Y.; Tam, P. K. H.; Yang, D. BODIPY-Based Fluorescent Probe for Peroxynitrite Detection and Imaging in Living Cells. *Org. Lett* **2009**, *11*, 1887-1890.

39. Ueno, T.; Urano, Y.; Kojima, H.; Nagano, T. Mechanism-based molecular design of highly selective fluorescence probes for nitrative stress. *J. Am. Chem. Soc.* **2006**, *128*, 10640-10641.
40. Maeda, H.; Yamamoto, K.; Nomura, Y.; Kohno, I.; Hafsi, L.; Ueda, N.; Yoshida, S.; Fukuda, M.; Fukuyasu, Y.; Yamauchi, Y. A design of fluorescent probes for superoxide based on a nonredox mechanism. *J. Am. Chem. Soc.* **2005**, *127*, 68-69.
41. Robinson, K. M.; Janes, M. S.; Pehar, M.; Monette, J. S.; Ross, M. F.; Hagen, T. M.; Murphy, M. P.; Beckman, J. S. Selective fluorescent imaging of superoxide in vivo using ethidium-based probes. *Proc. Natl Acad. Sci. USA* **2006**, *103*, 15038-15043.
42. Xu, K.; Liu, X.; Tang, B.; Yang, G.; Yang, Y.; An, L. Design of a phosphinate-based fluorescent probe for superoxide detection in mouse peritoneal macrophages. *Chem. Eur. J.* **2007**, *13*, 1411-1416.
43. Xu, K.; Liu, X.; Tang, B. A Phosphinate-Based Red Fluorescent Probe for Imaging the Superoxide Radical Anion Generated by RAW264.7 Macrophages. *ChemBioChem* **2007**, *8*, 453-458.
44. Umezawa, N.; Tanaka, K.; Urano, Y.; Kikuchi, K.; Higuchi, T.; Nagano, T. Novel Fluorescent Probes for Singlet Oxygen. *Angew. Chem. Int. Ed.* **1999**, *38*, 2899-2901.
45. Song, B.; Wang, G.; Tan, M.; Yuan, J. A Europium(III) Complex as an Efficient Singlet Oxygen Luminescence Probe. *J. Am. Chem. Soc.* **2006**, *128*, 13442-13450.
46. Garner, A. L.; St Croix, C. M.; Pitt, B. R.; Leikauf, G. D.; Ando, S.; Koide, K. Specific fluorogenic probes for ozone in biological and atmospheric samples. *Nat. Chem.* **2009**, *1*, 316-321.
47. Wolfbeis, O. S.; Dürkop, A.; Wu, M.; Lin, Z. A Europium-Ion-Based Luminescent Sensing Probe for Hydrogen Peroxide. *Angew. Chem. Int. Ed.* **2002**, *41*, 4495-4498.
48. Meng, O.; Lin, W. Z. A europium-ion-based luminescent sensing probe for hydrogen peroxide. *Angew. Chem. Int. Ed.* **2002**, *41*, 4495-4498.
49. Onoda, M.; Uchiyama, S.; Endo, A.; Tokuyama, H.; Santa, T.; Imai, K. First fluorescent photoinduced electron transfer (PET) reagent for hydroperoxides. *Org. Lett.* **2003**, *5*, 1459-1461.
50. Lo, L. C.; Chu, C. Y. Development of highly selective and sensitive probes for hydrogen peroxide. *Chem. Commun.* **2003**, 2728-2729.
51. Chang, M. C. Y.; Pralle, A.; Isacoff, E. Y.; Chang, C. J. A selective, cell-permeable optical probe for hydrogen peroxide in living cells. *J. Am. Chem. Soc* **2004**, *126*, 15392-15393.
52. Maeda, H.; Fukuyasu, Y.; Yoshida, S.; Fukuda, M.; Saeki, K.; Matsuno, H.; Yamauchi, Y.; Yoshida, K.; Hirata, K.; Miyamoto, K. Fluorescent Probes for Hydrogen Peroxide Based on a Non-Oxidative Mechanism. *Angew. Chem. Int. Ed.* **2004**, *43*, 2389-2391.
53. Miller, E. W.; Albers, A. E.; Pralle, A.; Isacoff, E. Y.; Chang, C. J. Boronate-based fluorescent probes for imaging cellular hydrogen peroxide. *J. Am. Chem. Soc.* **2005**, *127*, 16652-16659.
54. Kozhevnikov, V. N.; Mandl, C.; Miltschitzky, S.; Duerkop, A.; Wolfbeis, O. S.; Koenig, B. Strong emission increase of a dicarboxyterpyridene europium (III) complex in the presence of citrate and hydrogen peroxide. *Inorg. Chim. Acta* **2005**, *358*, 2445-2448.
55. Soh, N.; Sakawaki, O.; Makihara, K.; Odo, Y.; Fukaminato, T.; Kawai, T.; Irie, M.; Imato, T. Design and development of a fluorescent probe for monitoring hydrogen

peroxide using photoinduced electron transfer. *Bioorg. Med. Chem. Lett.* **2005**, *13*, 1131-1139.
56. Onoda, M.; Tokuyama, H.; Uchiyama, S.; Mawatari, K.; Santa, T.; Kaneko, K.; Imai, K.; Nakagomi, K. Fluorescence enhancement by hydroperoxides based on a change in the intramolecular charge transfer character of benzofurazan. *Chem. Commun.* **2005**, *2005*, 1848-1850.
57. Belousov, V. V.; Fradkov, A. F.; Lukyanov, K. A.; Staroverov, D. B.; Shakhbazov, K. S.; Terskikh, A. V.; Lukyanov, S. Genetically encoded fluorescent indicator for intracellular hydrogen peroxide. *Nat. Methods* **2006**, *3*, 281-286.
58. Albers, A. E.; Okreglak, V. S.; Chang, C. J. A FRET-based approach to ratiometric fluorescence detection of hydrogen peroxide. *J. Am. Chem. Soc.* **2006**, *128*, 9640-9641.
59. Lee, D.; Khaja, S.; Velasquez-Castano, J. C.; Dasari, M.; Sun, C.; Petros, J.; Taylor, W. R.; Murthy, N. In vivo imaging of hydrogen peroxide with chemiluminescent nanoparticles. *Nat. Mater.* **2007**, *6*, 765-769.
60. Srikun, D.; Miller, E. W.; Domaille, D. W.; Chang, C. J. An ICT-Based approach to ratiometric fluorescence imaging of hydrogen peroxide produced in living cells. *J. Am. Chem. Soc.* **2008**, *130*, 4596-4597.
61. Dickinson, B. C.; Chang, C. J. A Targetable Fluorescent Probe for Imaging Hydrogen Peroxide in the Mitochondria of Living Cells. *J. Am. Chem. Soc.* **2008**, *130*, 9638-9639.
62. Albers, A. E.; Dickinson, B. C.; Miller, E. W.; Chang, C. J. A red-emitting naphthofluorescein-based fluorescent probe for selective detection of hydrogen peroxide in living cells. *Bioorg. Med. Chem. Lett.* **2008**, *18*, 5948-5950.
63. Xu, K.; Liu, F.; Wang, H.; Wang, S.; Wang, L.; Tang, B. Sulfonate-based fluorescent probes for imaging hydrogen peroxide in living cells. *Sci. China, Ser. B Chem.* **2009**, *52*, 734-740.
64. Du Y, L.; Ni Y, N.; Li, M.; Wang, B. A fluorescent hydrogen peroxide probe based on a [`]click' modified coumarin fluorophore. *Tetrahedron Letters* **2010**, *51*, 1152-1154.
65. Srikun, D.; Albers, A. E.; Nam, C. I.; Ivarone, A. T.; Chang, C. J. Organelle-Targetable Fluorescent Probes for Imaging Hydrogen Peroxide in Living Cells via SNAP-Tag Protein Labeling. *J. Am. Chem. Soc.* **2010**, *132*, 4455-4465.
66. Kenmoku, S.; Urano, Y.; Kojima, H.; Nagano, T. Development of a highly specific rhodamine-based fluorescence probe for hypochlorous acid and its application to real-time imaging of phagocytosis. *J. Am. Chem. Soc.* **2007**, *129*, 7313-7318.
67. Sun, Z. N.; Liu, F. Q.; Chen, Y.; Tam, P. K. H.; Yang, D. A Highly Specific BODIPY-Based Fluorescent Probe for the Detection of Hypochlorous Acid. *Org. Lett.* **2008**, *10*, 2171-2174.
68. Setsukinai, K.; Urano, Y.; Kakinuma, K.; Majima, H. J.; Nagano, T. Development of novel fluorescence probes that can reliably detect reactive oxygen species and distinguish specific species. *J. Biol. Chem.* **2003**, *278*, 3170-3175.
69. Koide, Y.; Urano, Y.; Kenmoku, S.; Kojima, H.; Nagano, T. Design and Synthesis of Fluorescent Probes for Selective Detection of Highly Reactive Oxygen Species in Mitochondria of Living Cells. *J. Am. Chem. Soc.* **2007**, *129*, 10324-10325.
70. Panizzi, P.; Nahrendorf, M.; Wildgruber, M.; Waterman, P.; Figueiredo, J. L.; Aikawa, E.; McCarthy, J.; Weissleder, R.; Hilderbrand, S. A. Oxazine Conjugated Nanoparticle Detects in Vivo Hypochlorous Acid and Peroxynitrite Generation. *J. Am. Chem. Soc.* **2009**, *131*, 15739-15744.

71. Hempel, S. L.; Buettner, G. R.; O'Malley, Y. Q.; Wessels, D. A.; Flaherty, D. M. Dihydrofluorescein diacetate is superior for detecting intracellular oxidants: comparison with 2 , 7 -dichlorodihydrofluorescein diacetate, 5 (and 6)-carboxy-2 , 7 -dichlorodihydrofluorescein diacetate, and dihydrorhodamine 123. *Free Radical Biol. Med*. **1999**, *27*, 146-159.
72. Østergaard, H.; Henriksen, A.; Hansen, F. G.; Winther, J. R. Shedding light on disulfide bond formation: engineering a redox switch in green fluorescent protein. *EMBO J*. **2001**, *20*, 5853-5863.
73. Hanson, G. T.; Aggeler, R.; Oglesbee, D.; Cannon, M.; Capaldi, R. A.; Tsien, R. Y.; Remington, S. J. Investigating mitochondrial redox potential with redox-sensitive green fluorescent protein indicators. *J. Biol. Chem*. **2004**, *279*, 13044-13053.
74. Cline, D. J.; Thorpe, C.; Schneider, J. P. Structure-based design of a fluorimetric redox active peptide probe. *Anal. Biochem*. **2004**, *325*, 144-150.
75. Lee, K.; Dzubeck, V.; Latshaw, L.; Schneider, J. P. De Novo Designed Peptidic Redox Potential Probe: Linking Sensitized Emission to Disulfide Bond Formation. *J. Am. Chem. Soc*. **2004**, *126*, 13616-13617.
76. Cannon, M. B.; Remington, S. J. Re-engineering redox-sensitive green fluorescent protein for improved response rate. *Protein Sci*. **2006**, *15*, 45-57.
77. Miller, E. W.; Bian, S. X.; Chang, C. J. A fluorescent sensor for imaging reversible redox cycles in living cells. *J. Am. Chem. Soc*. **2007**, *129*, 3458-3459.
78. Ahn, Y. H.; Lee, J. S.; Chang, Y. T. Combinatorial Rosamine Library and Application to in Vivo Glutathione Probe. *J. Am. Chem. Soc*. **2007**, *129*, 4510-4511.
79. Wang, W.; Fang, H.; Groom, L.; Cheng, A.; Zhang, W.; Liu, J.; Wang, X.; Li, K.; Han, P.; Zheng, M. Superoxide flashes in single mitochondria. *Cell* **2008**, *134*, 279-290.
80. Gutscher, M.; Pauleau, A. L.; Marty, L.; Brach, T.; Wabnitz, G. H.; Samstag, Y.; Meyer, A. J.; Dick, T. P. Real-time imaging of the intracellular glutathione redox potential. *Nat. Methods* **2008**, *5*, 553-560.
81. Banerjee, S.; Kar, S.; Perez, J. M.; Santra, S. Quantum Dot-Based OFF/ON Probe for Detection of Glutathione. *J. Phys. Chem. C* **2009**, *113*, 9659-9663.
82. Shao, N.; Jin, J.; Wang, H.; Zheng, J.; Yang, R.; Chan, W.; Abliz, Z. Design of Bis-spiropyran Ligands as Dipolar Molecule Receptors and Application to in Vivo Glutathione Fluorescent Probes. *J. Am. Chem. Soc*. **2009**, *132*, 725-736.
83. Kundu, K.; Knight, S. F.; Willett, N.; Lee, S.; Taylor, W. R.; Murthy, N. Hydrocyanines: A Class of Fluorescent Sensors That Can Image Reactive Oxygen Species in Cell Culture, Tissue, and In Vivo. *Angew. Chem. Int. Ed*. **2009**, *48*, 299-303.
84. Oushiki, D.; Kojima, H.; Terai, T.; Arita, M.; Hanaoka, K.; Urano, Y.; Nagano, T. Development and Application of a Near-Infrared Fluorescence Probe for Oxidative Stress Based on Differential Reactivity of Linked Cyanine Dyes. *J. Am. Chem. Soc*. **2010**, *132*, 2795-2801.
85. Burdette, S. C.; Lippard, S. J. The Rhodafluor Family. An Initial Study of Potential Ratiometric Fluorescent Sensors for Zn2+. *Inorg. Chem*. **2002**, *41*, 6816-6823.
86. Clark, M. A.; Duffy, K.; Tibrewala, J.; Lippard, S. J. Synthesis and Metal-Binding Properties of Chelating Fluorescein Derivatives. *Org. Lett*. **2003**, *5*, 2051-2054.
87. Woodroofe, C. C.; Lim, M. H.; Bu, W.; Lippard, S. J. Synthesis of isomerically pure carboxylate- and sulfonate-substituted xanthene fluorophores. *Tetrahedron* **2005**, *61*, 3097-3105.

88. Hilderbrand, S. A.; Weissleder, R. One-pot synthesis of new symmetric and asymmetric xanthene dyes. *Tettrahedron Lett*. **2007**, *48*, 4383-4385.
89. Wu, L.; Burgess, K. Fluorescent Amino- and Thiopyronin Dyes. *Org. Lett*. **2008**, *10*, 1779-1782.
90. Li, J.; Yao, S. Q. "Singapore Green": A New Fluorescent Dye for Microarray and Bioimaging Applications. *Org. Lett*. **2008**, *11*, 405-408.
91. Li, J.; Hu, M.; Yao, S. Q. Rapid Synthesis, Screening, and Identification of Xanthone- and Xanthene-Based Fluorophores Using Click Chemistry. *Org. Lett*. **2009**, *11*, 3008-3011.
92. Peng, T.; Yang, D. Construction of a Library of Rhodol Fluorophores for Developing New Fluorescent Probes. *Org. Lett*. **2010**, *12*, 496-499.
93. Wrona, M.; Patel, K.; Wardman, P. Reactivity of 2',7'-dichlorodihydrofluorescein and dihydrorhodamine 123 and their oxidized forms toward carbonate, nitrogen dioxide, and hydroxyl radicals. *Free Radical Biol. Med*. **2005**, *38*, 262-270.
94. Li, H.; Li, Q.; Wang, X.; Xu, K.; Chen, Z.; Gong, X.; Liu, X.; Tong, L.; Tang, B. Simultaneous Determination of Superoxide and Hydrogen Peroxide in Macrophage RAW 264.7 Cell Extracts by Microchip Electrophoresis with Laser-Induced Fluorescence Detection. *Anal. Chem*. **2009**, *81*, 2193-2198.
95. Gong, X.; Li, Q.; Xu, K.; Liu, X.; Li, H.; Chen, Z.; Tong, L.; Tang, B.; Zhong, H. A new route for simple and rapid determination of hydrogen peroxide in RAW264. 7 macrophages by microchip electrophoresis. *Electrophoresis* **2009**, *30*, 1983-1990.
96. Hampton, M. B.; Kettle, A. J.; Winterbourn, C. C. Inside the neutrophil phagosome: oxidants, myeloperoxidase, and bacterial killing. *Blood* **1998**, *92*, 3007-3017.
97. Winterbourn, C. C.; Vissers, M.; Kettle, A. J. Myeloperoxidase. *Curr. Opin. Hematol*. **2000**, *7*, 53-58.
98. Karlsson, A.; Dahlgren, C. Assembly and activation of the neutrophil NADPH oxidase in granule membranes. *Antioxid. Redox Signal*. **2002**, *4*, 49-60.
99. van der Veen, B. S.; de Winther, M. P. J.; Heeringa, P.; Augusto, O.; Chen, J. W.; Davies, M.; Ma, X. L.; Malle, E.; Pignatelli, P.; Rudolph, T. Myeloperoxidase: Molecular Mechanisms of Action and Their Relevance to Human Health and Disease. *Antioxid. Redox Signal*. **2009**, *11*, 2899-2937.
100. Patel, S. V.; Patel, M. P.; Patel, R. G. Synthesis and characterization of novel substituted spiro [isobenzofuran-1 (3H), 9'-xanthene]-3-ones. *J. Serb. Chem. Soc*. **2005**, *70*, 931-936.
101. Sauers, R. R.; Husain, S. N.; Piechowski, A. P.; Bird, G. R. Shaping the absorption and fluorescence bands of a class of efficient, photoactive chromophores: synthesis and properties of some new 3H-xanthen-3. *Dyes Pigm*. **1987**, *8*, 35-53.
102. Whitaker, J. E.; Haugland, R. P.; Ryan, D.; Hewitt, P. C.; Haugland, R. P.; Prendergast, F. G. Fluorescent rhodol derivatives: Versatile, photostable labels and tracers. *Anal. Biochem*. **1992**, *207*, 267-279.
103. Mugherli, L.; Burchak, O. N.; Chatelain, F.; Balakirev, M. Y. Fluorogenic ester substrates to assess proteolytic activity. *Bioorg. Med. Chem. Lett*. **2006**, *16*, 4488-4491.
104. Heller, C. A.; Henry, R. A.; McLaughlin, B. A.; Bliss, D. E. Fluorescence spectra and quantum yields. Quinine, uranine, 9,10-diphenylanthracene, and 9,10-bis(phenylethynyl)anthracenes. *J. Chem. Eng. Data* **1974**, *19*, 214-219.

Chapter 2:

A Targetable Fluorescent Probe for Imaging Hydrogen Peroxide in the Mitochondria of Living Cells

Portions of this work were published in the following scientific journal:

Dickinson, B. C.; Chang, C. J. "A Targetable fluorescent probe for imaging hydrogen peroxide in the mitochondria of living cells." *Journal of the American Chemical Society* **2008**, 130, 9638–9639.

Introduction

Hydrogen peroxide (H_2O_2) is an increasingly recognized small-molecule mediator of physiology, aging, and disease in living organisms.[1-6] In this regard, aberrant production or accumulation of H_2O_2 within cellular mitochondria over time due to environmental stress(es) and/or genetic mutation(s) is connected to serious diseases where age is a risk factor, including cancer[7] and neurodegenerative Alzheimer's, Parkinson's, and Huntington's diseases.[8,9] Indeed, overexpression and mitochondrial targeting of catalase, a peroxide-detoxifying enzyme, can increase life span in mouse models.[10] On the other hand, newer data suggest that controlled bursts of mitochondrial H_2O_2 can also serve beneficial roles for cell survival, growth, differentiation, and maintenance.[2]

New imaging methods that allow visualization of localized production and accumulation of mitochondrial H_2O_2 in living samples are potentially useful for disentangling the complex contributions of this reactive oxygen species (ROS) to both healthy and diseased states. Synthetic fluorescent H_2O_2 indicators that can be targeted to precise subcellular locations offer one approach to this goal and do not require transfection like their protein counterparts,[11,12] but traditional ROS indicators such as dihydrorhodamine (DHR) are uncharged and hence not preferentially localized in cells before oxidation.[13] In addition, DHR and related dyes are not specific for H_2O_2 over other ROS. Accordingly, mitochondrial-targeted small molecules for detection of specific ROS remain rare[13,14] and none of the probes reported to date are selective for H_2O_2. We now report the synthesis and applications of Mitochondria Peroxy Yellow 1 (MitoPY1), a new type of fluorophore for imaging mitochondrial H_2O_2 in living cells with ROS and spatial specificity.

Results and Discussion

Our overall strategy for fluorescence imaging of mitochondrial H_2O_2 in living systems is to create bifunctional dyes that contain both a peroxide-responsive element and a mitochondrial-targeting moiety. For the latter purpose, we were inspired by the use of phosphonium head groups by Murphy and others to deliver antioxidants, electrophiles, and EPR and optical probes to mitochondria, as these and related lipophilic cations selectively accumulate in this organelle due to proton gradient considerations.[14-16] In addition, we sought a modular synthetic route that would allow facile introduction of a phosphonium or any other desired targeting group after installation of the boronate switch, which circumvents potential complications arising from sensitive functionalities that are incompatible with palladium-catalyzed Miyaura-Suzuki reactions typically used to introduce the H_2O_2-cleavable boronate cage. Both of these design criteria can be met by the approach outlined in Scheme 2-1 for the synthesis of MitoPY1. The ability to append additional groups post-boronation offers a host of opportunities for generating new multifunctional H_2O_2 imaging probes.

MitoPY1 features two major visible region absorptions (λ_{abs} = 489 nm, ε = 14,300 $M^{-1}cm^{-1}$; 510 nm, ε = 14,200 M-1cm-1) and a weak emission (λ_{em} = 540 nm, ϕ = 0.019, Figure 2-3) in 20 mM HEPES, pH 7. Reaction of MitoPY1 with H_2O_2 triggers a fluorescence increase by its conversion to MitoPY1ox (Figure 2-3), which possesses one major absorption band at 510 nm (ε = 22,300 $M^{-1}cm^{-1}$) and enhanced emission (λ_{em} = 528 nm, ϕ = 0.405). Kinetics measurements of the H_2O_2-mediated boronate deprotection were performed under pseudo-first-order conditions (5 μM dye, 10 mM H_2O_2), giving an observed rate constant of k = 2.0(1) x 10-3 s-1. Figure 2-1 shows the relative turn-on fluorescence responses of MitoPY1 to a panel of biologically relevant

ROS. Owing to its chemospecific boronate switch,[17,18] the probe is selective for H_2O_2 over ROS like superoxide, nitric oxide, and hydroxyl radical.

MitoPY1 was then tested for its ability to both target the mitochondria and respond to H_2O_2 in living biological systems. Cervical cancer HeLa cells loaded with 5 μM MitoPY1 for 1 h at 37 °C show faint but measurable levels of fluorescence in discrete subcellular locations as determined by confocal microscopy (Figure 2-2a). Co-staining experiments with 50 nM MitoTracker Deep Red, a commercially available mitochondrial indicator (Figure 2-2, b and c), or 500 nM LysoTracker Red, a lysosomal indicator (Figures 2-6), establish that the observed fluorescence from MitoPY1 is localized to the mitochondria of these live cells. Addition of 100 μM H_2O_2 to HeLa cells loaded with MitoPY1 display a marked localized increase in fluorescence compared to control cells (Figure 2-2, d-f). Again, co-staining with MitoTracker confirms that the dye is retained in the mitochondria and detects localized rises in H_2O_2 concentrations. Brightfield measurements and nuclear staining with Hoechst 33342 indicate that the cells are viable throughout the imaging experiments (Figure 2-2, b, e, and g). In addition, control experiments using a probe lacking the phosphonium targeting moiety (ContPY1, Figures 2-4 through 2-5 and Figures 2-11 through 2-14) or the oxidized probe (MitoPY1ox, Figure 2-15 through 2-19) confirm that only MitoPY1 targets the mitochondria, and complementary flow cytometry experiments (Figure 2-10) provide supporting data over a larger population of cells. Finally, analogous experiments in Cos-7, HEK293, and CHO.K1 cell lines give similar results and expand the scope of the probe (Figure 2-7 through 2-10). Taken together, these data establish that MitoPY1 is targeted to cellular mitochondria, where it can respond to localized changes in H_2O_2 levels in living samples.

Finally, we sought to utilize MitoPY1 to visualize endogenous production of H_2O_2 in the mitochondria of living cells. To this end, we treated HeLa cells with paraquat, a small-molecule inducer of oxidative stress that produces Parkinson's-like phenotypes.[19] The images in Figures 2-2, h-n show clear increases in mitochondrial-localized H_2O_2 levels detected with MitoPY1 within cells that had been exposed to 1 mM paraquat compared to control cells (IC_{50} of paraquat in HeLa cells is 1.02 mM).[20] These data indicate that MitoPY1 is sensitive enough to detect local mitochondrial H_2O_2 elevations associated with oxidative stress in this Parkinson's model.

Concluding Remarks

To close, we have presented the synthesis, properties, and biological applications of MitoPY1, a new targeted fluorescent probe that can selectively detect H_2O_2 in the mitochondria of living cells. Our data show that MitoPY1 is capable of imaging changes in the levels of H_2O_2 within the mitochondria of a variety of mammalian cell lines, as well as H_2O_2 elevations caused by an oxidative stress model of Parkinson's disease. In addition to applying MitoPY1 and related chemical tools for studies of mitochondrial redox biology, we anticipate that this modular probe scaffold should prove useful for creating new multifunctional probes for targeting, activation, and detection in living systems and are actively pursuing these possibilities.

Experimental Section

Synthetic Materials and Methods. All reactions were carried out under a dry nitrogen atmosphere. (4-Iodobutyl)triphenylphosphonium (IBTP)[21] and 2-(2,4-dihydroxybenzoyl)benzoic acid[22] were synthesized according to literature methods. Silica gel P60 (SiliCycle) was used for column chromatography. Analytical thin layer chromatography was performed using SiliCycle

60 F254 silica gel (precoated sheets, 0.25 mm thick). All chemicals were purchased from Sigma-Aldrich (St. Louis, MO) and used as received. MitoTracker Deep Red and LysoTracker Red were purchased from Invitrogen (Carlsbad, CA). ^{1}H NMR, ^{13}C NMR, and ^{31}P NMR spectra were collected in $CDCl_3$ or 9:1 $CDCl_3/CD_3OD$ (Cambridge Isotope Laboratories, Cambridge, MA) at 25 ºC on a Bruker AV-300, AVQ-400, or DRX-500 spectrometer at the College of Chemistry NMR Facility at the University of California, Berkeley. All chemical shifts are reported in the standard d notation of parts per million using the peak of residual proton signals of $CDCl_3$ as an internal reference. Mass spectral analyses were carried out at the College of Chemistry Mass Spectrometry Facility at the University of California, Berkeley. Microwave reactions were performed using a CEM Intelligent Explorer/Discover (Matthews, NC).

Fmoc-piperazine rhodol (3). (adopted from literature)[23] 2-(2,4-Dihydroxybenzoyl)benzoic acid (**1**, 1.24 g, 4.8 mmol) and 1-(3-hydroxyphenyl)-piperazine (**2**, 853 mg, 4.8 mmol) were added to a pressure flask and dissolved in 20 mL of TFA. The reaction was stirred for 3 hours at 95 °C. After cooling, the reaction mixture was poured into 300 mL of ether. The resulting precipitate was collected, immediately redissolved in methanol, and then evaporated to dryness under reduced pressure to yield a red solid. The crude product was carried on without further purification. The crude fluorophore (1.09 g), Fmoc-Cl (845 mg, 3.27 mmol), and $NaHCO_3$ (686 mg, 8.16 mmol) were added to a dry Schlenk tube. Then, 20 mL of dry acetonitrile was added and the reaction stirred under a nitrogen atmosphere at room temperature for 3 hours. The product was then extracted into ethyl acetate, washed with water, and dried under reduced pressure. Purification by flash chromatography (1:1 hexanes/ethyl acetate) provided **3** as a red solid (654 mg, 39% overall yield). ^{1}H NMR ($CDCl_3$, 400 MHz): d 7.99 (1H, d, *J* = 7.6 Hz), 7.74 (2H, d, *J* = 7.6 Hz), 7.57-7.66 (2H, m), 7.55 (2 H, d, *J* = 7.6 Hz), 7.37 (2H, t, *J* = 7.2 Hz), 7.29 (2H, t, *J* = 7.2 Hz), 7.14 (1H, d, *J* = 7.6 Hz), 6.71 (1H, d, *J* = 2.0 Hz), 6.65 (1H, d *J* = 2.0 Hz), 6.49-6.63 (4H, m), 4.47 (2H, d, *J* = 6.4 Hz), 4.22 (1H, t, *J* = 6.4 Hz), 3.55 (4H, bs), 3.14 (4H, bs). ^{13}C NMR ($CDCl_3$, 100 MHz): d 170.03, 159.59, 155.23, 152.82, 152.65, 152.58, 152.41, 143.76, 141.29, 134.92, 129.63, 129.15, 128.81, 127.73, 127.07, 127.00, 125.06, 124.82, 124.18, 129.97, 112.59, 112.18, 110.35, 109.87, 102.82, 102.33, 67.37, 47.99, 47.25, 43.20 (broad multiplet). HR-FABMS: calculated for [M^+] 623.2171, found 623.2182.

Fmoc-piperazine rhodol triflate (4). Rhodol **3** (400 mg, 0.64 mmol), *N*-phenyl bis(trifluoromethanesulfonamide) (458 mg, 1.28 mmol), and sodium carbonate (340 mg, 3.21 mmol) were added to a dry Schlenk tube. Then, 8 mL of dry DMF was added via syringe and the reaction stirred under a nitrogen atmosphere at room temperature for 12 hours. The reaction mixture was then extracted into ethyl acetate, washed with water, and dried under reduced pressure. Column chromatography (1:1 hexanes/ethyl acetate) afforded **4** as a white solid (222 mg, 46% yield). ^{1}H NMR ($CDCl_3$, 400 MHz): d 8.04 (1H, d, *J* = 7.2 Hz), 7.76 (2H, d, *J* = 7.6 Hz), 7.69 (1H, dt, *J* = 1.2, 7.6 Hz), 7.64 (1H, dt, *J* = 7.6, 1.2 Hz), 7.57 (2H, d, *J* = 7.2 Hz), 7.38 (2H, t, *J* = 7.2 Hz), 7.30 (2H, dt, *J* = 1.2, 7.2 Hz), 7.23 (1H, d, *J* = 2.4 Hz), 7.16 (1H, d, *J* = 7.2 Hz), 6.94 (1H, dd, *J* = 2.4, 8.8 Hz), 6.88 (1H, d, *J* = 8.8 Hz), 6.70 (1H, d, *J* = 2.0 Hz), 6.66 (1H, d, *J* = 8.8 Hz), 6.61 (1H, dd, *J* = 2.0, 8.8 Hz), 4.48 (2H, d, *J* = 2.4 Hz), 4.23 (1H, t, *J* = 2.4 Hz), 3.56 (4H, bs), 3.16 (4H, bs). ^{13}C NMR ($CDCl_3$, 100 MHz): d 169.18, 155.09, 152.77, 152.49, 152.18, 151.85, 149.93, 143.83, 141.31, 135.37, 130.14, 130.06, 128.73, 127.73, 127.07, 126.36, 125.23, 124.86, 123.87, 119.98, 119.86, 116.52, 112.78, 110.42, 108.77, 102.23, 81.96, 67.29, 47.87, 47.30, 43.33 (broad multiplet). HR-FABMS: calculated for [MNa^+] 777.1494, found 777.1501.

Fmoc-piperazine rhodol boronate (5). Triflate **4** (71 mg, 0.28 mmol), Pd (dppf) Cl_2•CH_2Cl_2 (68 mg, 0.08 mmol), potassium acetate (82 mg, 0.8 mmol), and 10 mL of toluene were added to a dry pressure tube in an inert atmosphere glove box. The pressure tube was then brought out of the box and microwave-heated for 4 hours at 110 °C. After cooling the reaction to room temperature, the contents of the pressure flask were washed into a round bottom flask with dichloromethane and evaporated to dryness. Purification by column chromatography (1:1 hexanes/ethyl acetate) delivered **5** as a white solid (151 mg, 74% yield). ^{1}H NMR ($CDCl_3$, 400 MHz): d 8.02 (1H, d, *J* = 6.4 Hz), 7.77 (3H, t, *J* = 7.6 Hz), 7.56-7.68 (4H, m), 7.37-7.45 (3H, m), 7.33 (2H, t, *J* = 8.0 Hz), 7.22 (1H, d, *J* = 6.8 Hz), 6.81 (1H, d, *J* = 8.0 Hz), 6.69 (2H, d, *J* = 7.6 Hz), 6.59 (1H, dd, *J* = 2.4, 8.8 Hz), 4.50 (2H, d, *J* = 6.8 Hz), 4.26 (1H, t, *J* = 6.4 Hz), 3.60 (4H, bs), 3.16 (4H, bs), 1.35 (12H, s). ^{13}C NMR ($CDCl_3$, 100 MHz): d 169.65, 155.09, 153.44, 152.69, 152.31, 150.84, 143.88, 141.34, 153.09, 129.70, 129.27, 128.73, 128.04, 127.75, 127.25, 127.09, 126.37, 125.07, 124.90, 123.82, 123.44, 121.60, 120.01, 112.27, 109.47, 102.60, 84.20, 82.85, 67.29, 48.13, 47.34, 24.86. (no signal for carbon attached to boronate observed). HR-FABMS: calculated for [MNa^+] 733.3082, found 733.3085.

MitoPY1 (6). Boronate **5** (35 mg, 48 µmol) was dissolved in 15% piperidine in acetonitrile and stirred at room temperature for 30 minutes. The reaction was then dried under reduced pressure and brought into an inert atmosphere glovebox, where IBTP (55 mg, 96 µmol), sodium bicarbonate (30 mg, 240 µmol), and 5 mL of acetonitrile were added. The contents were then stirred at room temperature for 24 hours inside the glove box. The reaction was then removed from the glove box, filtered, and dried under reduced pressure. Purification by column chromatography (4.5:4.5:0.5 dichloromethane/ethyl acetate/methanol) furnished MitoPY1 as a light pink solid (35 mg, 76% yield). ^{1}H NMR ($CDCl_3$/10% CD_3OD, 300 MHz): d 7.96 (1H, d, *J* = 7.2 Hz), 7.76-7.83 (3H, m), 7.55-7.75 (15H, m), 7.35 (1H, dd, *J* = 8.0, 1.2 Hz), 7.09 (1H, d, *J* = 7.2 Hz), 7.71 (1H, d, *J* = 7.6 Hz), 6.67 (1H, d, *J* = 3.2 Hz), 6.60 (1H, d, *J* = 8.8 Hz), 6.56 (1H, dd, *J* = 2.0, 8.8 Hz), 3.36-3.47 (2H, m), 3.23-3.29 (4H, m), 2.74-2.81 (4H, m), 2.62-2.70 (2H, m), 1.88-1.94 (2H, m), 1.65-1.76 (2H, m), 1.29 (12H, s). ^{13}C NMR ($CDCl_3$/10% CD_3OD, 125 MHz): d 170.08, 153.13, 152.27, 150.08, 135.30, 135.28, 133.55, 133.47, 130.64, 130.54, 129.81, 129.17, 128.64, 127.09, 126.16, 124.97, 123.85, 123.36, 121.31, 118.00, 117.32, 84.23, 83.36, 74.96, 56.25, 52.33, 49.95, 24.61, 20.07. (no signal for carbon attached to boronate observed). ^{31}P NMR ($CDCl_3$/10% CD_3OD, 162 MHz): d 23.80. HR-FABMS: calculated for [M^+] 827.3781, found 827.3780.

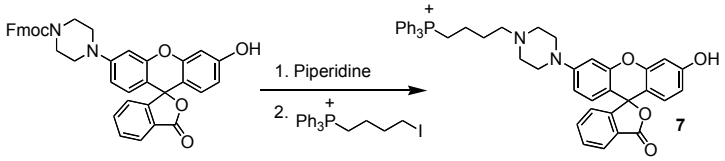

MitoPY1ox (7). Rhodol **3** (124 mg, 0.20 mmol) was dissolved in 15% piperidine in acetonitrile and stirred at room temperature for 30 minutes. The solvent was removed and the contents were brought into an inert atmosphere glovebox, where IBTP (226 mg, 0.39 mmol), sodium bicarbonate (167 mg, 1.99 mmol), and 6 mL of DMF were added. The reaction was then stirred at room temperature for 96 hours inside the glove box, removed from the glove box and dried under reduced pressure. Purification by column chromatography (gradient from 8.5:1.5:0.01 dichloromethane/methanol/water to 8.5:1.5:0.01:0.005 dichloromethane/methanol/water/HCl, then a second column gradient from 9:1 to 8.5:1.5 dichloromethane/methanol) furnished

MitoPY1ox as a red solid (30 mg, 22% yield). ^{1}H NMR (CD_3OD, 500 MHz): d 8.03 (1H, d, *J* = 7.0 Hz), 7.89 (4H, dt, *J* = 2.0, 6.5 Hz), 7.73-7.83 (12H, m), 7.66-7.73 (2H, m), 7.18 (1H, d, *J* = 6.5 Hz), 6.88 (2H, d, *J* = 5 Hz), 6.84 (1H, d, *J* = 9.5 Hz), 6.63 (1H, d, *J* = 2.5 Hz), 6.56 (1H, dd, *J* = 2.0, 9.0 Hz), 3.42-3.54 (6H, m), 2.89 (4H, bs), 2.71-2.78 (2H, m), 1.90 (2H, quintet, *J* = 7.5 Hz), 1.74 (2H, quintet, *J* = 7.5 Hz). ^{13}C NMR (10% CD_3OD/D_2O, 125 MHz): d 171.71, 156.18, 154.19, 153.59, 135.06, 135.03, 133.38, 133.30, 130.30, 130.20, 129.68, 129.44, 127.01, 126.53, 118.51, 117.83, 112.45, 111.34, 102.87, 100.17, 56.02, 51.71, 48.51, 29.19, 19.76. ^{31}P NMR (CD_3OD, 162 MHz) d 23.80. HR-FABMS: calculated for [M^+] 717.2877, found 717.2875.

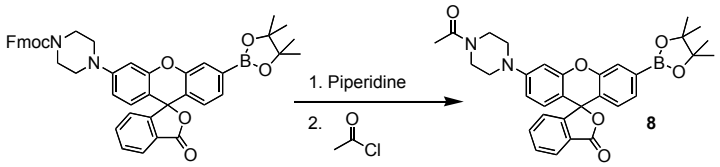

ContPY1 (8). Boronate **5** (10 mg, 13 μmol) was dissolved in 15% piperidine in acetonitrile and stirred at room temperature for 30 minutes. The reaction was then dried under reduced pressure. Acetyl chloride (2 μL, 27 μmol), cesium carbonate (9 mg, 27 μmol), and 3 mL of acetonitrile were added and the contents were then stirred at room temperature for 30 minutes at room temperature. The reaction was then filtered and dried under reduced pressure. Purification by column chromatography (20:1 dichloromethane/ methanol) furnished ContPY1 as a light pink solid (1.8 mg, 25% yield). ^{1}H NMR ($CDCl_3$/10% CD_3OD, 400 MHz): d 8.00 (1H, d, *J* = 6.4 Hz), 7.69 (1H, s), 7.63 (1H, dt, *J* = 1.6, 7.2 Hz), 7.59 (1H, dt, *J* = 1.6, 7.6 Hz), 7.39 (1H, d, *J* = 8.0 Hz), 7.10 (1H, d, *J* = 6.8 Hz), 6.76 (1H, d, *J* = 7.6 Hz), 6.66 (1H, d, *J* = 8.8 Hz), 6.60 (1H, dd, *J* = 2.0, 9.2 Hz), 3.71-3.78 (2H, m), 3.61 (2H, t, *J* = 4.8 Hz), 3.25 (2H, t, *J* = 4.8 Hz), 3.22 (2H, t, *J* = 4.8 Hz), 2.12 (3H, s), 1.32 (12H, s) ^{13}C NMR ($CDCl_3$/10% CD_3OD, 100 MHz): d 169.78, 169.45, 153.25, 152.31, 150.78, 133.07, 129.74, 129.25, 128.76, 127.96, 127.18, 126.28, 125.06, 123.80, 123.38, 121.47, 112.24, 102.63, 84.22, 74.88, 48.45, 48.17, 45.81, 41.01, 24.57, 21.16. (no signal for carbon attached to boronate observed). HR-FABMS: calculated for [M^+] 553.2523, found 553.2521.

Spectroscopic Materials and Methods. Millipore water was used to prepare all aqueous solutions. All spectroscopic measurements were performed in 20 mM HEPES buffer, pH 7. Absorption spectra were recorded on a Varian Cary 50 spectrophotometer (Walnut Creek, CA) and fluorescence spectra were recorded on a Photon Technology International Quanta Master 4 L-format scanning spectrofluorometer (Lawrenceville, NJ) equipped with an LPS-220B 75-W xenon lamp and power supply, A-1010B lamp housing with integrated igniter, switchable 814 photon-counting/analog photomultiplier detection unit, and MD5020 motor driver. Samples for absorption and emission measurements were contained in 1-cm × 1-cm quartz cuvettes (1.5-mL volume, Starna, Atascadero, CA). Fluorescence quantum yields were determined by reference to fluorescein in 0.1M NaOH (Φ = 0.95).

Preparation and Staining of Cell Cultures. HEK293 cells were cultured in DMEM (Invitrogen) supplemented with 10% fetal bovine serum (FBS, Hyclone) and glutamine (2 mM). CHO.K1 cells were cultured in DMEM with F-12 supplements, glutamax (Invitrogen), and 5% FBS. Cos-7 cells were cultured in DMEM with high glucose, glutamax, 10% FBS, and non-essential amino acids (Invitrogen). HeLa cells were cultured in DMEM with high glucose,

glutamax, and 10% FBS. Two days before imaging, cells were passaged and plated on 18-mm glass coverslips. For all experiments, solutions of dyes (from 5 mM stocks in DMSO) were made in DBPS with calcium chloride and magnesium chloride (Sigma). H_2O_2 was added by bath application to the medium from a 100 mM aqueous stock. For paraquat treatment, HeLa cells were cultured as described above. One day prior to imaging, 1 mM paraquat was added to cells from a 0.5 M stock solution in water. An equal amount of water was added to control cells at the same time. Cells were then incubated at 37 °C, 5% CO_2. After 24 hours, the media was exchanged for DPBS with 5 mM dye and incubated for 1 hour.

Fluorescence Imaging Experiments. Confocal fluorescence imaging studies were performed with a Zeiss LSM510 NLO Axiovert 200 laser scanning microscope and a 63x Achroplan IR water-immersion objective lens. Excitation of PY-loaded cells at 510 nm was carried out with an Ar laser and emission was collected using a META detector between 527-580 nm. MitoTracker Deep Red was excited with a 633-nm line and emission was collected between 666-698 nm. LysoTracker Red was excited with a 543-nm line and emission was collected between 580-644 nnm. Excitation of Hoechst 33342 was carried out using a MaiTai two-photon laser at 780-nm pulses (mode-locked Ti:sapphire laser, Tsunami Spectra Physics) and emission was collected between 452-537 nm. Image analysis was performed in Adobe Photoshop.

Flow Cytometry Experiments. Cells were treated as described in figure legends and analyzed on a Beckman-Coulter EPICS XV-MCL flow cytometer in the Flow Cytometry Facility at the University of California, Berkeley.

Figures and Schemes

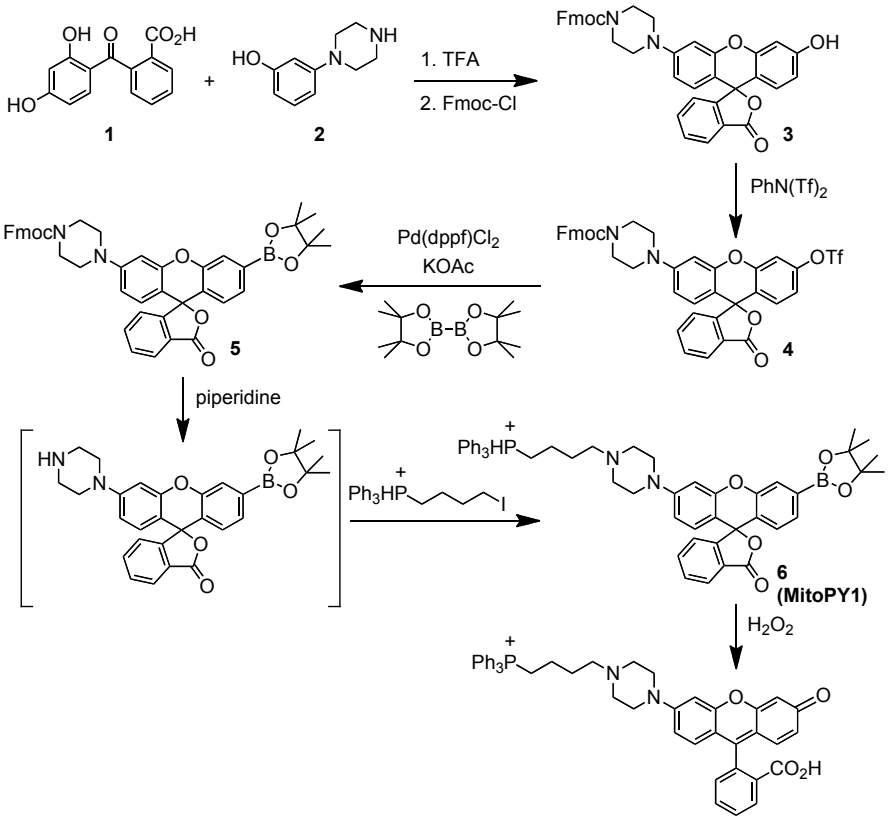

Scheme 2-1. Synthesis and activation of MitoPY1.

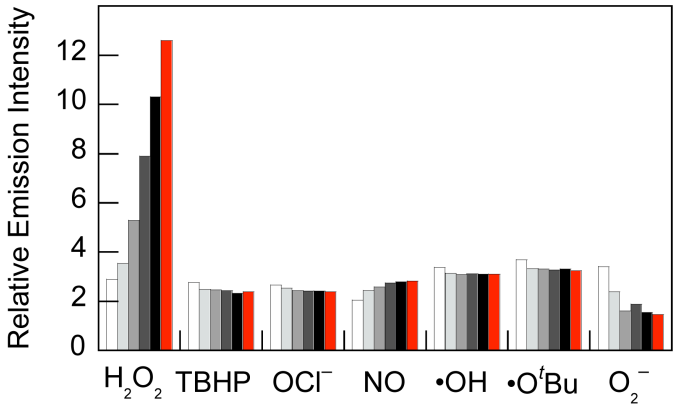

Figure 2-1. Fluorescence responses of 5 μM MitoPY1 to various reactive oxygen species (ROS). Bars represent relative responses at 0, 5, 15, 30, 45, and 60 min after addition of each ROS. Data shown are for 10 mM O_2^-, 200 μM NO, and 100 μM for all other ROS. Data were acquired at 25 ˚C in 20 mM HEPES, pH 7, with excitation λ = 503 nm and emission collected between 510 and 750 nm.

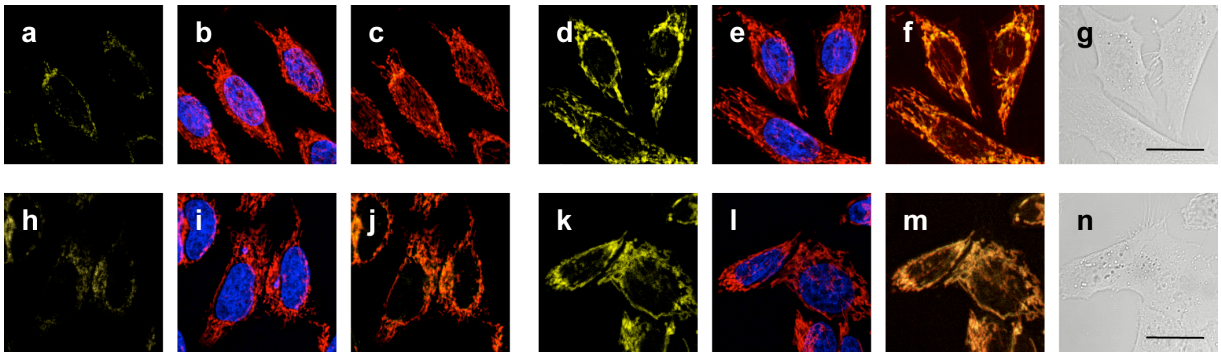

Figure 2-2. Confocal fluorescence images of live HeLa cells with increases in mitochondrial H_2O_2 levels visualized using MitoPY1. Images displayed represent emission intensities collected in optical windows between 527-601 nm upon excitation at 510 nm for MitoPY1. HeLa cells incubated with 5 μM MitoPY1 for 60 min at 37 °C and imaged with MitoPY1 (a), MitoTracker Red and Hoechst (overlay, b), and MitoPY1 with MitoTracker Red (overlay, c). HeLa cells incubated with 5 μM MitoPY1 for 60 min at 37 °C with 100 μM H_2O_2 added for the final 40 min and imaged with MitoPY1 (d), MitoTracker Red and Hoechst (overlay, e), MitoPY1 and MitoTracker Red (overlay, f), and brightfield (g) with 20 mm scale bar. HeLa cells incubated with 5 μM MitoPY1 for 60 min at 37 °C and imaged with MitoPY1 (h), MitoTracker Red and Hoechst (overlay, i), and MitoPY1 with MitoTracker Red (overlay, j). HeLa cells incubated for 24 h with 1 mM paraquat, then washed and incubated with 5 μM MitoPY1 for 60 min at 37 °C and imaged with MitoPY1 (k), MitoTracker Red and Hoechst (overlay, l), MitoPY1 and MitoTracker Red (overlay, m), and brightfield (n) with 20 mm scale bar.

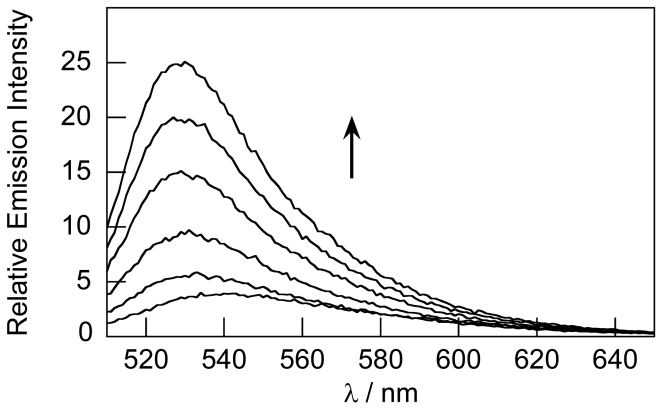

Figure 2-3. Fluorescence turn-on response of 5 μM MitoPY1 to H_2O_2. Data were acquired at 25 ºC in 20 mM HEPES, pH 7, with excitation at λ = 503 nm. Emission was collected between 510 and 750 nm. Time points represent 0, 5, 15, 30, 45, and 60 minutes after the addition of 100 μM H_2O_2. Reactions are not complete at these time points.

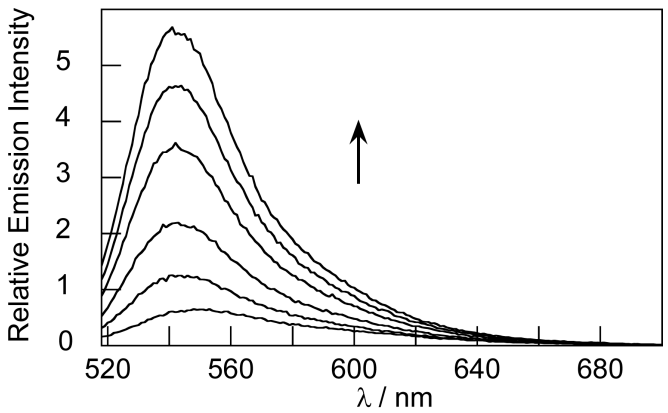

Figure 2-4. Fluorescence turn-on response of 5 μM ContPY1 to H_2O_2. Data were acquired at 25 ºC in 20 mM HEPES, pH 7, with excitation at λ = 510 nm. Emission was collected between 518 and 750 nm. Time points represent 0, 5, 15, 30, 45, and 60 minutes after the addition of 100 μM H_2O_2. The boronate dye features three major visible region absorption bands (λ_{abs} = 404 nm, e = 4,100 $M^{-1}cm^{-1}$; 490 nm, ε = 15,600 $M^{-1}cm^{-1}$; 510 nm, ε = 16,130 $M^{-1}cm^{-1}$) and a weak emission centered at λ_{em} = 549 nm (ϕ = 0.018). Reaction of ContPY1 with H_2O_2 triggers conversion to the corresponding rhodol, which possesses one major absorption band at 515 nm (e = 38,200 $M^{-1}cm^{-1}$) and enhanced emission (λ_{em} = 543 nm, ϕ =0.388). Reactions are not complete at these time points.

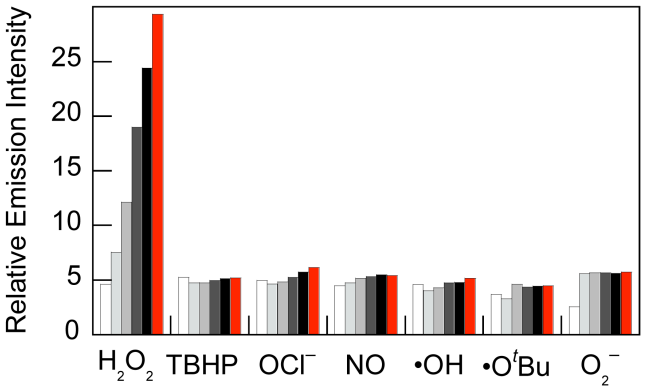

Figure 2-5. Fluorescence responses of 5 μM ContPY1 to various reactive oxygen species (ROS). Bars represent relative responses at 0, 5, 15, 30, 45, and 60 min after addition of each ROS. Data shown are for 10 mM O_2^- (with 10 μM catalase), 200 μM NO, and 100 μM for all other ROS. Data were acquired at 25 ºC in 20 mM HEPES, pH 7, with excitation at λ = 510 nm and emission collected between 518 and 750 nm.

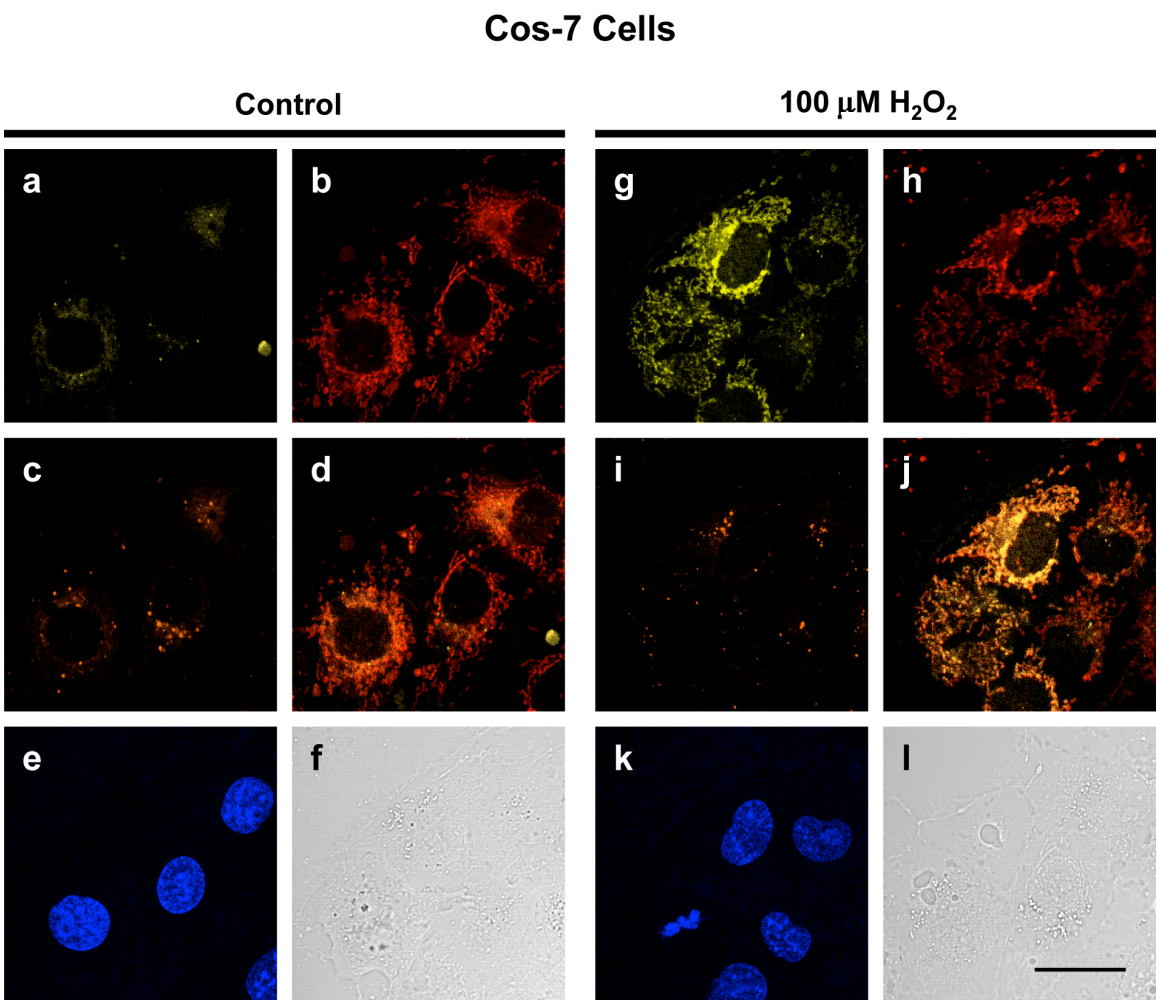

Figure 2-6. Confocal fluorescence images of H_2O_2 in live HeLa cells under oxidative stress with MitoPY1 with a nuclear stain and brightfields. HeLa cells (on two coverslips each in separate petri dishes) were incubated with 5 μM MitoPY1 in DPBS for 20 minutes. 100 μM H_2O_2 was then added to one of the petri dishes. At 20 minutes, 50 nM MitoTracker Deep Red, 500 nM Lysotracker Red, and 1 μM Hoechst 33342 were added to both dishes. After an additional 20 minutes (40 minute stimulation total), the two coverslips were put in a single, new petri dish filled with fresh DPBS and confocal images were taken (3.2 μsec pixel time, 100% laser power for 514 line, 4.1% laser power for the 633 line, 26% laser power for the 543 line, scanned using 12-bit multi-track scan mode using a constant receiver gain). Shown above are signals from MitoPY1 (a), MitoTracker Deep Red (b), LysoTracker Red (c), an overlay of MitoTracker Deep Red and MitoPY1 (d), Hoechst (e), and a brightfield image (f) of cells not treated with H_2O_2, as well as signals from MitoPY1 (g), MitoTracker Deep Red (h), LysoTracker Red (i), an overlay of MitoTracker Deep Red and MitoPY1 (j), Hoechst (k), and a brightfield image (l) of cells treated with H_2O_2. 20 μm scale bar shown for all images.

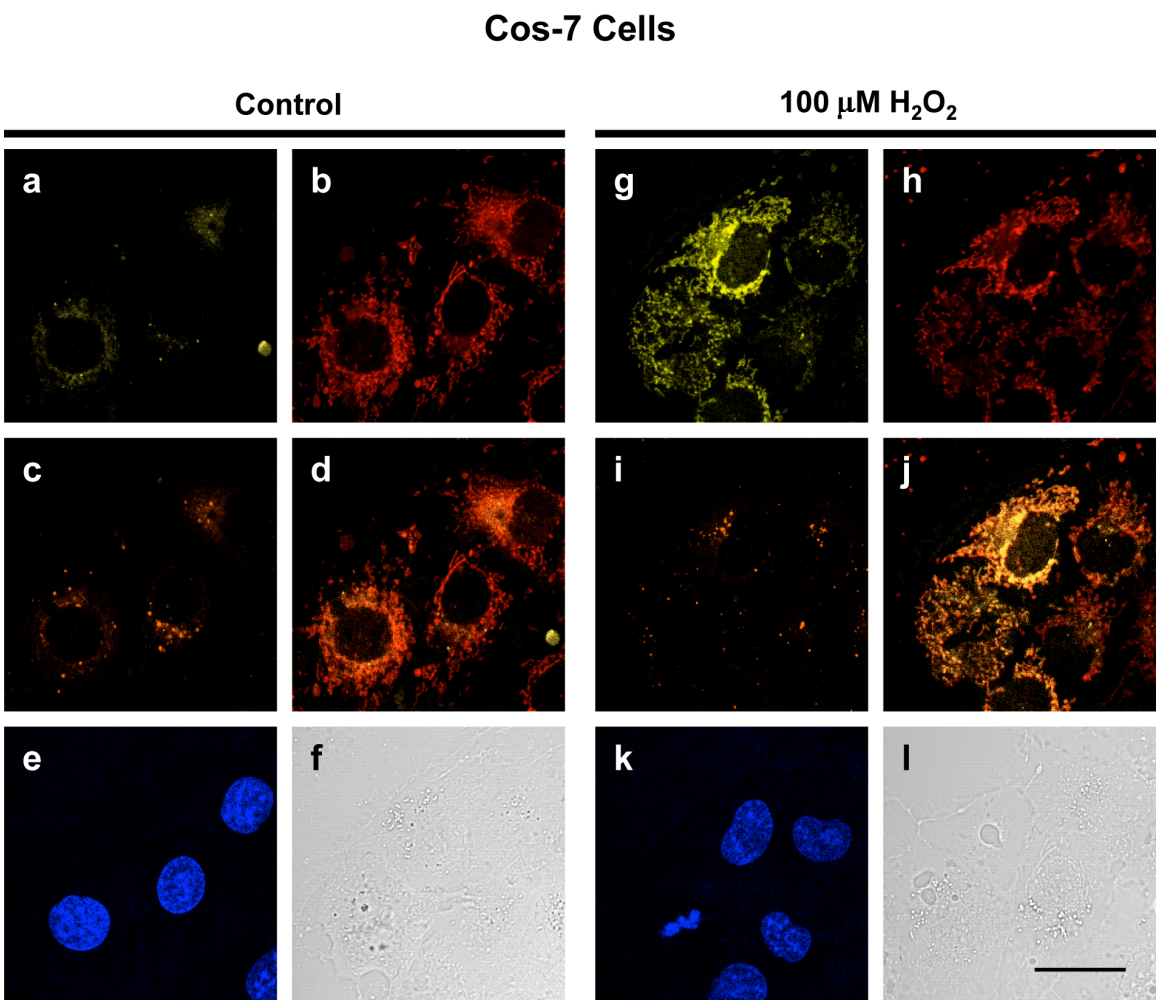

Figure 2-7. Confocal fluorescence images of H_2O_2 in live Cos-7 cells under oxidative stress with MitoPY1 with a nuclear stain and brightfields. Cos-7 cells (on two coverslips each in separate petri dishes) were incubated with 5 μM MitoPY1 in DPBS for 20 minutes. 100 μM H_2O_2 was then added to one of the petri dishes. At 20 minutes, 50 nM MitoTracker Deep Red, 500 nM Lysotracker Red, and 1 μM Hoechst 33342 were added to both dishes. After an additional 20 minutes (40 minute stimulation total), the two coverslips were put in a single, new petri dish filled with fresh DPBS and confocal images were taken (3.2 μsec pixel time, 100% laser power for 514 line, 4.1% laser power for the 633 line, 26% laser power for the 543 line, scanned using 12-bit multi-track scan mode using a constant receiver gain). Shown above are signals from MitoPY1 (a), MitoTracker Deep Red (b), LysoTracker Red (c), an overlay of MitoTracker Deep Red and MitoPY1 (d), Hoechst (e), and a brightfield image (f) of cells not treated with H_2O_2, as well as signals from MitoPY1 (g), MitoTracker Deep Red (h), LysoTracker Red (i), an overlay of MitoTracker Deep Red and MitoPY1 (j), Hoechst (k), and a brightfield image (l) of cells treated with H_2O_2. A 20 μm scale bar is shown for all images.

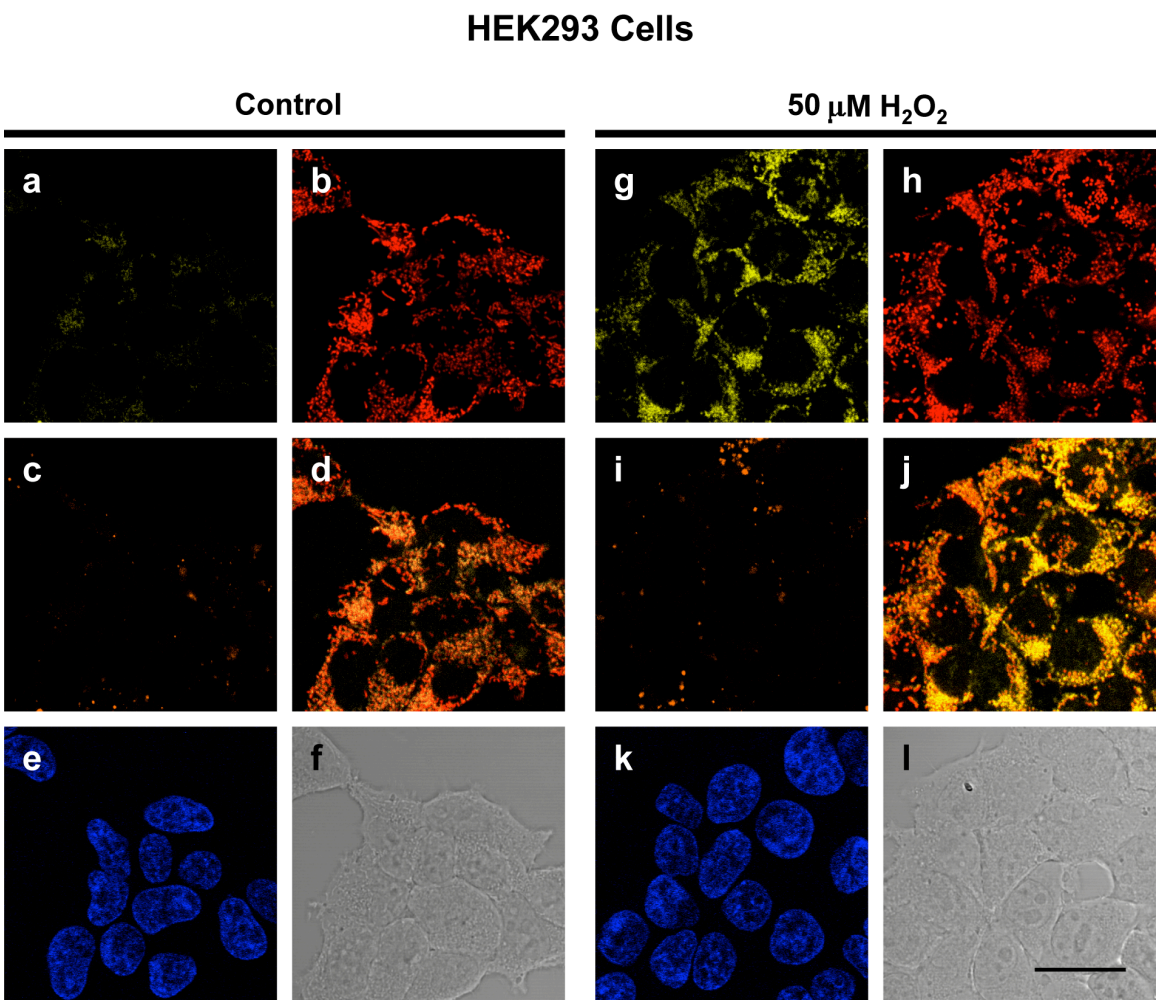

***Figure 2-8**:* Confocal fluorescence images of H_2O_2 in live HEK293 cells under oxidative stress with MitoPY1 with a nuclear stain and brightfields. HEK293 cells (on two coverslips each in separate petri dishes) were incubated with 5 μM MitoPY1 in DPBS for 20 minutes. 50 μM H_2O_2 was then added to one of the petri dishes. At 20 minutes, 50 nM MitoTracker Deep Red, 500 nM Lysotracker Red, and 1 μM Hoechst 33342 were added to both dishes. After an additional 20 minutes (40 minute stimulation total), the two coverslips were put in a single, new petri dish filled with fresh DPBS and confocal images were taken (3.2 μsec pixel time, 100% laser power for 514 line, 4.1% laser power for the 633 line, 26% laser power for the 543 line, scanned using 12-bit multi-track scan mode using a constant receiver gain). Shown above are signals from MitoPY1 (a), MitoTracker Deep Red (b), LysoTracker Red (c), an overlay of MitoTracker Deep Red and MitoPY1 (d), Hoechst (e), and a brightfield image (f) of cells not treated with H_2O_2, as well as signals from MitoPY1 (g), MitoTracker Deep Red (h), LysoTracker Red (i), an overlay of MitoTracker Deep Red and MitoPY1 (j), Hoechst (k), and a brightfield image (l) of cells treated with H_2O_2. A 20 μm scale bar is shown for all images.

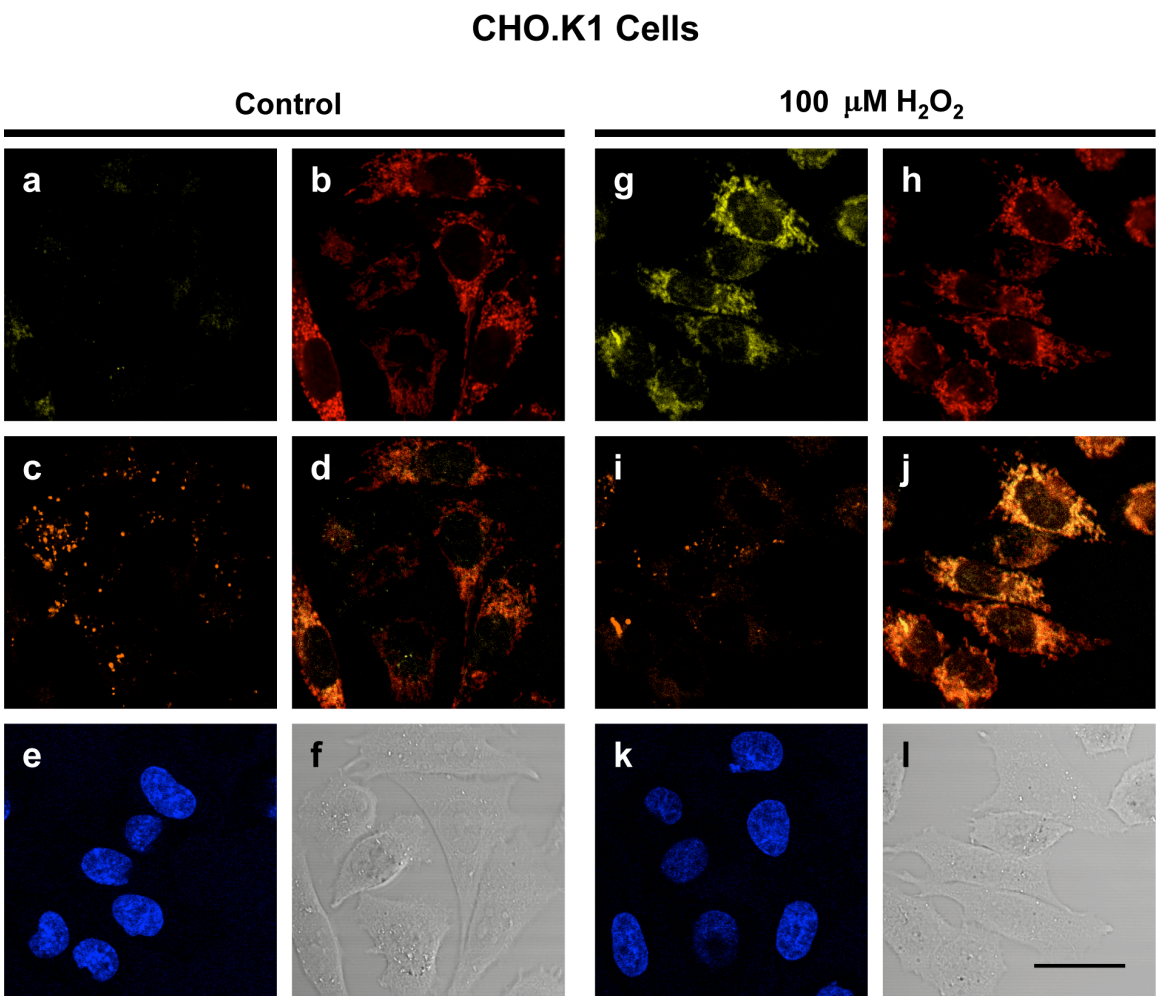

Figure 2-9*:* Confocal fluorescence images of H_2O_2 in live CHO.K1 cells under oxidative stress with MitoPY1 with a nuclear stain and brightfields. CHO.K1 cells (on two coverslips each in separate petri dishes) were incubated with 5 μM MitoPY1 in DPBS for 20 minutes. 100 μM H_2O_2 was then added to one of the petri dishes. At 20 minutes, 50 nM MitoTracker Deep Red, 500 nM Lysotracker Red, and 1 μM Hoechst 33342 were added to both dishes. After an additional 20 minutes (40 minute stimulation total), the two coverslips were put in a single, new petri dish filled with fresh DPBS and confocal images were taken (3.2 μsec pixel time, 100% laser power for 514 line, 4.1% laser power for the 633 line, 26% laser power for the 543 line, scanned using 12-bit multi-track scan mode using a constant receiver gain). Shown above are signals from MitoPY1 (a), MitoTracker Deep Red (b), LysoTracker Red (c), an overlay of MitoTracker Deep Red and MitoPY1 (d), Hoechst (e), and a brightfield image (f) of cells not treated with H_2O_2, as well as signals from MitoPY1 (g), MitoTracker Deep Red (h), LysoTracker Red (i), an overlay of MitoTracker Deep Red and MitoPY1 (j), Hoechst (k), and a brightfield image (l) of cells treated with H_2O_2. A 20 μm scale bar is shown for all images.

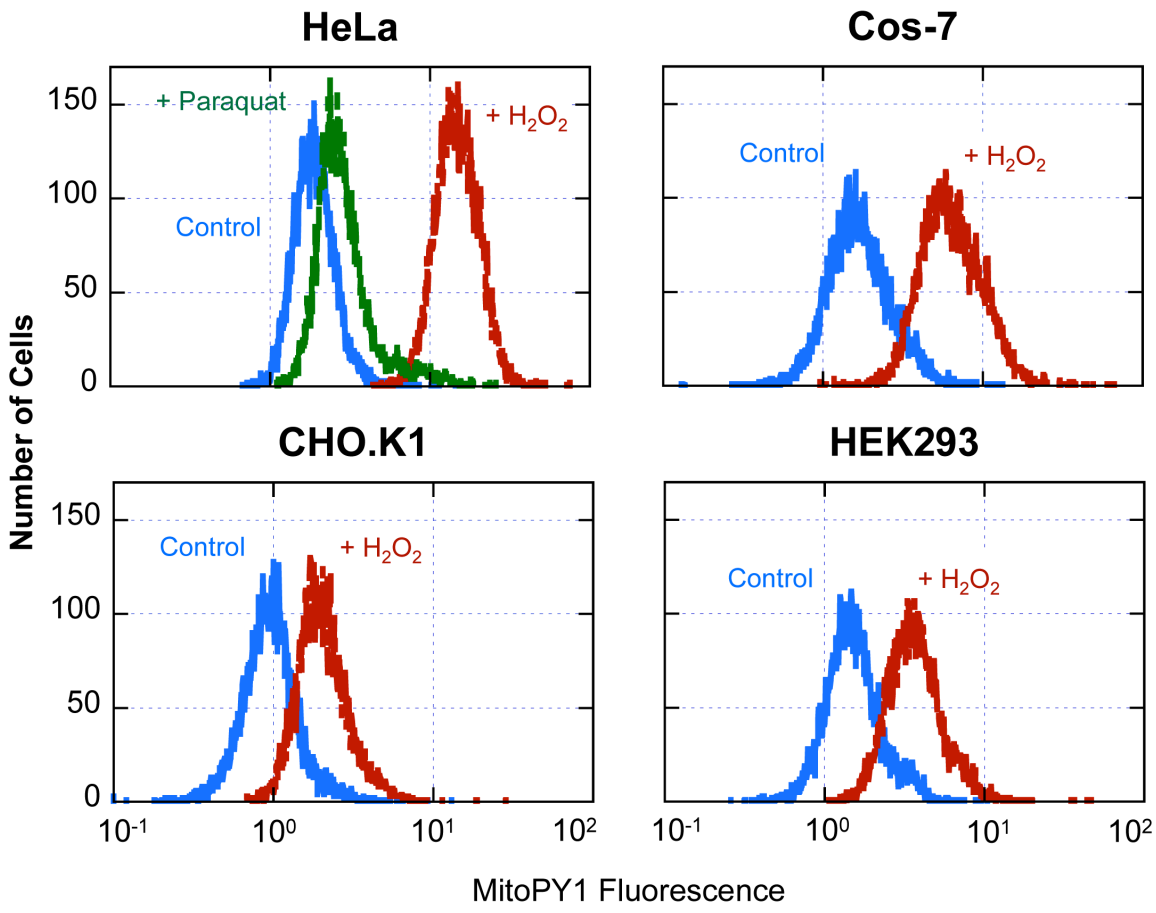

Figure 2-10. Quantification of fluorescence from MitoPY1 using flow cytometry. HeLa, Cos-7, CHO.K1, and HEK293 cells were grown in 35 mm tissue culture plates. Cells were washed with DBPS, detached with trypsin, and pelleted by centrifugation. The supernatant was removed and the pellets were each redissolved in 1 mL of 5 μM MitoPY1 in DPBS. The cell suspensions were then each split in half and incubated at 37 ºC for 20 minutes. H_2O_2 (50 μM for the HEK293, 100 μM for all other cells) was then added to one of the aliquots of each cell type and the cells incubated for a subsequent 40 minutes at 37 ºC. The cells were then subjected to analysis by flow cytometry using excitation by a 488 nm laser and collection by a 525 mm band pass filter (687 volts, 1.0 receiver gain). The paraquat-treated HeLa cells were analyzed identically as control cells except they were pretreated with 1 mM Paraquat the previous day. The data represents at least 10,000 cells for each analysis.

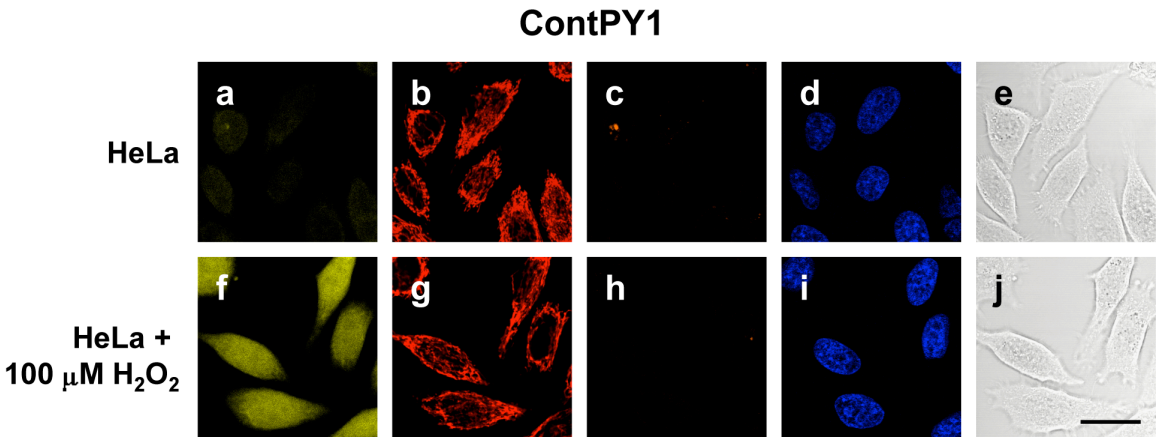

Figure 2-11. Confocal fluorescence images of H_2O_2 in live HeLa cells under oxidative stress with ContPY1 with a nuclear stain and brightfields. HeLa cells (on two coverslips each in separate petri dishes) were incubated with 5 μM ContPY1 in DPBS for 20 minutes. 100 μM H_2O_2 was then added to one of the petri dishes. At 20 minutes, 50 nM MitoTracker Deep Red, 500 nM Lysotracker Red, and 1 μM Hoechst 33342 were added to both dishes. After an additional 20 minutes (40 minute stimulation total), the two coverslips were put in a single, new petri dish filled with fresh DPBS and confocal images were taken (3.2 μsec pixel time, 100% laser power for 514 line, 4.1% laser power for the 633 line, 26% laser power for the 543 line, scanned using 12-bit multi-track scan mode using a constant receiver gain). Shown above are signals from ContPY1 (a), MitoTracker Deep Red (b), LysoTracker Red (c), Hoechst (d), and a brightfield image (e) of cells not treated with H_2O_2, as well as signals from ContPY1 (f), MitoTracker Deep Red (g), LysoTracker Red (h), Hoechst (i), and a brightfield image (j) of cells treated with H_2O_2. A 20 μm scale bar is shown for all images.

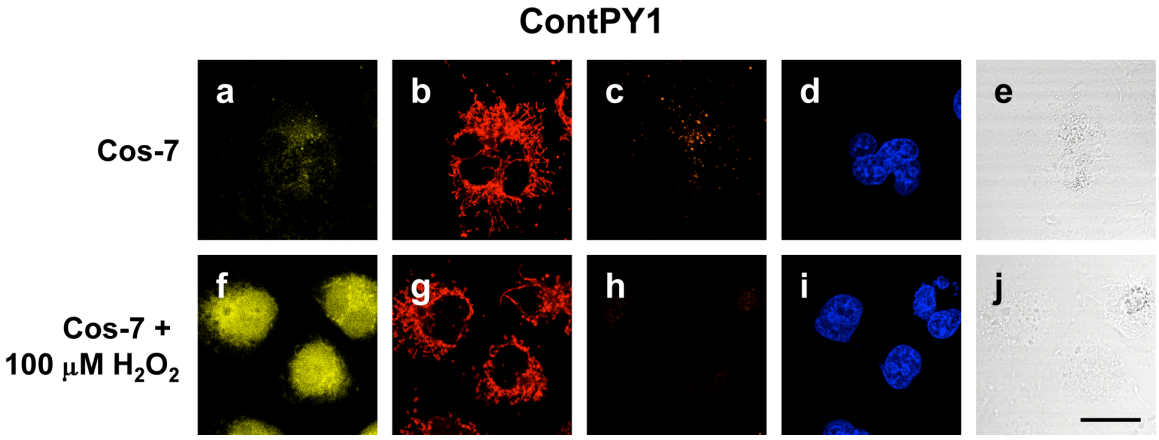

Figure 2-12. Confocal fluorescence images of H_2O_2 in live Cos-7 cells under oxidative stress with ContPY1 with a nuclear stain and brightfields. Cos-7 cells (on two coverslips each in separate petri dishes) were incubated with 5 μM ContPY1 in DPBS for 20 minutes. 100 μM H_2O_2 was then added to one of the petri dishes. At 20 minutes, 50 nM MitoTracker Deep Red, 500 nM Lysotracker Red, and 1 μM Hoechst 33342 were added to both dishes. After an additional 20 minutes (40 minute stimulation total), the two coverslips were put in a single, new petri dish filled with fresh DPBS and confocal images were taken (3.2 μsec pixel time, 100% laser power for 514 line, 4.1% laser power for the 633 line, 26% laser power for the 543 line, scanned using 12-bit multi-track scan mode using a constant receiver gain). Shown above are signals from ContPY1 (a), MitoTracker Deep Red (b), LysoTracker Red (c), Hoechst (d), and a brightfield image (e) of cells not treated with H_2O_2, as well as signals from ContPY1 (f), MitoTracker Deep Red (g), LysoTracker Red (h), Hoechst (i), and a brightfield image (j) of cells treated with H_2O_2. A 20 μm scale bar is shown for all images.

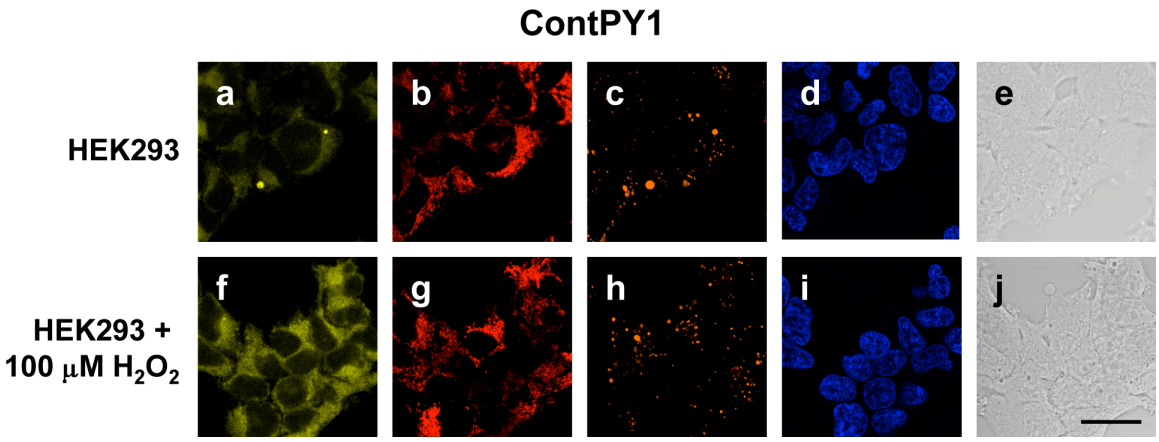

Figure 2-13. Confocal fluorescence images of H_2O_2 in live HEK293 cells under oxidative stress with ContPY1 with a nuclear stain and brightfields. HEK293 (on two coverslips each in separate petri dishes) were incubated with 5 μM ContPY1 in DPBS for 20 minutes. 100 μM H_2O_2 was then added to one of the petri dishes. At 20 minutes, 50 nM MitoTracker Deep Red, 500 nM Lysotracker Red, and 1 μM Hoechst 33342 were added to both dishes. After an additional 20 minutes (40 minute stimulation total), the two coverslips were put in a single, new petri dish filled with fresh DPBS and confocal images were taken (3.2 μsec pixel time, 100% laser power for 514 line, 4.1% laser power for the 633 line, 26% laser power for the 543 line, scanned using 12-bit multi-track scan mode using a constant receiver gain). Shown above are signals from ContPY1 (a), MitoTracker Deep Red (b), LysoTracker Red (c), Hoechst (d), and a brightfield image (e) of cells not treated with H_2O_2, as well as signals from ContPY1 (f), MitoTracker Deep Red (g), LysoTracker Red (h), Hoechst (i), and a brightfield image (j) of cells treated with H_2O_2. A 20 μm scale bar is shown for all images.

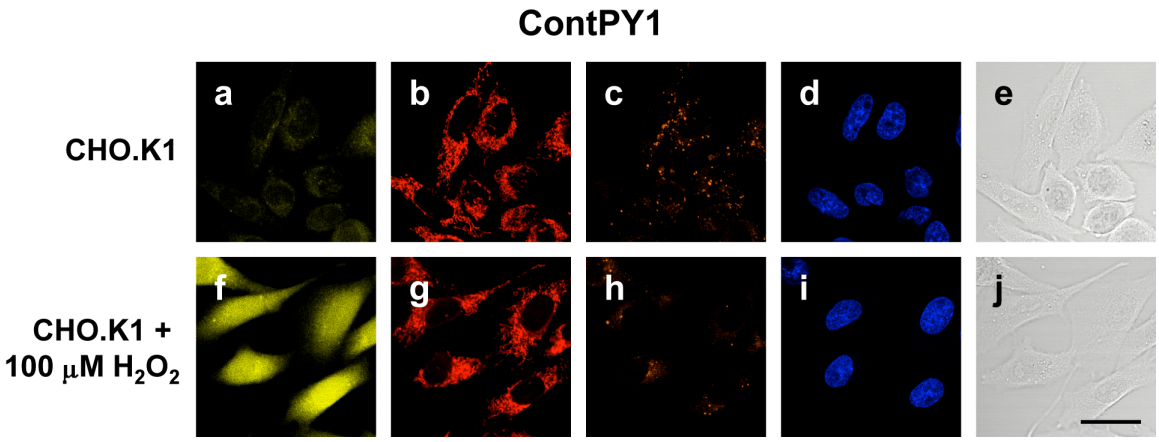

Figure 2-14. Confocal fluorescence images of H_2O_2 in live CHO.K1 cells under oxidative stress with ContPY1 with a nuclear stain and brightfields. CHO.K1 cells (on two coverslips each in separate petri dishes) were incubated with 5 μM ContPY1 in DPBS for 20 minutes. 100 μM H_2O_2 was then added to one of the petri dishes. At 20 minutes, 50 nM MitoTracker Deep Red, 500 nM Lysotracker Red, and 1 μM Hoechst 33342 were added to both dishes. After an additional 20 minutes (40 minute stimulation total), the two coverslips were put in a single, new petri dish filled with fresh DPBS and confocal images were taken (3.2 μsec pixel time, 100% laser power for 514 line, 4.1% laser power for the 633 line, 26% laser power for the 543 line, scanned using 12-bit multi-track scan mode using a constant receiver gain). Shown above are signals from ContPY1 (a), MitoTracker Deep Red (b), LysoTracker Red (c), Hoechst (d), and a brightfield image (e) of cells not treated with H_2O_2, as well as signals from ContPY1 (f), MitoTracker Deep Red (g), LysoTracker Red (h), Hoechst (i), and a brightfield image (j) of cells treated with H_2O_2. A 20 μm scale bar is shown for all images.

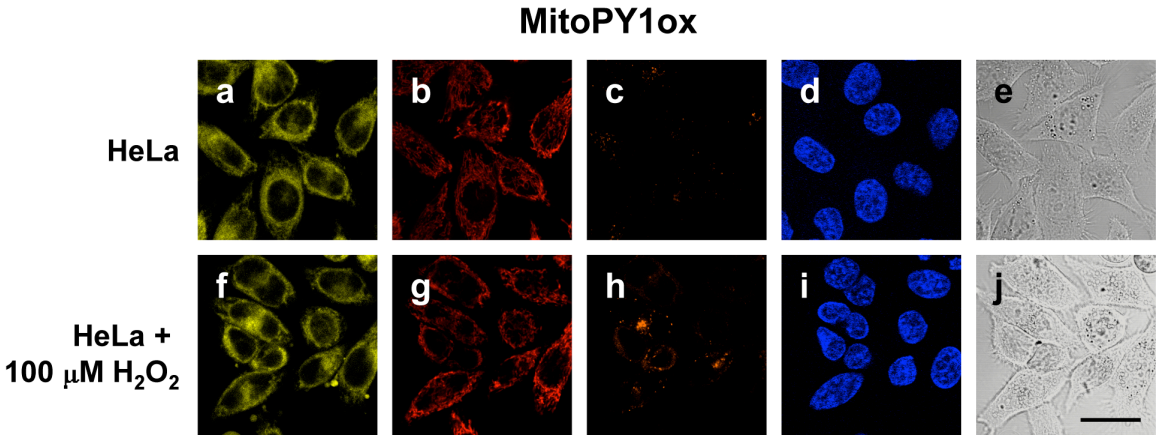

Figure 2-15. Confocal fluorescence images of H_2O_2 in live HeLa cells under oxidative stress with MitoPY1ox with a nuclear stain and brightfields. HeLa cells (on two coverslips each in separate petri dishes) were incubated with 5 μM MitoPY1ox in DPBS for 20 minutes. 100 μM H_2O_2 was then added to one of the petri dishes. At 20 minutes, 50 nM MitoTracker Deep Red, 500 nM Lysotracker Red, and 1 μM Hoechst 33342 were added to both dishes. After an additional 20 minutes (40 minute stimulation total), the two coverslips were put in a single, new petri dish filled with fresh DPBS and confocal images were taken (3.2 μsec pixel time, 100% laser power for 514 line, 4.1% laser power for the 633 line, 26% laser power for the 543 line, scanned using 12-bit multi-track scan mode using a constant receiver gain). Shown above are signals from MitoPY1ox (a), MitoTracker Deep Red (b), LysoTracker Red (c), Hoechst (d), and a brightfield image (e) of cells not treated with H_2O_2, as well as signals from MitoPY1ox (f), MitoTracker Deep Red (g), LysoTracker Red (h), Hoechst (i), and a brightfield image (j) of cells treated with H_2O_2. A 20 μm scale bar is shown for all images.

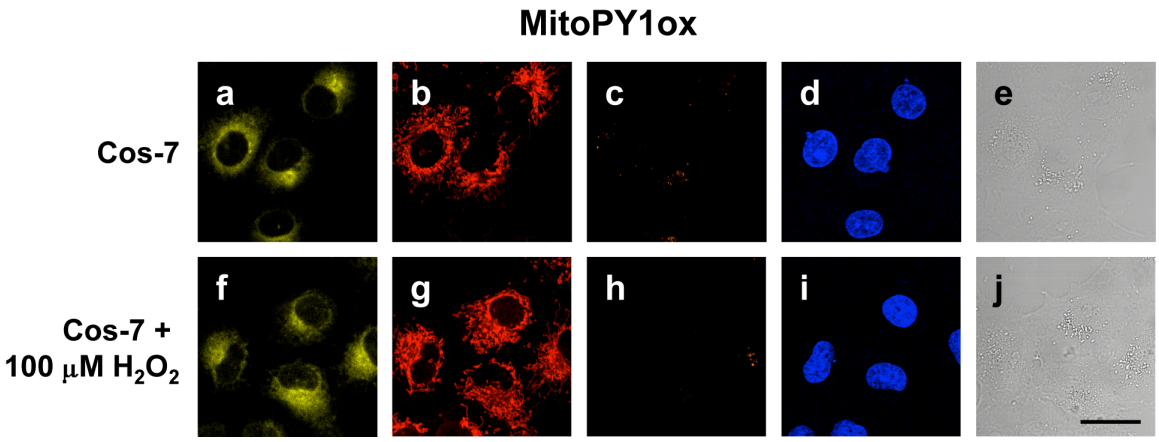

Figure 2-16. Confocal fluorescence images of H_2O_2 in live Cos-7 cells under oxidative stress with MitoPY1ox with a nuclear stain and brightfields. Cos-7 cells (on two coverslips each in separate petri dishes) were incubated with 5 μM MitoPY1ox in DPBS for 20 minutes. 100 μM H_2O_2 was then added to one of the petri dishes. At 20 minutes, 50 nM MitoTracker Deep Red, 500 nM Lysotracker Red, and 1 μM Hoechst 33342 were added to both dishes. After an additional 20 minutes (40 minute stimulation total), the two coverslips were put in a single, new petri dish filled with fresh DPBS and confocal images were taken (3.2 μsec pixel time, 100% laser power for 514 line, 4.1% laser power for the 633 line, 26% laser power for the 543 line, scanned using 12-bit multi-track scan mode using a constant receiver gain). Shown above are signals from MitoPY1ox (a), MitoTracker Deep Red (b), LysoTracker Red (c), Hoechst (d), and a brightfield image (e) of cells not treated with H_2O_2, as well as signals from MitoPY1ox (f), MitoTracker Deep Red (g), LysoTracker Red (h), Hoechst (i), and a brightfield image (j) of cells treated with H_2O_2. A 20 μm scale bar is shown for all images.

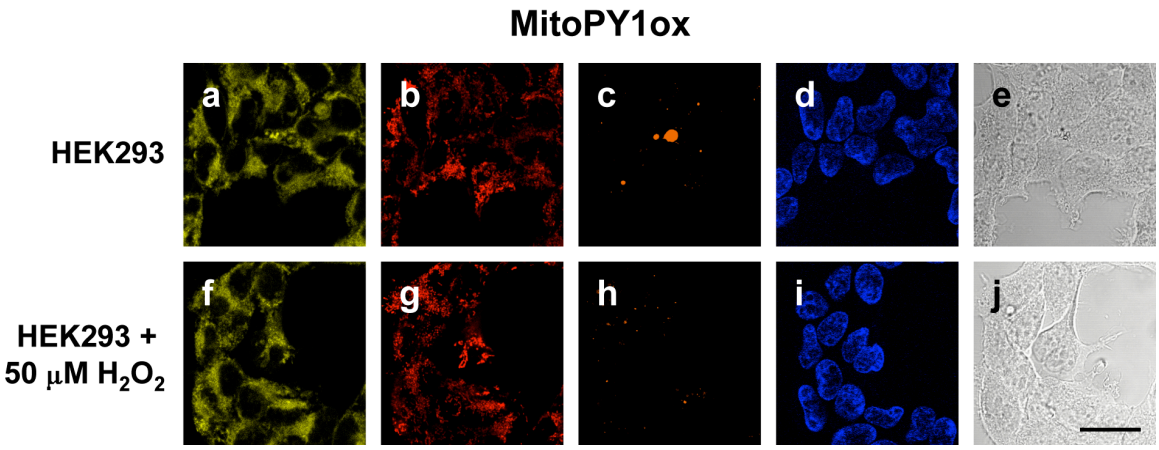

Figure 2-17. Confocal fluorescence images of H_2O_2 in live HEK293 cells under oxidative stress with MitoPY1ox with a nuclear stain and brightfields. HEK293 cells (on two coverslips each in separate petri dishes) were incubated with 5 μM MitoPY1ox in DPBS for 20 minutes. 50 μM H_2O_2 was then added to one of the petri dishes. At 20 minutes, 50 nM MitoTracker Deep Red, 500 nM Lysotracker Red, and 1 μM Hoechst 33342 were added to both dishes. After an additional 20 minutes (40 minute stimulation total), the two coverslips were put in a single, new petri dish filled with fresh DPBS and confocal images were taken (3.2 μsec pixel time, 100% laser power for 514 line, 4.1% laser power for the 633 line, 26% laser power for the 543 line, scanned using 12-bit multi-track scan mode using a constant receiver gain). Shown above are signals from MitoPY1ox (a), MitoTracker Deep Red (b), LysoTracker Red (c), Hoechst (d), and a brightfield image (e) of cells not treated with H_2O_2, as well as signals from MitoPY1ox (f), MitoTracker Deep Red (g), LysoTracker Red (h), Hoechst (i), and a brightfield image (j) of cells treated with H_2O_2. A 20 μm scale bar is shown for all images.

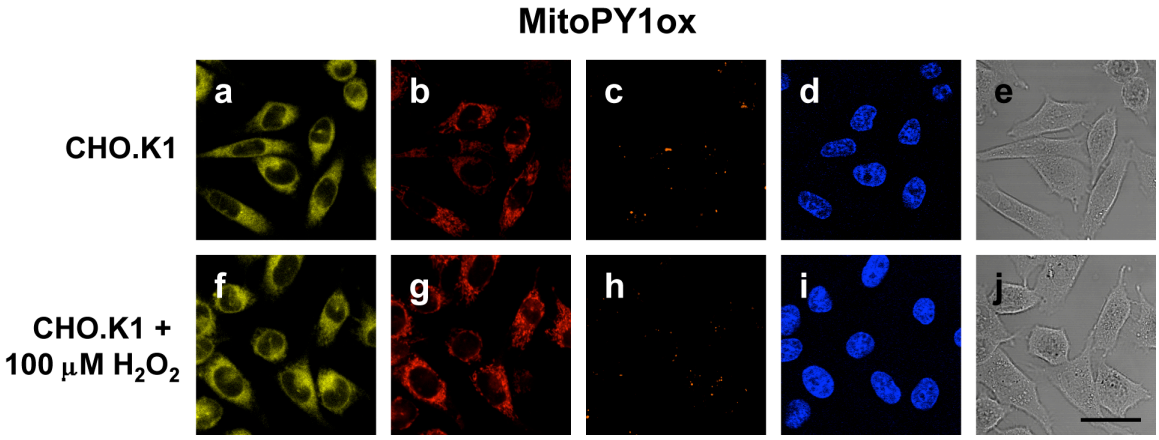

Figure 2-18. CHO.K1 cells (on two coverslips each in separate petri dishes) were incubated with 5 μM MitoPY1ox in DPBS for 20 minutes. 100 μM H_2O_2 was then added to one of the petri dishes. At 20 minutes, 50 nM MitoTracker Deep Red, 500 nM Lysotracker Red, and 1 μM Hoechst 33342 were added to both dishes. After an additional 20 minutes (40 minute stimulation total), the two coverslips were put in a single, new petri dish filled with fresh DPBS and confocal images were taken (3.2 μsec pixel time, 100% laser power for 514 line, 4.1% laser power for the 633 line, 26% laser power for the 543 line, scanned using 12-bit multi-track scan mode using a constant receiver gain). Shown above are signals from MitoPY1ox (a), MitoTracker Deep Red (b), LysoTracker Red (c), Hoechst (d), and a brightfield image (e) of cells not treated with H_2O_2, as well as signals from MitoPY1ox (f), MitoTracker Deep Red (g), LysoTracker Red (h), Hoechst (i), and a brightfield image (j) of cells treated with H_2O_2. A 20 μm scale bar is shown for all images.

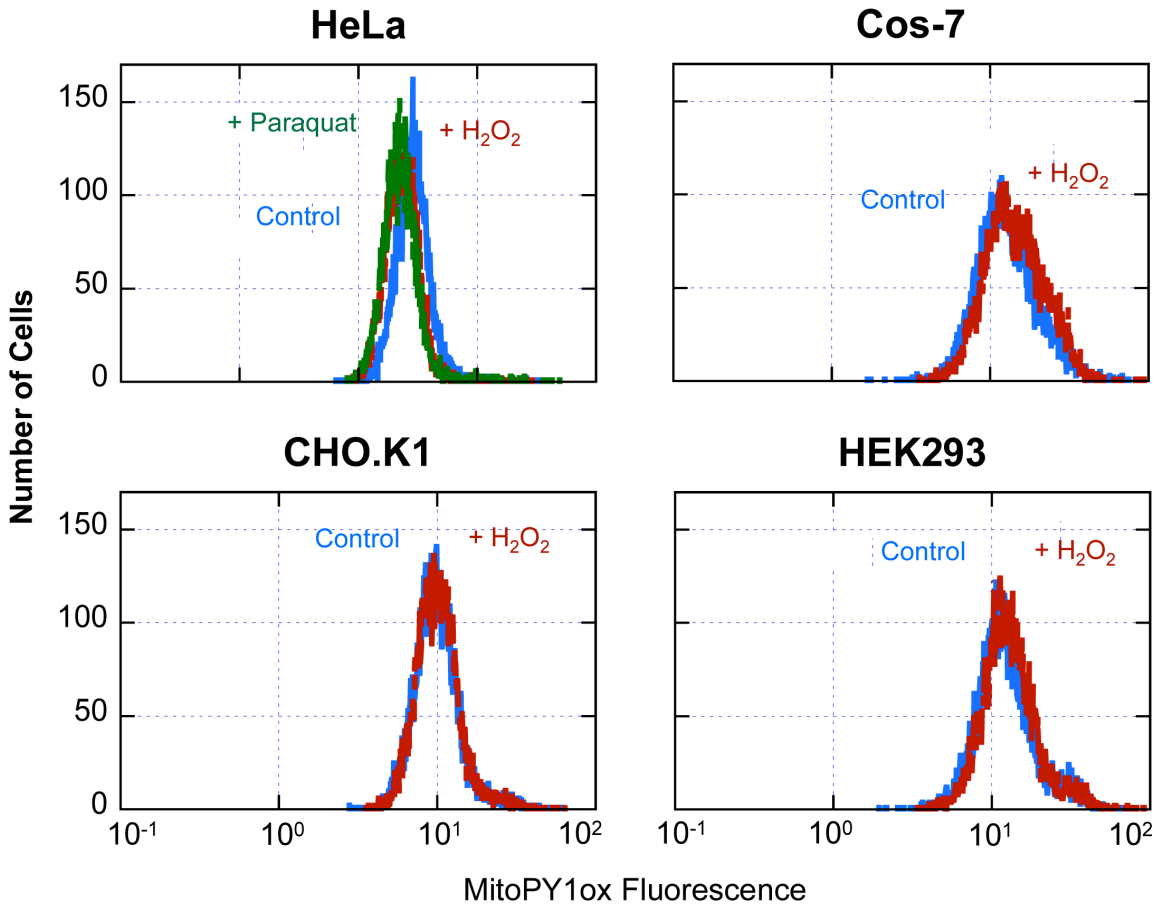

Figure 2-19. Quantification of fluorescence from MitoPY1ox using flow cytometry. HeLa, Cos-7, CHO.K1, and HEK293 cells were grown in 35 mm tissue culture plates. Cells were washed with DBPS, detached with trypsin, and pelleted by centrifugation. The supernatant was removed and the pellets were each redissolved in 1 mL of 5 µM MitoPY1ox in DPBS. The cell suspensions were then each split in half and incubated at 37 ºC for 20 minutes. H_2O_2 was then added to one of the aliquots (50 µM for the HEK293, 100 µM for all other cells) and the cells incubated for a subsequent 40 minutes at 37 ºC. The cells were then subjected to analysis by flow cytometry using excitation by a 488 nm laser and collection by a 525 mm band pass filter (687 volts, 1.0 receiver gain). The paraquat-treated HeLa cells were analyzed identically as control cells except they were treated with 1 mM paraquat the previous day. The data represents at least 10,000 cells for each analysis.

References

1. Rhee, S. G. H_2O_2, a necessary evil for cell signaling. *Science* **2006**, *312*, 1882-1883.
2. Poole, L. B.; Nelson, K. J. Discovering mechanisms of signaling-mediated cysteine oxidation. *Current Opinion in Chemical Biology* **2008**, *12*, 18-24.
3. Stone, J. R.; Yang, S. Hydrogen peroxide: a signaling messenger. *Antioxidants & Redox Signaling* **2006**, *8*, 243-270.
4. Veal, E. A.; Day, A. M.; Morgan, B. A. Hydrogen peroxide sensing and signaling. *Molecular Cell* **2007**, *26*, 1-14.
5. D'Autréaux, B.; Toledano, M. B. ROS as signalling molecules: mechanisms that generate specificity in ROS homeostasis. *Nature Reviews Molecular Cell Biology* **2007**, *8*, 813-824.
6. Giorgio, M.; Trinei, M.; Migliaccio, E.; Pelicci, P. G. Hydrogen peroxide: a metabolic by-product or a common mediator of ageing signals? *Nature Reviews Molecular Cell Biology* **2007**, *8*, 722-728.
7. Finkel, T.; Serrano, M.; Blasco, M. A. The common biology of cancer and ageing. *Nature* **2007**, *448*, 767-774.
8. Barnham, K. J.; Masters, C. L.; Bush, A. I. Neurodegenerative diseases and oxidative stress. *Nature Reviews Drug Discovery* **2004**, *3*, 205-214.
9. Lin, M. T.; Beal, M. F. Mitochondrial dysfunction and oxidative stress in neurodegenerative diseases. *Nature* **2006**, *443*, 787-795.
10. Schriner, S. E.; Linford, N. J.; Martin, G. M.; Treuting, P.; Ogburn, C. E.; Emond, M.; Coskun, P. E.; Ladiges, W.; Wolf, N.; Van Remmen, H. Extension of murine life span by overexpression of catalase targeted to mitochondria. *Science* **2005**, *308*, 1909-1911.
11. Hanson, G. T.; Aggeler, R.; Oglesbee, D.; Cannon, M.; Capaldi, R. A.; Tsien, R. Y.; Remington, S. J. Investigating mitochondrial redox potential with redox-sensitive green fluorescent protein indicators. *Journal of Biological Chemistry* **2004**, *279*, 13044-13053.
12. Belousov, V. V.; Fradkov, A. F.; Lukyanov, K. A.; Staroverov, D. B.; Shakhbazov, K. S.; Terskikh, A. V.; Lukyanov, S. Genetically encoded fluorescent indicator for intracellular hydrogen peroxide. *Nature Methods* **2006**, *3*, 281-286.
13. Koide, Y.; Urano, Y.; Kenmoku, S.; Kojima, H.; Nagano, T. Design and Synthesis of Fluorescent Probes for Selective Detection of Highly Reactive Oxygen Species in Mitochondria of Living Cells. *Journal of the American Chemical Society* **2007**, *129*, 10324-10325.
14. Robinson, K. M.; Janes, M. S.; Pehar, M.; Monette, J. S.; Ross, M. F.; Hagen, T. M.; Murphy, M. P.; Beckman, J. S. Selective fluorescent imaging of superoxide in vivo using ethidium-based probes. *Proceedings of the National Academy of Sciences* **2006**, *103*, 15038-15043.
15. Murphy, M. P.; Smith, R. A. J. Targeting antioxidants to mitochondria by conjugation to lipophilic cations. *Annual Reviews of Pharmacology Toxicology* **2007**, *47*, 629-565.
16. Hardy, M.; Chalier, F.; Ouari, O.; Finet, J. P.; Rockenbauer, A.; Kalyanaraman, B.; Tordo, P. Mito-DEPMPO synthesized from a novel NH 2-reactive DEPMPO spin trap: a new and improved trap for the detection of superoxide. *Chemical Communications* **2007**, *2007*, 1083-1085.
17. Chang, M. C. Y.; Pralle, A.; Isacoff, E. Y.; Chang, C. J. A selective, cell-permeable optical probe for hydrogen peroxide in living cells. *Journal of the American Chemical Society* **2004**, *126*, 15392-15393.

18. Miller, E. W.; Tulyathan, O.; Isacoff, E. Y.; Chang, C. J. Molecular imaging of hydrogen peroxide produced for cell signaling. *Nature Chemical Biology* **2007**, *3*, 263-267.
19. McCormack, A. L.; Thiruchelvam, M.; Manning-Bog, A. B.; Thiffault, C.; Langston, J. W.; Cory-Slechta, D. A.; Di Monte, D. A. Environmental risk factors and Parkinson's disease: selective degeneration of nigral dopaminergic neurons caused by the herbicide paraquat. *Neurobiology of disease* **2002**, *10*, 119-127.
20. Park, S. Y.; Choi, J. Cytotoxicity, genotoxicity and ecotoxicity assay using human cell and environmental species for the screening of the risk from pollutant exposure. *Environment international* **2007**, *33*, 817-822.
21. Lin, T. K.; Hughes, G.; Muratovska, A.; Blaikie, F. H.; Brookes, P. S.; Darley-Usmar, V.; Smith, R. A. J.; Murphy, M. P. Specific modification of mitochondrial protein thiols in response to oxidative stress. *Journal of Biological Chemistry* **2002**, *277*, 17048-17056.
22. Chang, C. J.; Nolan, E. M.; Jaworski, J.; Okamoto, K. I.; Hayashi, Y.; Sheng, M.; Lippard, S. J. ZP8, a neuronal zinc sensor with improved dynamic range; imaging zinc in hippocampal slices with two-photon microscopy. *Inorganic Chemistry* **2004**, *43*, 6774-6779.
23. Clark, M. A.; Hilderbrand, S. A.; Lippard, S. J. Synthesis of fluorescein derivatives containing metal-coordinating heterocycles. *Tetrahedron Letters* **2004**, *45*, 7129-7131.

Chapter 3:

A Nuclear-Localized Fluorescent Probe Reveals Sirtuin-Dependent Differences in Hydrogen Peroxide Levels and Responses in *C. Elegans*

Portions of this work were performed in collaboration with the following person:

The *C. Elegans* imaging was performed by Yan Tang (Peking University).

Abstract

We present Nuclear Peroxy Emerald 1 (NucPE1), a new type of nuclear-localized fluorescent probe for hydrogen peroxide (H_2O_2) in living cells and organisms. NucPE1 selectively accumulates in the nuclei of a variety of mammalian cell lines as well as in whole model organisms like *C. clegans*, where it can respond to subcellular changes in H_2O_2 fluxes. Moreover, *in vivo* NucPE1 imaging reveals a marked reduction in nuclear H_2O_2 levels in worms overexpressing sir-2.1 compared to wildtype congeners, supporting a link between this longevity-promoting sirtuin protein and enhanced regulation of nuclear ROS pools.

Introduction

Oxidative stress resulting from imbalances in the production of hydrogen peroxide (H_2O_2) and related reactive oxygen species (ROS) is an inevitable consequence of aerobic life.[1-10] Over time, this stress can lead to accumulation of ROS-mediated oxidative damage to genetic material (e.g., 8-oxoguanine) that is connected to aging and diseases where age is a risk factor, including cancer and Alzheimer's disease.[11,12] Accordingly, new methods for directly and specifically monitoring changes in nuclear H_2O_2 fluxes thus offer a potentially powerful set of tools for probing the relationships between nuclear oxidative stress, aging, and disease states. As current methods for targeting H_2O_2-responsive imaging reporters to the nucleus rely on transfection,[13] which varies in efficiency from cell type to cell type, we sought to pursue a complementary strategy using synthetic H_2O_2 indicators for nuclear localization. Nuclear-localized small-molecules remain rare[14-18] and no examples reported to date are H_2O_2 responsive. We now report the synthesis and properties of Nuclear Peroxy Emerald 1 (NucPE1), a new type of small-molecule chemical probe that selectively targets cellular nuclei and can report changes in H_2O_2 levels localized to this subcellular compartment in various mammalian cell lines and in the model organism *C. elegans*. Moreover, *in vivo* imaging experiments with this new chemical tool have allowed us to discover that worms overexpressing the longevity sirtuin gene sir-2.1 possess lower levels of nuclear H_2O_2 compared to wildtype counterparts, supporting a link between this gene and enhanced regulation of nuclear ROS pools.

Results and Discussion

Previous work from our laboratory has established the H_2O_2-mediated conversion of arylboronates to phenols as a general reaction-based strategy for selective and sensitive detection of cellular H_2O_2 in immune and neural signaling models,[13,19-23] but the vast majority of these probes do not possess a preferred subcellular localization. During the course of a systematic study of rhodol platforms to develop a family of H_2O_2 indicators that span a wider color palette,[24] we serendipidously discovered a boronate derivative that accumulates to the nuclei of live cells without the need for additional targeting groups. The synthetic route to this probe, NucPE1, is shown in Scheme 3-1. Condensation of 3-ethylamino-*p*-cresol and 2-(2,4-dihydroxybenzoyl)benzoic acid in TFA produces rhodol **1** in 67% yield. Treatment of **1** with *N*-phenyl bis(trifluoromethanesulfonamide) affords triflate **2** in 30% yield. Finally, palladium-mediated coupling with bis(pinacolato)diboron furnishes NucPE1 in 60% yield.

We evaluated the spectral characteristics and H_2O_2 response of NucPE1 in aqueous media buffered to physiological pH (20 mM HEPES, pH 7). NucPE1 features two major visible region absorptions (l_{abs} = 468 nm, e = 27,300 $M^{-1}cm^{-1}$; l_{abs} = 490 nm, e = 26,000 $M^{-1}cm^{-1}$) and a weak

emission (l_{em} = 530 nm, F = 0.117). Reaction of NucPE1 with H_2O_2 triggers a fluorescence increase upon its conversion to fluorophore **1**, which possesses one major absorption band at 505 nm (e = 19,100 $M^{-1}cm^{-1}$) with enhanced emission (l_{em} = 530 nm, F = 0.626). Kinetics measurements of the H_2O_2-mediated boronate deprotection were performed under pseudo-first-order conditions (5 μM dye, 10 mM H_2O_2), giving an observed rate constant of $k = 8.2 \times 10^{-3}$ s^{-1}. Figure 3-1a displays the H_2O_2-triggered fluorescence turn-on detected by NucPE1 over the course of 1 hour. As shown in Figure 3-1b, NucPE1 is selective for H_2O_2 over a panel of biologically relevant ROS, including superoxide, nitric oxide, and hydroxyl radical.

We next evaluated the subcellular distribution of NucPE1 in live mammalian cells. Images of HEK 293 cells loaded with NucPE1 and the nuclear stain Hoechst 33342 show good colocalization of the two dyes, establishing that NucPE1 accumulates specifically in the nucleus (Figure 3-2). Brightfield images coupled with nuclear staining demonstrate that the cells are viable throughout the imaging experiments (Figure 3-6). NucPE1 was then tested for its ability to respond to local changes in nuclear H_2O_2 levels. HEK 293 cells loaded with NucPE1 and Hoescht 33342 and then washed and treated with 100 μM H_2O_2 exhibit marked increases in green NucPE1 fluorescence that maintains nuclear localization (Figures 3-3 and 3-9). Similar images are observed in a wide variety of cell types, including HeLa, CHO.K1, NIH 3T3, Swiss 3T3, COS-7, A431, and Raw 264.7 Macrophages (Figures 3-10 through 3-17), demonstrating that NucPE1 can visualize changes in localized nuclear H_2O_2 pools in a range of mammalian cell systems. Importantly, compound **1** does not localize to the nucleus of cells (Figure 3-7), suggesting that the boronate moiety is required for this unexpected localization, but also confirming that any fluorescence change observed within the nucleus is due to nuclear H_2O_2 fluxes, as any NucPE1 deprotected outside of the nucleus will no longer localize to this organelle.

We performed several sets of experiments in an attempt to probe the origin of the observed nuclear localization of NucPE1. Initial studies focused on imaging mitotic cells stained with both NucPE1 and Hoescht 33342. Because this process involves breakdown of the nuclear envelope,[25] we reasoned that if the nuclear localization of NucPE1 depends on active nuclear import, we would expect mitotic cells to no longer maintain colocalization between NucPE1 and Hoechst 33342, as the latter dye relies on DNA intercalation for its nuclear targeting. However, we observed that cells in late anaphase still show pronounced colocalization of NucPE1 and Hoechst 33342, suggesting that DNA is involved in the selective nuclear accumulation of NucPE1 (Figures 3-2 and 3-6). However, our attempts to quantify this interaction *in vitro* by multiple methods, including monitoring absorption and emission changes, staining DNA gels with the NucPE1, or fluorescence polarization anisotropy measurements (Figure 3-8), have not revealed a confirmation of DNA binding, which is still the most likely mode of localization as is observed in other nuclear staining fluorophores. Nevertheless, NucPE1 selectively localizes to the nuclei of live mammalian cells, where it can respond to local changes in H_2O_2 levels.

With these cellular results in hand, we sought to expand the scope and utility of NucPE1 by applying this probe to *in vivo* nuclear H_2O_2 imaging in the model organism *C. elegans*. Worms loaded with 150 μM Hoechst 33342 and 50 μM NucPE1 for 8 h at 20 °C and imaged by scanning confocal microscopy show tight colocalization between the two fluorophores (Figures 3-4 and 3-18 through 3-20), confirming that NucPE1 maintains the ability to selectively target nuclei *in vivo*. We then used NucPE1 to interrogate nuclear redox responses to H_2O_2 in a *C. elegans* aging model. We focused our attention on sir-2.1,[26] an NAD-dependent histone deacetylase that when overexpressed can increase the lifespan of *C. elegans* and other model

organisms.[26,27] Interestingly, NucPE1 imaging of tail neurons in the control (N2) and sir-2.1-overexpressing worms reveals a lower basal level of nuclear H_2O_2 for the long-lived mutant strain (Figures 3-5 and 3-21). Moreover, addition of 10 mM H_2O_2 for 30 min causes a lower relative NucPE1 fluorescence increase for sir-2.1-overexpressing *C. elegans* compared to wildtype counterparts (Figures 3-5 and 3-21), suggesting that these longer-lived organisms possess enhanced nuclear protection to exogenous oxidative stressors.

Concluding Remarks

To close, we have discovered NucPE1, a new type of H_2O_2-specific fluorescent probe that localizes to cellular nuclei and is capable of visualizing local changes in H_2O_2 levels in a variety of mammalian cell lines and in the model organism *C. clegans*. Moreover, this probe can detect differences in nuclear H_2O_2 levels and responses between wildtype *C. elegans* and ones that overexpress the longevity gene sir-2.1. We are currently applying NucPE1 and related chemical tools to study the contributions of localized H_2O_2 fluxes to healthy, aging, and disease states in a variety of biological models.

Experimental Section

Synthetic Materials and Methods. All reactions were carried out under a dry nitrogen atmosphere. 2-(2,4-Dihydroxybenzoyl)benzoic acid[28] was synthesized according to literature methods. Silica gel P60 (SiliCycle) was used for column chromatography. Analytical thin layer chromatography was performed using SiliCycle 60 F254 silica gel (precoated sheets, 0.25 mm thick). All chemicals were purchased from Sigma-Aldrich (St. Louis, MO) and used as received. ^{1}H NMR, ^{13}C NMR, and ^{19}F NMR spectra were collected in $CDCl_3$ and $(CD_3)_2O$ (Cambridge Isotope Laboratories, Cambridge, MA) at 25 ºC on a Bruker AV-300, AVQ-400, or DRX-500 spectrometer at the College of Chemistry NMR Facility at the University of California, Berkeley. All chemical shifts are reported in the standard δ notation of parts per million using the peak of residual solvent proton signals as an internal reference. High-resolution mass spectral analyses were carried out at the College of Chemistry Mass Spectrometry Facility at the University of California, Berkeley. Low-resolution mass spectral analyses were carried out on an Agilent 6130 LC/MS system (Santa Clara, CA).

***N*-Ethyl (methyl) rhodol (1).** 3-Ethylamino-p-cresol (1.1 g, 7.0 mmol) and 2-(2,4-Dihydroxybenzoyl)benzoic acid (2.0 g, 7.7 mmol) were added to a heavy-walled pressure flask and dissolved in 10 mL of trifluoroacetic acid. The reaction contents were heated to 90 °C for 24 h. After cooling to room temperature, the contents were dried under reduced pressure. Purification by column chromatography (dichloromethane/10 % methanol) yielded **17** as a red solid (1.7 g, 67%). ^{1}H NMR (CD_3OD, 400 MHz): δ 8.54 (1H, d, J = 7.6 Hz), 7.86 (1H, t, J = 7.6 Hz), 7.81 (1H. t, J = 7.6 Hz), 7.41 (1H, d, J = 6.8 Hz), 7.20 (1H, d, J = 9.2 Hz), 7.15 (1H, d, J = 2.4 Hz), 7.05 (1H, s), 7.02 (1H, s), 6.98 (1H, dd, J = 2.4, 9.2 Hz), 6.61 (2H, q, J = 7.2 Hz), 2.17 (3H, s), 1.35 (3H, t, J = 7.2 Hz). ^{13}C NMR (CD_3OD, 100 MHz): δ 166.8, 161.0, 159.3, 158.8, 156.5, 133.8, 132.5, 131.2, 130.8, 130.2, 129.9, 129.4, 128.0, 116.9, 115.7, 115.2, 101.7, 93.6, 38.4, 16.1, 12.5. LR-MS (ESI): calculated for [M^+] 374.4, found 373.9.

***N*-Ethyl (methyl) rhodol triflate (2).** Compound **1** (1.0 g, 2.7 mmol), *N*-phenyl bis(trifluoromethanesulfonamide) (1.9 g, 5.4 mmol), and potassium carbonate (1.5 g, 10.7 mmol) were added to a glass vial, dissolved in 5 mL of acetonitrile, and stirred at room temperature for

5 h. The reaction contents were dried under reduced pressure. Purification by column chromatography (2:1 hexanes/ethyl acetate) yielded **18** as a faintly-yellow solid (0.40 g, 30%). ^{1}H NMR ($CDCl_3$ /5% CD_3OD, 400 MHz): δ 8.01 (1H, d, *J* = 7.6 Hz), 7.67 (1H, t, *J* = 7.2 Hz), 7.62 (1H, t, *J* = 7.2 Hz), 7.19 (1H, d, *J* = 2.4 Hz), 7.15 (1H, d, *J* = 7.6 Hz), 6.88 (1H, dd, *J* = 2.0, 8.8 Hz), 6.83 (1H, d, *J* = 8.8 Hz), 6.39 (1H, s), 6.34 (1H, s), 3.19 (2H, q, *J* = 6.8 Hz), 1.92 (3H, s), 1.29 (3H, t, *J* = 6.8 Hz). ^{13}C NMR ($CDCl_3$ /5% CD_3OD, 100 MHz): δ 169.6, 152.7, 152.4, 150.8, 149.8, 148.7, 135.3, 130.0, 129.9, 128.1, 126.5, 125.1, 124.0, 119.9, 119.1, 116.0, 110.3, 104.5, 96.1, 83.1, 38.1, 16.7, 14.4. ^{19}F NMR ($CDCl_3$ /10% CD_3OD, 376.5 MHz): δ –71.995. LR-MS (ESI): calculated for [M^+] 506.5, found 505.5.

***N*-Ethyl (methyl) rhodol boronate, NucPE1 (3).** Compound **2** (150 mg, 0.30 mmol), bis(pinacolato)diboron (120 mg, 0.47 mmol), palladium acetate (63 mg, 0.10 mmol), and cyclo-hexyl JohnPhos (66 mg, 0.20 mmol) were added to a glass vial in an inert atmosphere glove box and dissolved in 3 mL of dioxane. Diisopropylethamine (0.31 mL, 1.79 mmol) was then added the vial and the contents stirred at room temperature overnight. The contents were then brought out of the box and dried under reduced pressure. Purification by column chromatography (1:1 hexanes/ethyl acetate) yielded Nuc-PE1 as a light orange solid (87 mg, 60%). ^{1}H NMR ($CDCl_3$/5% CD_3OD, 400 MHz): δ 8.00 (1H, d, *J* = 6.8 Hz), 7.68 (1H, s), 7.63 (1H, t, *J* = 8.0 Hz), 7.58 (1H, t, *J* = 7.2 Hz), 7.36 (1H, d, *J* = 8.0 Hz), 7.10 (1H, d, *J* = 7.2 Hz), 6.73 (1H, d, *J* = 7.6 Hz), 6.39 (1H, s), 6.35 (1H, s), 3.21 (2H, q, *J* = 7.2 Hz), 1.92 (3H, s), 1.26-1.33 (15H, m). ^{13}C NMR ($CDCl_3$ /5% CD_3OD, 100 MHz): δ 170.1, 153.6, 151.3, 151.0, 148.5, 135.0 129.5, 128.8, 128.2, 127.2, 126.5, 124.9, 123.9, 123.4, 121.6, 118.3, 105.1, 96.4, 84.2, 36.2, 24.7, 24.7, 16.7, 14.5. HR-FABMS: calculated for [M^+] 484.2290, found 484.2297.

Spectroscopic Materials and Methods. Millipore water was used to prepare all aqueous solutions. All spectroscopic measurements were performed in 20 mM HEPES buffer, pH 7. Absorption spectra were recorded on a Varian Cary 50 spectrophotometer (Walnut Creek, CA) and fluorescence spectra were recorded on a Photon Technology International Quanta Master 4 L-format scanning spectrofluorometer (Lawrenceville, NJ) equipped with an LPS-220B 75-W xenon lamp and power supply, A-1010B lamp housing with integrated igniter, switchable 814 photon-counting/analog photomultiplier detection unit, and MD5020 motor driver. Samples for absorption and emission measurements were contained in 1-cm x 1-cm quartz cuvettes (1.5-mL volume, Starna, Atascadero, CA). Fluorescence quantum yields were determined by reference to fluorescein in 0.1 M NaOH (Φ = 0.94).

Selectivity Measurements. Data shown are for 10 mM O_2^-, 200 μM NO, and 100 μM for all other ROS as described previously.[20] Data were acquired at 25 ˚C in 20 mM HEPES, pH 7, with excitation λ = 500 nm and emission collected between 510 and 750 nm with all slits at 0.5 mm.

Fluorescence Polarization. A 500 nM NucPE1 solution was made up in 20 mM HEPES buffer, pH 7, with 2.5 mM $MgCl_2$. 1 mg DNA from calf thymus (Sigma) or 1 mg RNA from torula yeast (Sigma) were then dissolved in 1 mL of the NucPE1 solution. The samples were then measured in triplicate in a 384-well plate using the FITC filter sets in a plate reader.

Preparation and Staining of Cell Cultures HEK 293, HeLa, A431, NIH 3T3, Swiss 3T3, COS-7, and RAW264.7 macrophages were cultured in Dulbecco's Modified Eagle Medium (DMEM) containing high glucose with GlutaMAX™ (Invitrogen, Carlsbad, CA) and supplemented with 10% Fetal Bovine Serum (FBS, Hyclone). CHO.K1 cells were cultured in DMEM with F-12 supplements, glutamax (Invitrogen), and 5% Fetal Bovine Serum (FBS, Hyclone). Two days

before imaging, cells were passaged and plated on 18-mm glass coverslips. For all experiments, solutions of NucPE1 (from 5 mM stocks in DMSO) were made in DBPS with calcium chloride and magnesium chloride (Sigma). H_2O_2 was added by bath application to the medium from a 100 mM aqueous stock (Millipore H_2O). The cells were then kept in an incubator (37 °C, 5% CO_2) during the course of all experiments.

Fluorescence Cell Imaging Experiments. Confocal fluorescence imaging studies were performed with a Zeiss LSM510 NLO Axiovert 200 laser scanning microscope and a 40x Achroplan IR water-immersion objective lens. Excitation of NucPE1-loaded cells at 514 nm was carried out with an Ar laser and emission was collected using a META detector between 522-554 nm. Excitation of Hoechst 33342 was carried out using a MaiTai two-photon laser at 780-nm pulses (mode-locked Ti:sapphire laser, Tsunami Spectra Physics) and emission was collected between 436-501 nm. Image analysis was performed in Image J.

***C. elegans* Experiments.** Standard nematode growth medium (NGM) plates seeded with E. coli OP50-1 bacteria were used for C. elegans culture.[29] Worms were maintained at 20 ºC N2 Bristol were used the wild-type strain and sir-2.1(geIn3) mutants were used as the sir-2.1 overexpressing strain. Stock solutions of NucPE1 were freshly dissolved in M9 to make working solutions of 50 μM. Worms were collected, washed with M9 twice, and bathed in 100 μL NucPE1 (50 μM) and Hoechst 33342 (150 μM) solution for 8 h at 20 °C with mild shaking in the dark. Worms were washed twice with M9 before imaging. Confocal fluorescence images were captured with a Zeiss LSM710 NLO laser scanning microscope and a X40 water-immersion objective lens. NucPE1 and Hoechst double-loaded worms were excited at 514 nm and 405 nm respectively and emissions were collected from 525 to 555 nm for NucPE1 and from 440 to 480 nm for Hoechst 33342. The images were collected at 16-bit with the raw pixel values within the linear range of the PMT. Nuclei were segmented by adaptive threshold of the Hoechst channel and watershed segmentation. Inverse flood fill was used to remove nuclei internal holes. To calculate the fluorescence intensity for both NucPE1 and Hoechst, the mean pixel intensity of all fluorescence staining nuclei was divided by the multiply of corresponding laser power and master gain value of PMT. All other imaging parameters including digital gain, scaling, and scanning speed were kept constant for all images. The mean intensity of NucPE1 was normalized by the corresponding nuclear mean intensity of Hoechst 33342. For each treatment more than 55 nuclei in at least 5 worms were analyzed. All experiments were performed in duplicate.

Figures and Schemes

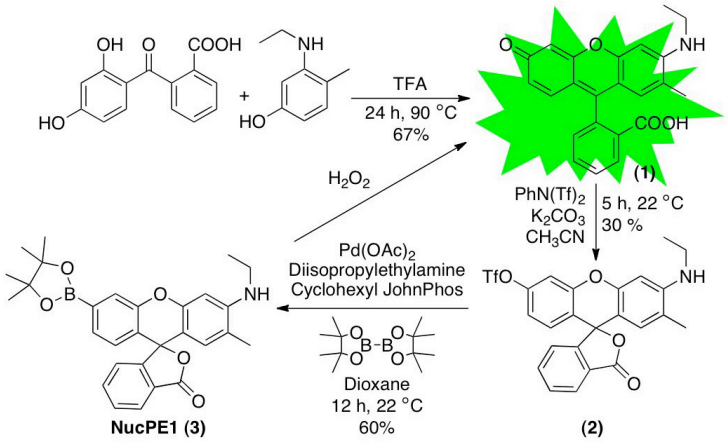

Scheme 3-1. Synthesis and activation of NucPE1.

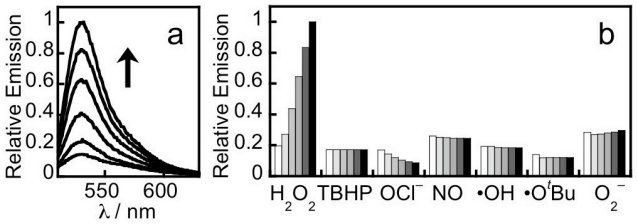

Figure 3-1. Fluorescence response and selectivity of NucPE1. (a) Fluorescence response of 5 μM NucPE1 to H_2O_2. Time points represent 0, 5, 15, 30, 45, and 60 min after the addition of 100 μM H_2O_2. (b) Fluorescence responses of NucPE1 to various reactive oxygen species (ROS). Bars represent relative responses at 0, 5, 15, 30, 45, and 60 min after addition of each ROS.

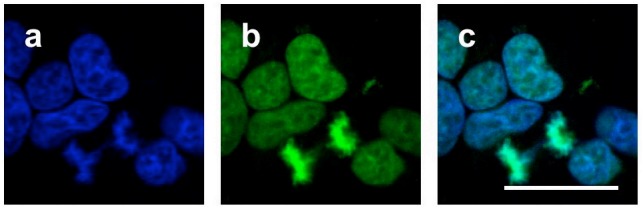

Figure 3-2. HEK 293 cells loaded with 5 μM NucPE1 and 1 μM Hoechst 33342 for 15 min in DPBS, washed with DPBS, incubated 20 minutes in DPBS, and imaged for Hoechst 33342 (a) NucPE1 (b), and Hoechst 33342 and NucPY1 overlay with 25 μm scale bar (c).

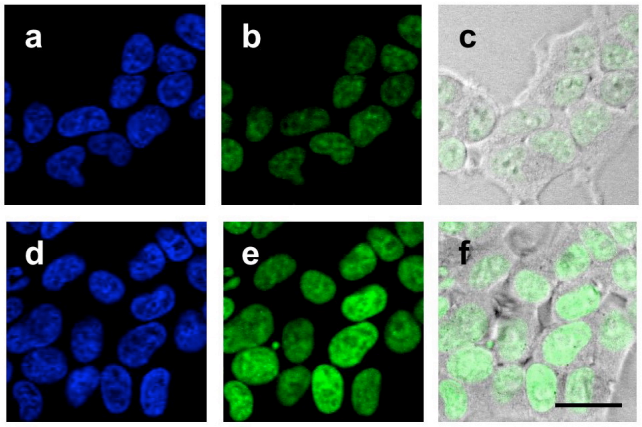

Figure 3-3. HEK 293 cells loaded with 5 μM NucPE1 and 1 μM Hoechst 33342 for 15 min in DPBS, washed with DPBS, incubated 20 minutes in DPBS, and imaged for Hoechst 33342 (a), NucPE1 (b), and a brightfield with NucPE1 overlay (c). HEK 293 cells loaded with 5 μM NucPE1 and 1 μM Hoechst 33342 for 15 min in DPBS, washed with DPBS, incubated 20 min in DPBS with 100 μM H_2O_2, and imaged for Hoechst 33342 (d), NucPE1 (e), and bright field with NucPE1 overlay with 20 μm scale bar (f).

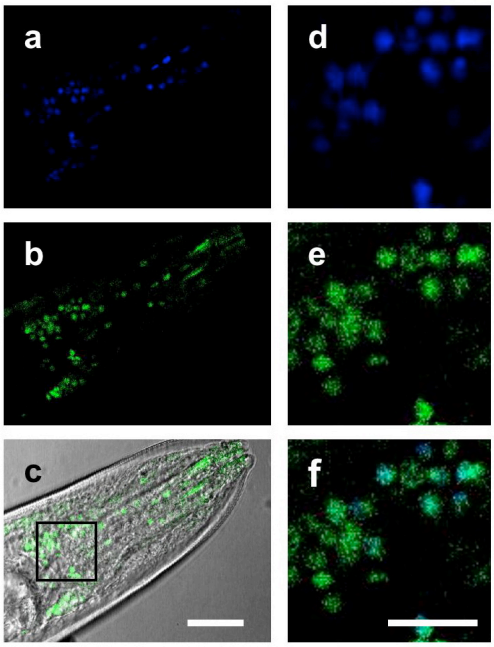

Figure 3-4. *C. elegans* loaded with 150 μM Hoechst 33342 and 50 μM NucPE1 for 8 h and imaged for Hoechst 33342 (a), NucPE1 (b), and NucPE1 and DIC overlay with a 20 μm scale bar (c). The portion illustrated by a squares in (c) is enlarged and the signal from Hoechst 33342 (d), NucPE1 (e), and Hoechst 33342 and NucPY1 overlay (f) are shown with a 10 μm scale bar.

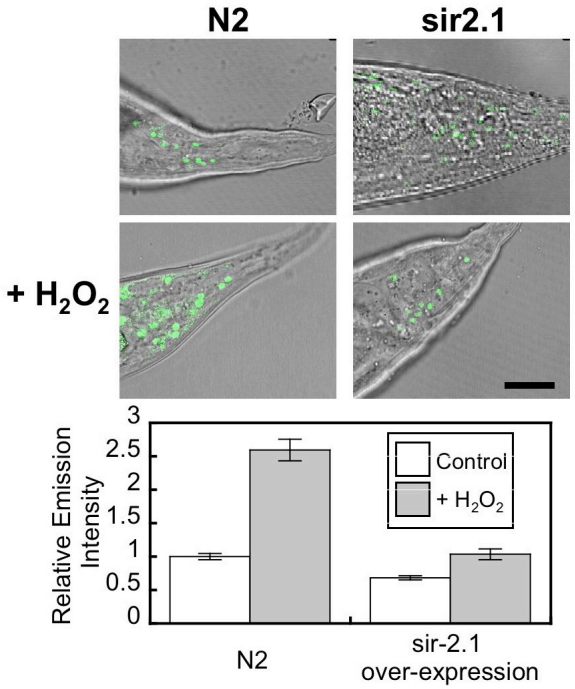

Figure 3-5. Wild-type (N2) or sir-2.1-overexpressing *C. elegans* loaded with 150 μM Hoechst 33342 and 50 μM NucPE1 for 8 h, stimulated with either carrier or 10 mM H_2O_2 for 30 min, and tail neurons analyzed by confocal microscopy. Representative images of NucPE1 and a bright field overlay are displayed for one worm from each condition as well as quantification of NucPE1 fluorescence as described in *Methods*. 20 μm scale bar shown. Error bars are ± s.e.m.

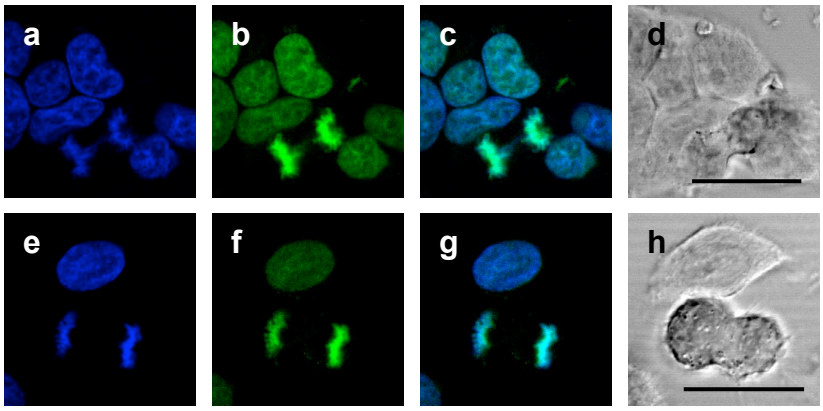

Figure 3-6. HEK 293 cells loaded with 5 μM NucPE1 and 1 μM Hoechst 33342 for 15 min in DPBS, washed with DPBS, incubated 20 minutes in DPBS, and imaged for Hoechst 33342 (a) NucPE1 (b), Hoechst 33342 and NucPE1 overlay (c), and brightfield (d). HeLa cells loaded with 5 μM NucPE1 and 1 μM Hoechst 33342 for 15 min in DPBS, washed with DPBS, incubated 20 minutes in DPBS, and imaged for Hoechst 33342 (e) NucPE1 (f), Hoechst 33342 and NucPE1 overlay (g), and brightfield (h). 25 μm scale bar shown.

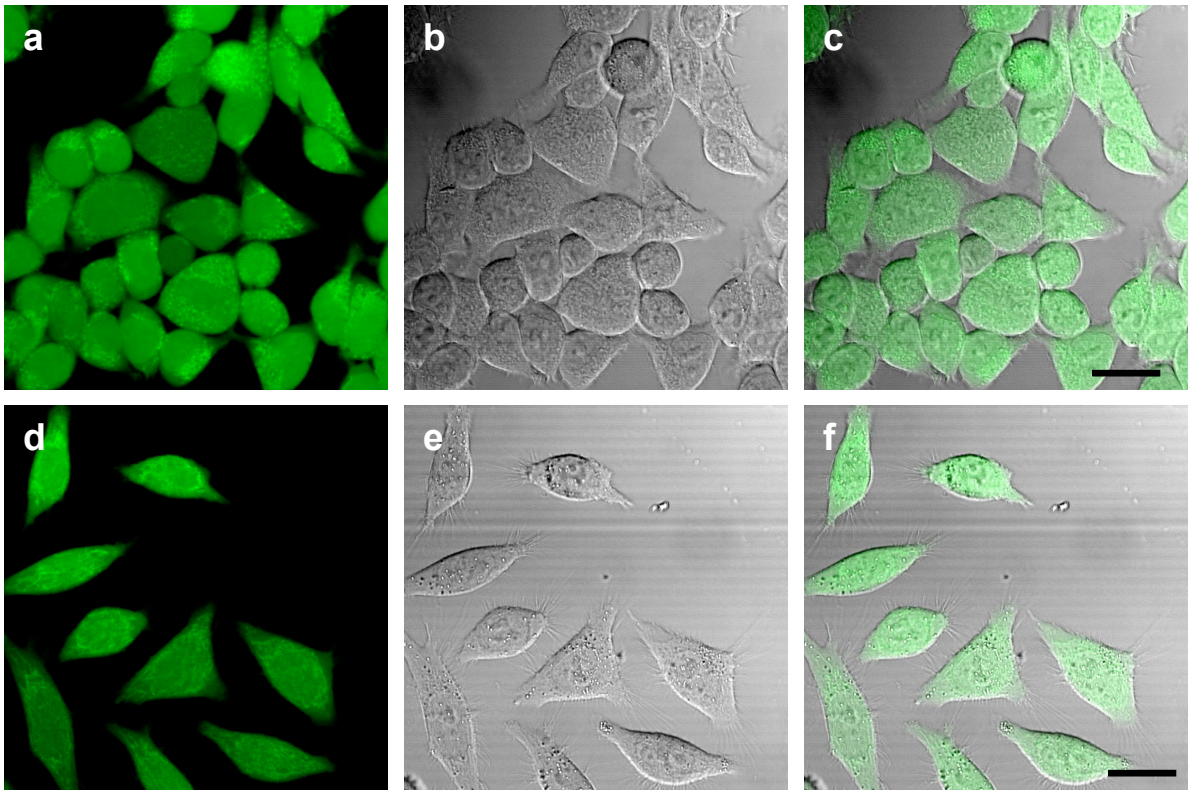

Figure 3-7. HEK 293 cells loaded with 5 μM **1** for 40 min in DPBS, washed with DPBS, and imaged for **1** (a), brightfield (b), and **1** and brightfield overlay (c). HeLa cells loaded with 5 μM **1** for 40 min in DPBS, washed with DPBS, and imaged for **1** (a), brightfield (b), and **1** and brightfield overlay (c). 20 μm scale bar shown.

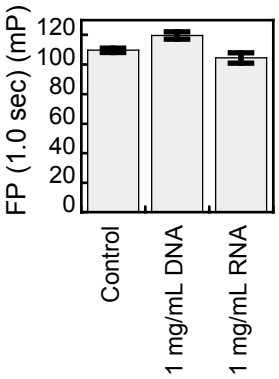

Figure 3-8. Fluorescence polarization anisotropy of NucPE1 in the presence of DNA and RNA. 500 nM NucPE1 solution in 20 mM HEPES buffer, pH 7, with 2.5 mM $MgCl_2$, with either carrier (control), 1 mg/mL DNA from calf thymus, or 1 mg/mL RNA from torula yeast. Error bars are ± s.e.m.

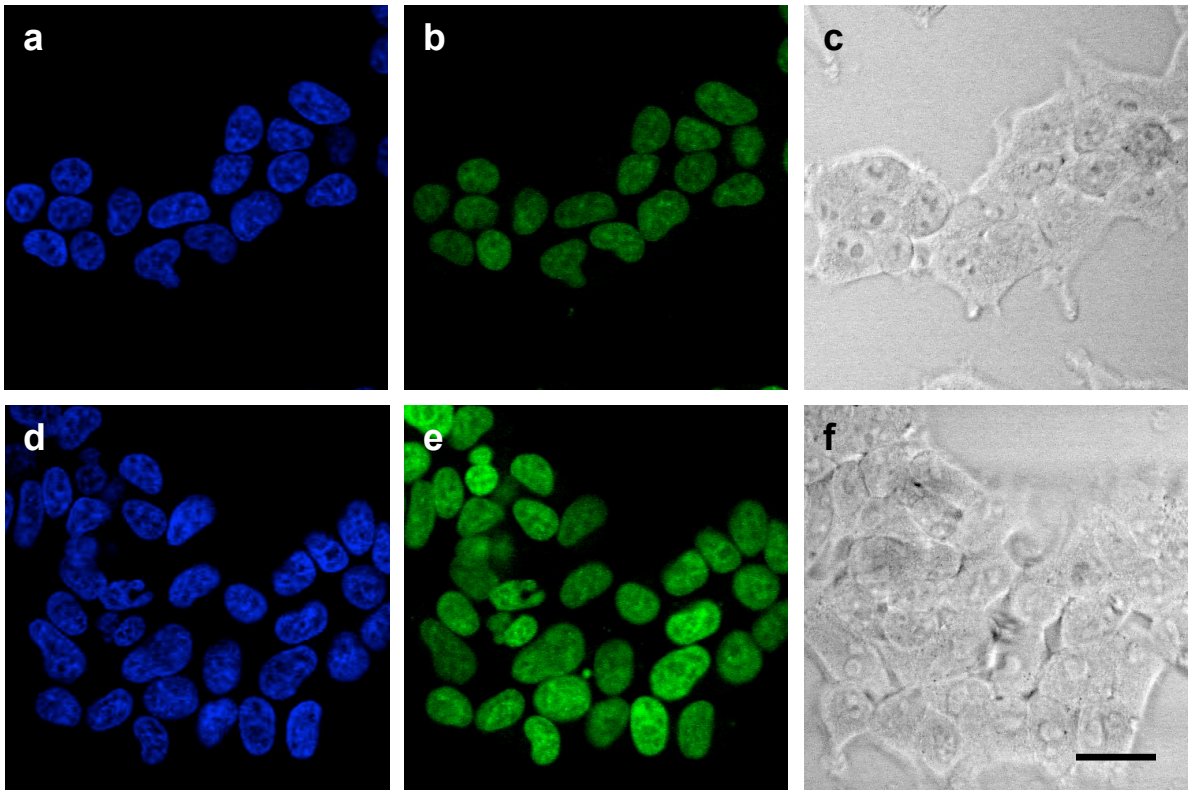

Figure 3-9. HEK 293 cells loaded with 5 μM NucPE1 and 1 μM Hoechst 33342 for 15 min in DPBS, washed with DPBS, incubated 20 minutes in DPBS, and imaged for Hoechst 33342 (a), NucPE1 (b), and a brightfield (c). HEK 293 cells loaded with 5 μM NucPE1 and 1 μM Hoechst 33342 for 15 min in DPBS, washed with DPBS, incubated 20 minutes in DPBS with 100 μM H_2O_2, and imaged for Hoechst 33342 (d), NucPE1 (e), and brightfield (f). 20 μm scale bar shown.

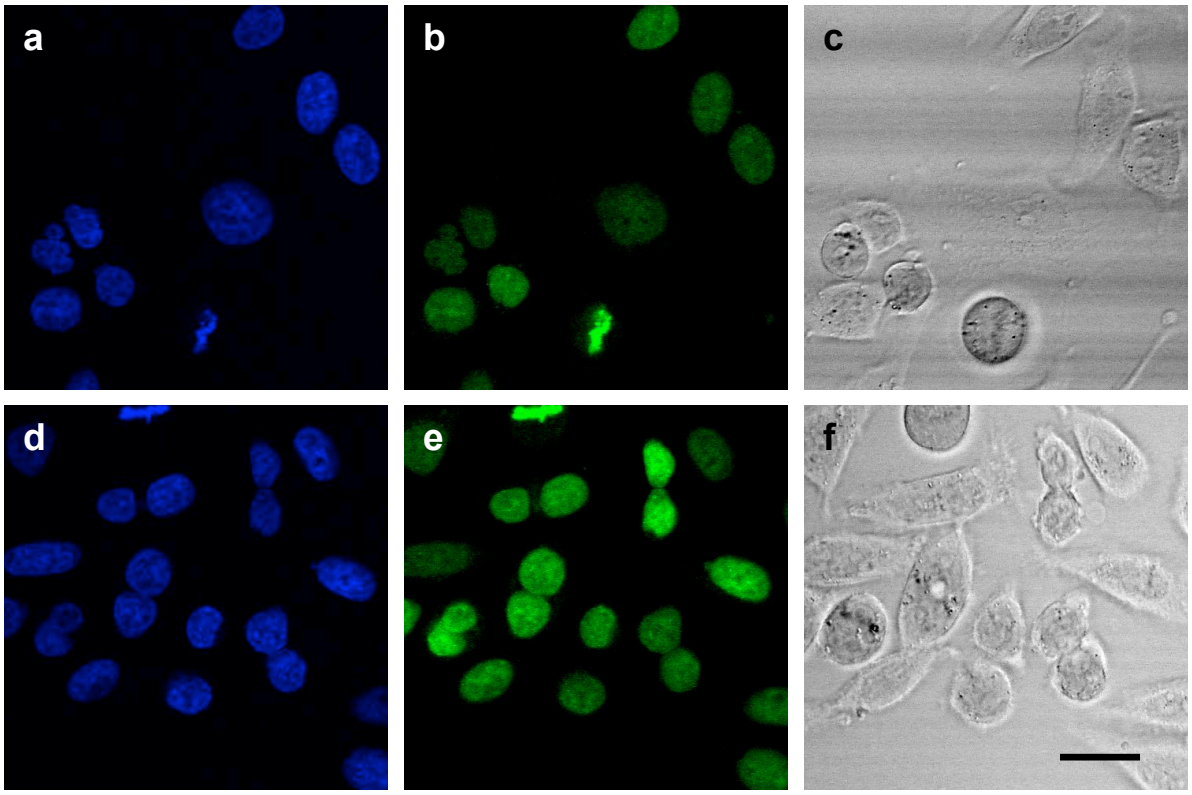

Figure 3-10. HeLa cells loaded with 5 μM NucPE1 and 1 μM Hoechst 33342 for 15 min in DPBS, washed with DPBS, incubated 20 minutes in DPBS, and imaged for Hoechst 33342 (a), NucPE1 (b), and a brightfield (c). HeLa cells loaded with 5 μM NucPE1 and 1 μM Hoechst 33342 for 15 min in DPBS, washed with DPBS, incubated 20 minutes in DPBS with 100 μM H_2O_2, and imaged for Hoechst 33342 (d), NucPE1 (e), and brightfield (f). 20 μm scale bar shown.

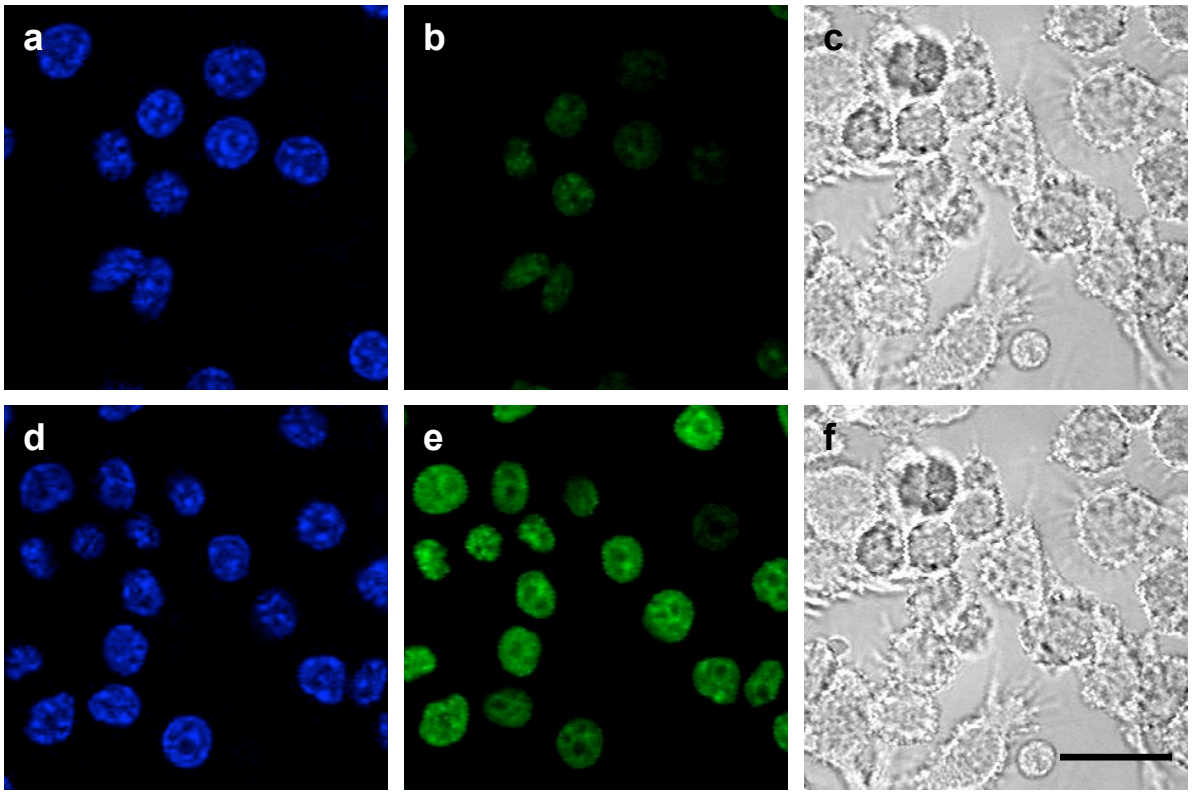

Figure 3-11. RAW 264.7 macrophages loaded with 5 μM NucPE1 and 1 μM Hoechst 33342 for 15 min in DPBS, washed with DPBS, incubated 20 minutes in DPBS, and imaged for Hoechst 33342 (a), NucPE1 (b), and a brightfield (c). RAW 264.7 macrophages cells loaded with 5 μM NucPE1 and 1 μM Hoechst 33342 for 15 min in DPBS, washed with DPBS, incubated 20 minutes in DPBS with 100 μM H_2O_2, and imaged for Hoechst 33342 (d), NucPE1 (e), and brightfield (f). 20 μm scale bar shown.

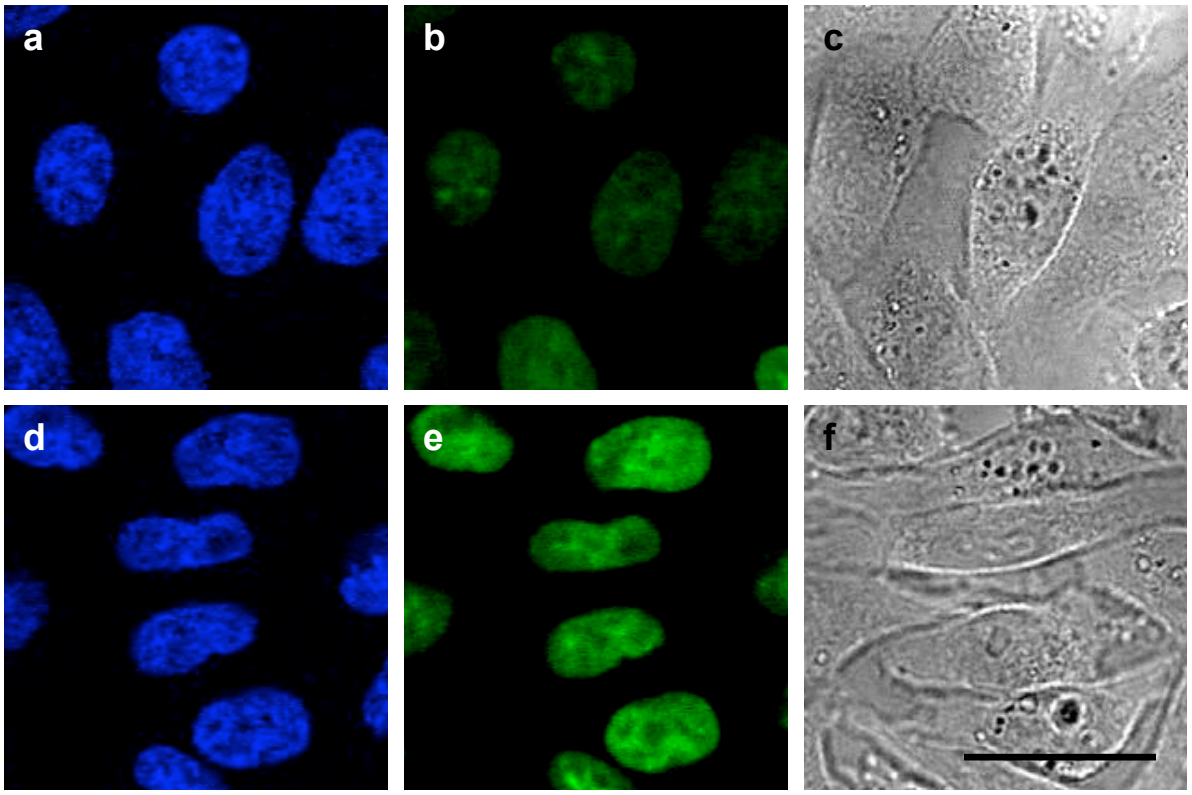

Figure 3-12. CHO.K1 cells loaded with 5 μM NucPE1 and 1 μM Hoechst 33342 for 15 min in DPBS, washed with DPBS, incubated 20 minutes in DPBS, and imaged for Hoechst 33342 (a), NucPE1 (b), and a brightfield (c). CHO.K1 cells loaded with 5 μM NucPE1 and 1 μM Hoechst 33342 for 15 min in DPBS, washed with DPBS, incubated 20 minutes in DPBS with 100 μM H_2O_2, and imaged for Hoechst 33342 (d), NucPE1 (e), and brightfield (f). 20 μm scale bar shown.

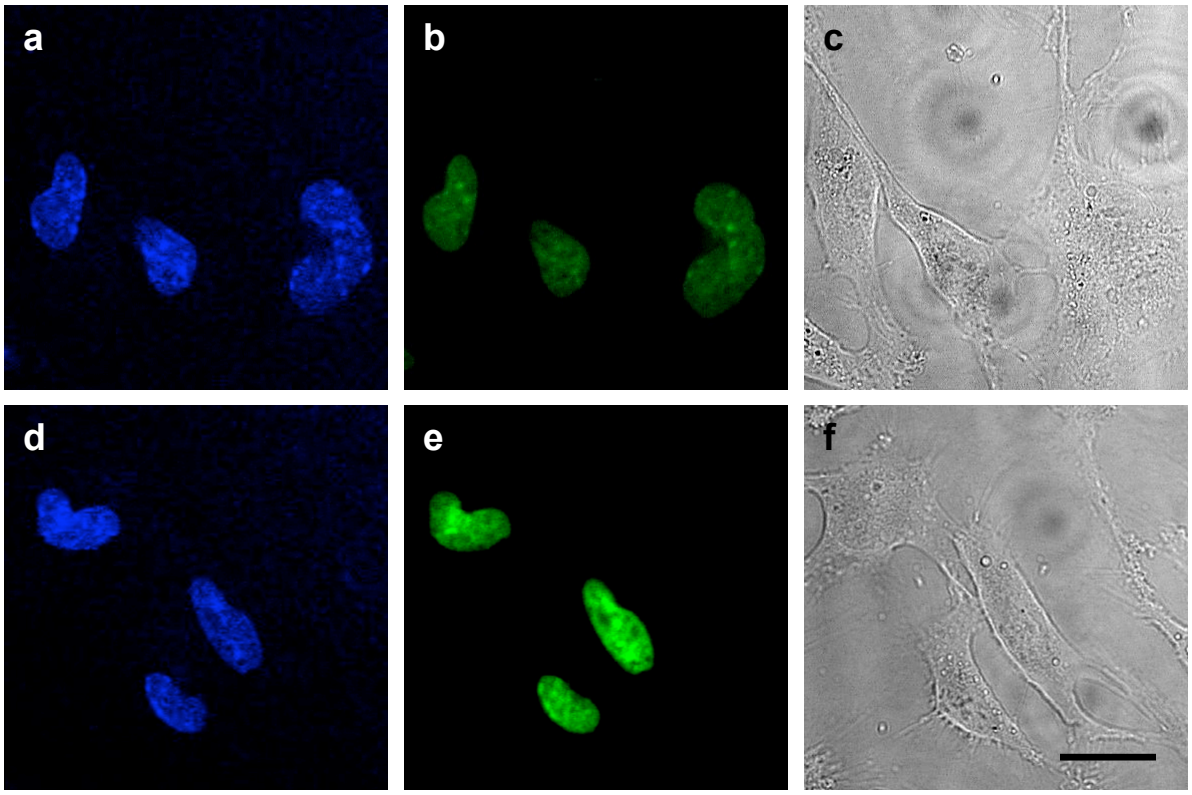

Figure 3-13. Swiss 3T3 cells loaded with 5 μM NucPE1 and 1 μM Hoechst 33342 for 15 min in DPBS, washed with DPBS, incubated 20 minutes in DPBS, and imaged for Hoechst 33342 (a), NucPE1 (b), and a brightfield (c). Swiss 3T3 cells loaded with 5 μM NucPE1 and 1 μM Hoechst 33342 for 15 min in DPBS, washed with DPBS, incubated 20 minutes in DPBS with 100 μM H_2O_2, and imaged for Hoechst 33342 (d), NucPE1 (e), and brightfield (f). 20 μm scale bar shown.

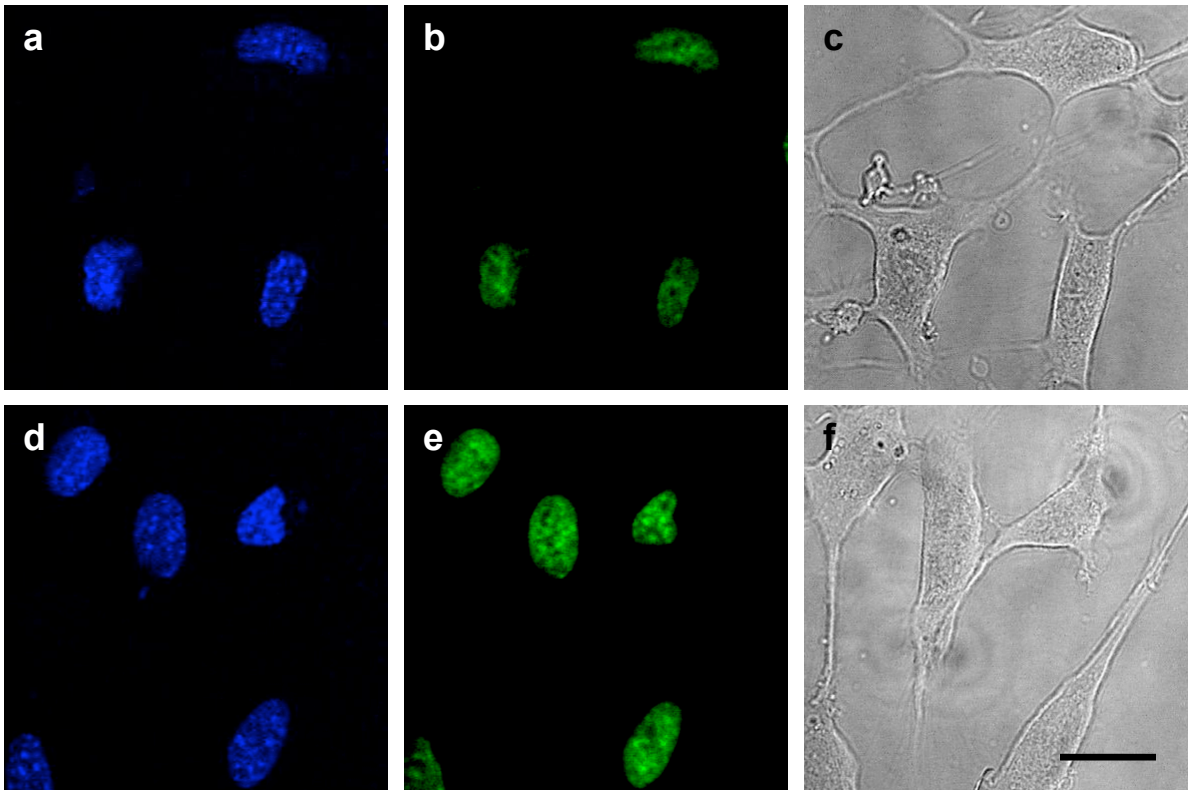

Figure 3-14. NIH 3T3 cells loaded with 5 μM NucPE1 and 1 μM Hoechst 33342 for 15 min in DPBS, washed with DPBS, incubated 20 minutes in DPBS, and imaged for Hoechst 33342 (a), NucPE1 (b), and a brightfield (c). NIH 3T3 cells loaded with 5 μM NucPE1 and 1 μM Hoechst 33342 for 15 min in DPBS, washed with DPBS, incubated 20 minutes in DPBS with 100 μM H_2O_2, and imaged for Hoechst 33342 (d), NucPE1 (e), and brightfield (f). 20 μm scale bar shown.

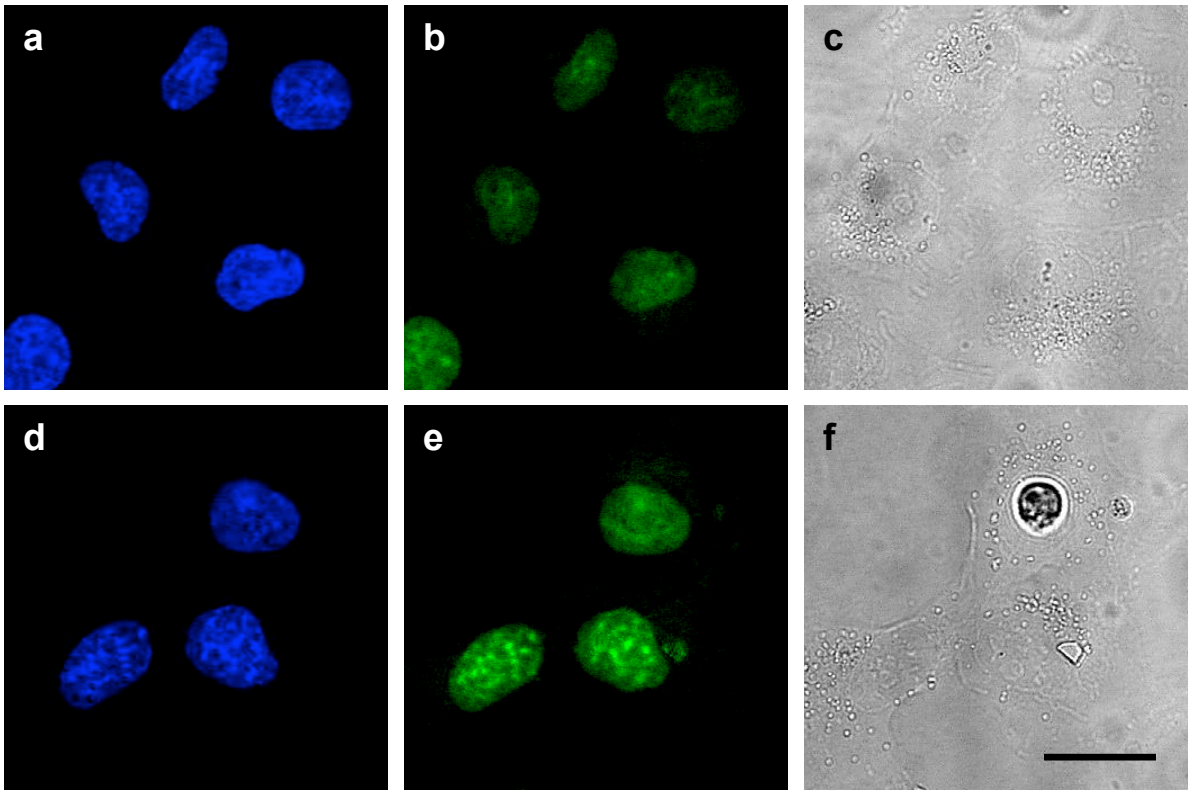

Figure 3-15. COS-7 cells loaded with 5 μM NucPE1 and 1 μM Hoechst 33342 for 15 min in DPBS, washed with DPBS, incubated 20 minutes in DPBS, and imaged for Hoechst 33342 (a), NucPE1 (b), and a brightfield (c). COS-7 cells loaded with 5 μM NucPE1 and 1 μM Hoechst 33342 for 15 min in DPBS, washed with DPBS, incubated 20 minutes in DPBS with 100 μM H_2O_2, and imaged for Hoechst 33342 (d), NucPE1 (e), and brightfield (f). 20 μm scale bar shown.

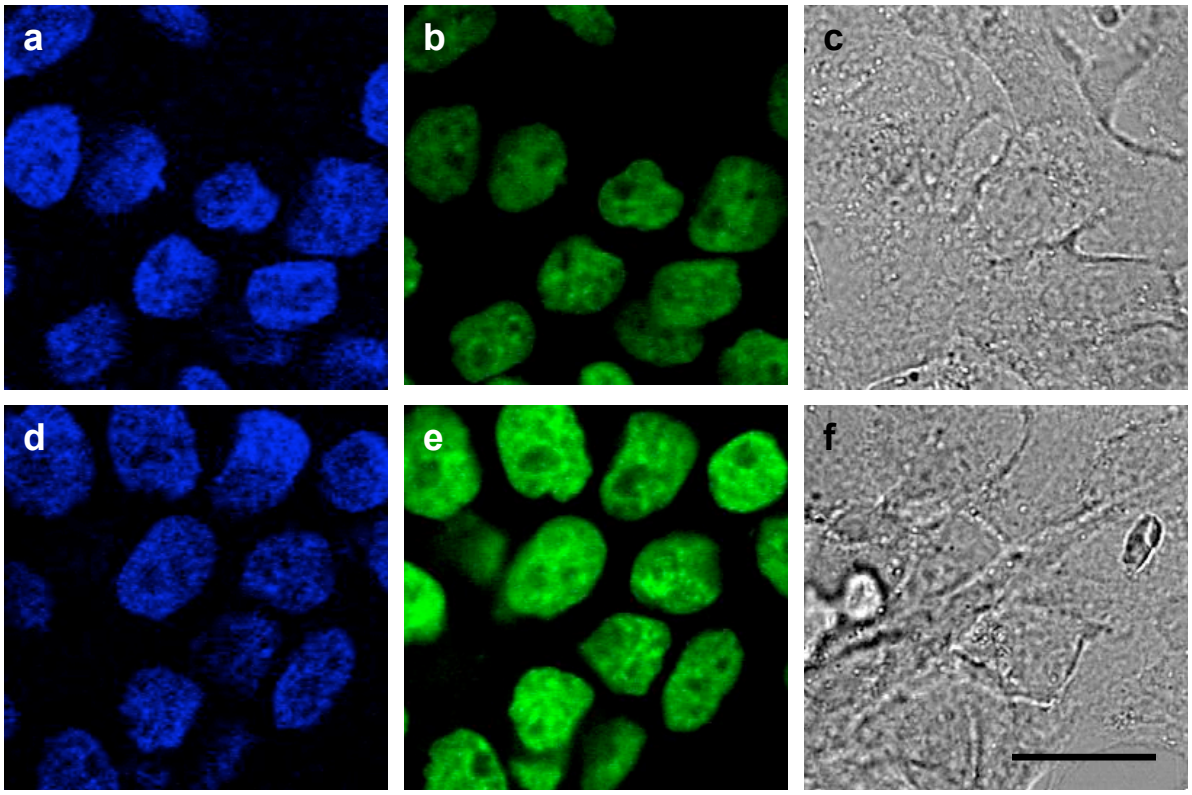

Figure 3-16. A431 cells loaded with 5 μM NucPE1 and 1 μM Hoechst 33342 for 15 min in DPBS, washed with DPBS, incubated 20 minutes in DPBS, and imaged for Hoechst 33342 (a), NucPE1 (b), and a brightfield (c). A431 cells loaded with 5 μM NucPE1 and 1 μM Hoechst 33342 for 15 min in DPBS, washed with DPBS, incubated 20 minutes in DPBS with 100 μM H_2O_2, and imaged for Hoechst 33342 (d), NucPE1 (e), and brightfield (f). 20 μm scale bar shown.

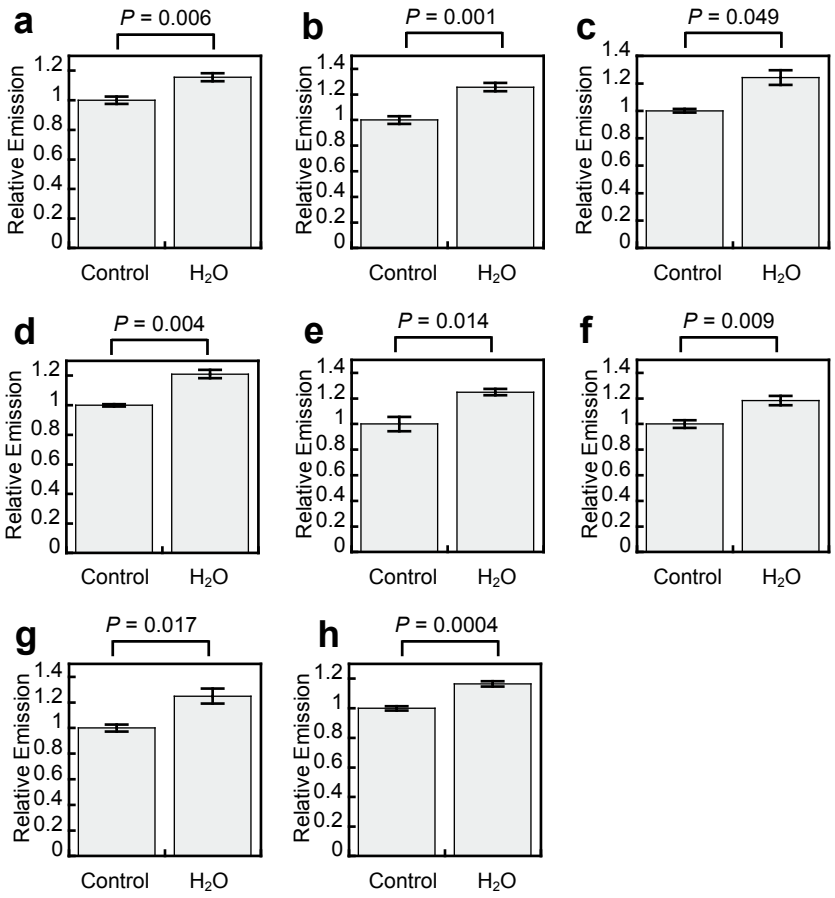

Figure 3-17. Quantification of experiments as shown in Figure S3-S10. HEK 293 (a), HeLa (b), Raw 264.7 Macrophages (c), CHO.K1 (d), Swiss 3T3 (e), NIH 3T3 (f), COS-7 (g), or A431 (h) cells loaded with 5 μM NucPE1 and 1 μM Hoechst 33342 for 15 min in DPBS, washed with DPBS, incubated 20 minutes in DPBS or 100 μM H_2O_2, and imaged for NucPE1. Statistical analysis were performed with a Student's *t*-test (n = 4) and error bars are ± s.e.m.

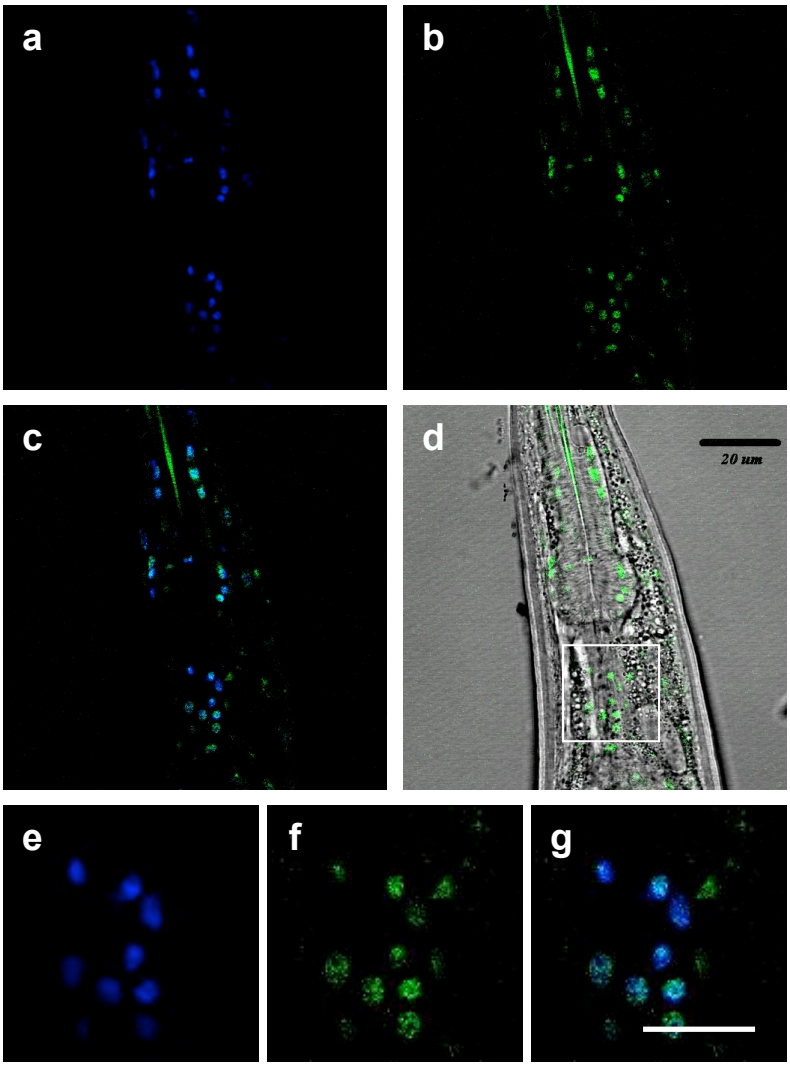

Figure 3-18. Image of LG100 *C. elegans* loaded with 150 µM Hoechst 33342 and 50 µM NucPE1 for 8 h at 20 °C and imaged by confocal microscopy for Hoechst 33342 (a), NucPE1 (b), Hoechst 33342 and NucPE1 overlay (c), and NucPE1 and brightfield overlay (d) with a 20 µm scale bar. The region indicated in (a) is enlarged and images shown for Hoechst 33342 (e), NucPE1 (f), and NucPE1 and Hoechst 33342 overlay (g) with a 10 µm scale bar.

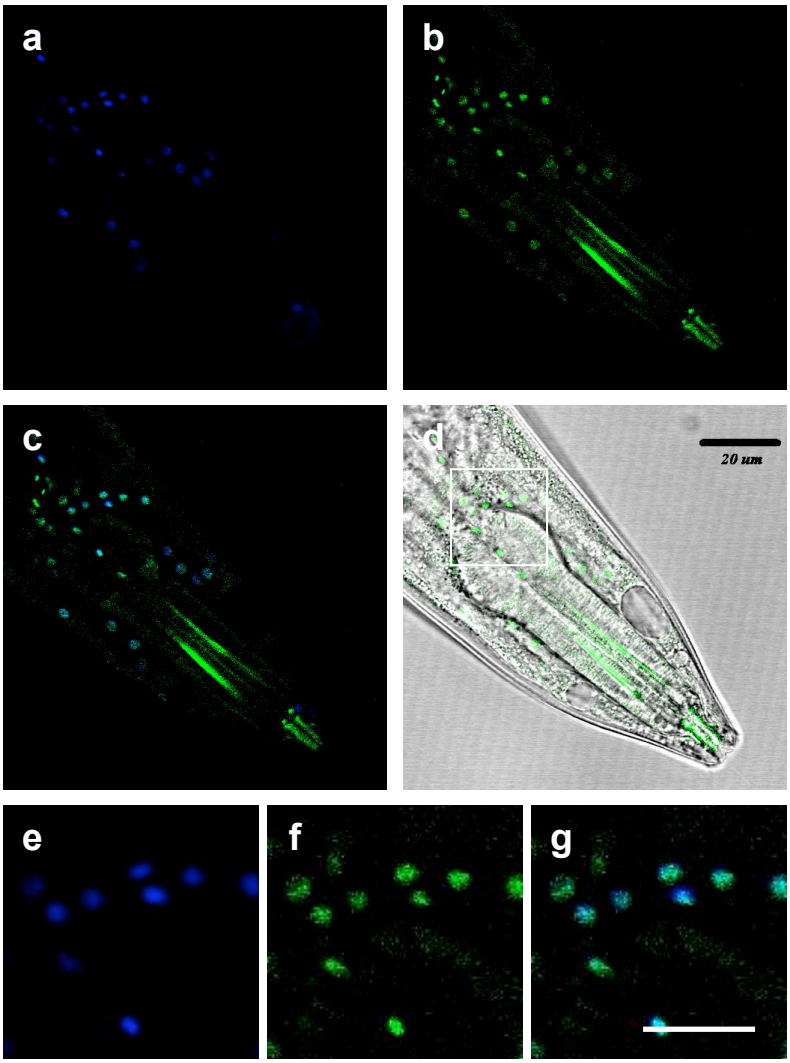

Figure 3-19. Image of N2 *C. elegans* loaded with 150 µM Hoechst 33342 and 50 µM NucPE1 for 8 h at 20 °C and imaged by confocal microscopy for Hoechst 33342 (a), NucPE1 (b), Hoechst 33342 and NucPE1 overlay (c), and NucPE1 and brightfield overlay (d) with a 20 µm scale bar. The region indicated in (a) is enlarged and images shown for Hoechst 33342 (e), NucPE1 (f), and NucPE1 and Hoechst 33342 overlay (g) with a 10 µm scale bar.

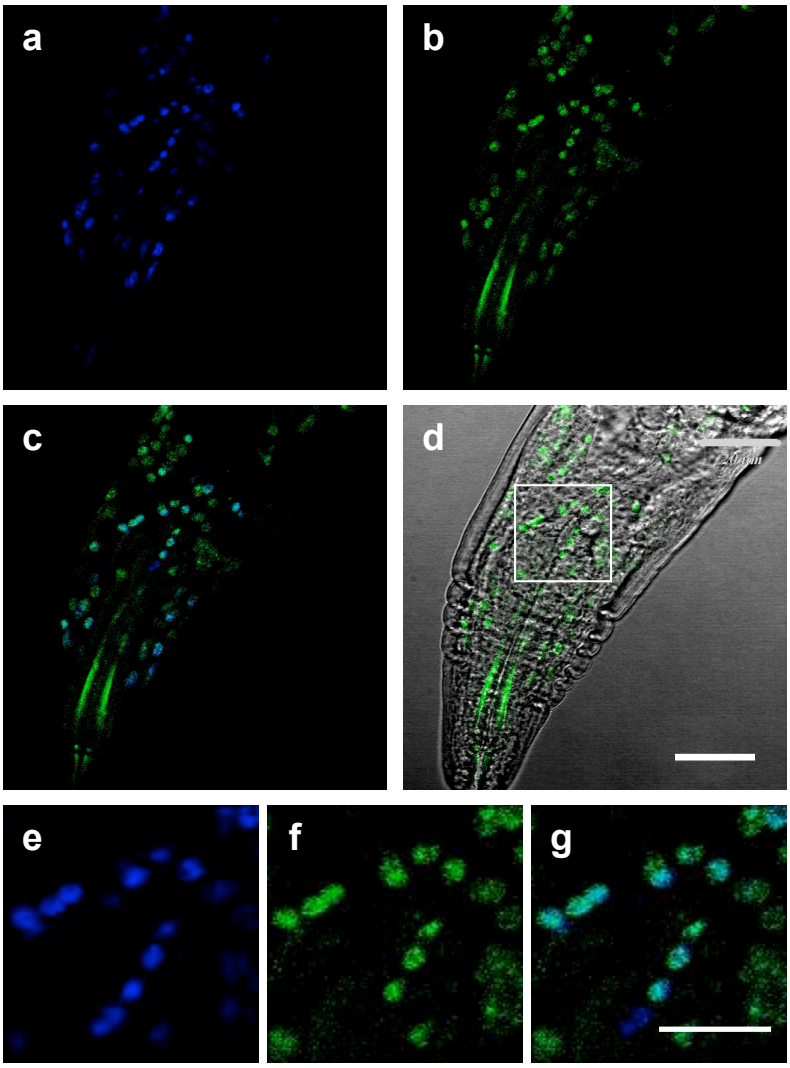

Figure 3-20. Image of LG100 *C. elegans* loaded with 150 µM Hoechst 33342 and 50 µM NucPE1 for 8 hours at 20 °C and imaged by confocal microscopy for Hoechst 33342 (a), NucPE1 (b), Hoechst 33342 and NucPE1 overlay (c), and NucPE1 and brightfield overlay (d) with a 20 µm scale bar.

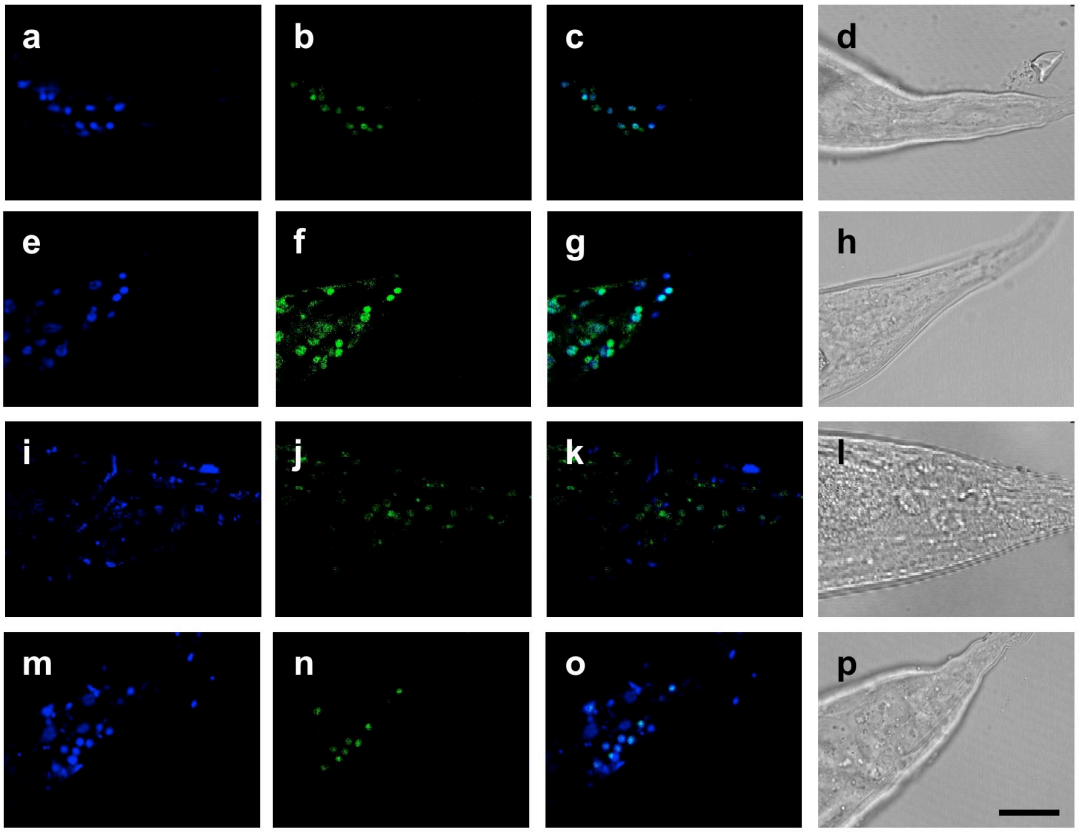

Figure 3-21. Wild-type *C. elegans* loaded with 150 µM Hoechst 33342 and 50 µM NucPE1 for 8 h at 20 °C, washed, stimulated with carrier for 30 min and imaged by confocal microscopy for Hoechst 33342 (a), NucPE1 (b), Hoechst 33342 and NucPE1 overlay (c), and brightfield (d). Wild-type *C. elegans* loaded with 150 µM Hoechst 33342 and 50 µM NucPE1 for 8 h at 20 °C, washed, stimulated with 10 mM H_2O_2 for 30 min and imaged by confocal microscopy for Hoechst 33342 (e), NucPE1 (f), Hoechst 33342 and NucPE1 overlay (g), and brightfield (h). Sir2.1-overexpressing *C. elegans* loaded with 150 µM Hoechst 33342 and 50 µM NucPE1 for 8 h at 20 °C, washed, stimulated with carrier for 30 min and imaged by confocal microscopy for Hoechst 33342 (i), NucPE1 (j), Hoechst 33342 and NucPE1 overlay (k), and brightfield (l). Sir2.1-overexpressing *C. elegans* loaded with 150 µM Hoechst 33342 and 50 µM NucPE1 for 8 h at 20 °C, washed, stimulated with 10 mM H_2O_2 for 30 min and imaged by confocal microscopy for Hoechst 33342 (m), NucPE1 (n), Hoechst 33342 and NucPE1 overlay (o), and brightfield (p). 20 µm scale bar shown.

References

1. Finkel, T.; Serrano, M.; Blasco, M. A. The common biology of cancer and ageing. *Nature* **2007**, *448*, 767.
2. D'Autréaux, B.; Toledano, M. B. ROS as signalling molecules: mechanisms that generate specificity in ROS homeostasis. *Nature Reviews Molecular Cell Biology* **2007**, *8*, 813.
3. Winterbourn, C. C. Reconciling the chemistry and biology of reactive oxygen species. *Nat. Chem. Biol.* **2008**, *4*, 278.
4. Murphy, M. P. How mitochondria produce reactive oxygen species. *Biochem. J.* **2009**, *417*, 1.
5. Dickinson, B. C.; Srikun, D.; Chang, C. J. Mitochondrial-targeted fluorescent probes for reactive oxygen species. *Curr. Opin. Chem. Biol.* **2010**, *14*, 50.
6. Paulsen, C. E.; Carroll, K. S. Orchestrating Redox Signaling Networks through Regulatory Cysteine Switches. *ACS Chemical Biology* **2009**, *5*, 47-62.
7. Frey, R. S.; Ushio–Fukai, M.; Malik, A. B. NADPH oxidase-dependent signaling in endothelial cells: role in physiology and pathophysiology. *Antioxidants & redox signaling* **2009**, *11*, 791.
8. Sundaresan, M.; Yu, Z. X.; Ferrans, V. J.; Irani, K.; Finkel, T. Requirement for generation of H2O2 for platelet-derived growth factor signal transduction. *Science* **1995**, *270*, 296.
9. Bae, Y. S.; Kang, S. W.; Seo, M. S.; Baines, I. C.; Tekle, E.; Chock, P. B.; Rhee, S. G. Epidermal growth factor (EGF)-induced generation of hydrogen peroxide. Role in EGF receptor-mediated tyrosine phosphorylation. *J. Biol. Chem.* **1997**, *272*, 217.
10. Niethammer, P.; Grabher, C.; Look, A. T.; Mitchison, T. J. A tissue-scale gradient of hydrogen peroxide mediates rapid wound detection in zebrafish. *Nature* **2009**, *459*, 996.
11. Markesbery, W. R.; Lovell, M. A. DNA oxidation in Alzheimer's disease. *Antioxidants & redox signaling* **2006**, *8*, 2039.
12. Bohr, V. A. Repair of oxidative DNA damage in nuclear and mitochondrial DNA, and some changes with aging in mammalian cells. *Free radical biology & medicine* **2002**, *32*, 804.
13. Srikun, D.; Albers, A. E.; Nam, C. I.; Ivarone, A. T.; Chang, C. J. Organelle-Targetable Fluorescent Probes for Imaging Hydrogen Peroxide in Living Cells via SNAP-Tag Protein Labeling. *J. Am. Chem. Soc.* **2010**, *132*, 4455.
14. Dooley, C. T.; Dore, T. M.; Hanson, G. T.; Jackson, W. C.; Remington, S. J.; Tsien, R. Y. Imaging dynamic redox changes in mammalian cells with green fluorescent protein indicators. *Journal of Biological Chemistry* **2004**, *279*, 22284.
15. Koide, Y.; Urano, Y.; Yatsushige, A.; Hanaoka, K.; Terai, T.; Nagano, T. Design and Development of Enzymatically Activatable Photosensitizer Based on Unique Characteristics of Thiazole Orange. *Journal of the American Chemical Society* **2009**, *131*, 6058-6059.
16. Halvey, P. J.; Hansen, J. M.; Johnson, J. M.; Go, Y. M.; Samali, A.; Jones, D. P. Selective oxidative stress in cell nuclei by nuclear-targeted D-amino acid oxidase. *Antioxid. Redox Signal.* **2007**, *9*, 807.
17. Mahon, K. P.; Potocky, T. B.; Blair, D.; Roy, M. D.; Stewart, K. M.; Chiles, T. C.; Kelley, S. O. Deconvolution of the cellular oxidative stress response with organelle-specific Peptide conjugates. *Chem. & Biol.* **2007**, *14*, 923.

18. Feng, S.; Kim, Y. K.; Yang, S.; Chang, Y. T. Discovery of a green DNA probe for live-cell imaging. *Chem. Comm.*, *46*, 436.
19. Chang, M. C. Y.; Pralle, A.; Isacoff, E. Y.; Chang, C. J. A selective, cell-permeable optical probe for hydrogen peroxide in living cells. *J. Am. Chem. Soc* **2004**, *126*, 15392.
20. Miller, E. W.; Albers, A. E.; Pralle, A.; Isacoff, E. Y.; Chang, C. J. Boronate-based fluorescent probes for imaging cellular hydrogen peroxide. *J. Am. Chem. Soc.* **2005**, *127*, 16652.
21. Miller, E. W.; Tulyathan, O.; Isacoff, E. Y.; Chang, C. J. Molecular imaging of hydrogen peroxide produced for cell signaling. *Nat. Chem. Biol.* **2007**, *3*, 263.
22. Albers, A. E.; Dickinson, B. C.; Miller, E. W.; Chang, C. J. A red-emitting naphthofluorescein-based fluorescent probe for selective detection of hydrogen peroxide in living cells. *Bioorg. Med. Chem. Lett.* **2008**, *18*, 5948.
23. Dickinson, B. C.; Chang, C. J. A Targetable Fluorescent Probe for Imaging Hydrogen Peroxide in the Mitochondria of Living Cells. *J. Am. Chem. Soc.* **2008**, *130*, 9638.
24. Dickinson, B. C.; Huynh, C.; Chang, C. J. A Palette of Fluorescent Probes with Varying Emission Colors for Imaging Hydrogen Peroxide Signaling in Living Cells. *J. Am. Chem. Soc.* **2010**, ASAP.
25. Güttinger, S.; Laurell, E.; Kutay, U. Orchestrating nuclear envelope disassembly and reassembly during mitosis. *Nat. Rev. Mol. Cell Biol.* **2009**, *10*, 178.
26. Tissenbaum, H. A.; Guarente, L. Increased dosage of a sir-2 gene extends lifespan in Caenorhabditis elegans. *Nature* **2001**, *410*, 227.
27. Chen, D.; Guarente, L. SIR2: a potential target for calorie restriction mimetics. *Trends Mol. Med.* **2007**, *13*, 64.
28. Chang, C. J.; Nolan, E. M.; Jaworski, J.; Okamoto, K. I.; Hayashi, Y.; Sheng, M.; Lippard, S. J. ZP8, a neuronal zinc sensor with improved dynamic range; imaging zinc in hippocampal slices with two-photon microscopy. *Inorg. Chem* **2004**, *43*, 6774.
29. Brenner, S. The genetics of Caenorhabditis elegans. *Genetics* **1974**, *77*, 71.

Chapter 4:

Nox2 Redox Signaling Maintains Essential Cell Populations in the Brain

Portions of this work were accepted for publication in the following scientific journal:

Dickinson, B. C.; Peltier, J.; Stone, D.; Schaffer, D.V.; Chang, C. J. "Nox2 Redox Signaling Matintains Essential Cell Populations in the Brain." *Nat. Chem. Biol.*

Portions of this work were performed in collaboration with the following persons:

RT-PCR was performed by Dr. Joeseph Peltier.
Animal work was performed with Dr. Joseph Peltier and Dr. Daniel Stone.

Abstract

Reactive oxygen species (ROS) are conventionally classified as toxic consequences of aerobic life, and the brain is particularly susceptible to ROS-induced oxidative stress and damage owing to its high energy and oxygen demands. In this context, NAPDH oxidases (Nox) are a widespread source of brain ROS implicated in seizures, stroke, and neurodegeneration. A physiological role for ROS generation in normal brain function has not been established, despite the fact that mice and humans lacking functional Nox proteins exhibit cognitive deficits. Using molecular imaging with Peroxyfluor-6 (PF6), a new selective fluorescent indicator for hydrogen peroxide (H_2O_2), we show that adult hippocampal stem/progenitor cells (AHPs) generate H_2O_2 through Nox2 to regulate intracellular growth signaling pathways, which in turn maintains their normal proliferation *in vitro* and *in vivo*. Our results challenge the traditional view that brain ROS are solely deleterious by demonstrating that controlled ROS chemistry is needed for maintaining specific cell populations.

Introduction

Aberrant accumulation of reactive oxygen species (ROS) over time can trigger oxidative stress and damage[1] of proteins, lipids, and nucleic acids that form the molecular underpinning of the free-radical theory of aging.[2] The brain is particularly sensitive to ROS damage owing to its high oxygen demand and low antioxidant capacity, and oxidative stress is connected to stroke and neurodegenerative diseases where age is a risk factor.[3] However, this organ also purposefully produces ROS throughout development and adult life, and a major source of brain ROS are the NAPDH oxidase enzymes (Nox) that are expressed throughout the central nervous system (CNS).[4,5] These membrane-spanning protein complexes generate hydrogen peroxide (H_2O_2) as their final chemical product by the direct two-electron reduction of molecular oxygen by NAPDH,[5,6] or through the one-electron reduction to superoxide ($O_2^{\cdot-}$) followed by conversion to H_2O_2.[4,5] The established physiological function for Nox proteins is in the immune system, where they participate in phagocytic killing of pathogen invaders.[5] More recently, however, the discovery of Nox enzymes in nonphagocytic cell types throughout the body[6,7] has greatly expanded the scope and potential roles for these complexes, and emerging data links their H_2O_2-producing activity to beneficial cell signaling events.[4-15]

The H_2O_2 generated from Nox proteins in the brain and CNS has been traditionally associated with stroke,[16] aging,[17] seizures,[18] and neurodegenerative Alzheimer's[19] and Parkinson's[20] diseases. However, the presence of these proteins in the brain and CNS throughout adult life presages a beneficial role for endogenous ROS production that remains insufficiently understood.[21] Along these lines, both mice and humans that lack functional Nox2 exhibit cognitive deficits,[22,23] most notably in learning and memory, suggesting a role for this Nox isoform within the hippocampus. In this context, a population of neural stem/progenitor cells reside within the dentate gyrus of the hippocampus and form new neural tissue in the adult brain that plays a role in memory formation.[24] We hypothesized that Nox-generated H_2O_2, which acts as a molecular signal for growth within cultured cell lines,[8,9] could help maintain the proliferation of these stem cell populations in the brain.

In this report, we show that H_2O_2 redox signaling derived from Nox2 is essential for normal growth and proliferation of neural stem cells *in vitro* and *in vivo*. Motivated by the dearth of chemical tools to selectively probe H_2O_2 production in cell types that would not be expected to produce high concentrations of this ROS, we developed Peroxyfluor-6 acetoxymethyl ester (PF6-

AM), a new chemoselective fluorescent indicator for H_2O_2 with improved sensitivity. This fluorescent probe features a boronate chemical switch that allows for selective detection of H_2O_2 over other ROS, combined with acetoxymethylester (AM) protected phenol and carboxylic acid groups for enhanced cellular retention and sensitivity. After validating that PF6 is more responsive than previous boronate H_2O_2 reporters, we use this new trappable probe to demonstrate that adult hippocampal stem/progenitor (AHP) cells produce H_2O_2 when stimulated with fibroblast growth factor 2 (FGF-2), a mitogen that regulates their proliferation.[25] We then show that endogenous H_2O_2 production is important for normal cell signaling through the kinase hub Akt and is mediated by the H_2O_2-producing enzyme Nox2. Moreover, RNAi knockdown of Nox2 in cell culture and gene knockout of Nox2 in mice abrogates normal Akt signaling and AHP function *in vitro* and *in vivo*. Our results highlight the utility of PF6-AM as a tool to help discover new redox chemistry in biological systems and provide evidence that the controlled production of H_2O_2 in the brain can be beneficial to its physiology.

Results

Synthesis and evaluation of Peroxyfluor-6 (PF6)

Redox signaling mediated by H_2O_2 has been studied primarily in proliferating cell culture models stimulated with mitogens.[9] As the majority of brain tissue is comprised of terminally differentiated cells, we turned our attention to AHPs, which grow and proliferate throughout development and adult life to feed into neuronal and glial populations. Accordingly, we first sought to test whether these neural stem cells produce endogenous H_2O_2 under growth conditions. In this regard, traditional methodologies for imaging H_2O_2 and related ROS in living cells typically utilize non-specific indicators that rely on general oxidation and therefore detect an assortment of oxidants.[26] Because neural tissue is highly susceptible to oxidative stress[1,2,21,27] the specific ROS that the AHPs come in contact with is a critical determinant of the ultimate downstream cellular responses. We have shown that the conversion of aryl boronates to phenols is a useful chemoselective methodology for the detection of H_2O_2 in biological systems.[28] The first generation of Peroxy dyes, exemplified by PF1 (Figure 4-6), possess two boronate protecting groups, which after reaction with two equivalents of H_2O_2, yield fluorescent products.[29-32] This initial work established that boronate cages offer a general motif for creating fluorescent indicators that can selectively image H_2O_2 over other biologically relevant ROS. Second generation boronate probes such as PG1 and MitoPY1 (Figure 4-6) utilize a single boronate deprotection to increase sensitivity and allow for detection of H_2O_2 generated in oxidative stress,[33] neurodegenerative disease,[34,35] immune,[36] and growth factor signaling models.[37,38] Unfortunately, these available boronate dyes were not sufficiently sensitive to visualize potential H_2O_2 production in AHPs after stimulation with the endogenous mitogen FGF-2 (Figure 4-7).

We sought to improve the sensitivity of boronate-based probes while maintaining their high selectivity for H_2O_2. Inspired by work showing that increasing cellular retention of fluorescent probes is a practical strategy to improve sensitivity,[39-43] we designed and synthesized PF6-AM, a carboxyfluorescein-based probe combining a boronate-masked phenol for H_2O_2 detection and AM groups to cap phenol and carboxylic acid functionalities for enhanced cellular retention (Scheme 4-1). Briefly, monotriflation of 6-carboxyfluorescein using stoichiometric *N*-phenyl bis(trifluoromethanesulfonamide) affords triflate **2** in 60% yield. Palladium-mediated borylation of **2** with cyclohexyl JohnPhos, bis(pinacolato)diboron, and diisopropylethylamine in

anhydrous 1,4-dioxane at room temperature provides PF6 in 80% yield. Finally, protection with bromomethyl acetate furnishes AM-ester protected PF6-AM. The lipophilic AM esters allow the probe to pass readily through cell membranes, where esterases can then deprotect the AM groups to reveal PF6, a dianionic form of the probe that is membrane impermeable and thus trapped inside the cell, where it can respond to changes in intracellular H_2O_2 levels. We reasoned that this trappable probe should have increased sensitivity owing to a combination of increased local concentration of probe substrate retained within cells as well as a decreased rate of deprotected probe product leaking out of cells. PF6 features two visible region absorptions (l_{abs} = 460 nm, e = 14,000 $M^{-1}cm^{-1}$; 370 nm, e = 10,000 $M^{-1}cm^{-1}$) and a weak emission (l_{em} = 530 nm, F = 0.10). Spectrophotometric studies confirm that PF6 responds to H_2O_2 by a turn-on fluorescence response and is selective for H_2O_2 over a host of other ROS oxidants (Figure 4-1a,b). Kinetics measurements of the H_2O_2-mediated boronate deprotection were performed under pseudo-first-order conditions (5 mM dye, 10 mM H_2O_2), giving an observed rate constant of k = 3.3(1) x 10^{-3} s^{-1}.

Validation of PF6 for molecular imaging in cell culture

With data characterizing the properties and H_2O_2-induced turn-on response of PF6 *in vitro*, we sought to evaluate its utility for molecular imaging in cell culture model systems. First, we assayed whether the AM ester cage groups were sufficient to increase retention of the probe within living cells. We utilized the boronate-based H_2O_2 probe Peroxy Green 1 (PG1), which is sensitive to signaling levels of H_2O_2 but does not possess esterase-cleavable groups, as a benchmark for these studies. PG1 and PF6 utilize the same excitation and emission wavelengths and exhibit similar emission characteristics, allowing for direct comparison of the uptake and retention these probes in cell culture by scanning confocal microscopy. After loading HeLa cells with either PG1 or PF6-AM, excess dye was thoroughly washed away. The cells were then imaged immediately after washing and visualized again after 10, 30, and 60 minutes (Figure 4-1c,d**)**. Cells loaded with PG1 show modest intracellular fluorescence immediately after washing, but the signal drops off markedly by the 10-minute time point. In contrast, cells loaded with PF6-AM exhibit intracellular fluorescence immediately after washing that is approximately twice as bright as PG1-loaded cells and maintain this emission intensity throughout the time course of the measurements. A similar trend is observed in analogous experiments using HEK 293 cells (Figure 4-8).

We next established whether this increased cellular uptake and retention would permit PF6 to detect low levels of H_2O_2 in live samples. HeLa cells were loaded with PF6-AM and then stimulated with either 10 μM H_2O_2 or carrier for 30 minutes (Figure 4-1e,f). Cells treated with H_2O_2 show increased intracellular fluorescence compared to control samples, even at this relatively low level of exogenously added H_2O_2. Similar results are seen in HEK 293 cells (Figure 4-8). A drawback to this approach is the probe is not retained after fixation, making it incompatible with immunostaining in fixed cell and tissue samples. Future synthetic directions include enhancing the photostability of these dyes, adding functional groups that allow for maintenance of the probe upon fixation, and expanding the color palette of trappable H_2O_2 probes for multicolor imaging experiments. Nevertheless, these experiments confirm that PF6 is a selective and sensitive reporter for intracellular H_2O_2 in live cells and further validate the strategy of increased cellular uptake and retention as a general method for increasing the sensitivity of small-molecule fluorescent probes. In this context, PF6 adds a H_2O_2-specific fluorescent probe with selectivity and sensitivity to signaling levels of this oxygen metabolite to

the arsenal of currently available ROS probes, including those for general oxidants[44] and superoxide[35,45].

PF6 reveals that AHPs produce H_2O_2 upon FGF stimulation

After validation of PF6 in model systems, we sought to apply this new tool to the study of AHP cells. To this end, AHPs were isolated from the hippocampi of 6-week-old female Fisher 344 rats as previously described[25]. After growth factor withdrawal, AHPs were loaded with PF6-AM and treated with either FGF-2 mitogen or carrier. Cells stimulated with FGF-2 show increased intracellular fluorescence compared to unstimulated control AHPs as shown by PF6 imaging (Figure 4-2, 4-12). Toxicity studies demonstrate that PF6-AM is non-toxic at the concentration utilized in this study (Figures 4-9, 4-10). When coupled with the *in vitro* selectivity characterization of PF6, these data indicate that FGF-2 induces the endogenous production of H_2O_2 in AHPs. Furthermore, these data illustrate the utility of this new chemical tool for detecting changes in low levels of H_2O_2 in live-cell settings. Intrigued at that finding that AHPs, an essential cell population of the central nervous system from development throughout adult life, produce a compound known to have potential toxic consequences in the brain,[46] we next turned our attention to elucidating potential roles for H_2O_2 in physiological (rather than pathological) processes of these cells.

H_2O_2 is required for growth signaling in AHPs

With molecular imaging data establishing that AHPs produce H_2O_2 upon mitogen stimulation, we then probed whether FGF-2-induced H_2O_2 generation could influence downstream cell signaling cascades. In this regard, an intriguing relationship has emerged between endogenous H_2O_2 production and PI3-kinase-dependent (PI3K) activation of the kinase Akt, a signaling pathway that has several potentially redox-regulated components. For example, previous studies have demonstrated that PTEN, a phosphatase that opposes forward PI3K signaling, contains a catalytic active site residue Cys-124 that is reversibly oxidized by H_2O_2 to form a disulfide with Cys-71. This oxidative redox switch turns off the activity of the phosphatase, allowing the PI3K/Akt signaling cascade to propagate forward; re-reduction of this disulfide to the corresponding thiols restores PTEN phosphatase activity, resetting the cycle.[47] The PI3K-dependent activatpion of Akt is critical for the growth and proliferation of AHPs, as previous studies using either pharmacological inhibition of Akt or the expression of a dominant negative Akt inhibited their proliferation.[48] Accordingly, we first investigated the effects of exogenous H_2O_2 addition to AHPs by monitoring the phosphorylation status of Akt. Toxicity studies demonstrate that AHPs can withstand H_2O_2 to surprisingly high concentrations (Figure 4-11). Treatment of AHPs with H_2O_2 in the absence of FGF-2 stimulation is sufficient to trigger a marked dose-dependent increase in phospho-Akt, without increasing the phosphorylation status of another major signaling hub, the MAP kinase ERK1/2 (Figure 4-3a, 4-13). Previous work has shown that pharmological inhibition of the ERK1/2 MAP kinase pathway does not strongly affect AHP proliferation.[48]

We then probed the role of endogenously produced H_2O_2 on the phosphorylation status of Akt. FGF-2 stimulation of AHPs triggers a time dependent increase in the phosphorylation of Akt compared to control samples. In contrast, cells expressing Catalase, an enzyme that quickly destroys H_2O_2, have diminished FGF-2-induced phosphorylation of Akt (Figure 4-3b) and produce less detectable H_2O_2 by PF6-AM imaging (Figure 4-2b, 4-12). Additionally, pretreatment with the general antioxidant *N*-acetylcysteine (NAC), which will quench H_2O_2, or

the flavin/Nox inhibitor diphenyliodonium (DPI), which inhibits the majority of potential intracellular sources of H_2O_2, both block the FGF-2-induced phosphorylation of Akt, as well as affect the phosphorylation of ERK1/2 to a lesser extent (Figure 3c). To confirm that DPI at this concentration is concomitantly blocking the H_2O_2 signal and Akt phosphorylation, pretreatment of PF6-AM-loaded AHPs with DPI was shown to abolish FGF-2-induced H_2O_2 production (Figure 4-2a, 4-12). These experiments demonstrate that AHPs utilize redox chemistry to modulate this growth-signaling kinase pathway. We then attempted to identify potential targets of the H_2O_2 along the Akt pathway. We utilized a methodology for assaying the oxidation status of PTEN that relies on differences in gel mobility between the oxidized, disulfide form and the reduced form of the protein[49] to demonstrate that FGF stimulation does indeed produce a small but detectable amount of oxidized PTEN (Figure 4-14). However, this approach toward assaying the oxidation state of PTEN is not very sensitive or consistent in this system, which is why we continued to monitor Akt phosphorylation, a much more reliable readout of redox signaling.

Nox2 is the source of H_2O_2-mediated signaling in AHPs

We next elucidated the molecular source of the redox signal within the AHPs. Given the vast expression of Nox2 in the CNS,[21] we looked to this protein as a potential redox modulator in AHPs. Both RT-PCR (Figure 4-3d) and western blot analysis using two separate Nox2 antibodies, a rabbit and a mouse (Figure 4-3e), confirm its presence in AHPs. Both antibodies show a band at the same molecular weight that corresponds to the approximate molecular weight of Nox2 (c.a. 65 kDa) and whose intensity selectively decreases upon genetic manipulation with Nox2-targeted shRNA. The mouse antibody has a nonspecific band slightly below the Nox2 band that does not change upon treatment with Nox2 shRNA, which can serve as a loading control. We utilized genetic manipulation of Nox2 to elucidate the contributions of this protein to Akt proliferation/signaling pathways as well as the fluorescent signal measured by PF6-AM. AHPs transfected with Nox2-targeted shRNA exhibit decreased Nox2 levels and show a concomitant marked decrease in FGF-2-induced phosphorylation of Akt compared to control cells transfected with an empty vector (Figure 4-3f). As was observed for chemical inhibition by NAC or DPI, the ERK1/2 pathway in AHPs also appears to be affected by the lack of Nox2. AHPs transfected with Nox2-targeted shRNA also show less H_2O_2 production in response to FGF-2 stimulation (Figure 4-2c, 4-12). As a further validation of the shRNA knockdown experiments, we designed and tested another shRNA construct to target an alternative member of the Nox family, Nox3. Again, Nox2-shRNA transfected cells show reduced levels of Nox2 compared to Nox3-shRNA transfected cells and concomitantly exhibit a decreased response to FGF-2-induced phospho-Akt production (Fig. 4-3g), confirming the specific effects of the Nox2 shRNA. Taken together, these data demonstrate that Nox2-generated H_2O_2 contributes to the regulation of growth-signaling pathways within the AHPs.

Nox2 is required for normal AHP proliferation *in vitro*

With data establishing that intracellular redox changes affect signaling at the protein level, we then sought to determine whether decreased redox signaling would also manifest similar results in functional assays. We therefore investigated the effects of diminished redox signaling on AHP proliferation in the presence of FGF-2. First, 5-day *in vitro* proliferation experiments were performed in the presence of varying levels of DPI. We observed a dose-dependent decrease in growth rate with DPI inhibition, with concentrations as low as 50 nM having an inhibitory effect (Figure 4-4a). As DPI is relatively non-specific and will block all

flavin-containing sources of ROS, we sought to elucidate the role of Nox2 specifically. We therefore transfected AHPs with shRNA constructs targeting Nox2 or the empty vector. In agreement with the chemical inhibition experiments and western blot analysis, the Nox2 shRNA transfected cells show a diminished proliferation rate compared to AHPs containing the empty vector (Figure 4-4b), or compared to cells expressing Nox3 shRNA as a control (Figure 4-4c). Taken together, these data indicate that FGF-2 signaling involves the production of H_2O_2 through the activation of Nox2, which influences signaling through Akt and ultimately the downstream phenotype of growth rate.

Nox2 is required for normal AHP function *in vivo*

We then sought to extend these *in vitro* findings to an *in vivo* system. To this end, we performed bromodeoxyuridine (BrdU) incorporation experiments in Nox2 knockout (Nox2-/-) mice and CL57BL/6J control mice. BrdU incorporates into the genome of dividing cells, which can then be detected by immunohistochemistry post fixation along with stem cell or neuronal markers. Therefore, cells that stain for both BrdU as well as a stem cell marker are AHPs that proliferated during the course of the injections. Mice were injected with BrdU daily for 7 days and perfused 24 h after the final injection. Immunohistochemical assessments of the dentate gyri from Nox2-/- and control mice show no morphological abnormalities (Figure 4-4d,e), suggesting that the dentate gyrus develops normally in the Nox2-/- mice. However, quantification of the proliferating AHP populations based on colocalization of BrdU and Sox2, a stem cell marker,[50] reveals a marked decrease in the number of proliferating AHPs in the Nox2-/- mice (Figure 4f-h), establishing that Nox2 contributes to the normal proliferation of AHPs *in vivo*.

Finally, we assayed the effects of Nox2 deficiency on adult neurogenesis *in vivo*. For these experiments mice were injected with BrdU daily for 7 days and were then perfused 28 days after the final injection. The brains were then analyzed for cells that stain for both BrdU and NeuN, a neuronal marker, which would indicate neurons that had differentiated from AHPs within the time course of the experiment. Quantification of the colocalization of BrdU and NeuN reveals a reduction in the number of newborn neurons in the Nox2-/- mice (Figure 4i-k), establishing that Nox2 also contributes to adult neurogenesis *in vivo*.

Discussion

H_2O_2 is emerging as a newly recognized messenger for cell signaling, and a major source of peroxide produced through stimulation of various cell surface receptors is the Nox family of proteins[5,9,10,26]. These ROS-generating enzymes are classically associated with phagocytic cells during immune responses, where they are used to combat pathogens by attacking them with controlled oxidative bursts. More recent results have revealed the widespread distribution of Nox complexes in non-phagocytic cell types throughout the body[5], presaging that H_2O_2 generation is a necessary component for physiological purposes; however, many aspects of how and why this small-molecule oxidant is required and used for the benefit of living organisms remain elusive. To address these questions, we developed a novel H_2O_2-specific fluorescent probe, PF6, and applied this new chemical tool to help demonstrate that AHPs, an essential population of cells that proliferate in the brain from development throughout adult life, respond to growth conditions by producing H_2O_2. Through a combination of imaging, pharmacological, and genetic experiments, we reveal that Nox2 and H_2O_2 are important for maintaining normal signaling and proliferation of AHPs *in vitro*. Moreover, we show that mice lacking functional Nox2 have a

decreased number of proliferating neural stem cells and less adult neurogenesis in the hippocampus, which establishes that H_2O_2-mediated redox signaling is essential on the whole organism scale.

The collective data provide a molecular model for the cognitive deficits observed in mice and humans lacking the ROS-generating Nox2 enzyme (Figure 4-5) and establish that ROS are not exclusively detrimental to brain tissue in the context of seizures, stroke, and neurodegeneration. Since various isoforms of the Nox family are present throughout the brain and CNS,[4] there are likely many other beneficial roles for these ROS-producing proteins in this system. Indeed, the *in vivo* effects observed in the Nox2 knockout mice could also be influenced by a lack of Nox2 in other cell types within brain. In a broader sense, our findings show that controlled ROS production and signaling can be used as a strategy for maintaining proliferation of essential cell populations in the body. Finally, these results suggest caution when applying antioxidant therapeutics in a non-specific fashion, as ROS production can be a necessary component for the fitness of a given system.

Materials and Methods

Synthetic Materials and Methods. Silica gel P60 (SiliCycle) was used for column chromatography. Analytical thin layer chromatography was performed using SiliCycle 60 F254 silica gel (precoated sheets, 0.25 mm thick). All chemicals were purchased from Sigma-Aldrich (St. Louis, MO) and used as received. 6-Carboxyfluorescein was synthesized according to literature methods.[51] ^{1}H NMR, ^{13}C NMR, and ^{19}F NMR spectra were collected in 20:1 $CDCl_3/CD_3OD$, 9:1 $CDCl_3/CD_3OD$, or $(CD_3)_2O$ (Cambridge Isotope Laboratories, Cambridge, MA) at 25 ºC using a Bruker AVQ-400 or DRX-500 spectrometer at the College of Chemistry NMR Facility at the University of California, Berkeley. All chemical shifts are reported in the standard δ notation of parts per million using the peak of residual proton signals of $CDCl_3$ or $(CD_3)_2O$ as an internal reference. High-resolution mass spectral analyses were carried out at the College of Chemistry Mass Spectrometry Facility at the University of California, Berkeley. Low-resolution mass spectral analyses were carried out on an Agilent 6130 LC/MS system (Santa Clara, CA).

6-Carboxyfluorescein monotriflate (2). 6-Carboxyfluorescein (512 mg, 1.36 mmol) was added to a vial and dissolved in 15 mL of 2:1 acetonitrile/DMF. Diisopropylethylamine (2.2 mL, 13.3 mmol) was then added and the reaction stirred for 10 min. *N*-Phenyl bis(trifluoromethanesulfonamide) (487 mg, 1.36 mmol) was then added and the reaction was stirred overnight at room temperature. The reaction mixture was then dried under reduced pressure. Purification by column chromatography (19:1 dichloromethane/methanol) afforded compound **2** as a yellow oil (412 mg, 60% yield). ^{1}H NMR ($CDCl_3$ /10% CD_3OD, 400 MHz): δ 8.26 (1H, d, J = 8.0 Hz), 8.02 (1H, d, J = 8.2 Hz), 7.77 (1H, s), 7.19 (1H, d, J = 2.4 Hz), 6.90 (1H, dd, J = 2.4, 8.8 Hz), 6.82 (1H, d, J = 8.8 Hz), 6.76 (1H, d, J = 2.4 Hz), 6.59 (1H, dd, J = 2.4, 8.8 Hz), 6.54 (1H, d, J = 8.8Hz). ^{13}C NMR ($CDCl_3$ /10% CD_3OD, 100 MHz): δ 168.6, 159.8, 152.5, 152.1, 151.8, 150.0, 138.4, 131.5, 130.0, 129.1, 128.9, 125.3, 125.1, 119.2, 116.5, 113.4, 110.5, 108.5, 103.0, 82.5. ^{19}F NMR ($CDCl_3$ /10% CD_3OD, 376.5 MHz): δ -71.97. HR-FABMS: calculated for [M^+] 509.0149, found 509.0158.

PF6/PF6-AM (3/4). Compound **2** (412 mg, 0.81 mmol), $Pd(OAc)_2$ (55 mg, 0.081 mmol), Bis(pinacolato)diboron (308 mg, 1.22 mmol), Cyclohexyl JohnPhos (114 mg, 0.32 mmol),

diisopropylethylamine (594 mg, 4.63 mmol), and 5 mL of dioxane were added to a vial in an inert atmosphere glove box and the reaction was stirred overnight at room temperature. The vial was then brought out of the glove box and the contents were evaporated to dryness. Purification by column chromatography (19:1 dichloromethane/methanol) furnished **PF6** as a yellow solid (317 mg, 80% yield). ^{1}H NMR ($CDCl_3$ /5% CD_3OD, 400 MHz): δ 8.26 (1H, d, *J* = 8.0 Hz), 8.06 (1H, d, *J* = 8.0 Hz), 7.78 (1H, s), 7.71 (1H, s), 7.39 (1H, d, *J* = 8.0 Hz), 6.72-6.76 (2H, m), 6.58 (1H, d, *J* = 8.8 Hz), 6.53 (1H, dd, *J* = 2.4, 8.8 Hz), 1.32 (12H, s). ^{13}C NMR ($CDCl_3$ /10% CD_3OD, 100 MHz): δ 169.1, 167.5, 159.1, 153.5, 152.3, 150.7, 136.9, 131.3, 129.7, 129.2, 129.0, 127.1, 125.5, 125.1, 123.6, 120.7, 112.6, 109.2, 103.1, 20.7. HR-FABMS: calculated for [M^+] 487.1559, found 487.1567. **PF6** (40 mg, 0.08 mmol), bromomethyl acetate (51 mg, 0.33 mmol), diisopropylethylamine (32 mg, 0.25 mmol), and 1 mL of DMF added to a vial and stirred at room temperature overnight. The reaction mixture was then extracted into dichloromethane, washed three times with water, washed once with brine, dried over magnesium sulfate, and dried under reduced pressure. Purification by column chromatography (7:3 ethyl acetate/hexanes) delivered **PF6-AM** as a white solid (11 mg, 22% yield). ^{1}H NMR ((CD_3)$_2$O, 500 MHz): δ 7.99-8.06 (1H, m), 7.81 (1H, t, *J* = 6.0 Hz), 7.72-7.79 (1H, m), 7.66 (1H, s), 7.43-7.50 (1H, m), 7.26-7.31 (1H, m), 6.97-7.10 (1H, m), 6.87-6.95 (1H, m), 6.81-6.88 (1H, m), 5.30-6.00 (4H, m), 2.01-2.11 (6H, m), 1.34 (12H, m). HR-FABMS: calculated for [M^+] 631.1981, found 631.1979.

Cell Culture. AHPs were cultured on tissue culture polystyrene coated with poly-ornithine and 5 μg/mL of laminin (Invitrogen) and grown in Dulbecco's modified Eagle medium (DMEM)/F-12 (1:1) high-glucose medium (Invitrogen) containing N-2 supplement (Invitrogen) and 20 ng/mL recombinant human FGF-2 (Peprotech). For FGF starvation, AHPs were washed once with (DMEM)/F-12 (1:1) high-glucose medium, and then placed in (DMEM)/F-12 (1:1) high-glucose medium without FGF for 12-16 hours.

AHP Fluorescence Imaging Experiments. Confocal fluorescence imaging studies on AHPS were performed with a Zeiss LSM510 NLO Axiovert 200 laser scanning inverted microscope and a 40x oil-immersion objective lens. Excitation of PF6-AM-loaded AHPs at 488 nm was carried out with an Ar laser and emission was collected using a 500-550 nm filter set. AHPs were incubated with 5 μM PF6-AM in DMEM/F12 + N-2 for 30 minutes at 37 ºC. The cells were then washed with fresh DMEM/F12 + N-2 twice. The cells were then incubated in DMEM/F12 + N-2 either with or without 20 ng/mL FGF-2 for 30 minutes, then imaged. For the DPI inhibited cells, 5 μM DPI was included in the DMEM/F12 + N-2 media for all incubations. Image analysis was performed in ImageJ (Wayne Rasband, NIH) with at least 10 cells counted per field in 4 separate fields for each condition.

Stock Solutions. DPI (Sigma) stock solutions were made at a concentration of 5 mM in DMSO. NAC (Sigma) stocks were made at a concentration of 250 mM in DMEM/F12 + N-2. PG1, PF6, and PF6-AM stocks were made at a concentration of 5 mM in DMSO. H_2O_2 stock solutions were made at a concentration of 100 mM in Millipore water.

Spectroscopic Materials and Methods. Millipore water was used to prepare all aqueous solutions. All spectroscopic measurements were performed in 20 mM HEPES buffer, pH 7. Absorption spectra were recorded using a Varian Cary 50 spectrophotometer (Walnut Creek, CA) and fluorescence spectra were recorded on a Photon Technology International Quanta Master 4 L-format scanning spectrofluorometer (Lawrenceville, NJ) equipped with an LPS-220B 75-W xenon lamp and power supply, A-1010B lamp housing with integrated igniter, switchable

814 photon-counting/analog photomultiplier detection unit, and MD5020 motor driver. Samples for absorption and emission measurements were contained in 1-cm x 1-cm quartz cuvettes (1.5-mL volume, Starna, Atascadero, CA). Fluorescence quantum yields were determined by reference to rhodamine B in water (quantum yield $\Phi = 0.31$).

Comparison of PG1 and PF6-AM in cell culture. Confocal fluorescence imaging studies were performed with a Zeiss LSM510 NLO Axiovert 200 laser scanning microscope and a 40x Achroplan IR water-immersion objective lens. Excitation of PG1- or PF6-AM-loaded cells at 488 nm was carried out with an Ar laser and emission was collected using a META detector between 501 - 554 nm. HEK 293 cells were cultured in DMEM (Invitrogen) supplemented with 10% fetal bovine serum (FBS, Hyclone) and glutamine (2 mM). HeLa cells were cultured in DMEM with high glucose, glutamax, and 10% FBS. Two days before imaging, cells were passaged and plated on 18-mm glass coverslips. Solutions of dyes were made in DBPS with calcium chloride and magnesium chloride (Sigma). For washout experiments, the cells were washed twice with fresh DPBS. H_2O_2 was added by bath application to the medium. Identical microscope settings were utilized for all imaging and PG1 and PF6-AM-loaded cells were imaged side-by-side in simultaneous experiments. For data analysis, the average fluorescence intensity per image in each experimental condition was obtained. The background was then subtracted from each intensity and the data normalized to the brightest condition of each experiment. Analyses were performed in ImageJ (Wayne Rasband, NIH).

Flow cytometry evaluation of cell viability. AHPs were passaged and suspended at a concentration of 1 x 10^6 cells/mL. The cells were then aliquoted out into microcentrifuge tubes at 2 x 10^5 cells per tube. The cells were then treated with either H_2O_2 of PF6-AM and incubated at 37 °C for the indicated times. For the final 15 min of incubation, 3 μM propidium iodide (PI) was added to each tube from a 1.5 mM stock. The cells were then analyzed on an LSR Fortessa cell analyzer (BD Biosciences, Franklin Lakes, NJ). The instrument settings were calibrated using ethanol-treated AHPs as a positive control. Briefly, 5 x 10^5 cells were pelleted by centrifugation and then resuspended in 1 mL phosphate-buffered saline (PBS). The cells were then transferred into 4 mL absolute ethanol at -20 °C while vortexing. The mixture was then incubated at -20 °C for 10 min, then pelleted by centrifugation. The cells were resuspended in PBS for 15 min at RT to rehydrate, pelleted by centrifugation, and resuspended in 200 μL of Tris buffer (100 mM Tris, pH 7.4, 100 mM NaCl, 0.5 mM $CaCl_2$, 0.5 mM $MgCl_2$, 0.1% Nonidet P-40) with 3 μM PI.

Trypan blue evaluation of cell viability. AHPs were passaged and resuspended at a concentration of 1 x 10^6 cells/mL. The cells were then aliquoted into microcentrifuge tubes at 2 x 10^5 cells per tube. The cells were then either treated with DMSO carrier of PF6-AM at the indicated concentrations and incubated at 37 °C for 1 hour. The cell suspensions were then mixed with an equal volume of trypan blue solution (0.4% w/v) for 3 min. The cells were then analyzed with a hemacytometer by counting under a microscope.

Western Blotting. Cells were lysed with RIPA buffer (50 mM Tris, pH 7.4, 150 mM NaCl, 1% Triton X-100, 0.5% sodium deoxycholate, and 0.1% SDS) supplemented with protease inhibitors (Roche Complete MiniTab) and 2 mM Na_3VO_4 for 30 minutes on ice, and clarified by centrifugation at 13.2 x 10^3 rpm for 10 minutes at 4 °C. The protein concentration was determined by BCA assay (Pierce), and then 4x Laemmli buffer (0.25 mM Tris, 2% SDS, 40% glycerol, 20% beta-mercaptoethanol, 0.04% bromophenol blue) was added, the samples were

denatured at 90 °C for 5 minutes, and equal amounts of total protein were loaded onto 12% SDS-PAGE gels. Proteins were transferred to PVDF membranes (Immobilon, Millipore) and incubated overnight at 4 °C in 5% non-fat dry milk in wash buffer (10 mM Tris, pH 7.5, 100 mM NaCl, 0.1% Tween-20) with 1:1000 primary antibodies (rabbit anti-pAkt1/2/3, rabbit anti-Akt1/2/3, mouse anti-pERK1/2, rabbit anti-ERK1, goat anti-catalase, goat anti-mouse IgG-HRP, goat anti-rabbit IgG-HRP, mouse anti-PTEN, and donkey anti-goat IgG-HRP from Santa Cruz Biotechnology; mouse anti-actin from Millipore, mouse monoclonal anti-Nox2 and rabbit polyclonal anti-Nox2 were a gift from Mark Quinn). Membranes were washed 5 times for 5 minutes in wash buffer, incubated for 1 hour at room temperature with 1:2000 secondary antibody (HRP conjugates, Santa Cruz Biotechnology) in 5% non-fat dry milk in wash buffer, washed 5 times for 5 minutes in wash buffer, and then visualized using enhanced chemiluminescence (Western Lightning, Perkin-Elmer) recorded on a BioRad GelDoc imaging station. Blots were stripped by incubating in pH 6.8 Tris with 2% SDS and 100 mM beta-mercaptoethanol at 55 °C for 17 minutes, washed three times with wash buffer, then reprobed as above.

RT-PCR. AHP RNA was isolated by Trizol (Invitrogen) according to manufacturer's instructions, and cDNAs were then generated using Thermoscript RT-PCR kit (Invitrogen) according to manufacturer's instructions. PCR was performed for Nox2 with the 18S ribosomal subunit as an internal control. Nox2 expected amplicon: 165 base pairs. 18S expected amplicon: 150 base pairs. Bands were excised and confirmed by sequence analysis. All bands are from the same gel, but intervening lanes have been removed for clarity. Primer sequences were as follows:

NOX2:	TTGCCATCCATGGAGCTGA
	CTATCCATTTCCAAGTCATAGGAGG
18S:	GTAACCCGTTGAACCCCATTC
	CCATCCAATCGGTAGTAGCGA

shRNA and Transfection. *Mus musculus* Catalase was obtained from Origene in a pCMV6 vector. A previously verified shRNA construct directed against rat Nox2 (NM_023965)[52] or a new construct directed against rat Nox3 (AY573239) were designed and verified using OligoEngine design tools and incorporated into a pSuper.retro.neo.GFP (for cell signaling and growth assays) or a pSuper.retro.neo.mCherry (for H_2O_2 imaging experiment) vector according to the manufacturer's instructions.

Rat Nox2 370: 5' GAGTGGTGTGTGAATGCCAGA 3'
Rat Nox3 578: 5' GTTTATCAGGCAGTCCTCT 3'

AHPs were transfected using the Nucleofector II device (Lonza) following the manufacturer's instructions using program A-33 and allowed to grow for 24 hours after transfection prior to replating for imaging, western blot analysis, or growth assays.

***In vitro* Growth Assays**. For DPI growth assays, AHPs were plated at low density (1000 cells/well) on 96-well poly-ornithine/laminin-coated tissue culture plates with 20 ng/mL FGF-2 in the presence of DPI or control carrier (DMSO). Fifty percent media changes were conducted daily with media containing 20 ng/mL FGF-2. After 5 days in culture the cell numbers were quantified using the WST-1 assay (Roche) and utilizing a standard growth curve generated with known cell numbers. For shRNA growth assays, AHPs were transfected as above, allowed to grow for 24 hours, then plated at 40,000 cells per well in 24-well poly-ornithine/laminin-coated tissue culture plates containing 20 ng/mL FGF-2. Fifty percent media changes were conducted daily with media containing 20 ng/mL FGF-2. After 5 days in cell culture, the cells were

removed with Accutase and cell numbers were quantified using a hemacytometer. Cells for H_2O_2 stimulations and DPI growth assays were grown in homemade incubators[53] under an atmosphere of 2% O_2 / 5% CO_2 / 94% N_2.

***In vivo* BrdU Assays**. All animal protocols were approved by the University of California, Berkeley Animal Care and Use Committee and conducted in accordance with National Institutes of Health guidelines. Eight week-old matched control (C57BL/6J) or Nox2-/- (B6.129S6-*Cybb*^{tm1Din}/J, The Jackson Laboratory, Bar Harbor, Maine) mice were injected intraperitoneally once daily for 7 days with either saline or BrdU resuspended in 0.9% saline (50 μg per g body weight) in a total volume of 100 μL. The mice were perfused transcardially with 0.9% saline followed by 4% PFA either 8 or 35 days after the start of the BrdU injections. The brains were then post-fixed overnight in 4% PFA at 4 °C, rinsed with PBS, transferred to 30% sucrose at 4 °C for three days, and then sectioned at 40 μm with a freezing microtome. Every fourth coronal section of the hippocampus was evaluated after immunostaining for NeuN (Mouse, 1:100, Millipore) and BrdU (Rat, 1:100, Abcam) for the 35-day experiments, or NeuN, BrdU, and Sox2 (Y-17, Goat, 1:100, Santa Cruz) for the 8-day experiments. Sections were processed for BrdU staining as previously described.[54] Confocal fluorescence slices were analyzed using a Zeiss LSM510 NLO Axiovert 200 laser scanning microscope and a Plan-Neofluar 40x oil-immersion objective lens utilizing confocal slices less than 1 μm. Both dentate gyri of each section were fully counted for the number of cells colabeled for both BrdU and Sox2.

Figures and Schemes

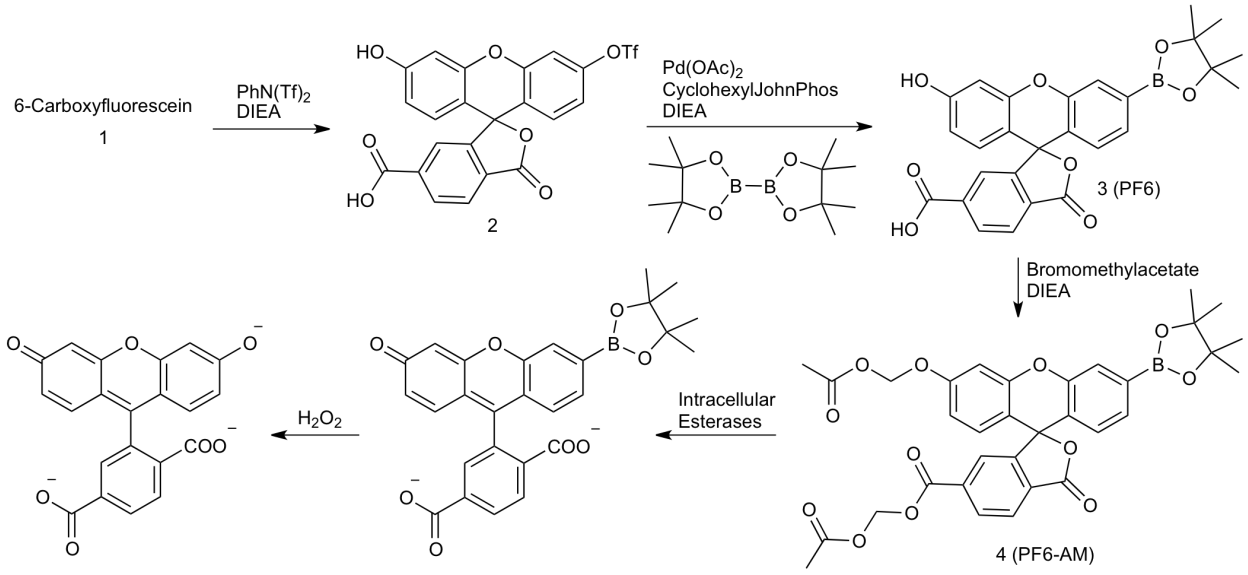

Scheme 4-1. Design and synthesis of Peroxyfluor-6 Acetoxymethyl Ester, PF6-AM.

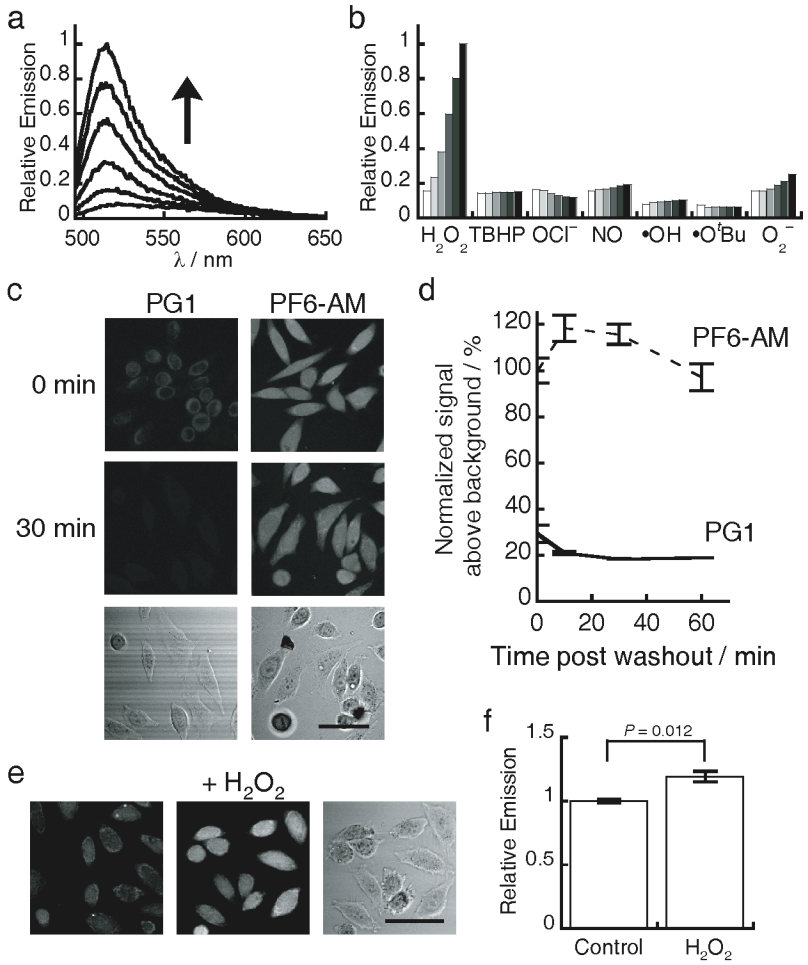

Figure 4-1. Spectroscopic characterization and cell culture validation of PF6-AM. **(a)** Fluorescence turn-on response of 5 mM PF6 at 0, 5, 15, 30, 45, and 60 minutes after the addition of 100 mM H_2O_2. **(b)** Fluorescence responses of 5 mM PF6 to various reactive oxygen species (ROS). Bars represent relative responses at 0, 5, 15, 30, 45, and 60 min after addition of each ROS. Data shown are for 10 mM O_2^- (with 10 mM Catalase), 200 mM NO, and 100 mM for all other ROS. **(c)** HeLa cells were loaded with either 5 μM PG1 or 5 μM PF6-AM for 15 minutes, then washed twice with DPBS and imaged at 0, 10, 30 and 60 minutes post dye washing. **(d)** Quantification of the experiment as conducted in (c). **(e)** HeLa cells were loaded with 5 μM PF6-AM for 15 minutes, stimulated with either water carrier or 10 μM H_2O_2 for 30 minutes, and imaged. **(f)** Quantification of the experiment as conducted in (e). Statistical analyses were performed with a two-tailed Student's *t*-test and error bars are ± s.e.m. 50 μm scale bars are shown.

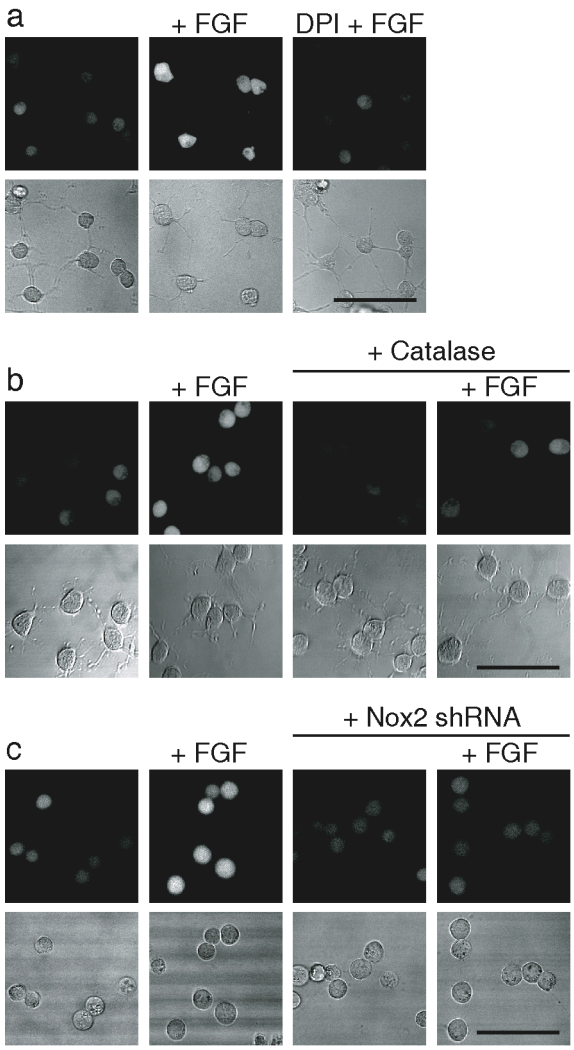

Figure 4-2. Application of PF6 to demonstrate that adult hippocampal stem/progenitor cells (AHPs) produce H_2O_2 upon FGF-2 stimulation. **(a)** After FGF-2 starvation, AHPs were loaded with 5 mM PF6-AM for 30 minutes, stimulated with 20 ng/mL FGF-2 or media for 30 minutes, and then imaged. For DPI treatment, cells were preincubated in media containing 5 mM DPI before FGF-2 stimulation. **(b)** AHPs were transfected with either Catalase or control vector and treated as in (a). **(c)** AHPs were transfected with either Nox2-shRNA or control vector and treated as in (a). Brightfield images are shown for each representative image with a 50 μm scale bar.

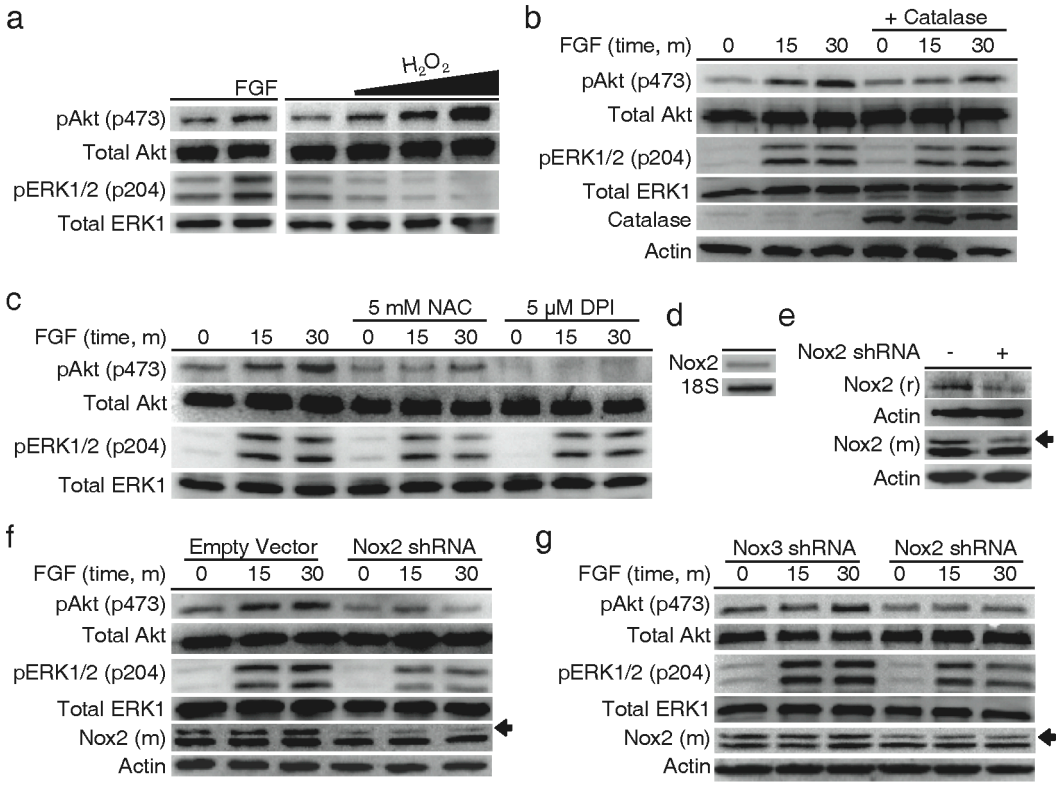

Figure 4-3. Cellular redox status affects AHP growth signaling. (**a**) After FGF-2 starvation, AHPs were stimulated with vehicle control (buffer), 20 ng/mL FGF-2, 300, 500, or 1000 mM H_2O_2 for 30 min. **(b)** AHPs transfected with either Catalase or a control vector. After FGF-2 starvation, AHPs were stimulated with 20 ng/mL and lysed at the given time points. **(c)** After FGF-2 starvation, AHPs were incubated with NAC, DPI, or vehicle control (DMSO) for 40 minutes, then stimulated with 20 ng/mL FGF-2 and lysed at the given time points. **(d)** Nox2 mRNA detection in AHPs measured by RT-PCR. **(e)** Nox2 expression of AHP whole cell extracts transfected with either Nox2 shRNA or an empty vector as measured by western blot analysis using either a mouse monoclonal (m) or a rabbit polyclonal (r) Nox2 antibody, followed by stripping and reprobing for actin as a loading control. An arrow shows the band in the Nox2 monoclonal antibody blot that matches the band in the Nox2 polyclonal blot, which corresponds to the molecular weight of Nox2. **(f)** AHPs transfected with either Nox2 shRNA or the empty vector. **(g)** AHPs transfected with either Nox2 shRNA or Nox3 shRNA. After 12 hour FGF-2 starvation, AHPs were stimulated with 20 ng/mL and lysed at the given time points. phospho-Akt, phospho-ERK, or mouse monoclonal Nox2 were measured by western blot analysis of whole cell extracts, and blots were stripped and reprobed for total protein or actin as loading controls.

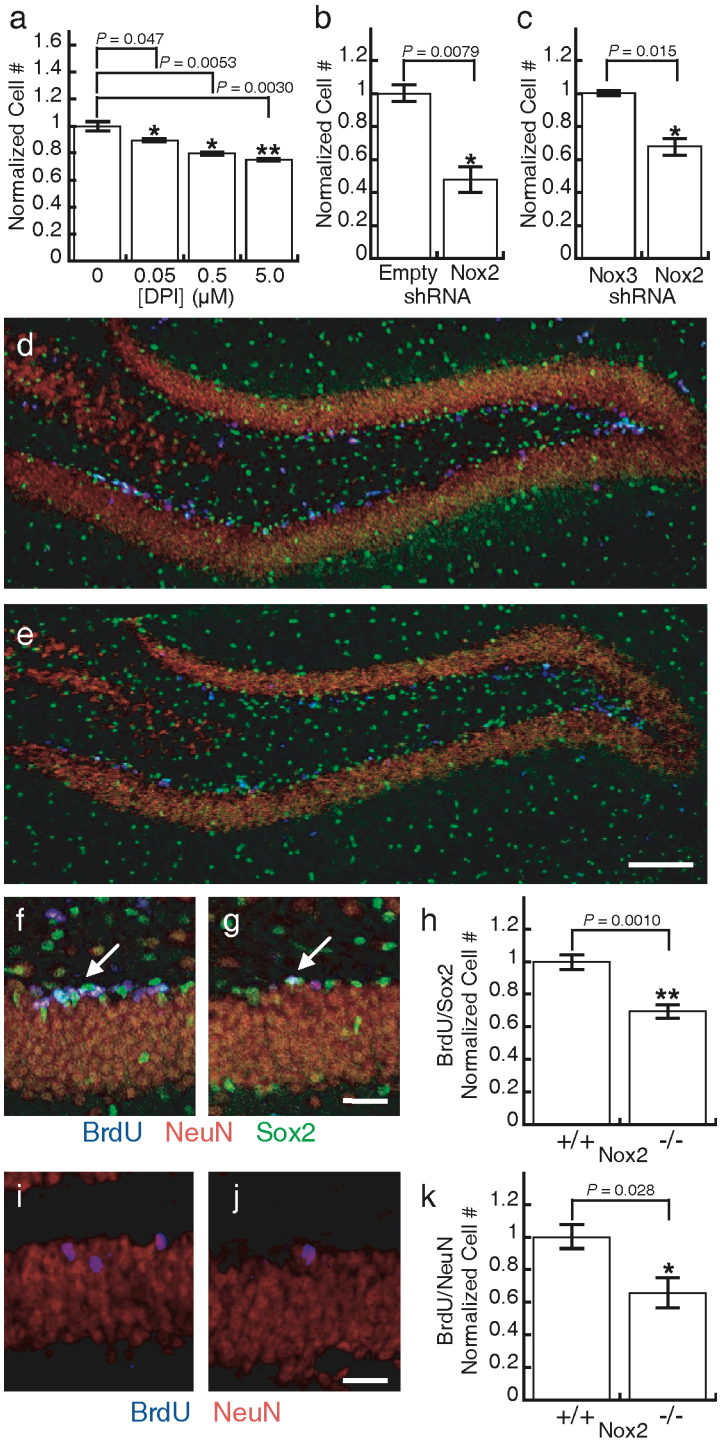

Figure 4-4. Nox2 is essential for normal proliferation of AHPs *in vitro* and *in vivo*. **(a)** 5-day growth assay of AHPs grown in the presence of FGF and varying concentrations of DPI (n = 4). **(b)** 5-day growth assay of AHPs transfected with either Nox2 shRNA or the empty vector and grown in the presence of FGF (n = 3). **(c)** 5-day growth assay of AHPs transfected with either Nox2 shRNA or Nox3 shRNA and grown in the presence of FGF (n = 3). **(d)** Dentate gyrus of a CL57BL/6J mouse after 7 days of BrdU injections. **(e)** Dentate gyrus of a Nox2-/- mouse after 7 days of BrdU injections with 100 μm scale bar. **(f)** Example of a cluster of BrdU/Sox2 positive AHPs in a CL57BL/6J control after seven days of BrdU injections. **(g)** Example of a single BrdU/Sox2 positive cell in a Nox2-/- mouse after 7 days of BrdU injections with 20 μm

scale bar. Sections stained for BrdU (blue), NeuN (red) and Sox2 (green). **(h)** Quantification of BrdU/Sox2 positive cells in either control or Nox2-/- mice after 7 days of BrdU injections (n = 5). (**i**) Example of newborn neurons in a CL57BL/6J control mouse 28 days after 7 days of BrdU injections. (**j**) Example of a newborn neuron in a Nox2-/- mouse 28 days after 7 days of BrdU injections with 20 μm scale bar. **(k)** Quantification of BrdU/NeuN positive cells in either control or Nox2-/- mice 28 days after 7 days of BrdU injections (n = 4). For all panels data were normalized to controls and statistical analyses were performed with a two-tailed Student's *t*-test. $*P \leq 0.05$, $**P \leq 0.005$ and error bars are ± s.e.m.

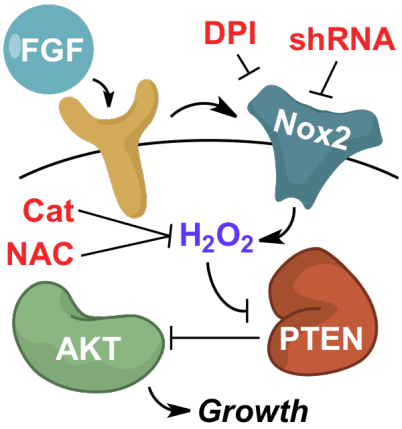

Figure 4-5. Model for the role of Nox2 in FGF-2 redox signaling in AHPs. The mitogen FGF-2 induces the production of H_2O_2 in AHPs, which can be blocked by either the general flavin inhibitor DPI, the antioxidant NAC, the expression of Catalase or genetic manipulation of Nox2. Nox2-generated H_2O_2 oxidizes and deactivates PTEN, which enhances signaling through Akt and manifest phenotypes in growth rates of AHPs *in vitro* and *in vivo*.

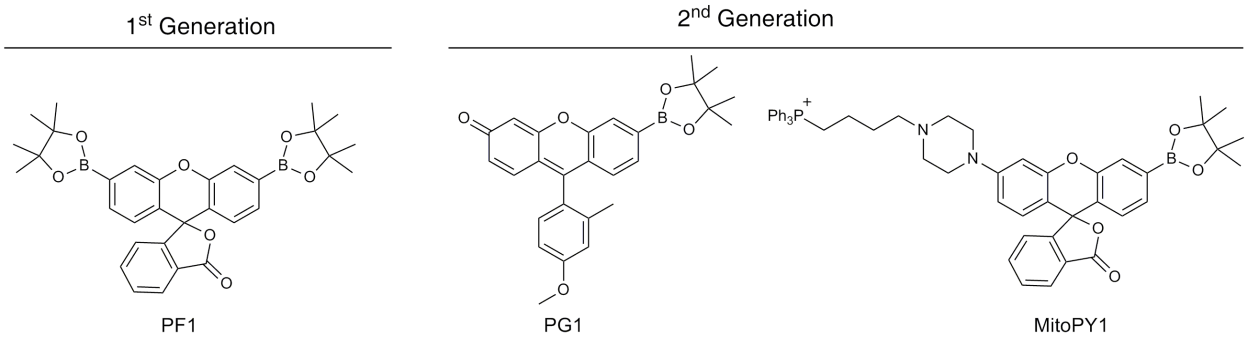

Figure 4-6. Structures of representative examples of 1st and 2nd generation boronate-based H_2O_2 probes. First-generation probes such as Peroxyfluor-1 (PF1) utilize two boronate-protected phenol cages to confer H_2O_2 specificity. Second-generation probes such as Peroxy Green 1 (PG1) and Mitochondrial Peroxy Yellow 1 (MitoPY1) feature a single boronate-masked phenol, which increases sensitivity by only requiring a single equivalent of H_2O_2 to yield a fluorescent product.

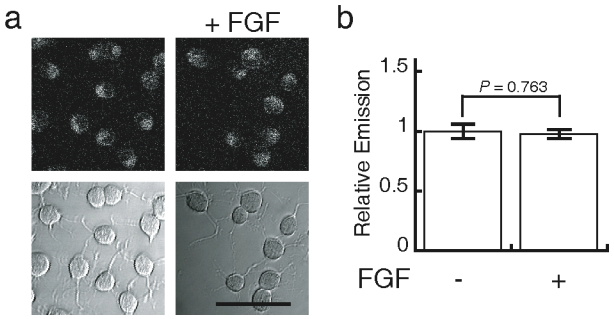

Figure 4-7. Application of PG1 to attempt to detect H_2O_2 in adult hippocampal stem/progenitor cells (AHPs) upon FGF-2 stimulation. **(a)** After FGF-2 starvation, AHPs were loaded with 5 μM PG1 for 30 minutes, stimulated with 20 ng/mL FGF-2 or media for 30 minutes, and then imaged. Brightfield images are shown for each representative image with a 50 μm scale bar. **(b)** Quantification of the experiment as conducted in (a). Statistical analyses were performed with a two-tailed Student's *t*-test. $^{**}P \leq 0.005$ (n = 4) and error bars are ± s.e.m.

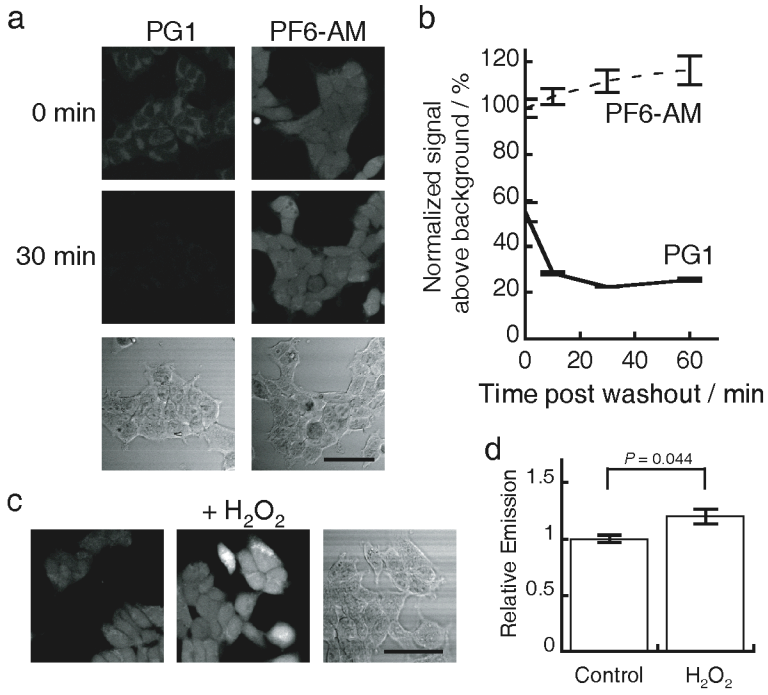

Figure 4-8. Validation of increased uptake and retention of PF6-AM for molecular imaging. **(a)** HEK 293 cells were loaded with either 5 μM PG1 or 5 μM PF6-AM for 15 minutes, then washed twice with DPBS and imaged at 0, 10, 30 and 60 minutes post washing. **(b)** Quantification of the experiment as conducted in (a). **(c)** HEK 293 cells were loaded with 5 μM PF6-AM for 15 minutes, stimulated with either water carrier or 10 μM H_2O_2 for 30 minutes, and imaged. **(d)** Quantification of the experiment as conducted in (c). Statistical analyses were performed with a two-tailed Student's *t*-test and error bars are ± s.e.m. 50 μm scale bars are shown.

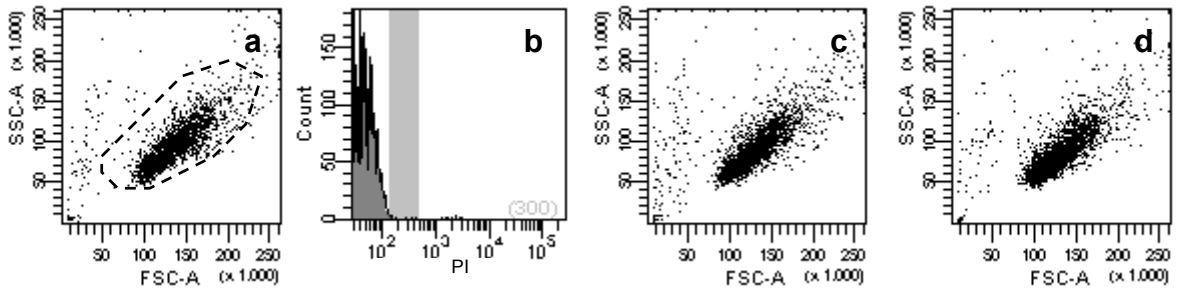

PF6-AM (μM)	% Cells in ROI
0	93.3
5	90.8
10	93.2

Figure 4-9. Flow cytometry evaluation of cell viability of AHPs treated with PF6-AM. AHPs treated with 0 (a/b), 5 (c), or 10 (d) μM PF6-AM for 60 minutes with 3 μM propidium iodide (PI) added for the final 15 minutes and then analyzed by flow cytometry. FS and SS dot plots are shown for each concentration of PF6-AM. (b) PI staining of cells within indicated ROI of (a) indicates that the cells within this ROI are viable. No morphological abnormalities are seen in the FS/SS dot plot, indicating that PF6-AM at these concentrations is non-toxic. PI staining was not possible with PF6-AM loading due to the signal from PF6-AM leaking into the PI channel.

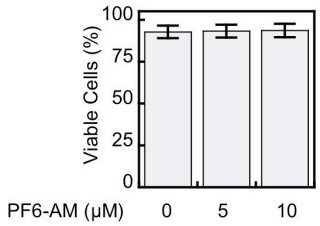

Figure 4-10. Trypan blue evaluation of cell viability studies of AHPs treated with PF6-AM. AHPs were treated with 0, 5, or 10 μM PF6-AM for 60 minutes and then incubated with trypan blue (0.4% w/v) for 3 minutes at room temperature and then analyzed on a hemacytometer. Three independent counts were conducted for each concentration. Error bars are s.e.m.

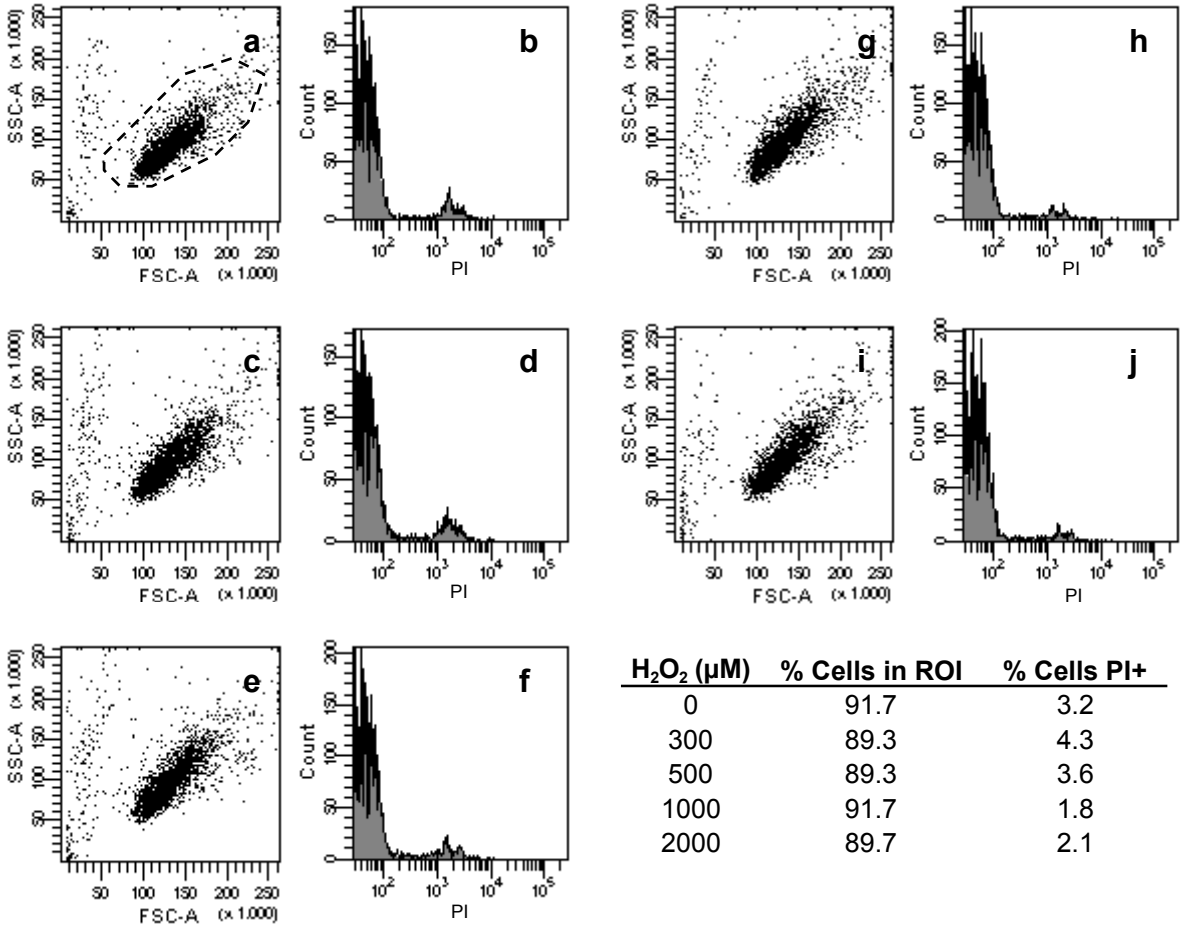

H_2O_2 (μM)	% Cells in ROI	% Cells PI+
0	91.7	3.2
300	89.3	4.3
500	89.3	3.6
1000	91.7	1.8
2000	89.7	2.1

Figure 4-11. Flow cytometry evaluation of cell viability studies of AHPs treated with H_2O_2. AHPs treated with 0 (a, b), 300 (c, d), 500 (e, f), 1000 (g, h), or 2000 (i, j) μM H_2O_2 for 30 minutes with 3 μM propidium iodide (PI) added for the final 15 minutes and then analyzed by flow cytometry. FS and SS dot plots as well as PI histograms are shown for each concentration of H_2O_2. Ethanol-fixed cells were used as a positive control to calibrate flow cytometer settings. Quantification of the percent of cells that fall within the ROI outlined in (a) as well as the total number of cells that are PI positive are listed. These data indicated that these levels of H_2O_2 are not causing cell death within the time scale of this experiment.

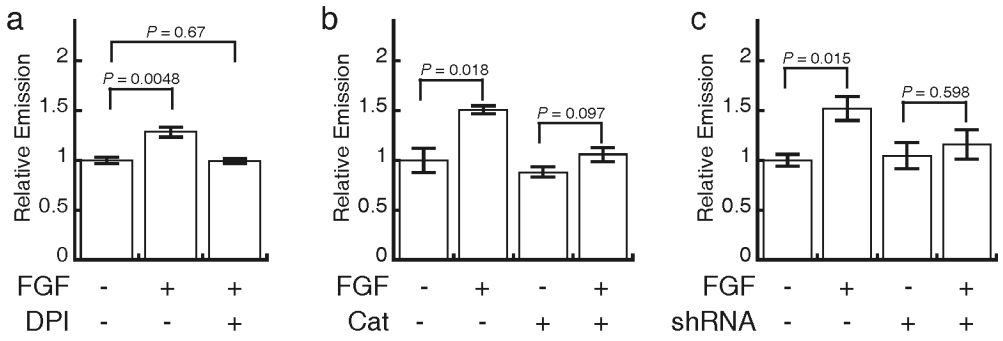

Figure 4-12. Quantification of imaging to demonstrate that adult hippocampal stem/progenitor cells (AHPs) produce H_2O_2 upon FGF-2 stimulation. **(a)** After FGF-2 starvation, AHPs were loaded with 5 μM PF6-AM for 30 minutes, stimulated with 20 ng/mL FGF-2 or media for 30 minutes, and then imaged. For DPI treatment, cells were preincubated in media containing 5 μM DPI before FGF-2 stimulation **(b)** AHPs were transfected with either Catalase or a control vector. After FGF-2 starvation, AHPs were loaded with 5 μM PF6-AM for 30 minutes, stimulated with 20 ng/mL FGF-2 or media for 30 minutes, and then imaged. **(c)** AHPs were transfected with either Nox2-shRNA or a control vector. After FGF-2 starvation, AHPs were loaded with 5 μM PF6-AM for 30 minutes, stimulated with 20 ng/mL FGF-2 or media for 30 minutes, and then imaged. Statistical analyses were performed with a two-tailed Student's *t*-test (n = 4) and error bars are ± s.e.m.

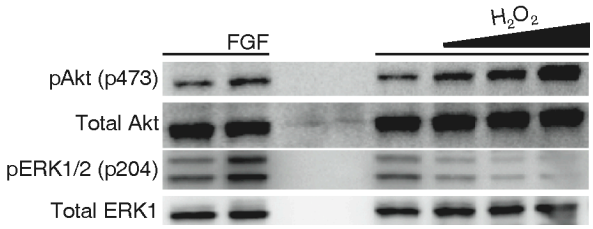

Figure 4-13. Uncut blot from Figure 4-3a. After FGF-2 starvation, AHPs were stimulated with vehicle control (buffer), 20 ng/mL FGF-2, 300, 500, or 1000 mM H_2O_2 for 30 min and analyzed by western blot analysis.

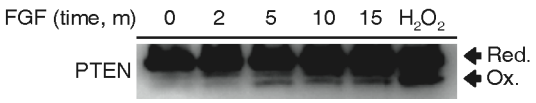

Figure 4-14. Detection of PTEN oxidation in AHPs. After FGF-2 starvation, AHPs were stimulated with 20 ng/mL FGF-2 and lysed at the various times points or stimulated with 100 μM H_2O_2 and lysed after 15 min. Cells were lysed with lysis buffer containing 40 mM N-ethylmaleimide and whole cell extracts were run on a non-reducing gel and probed for PTEN using western blot analysis.

References

1 Floyd, R. A. Oxidative damage to behavior during aging. *Science* **254**, 1597-1597, (1991).

2 Harman, D. The aging process. *Proc. Natl. Acad. Sci. USA* **78**, 7124-7128, (1981).

3 Andersen, J. K. Oxidative stress in neurodegeneration: cause or consequence? *Nature Med.* **10**, S18-25, (2004).

4 Bedard, K. & Krause, K. H. The NOX family of ROS-generating NADPH oxidases: physiology and pathophysiology. *Physiol. Rev.* **87**, 245-313, (2007).

5 Lambeth, J. D. NOX enzymes and the biology of reactive oxygen. *Nat. Rev. Immunol.* **4**, 181-189, (2004).

6 Geiszt, M., Kopp, J. B., Várnai, P. & Leto, T. L. Identification of Renox, an NAD(P)H oxidase in kidney. *Proc. Natl. Acad. Sci. USA* **97**, 8010-8014, (2000).

7 Suh, Y. A. *et al*. Cell transformation by the superoxide-generating oxidase Mox1. *Nature* **401**, 79-82, (1999).

8 Sundaresan, M., Yu, Z. X., Ferrans, V. J., Irani, K. & Finkel, T. Requirement for generation of H2O2 for platelet-derived growth factor signal transduction. *Science* **270**, 296-299, (1995).

9 Rhee, S. G. H2O2, a necessary evil for cell signaling. *Science* **312**, 1882-1883, (2006).

10 D'Autreaux, B. & Toledano, M. B. ROS as signalling molecules: mechanisms that generate specificity in ROS homeostasis. *Nat. Rev. Mol. Cell. Biol.* **8**, 813-824, (2007).

11 Poole, L. B. & Nelson, K. J. Discovering mechanisms of signaling-mediated cysteine oxidation. *Curr. Opin. Chem. Biol.* **12**, 18-24, (2008).

12 Woo, H. *et al*. Inactivation of Peroxiredoxin I by phosphorylation allows localized H2O2 accumulation for cell signaling. *Cell* **140**, 517-528, (2010).

13 Niethammer, P., Grabher, C., Look, A. T. & Mitchison, T. J. A tissue-scale gradient of hydrogen peroxide mediates rapid wound detection in zebrafish. *Nature* **459**, 996-999, (2009).

14 Paulsen, C. E. & Carroll, K. S. Orchestrating Redox Signaling Networks through Regulatory Cysteine Switches. *ACS Chem. Biol.* **5**, 47-62, (2010).

15 Miller, E. W., Dickinson, B. C. & Chang, C. J. Aquaporin-3 mediates hydrogen peroxide uptake to regulate downstream intracellular signaling. *Proc. Natl. Acad. Sci. USA* **107**, 15681-15686, (2010).

16 Walder, C. E. *et al*. Ischemic stroke injury is reduced in mice lacking a functional NADPH oxidase. *Stroke* **28**, 2252, (1997).

17 Park, L., Anrather, J., Girouard, H., Zhou, P. & Iadecola, C. Nox2-derived reactive oxygen species mediate neurovascular dysregulation in the aging mouse brain. *J. Cereb. Blood Flow Metab.* **27**, 1908-1918, (2007).

18 Behrens, M. M. *et al*. Ketamine-induced loss of phenotype of fast-spiking interneurons is mediated by NADPH-oxidase. *Science* **318**, 1645-1647, (2007).

19 Park, L. *et al*. Nox2-derived radicals contribute to neurovascular and behavioral dysfunction in mice overexpressing the amyloid precursor protein. *Proc. Natl. Acad. Sci. USA* **105**, 1347-1352, (2008).

20 Zhang, W. E. I. *et al*. Neuroprotective effect of dextromethorphan in the MPTP Parkinson's disease model: role of NADPH oxidase. *FASEB J.* **18**, 589-591, (2004).

21 Sorce, S. & Krause, K. H. NOX enzymes in the central nervous system: from signaling to disease. *Antioxid. Redox Signal.* **11**, 2481-2503, (2009).

22 Pao, M. *et al*. Cognitive function in patients with Chronic Granulomatous Disease: a preliminary report. *Psychosomatics* **45**, 230-234, (2004).
23 Kishida, K. T. *et al*. Synaptic plasticity deficits and mild memory impairments in mouse models of chronic granulomatous disease. *Mol. Cell Biol.* **26**, 5908-5920, (2006).
24 Zhao, C., Deng, W. & Gage, F. H. Mechanisms and functional implications of adult neurogenesis. *Cell* **132**, 645-660, (2008).
25 Palmer, T. D., Markakis, E. A., Willhoite, A. R., Safar, F. & Gage, F. H. Fibroblast Growth Factor-2 Activates a Latent Neurogenic Program in Neural Stem Cells from Diverse Regions of the Adult CNS. *J. Neurosci.* **19**, 8487-8497, (1999).
26 Winterbourn, C. C. Reconciling the chemistry and biology of reactive oxygen species. *Nat. Chem. Biol.* **4**, 278-286, (2008).
27 Barnham, K. J., Masters, C. L. & Bush, A. I. Neurodegenerative diseases and oxidative stress. *Nat. Rev. Drug. Discov.* **3**, 205-214, (2004).
28 Miller, E. W. & Chang, C. J. Fluorescent probes for nitric oxide and hydrogen peroxide in cell signaling. *Curr. Opin. Chem. Biol.* **11**, 620-625, (2007).
29 Chang, M. C. Y., Pralle, A., Isacoff, E. Y. & Chang, C. J. A selective, cell-permeable optical probe for hydrogen peroxide in living cells. *J. Am. Chem. Soc* **126**, 15392-15393, (2004).
30 Miller, E. W., Albers, A. E., Pralle, A., Isacoff, E. Y. & Chang, C. J. Boronate-based fluorescent probes for imaging cellular hydrogen peroxide. *J. Am. Chem. Soc.* **127**, 16652-16659, (2005).
31 Albers, A. E., Okreglak, V. S. & Chang, C. J. A FRET-based approach to ratiometric fluorescence detection of hydrogen peroxide. *J. Am. Chem. Soc.* **128**, 9640-9641, (2006).
32 Albers, A. E., Dickinson, B. C., Miller, E. W. & Chang, C. J. A red-emitting naphthofluorescein-based fluorescent probe for selective detection of hydrogen peroxide in living cells. *Bioorg. Med. Chem. Lett.* **18**, 5948-5950, (2008).
33 Srikun, D., Albers, A. E., Nam, C. I., Ivarone, A. T. & Chang, C. J. Organelle-Targetable Fluorescent Probes for Imaging Hydrogen Peroxide in Living Cells via SNAP-Tag Protein Labeling. *J. Am. Chem. Soc.* **132**, 4455-4465, (2010).
34 Dickinson, B. C. & Chang, C. J. A targetable fluorescent probe for imaging hydrogen peroxide in the mitochondria of living cells. *J. Am. Chem. Soc* **130**, 9638-9639, (2008).
35 Dickinson, B. C., Srikun, D. & Chang, C. J. Mitochondrial-targeted fluorescent probes for reactive oxygen species. *Curr. Opin. Chem. Biol.* **14**, 50-56, (2010).
36 Srikun, D., Miller, E. W., Domaille, D. W. & Chang, C. J. An ICT-based approach to ratiometric fluorescence imaging of hydrogen peroxide produced in living cells. *J. Am. Chem. Soc.* **130**, 4596-4597, (2008).
37 Miller, E. W., Tulyathan, O., Isacoff, E. Y. & Chang, C. J. Molecular imaging of hydrogen peroxide produced for cell signaling. *Nat. Chem. Biol.* **3**, 263-267, (2007).
38 Dickinson, B. C., Huynh, C. & Chang, C. J. A Palette of Fluorescent Probes with Varying Emission Colors for Imaging Hydrogen Peroxide Signaling in Living Cells. *J. Am. Chem. Soc* **132**, 5906-5915, (2010).
39 Tsien, R. Y. A non-disruptive technique for loading calcium buffers and indicators into cells. *Nature* **290**, 527-528, (1981).
40 Izumi, S., Urano, Y., Hanaoka, K., Terai, T. & Nagano, T. A simple and effective strategy to increase the sensitivity of fluorescence probes in living cells. *J. Am. Chem. Soc* **131**, 10189-10200, (2009).

41 Pluth, M. D., McQuade, L. E. & Lippard, S. J. Cell-trappable fluorescent probes for nitric oxide visualization in living cells. *Org. Lett.* **12**, 2318-2321, (2010).
42 McQuade, L. E. & Lippard, S. J. Cell-Trappable Quinoline-Derivatized Fluoresceins for Selective and Reversible Biological Zn(II) Detection. *Inorg. Chem.*, (2010).
43 McQuade, L. E. *et al.* Visualization of nitric oxide production in the mouse main olfactory bulb by a cell-trappable copper(II) fluorescent probe. *Proc. Natl. Acad. Sci. USA* **107**, 8525-8530, (2010).
44 Hempel, S. L., Buettner, G. R., O'Malley, Y. Q., Wessels, D. A. & Flaherty, D. M. Dihydrofluorescein diacetate is superior for detecting intracellular oxidants: comparison with 2',7'-dichlorodihydrofluorescein diacetate, 5(and 6)-carboxy-2',7'-dichlorodihydrofluorescein diacetate, and dihydrorhodamine 123. *Free Radic. Biol. Med.* **27**, 146-159, (1999).
45 Robinson, K. M. *et al.* Selective fluorescent imaging of superoxide in vivo using ethidium-based probes. *Proc Natl Acad Sci U S A* **103**, 15038-15043, (2006).
46 Prozorovski, T. *et al.* Sirt1 contributes critically to the redox-dependent fate of neural progenitors. *Nat. Cell Biol.* **10**, 385-394, (2008).
47 Kwon, J. *et al.* Reversible oxidation and inactivation of the tumor suppressor PTEN in cells stimulated with peptide growth factors. *Proc. Natl. Acad. Sci. USA* **101**, 16419-16424, (2004).
48 Peltier, J., O'Neill, A. & Schaffer, D. V. PI3K/Akt and CREB regulate adult neural hippocampal progenitor proliferation and differentiation. *Dev. Neurobiol.* **67**, 1348-1361, (2007).
49 Lee, S. R. *et al.* Reversible inactivation of the tumor suppressor PTEN by H2O2. *J. Biol. Chem.* **277**, 20336-20342, (2002).
50 Suh, H. *et al.* In Vivo Fate Analysis Reveals the Multipotent and Self-Renewal Capacities of Sox2+ Neural Stem Cells in the Adult Hippocampus. *Cell Stem Cell* **1**, 515-528, (2007).
51. M. V. Kvach *et al.*, 5(6)-Carboxyfluorescein revisited: new protecting group, separation of isomers, and their spectral properties on oligonucleotides. *Bioconjugate Chem.* **18**, 1691 (2007).
52. S. D. Hingtgen *et al.*, Nox2-containing NADPH oxidase and Akt activation play a key role in angiotensin II-induced cardiomyocyte hypertrophy. *Physiol. Genomics* **26**, 180 (2006).
53. W. E. Wright, J. W. Shay, Inexpensive low-oxygen incubators. *Nat. Protocols* **1**, 2088 (2006).
54. K. Lai, B. K. Kaspar, F. H. Gage, D. V. Schaffer, Sonic hedgehog regulates adult neural progenitor proliferation in vitro and in vivo. *Nat. Neurosci.* **6**, 21 (2003).

Chapter 5:

Aquaporin-3 Mediates Hydrogen Peroxide Uptake to Regulate Downstream Intracellular Signaling

Portions of this work were published in the following scientific journal:

Miller, E. W.; Dickinson, B. C.; Chang, C. J. "Aquaporin-3 mediates hydrogen peroxide uptake to regulate downstream intracellular signaling." *Proceedings of the National Acadademy of Sciences, U.S.A.* **2010**, *107*, 15681–15686.

This work was performed in collaboration with Dr. Evan Miller.

Abstract

Hydrogen peroxide (H_2O_2) produced by cell-surface NADPH Oxidase (Nox) enzymes is emerging as an important signaling molecule for growth, differentiation, and migration processes. However, how cells spatially regulate H_2O_2 to achieve physiological redox signaling over non-specific oxidative stress pathways is insufficiently understood. Here we report that the water channel Aquaporin-3 (AQP3) can facilitate the uptake of H_2O_2 into mammalian cells and mediate downstream intracellular signaling. Molecular imaging with Peroxy Yellow 1 Methyl-Ester (PY1-ME), a new chemoselective fluorescent indicator for H_2O_2, directly demonstrates that aquaporin isoforms AQP3 and AQP8, but not AQP1, can promote uptake of H_2O_2 specifically through membranes in mammalian cells. Moreover, we show that intracellular H_2O_2 accumulation can be modulated up or down based on endogenous AQP3 expression, which in turn can influence downstream cell signaling cascades. Finally, we establish that AQP3 is required for Nox-derived H_2O_2 signaling upon growth factor stimulation. Taken together, our findings demonstrate that the downstream intracellular effects of H_2O_2 can be regulated across biological barriers, a discovery that has broad implications for the controlled use of this potentially toxic small molecule for beneficial physiological functions.

Introduction

Hydrogen peroxide (H_2O_2) is garnering increased attention as a molecule involved not only in immune response and oxidative stress, but also as a physiological effector in essential cellular processes.[1-5] Seminal contributions have elucidated ligand stimulants[6-10] and enzymatic sources [11-13] for cellular H_2O_2 production as well as putative downstream targets,[14-24] but principles of how this reactive oxygen species (ROS) is spatially and temporally regulated to promote redox signaling over oxidative stress pathways remain insufficiently understood. Because many of the signaling functions of H_2O_2 rely on its generation by nonphagocytic forms of NADPH (Nox) proteins on the extracellular side of cell membranes, understanding how cells funnel H_2O_2 toward beneficial pathways in these locales is of significant interest.

Despite its reactive nature, H_2O_2 has been long thought to be freely diffusible across biological membranes in a manner akin to the related canonical small-molecule signal nitric oxide (NO).[25] More recent studies implicate the role of AQP water channels, a class of membrane-spanning proteins that facilitate the diffusion of water and other substrates with varying specificity,[26-28] in mediating H_2O_2 passage across the plasma membrane of reconstituted yeast[29] and plant[30] cells. However, given that the experiments described in these reports utilized non-specific chemical reagents for determination of the redox signal that was passed into the cell, direct evidence that aquaporins influence the cellular uptake of H_2O_2 in a native context remains elusive, and no studies have addressed higher-order mammalian systems. More importantly, the potential physiological consequences of regulating H_2O_2 have not been elucidated.

We now report a H_2O_2-selective small-molecule fluorescent indicator, Peroxy Yellow 1 Methyl Ester (PY1-ME), and apply this novel chemical tool to show that members of two of the three main types of aquaporins (e.g., aquaglyceroporins and unorthodox aquaporins), but not the other type (e.g., classical aquaporins), can mediate H_2O_2 uptake across the plasma membrane of mammalian cells. Molecular imaging with PY1-ME in flow cytometry or confocal microscopy experiments reveals that canonical examples of an aquaglyceroporin and unorthodox aquaporin (AQP3 and AQP8, respectively), which are known to be permeated by molecules in addition to

water, can facilitate H_2O_2 uptake into mammalian cells, whereas an example of a classical aquaporin that is known only to transport water (AQP1) does not enhance membrane H_2O_2 permeability. Moreover, we go on to show the physiological consequences of this newly discovered form of membrane H_2O_2 regulation in mammalian cells. We focused these studies on the aquaglyceroporin isoform AQP3 owing to its wide expression in many tissues, including the kidney, skin, colon, spleen, stomach, small intestine, uninary bladder, and respiratory tract, with AQP3-knockout mice showing loss of kidney function, polyuric behavior, deficiencies in epidermal hydration, and propensity towards colitis.[31] Along these lines, we demonstrate at the cellular level that H_2O_2 uptake mediated by AQP3 can amplify or diminish downstream native signaling pathways that rely on this ROS as a physiological messenger. Our findings challenge the notion that H_2O_2 is freely diffusible through cell membranes and define a link between its membrane regulation and consequences for downstream signal transduction.

Results and Discussion

Design, Synthesis, and Properties of the New Chemoselective H_2O_2 Indicator Peroxy Yellow 1 Methyl Ester (PY1-ME). Traditional fluorescent dyes used to probe H_2O_2 typically rely on non-specific general oxidations that can be modulated by a variety of ROS, which can complicate data interpretation.[32] We therefore sought to ensure that we could directly discriminate between H_2O_2 uptake and transfer of the redox signal by other means. Accordingly, we developed a new H_2O_2-specific fluorescent indicator, Peroxy Yellow 1 Methyl Ester (PY1-ME, Figure 5-5 A), which combines a boronate-masked phenol for the selective detection of H_2O_2[10,33-39] and an appended methyl ester group designed to increase cellular uptake and retention upon cleavage by intracellular esterases; this latter feature makes the dye suitable for both fluorescence imaging and flow cytometry experiments. Because this probe relies on a specific molecular reaction between H_2O_2 and the boronate to generate a fluorescence signal, rather than thiol-based chemistry that can occur by non-specific ROS oxidation or disulfide exchange, our chemical method affords a direct measure of H_2O_2 in cellular specimens. Spectroscopic data show that PY1-ME features high selectivity for H_2O_2 over other ROS, visible excitation and emission profiles, and a 12-fold turn-on dynamic range with sensitivity to micromolar levels of H_2O_2 (Figure 5-5 B and C).

Application of PY1-ME to Directly Establish that Select Types of AQP Channels Mediate H_2O_2 Uptake in Mammalian Cells. Initial experiments tested whether overexpression of various types of AQPs would lead to increased intracellular H_2O_2 uptake in a reconstituted mammalian system. Previous work established that the unorthodox aquaporin AQP8 but not the classical aquaporin AQP1 can facilitate the uptake of H_2O_2 in yeast models.[29] We sought to test whether this same pattern would hold in mammalian cells, as well as explore whether aquaglyceroporins, the third major type of these channels, could affect membrane H_2O_2 permeability. To this end, we transfected HEK 293 cells with either AQP expression or control vectors. Overexpression of each AQP was confirmed by Western blot analysis on cell lysates (Figure 5-6 A and B). Aquaporin expressing or control cells were then loaded with PY1-ME, stimulated with H_2O_2 or vehicle control, and analyzed by flow cytometry. As shown in Figure 5-1A, the addition of H_2O_2 to both control and AQP1 expressing HEK 293 cells results in enhanced PY1-ME fluorescent signal, indicating that this new fluorescent probe is capable of measuring intracellular uptake of H_2O_2. AQP1 expression does not cause an increased signal from PY1-ME upon H_2O_2 stimulation as compared to control cells also stimulated with H_2O_2. However, as

shown in Figure 5-1B, addition of 50 μM H_2O_2 to AQP8-overexpressing HEK 293 cells loaded with PY1-ME results in a greater relative increase in intracellular fluorescence compared to control cells. These results confirm the yeast studies and demonstrate that some members of the AQP family of proteins are capable of allowing enhanced uptake of H_2O_2 into mammalian cells, while others appear to lack this ability.

We next turned our attention to evaluating whether an aquaglyceroporin-type AQP would regulate membrane H_2O_2 uptake in mammalian cells. We focused these studies on AQP3, owing to the wide tissue distribution of this aquaglyceroporin and phenotypes shown by AQP3 knockout mice,[31] including kidney duct malfunctions and polyuric behavior,[40] epidermal hydration deficiencies,[41] and propensity towards colitis.[42] At the cellular level, this aquaglyceroporin is known to facilitate diffusion of larger, alternative substrates to water[26] and is involved in cell migration and wound healing processes.[43] Because some of these cell migration and wound healing processes are redox dependent,[43,44] we hypothesized that AQP3 may be involved in second-messenger signaling cascades utilizing H_2O_2. Indeed, many cell types, particularly colon cells[45,46] and keratinocytes,[47,48] possess the endogenous machinery to produce H_2O_2 at the membrane through NADPH oxidase (Nox) proteins as well as high levels of AQP channels.

Overexpression of AQP3 was confirmed by Western blot analysis on cell lysates as well as immunostaining (Figure 5-6 C and D). As shown in Figure 5-1C, addition of 50 μM H_2O_2 to AQP3-overexpressing HEK 293 cells loaded with PY1-ME results in a greater relative increase in intracellular fluorescence compared to control cells. These results were further verified by live cell imaging (Figure 5-1 D and E). AQP3-expressing cells exhibit a 130 ± 9% increase in fluorescence upon treatment with H_2O_2, whereas control cells show only a 80 ± 18% increase upon H_2O_2 addition (Figure 5-1E). These experiments directly demonstrate that AQP3 is also able to increase the permeability of mammalian cells to exogenous H_2O_2.

Application of HyPer to Further Validate that AQP3 Facilitates H_2O_2 Uptake in Mammalian Cells. After establishing that AQP3 and AQP8 but not AQP1 mediate H_2O_2 uptake utilizing a chemoselective small-molecule, we sought to utilize a secondary method of H_2O_2 measurement. For these experiments, we utilized the genetically encoded fluorescent H_2O_2 sensor HyPer,[49] which has reasonable selectivity for and high sensitivity to H_2O_2 and thus should permit the detection of very low levels of H_2O_2 uptake and assure intracellular localization of the fluorescent reporter. Control HEK 293 cells exposed to 10 μM H_2O_2 show no statistically significant fluorescence enhancements as determined by HyPer fluorescence (Figures 5-2A and 5-10). In contrast, AQP3-overexpressing HEK 293 cells exhibit a fluorescence increase within 2 min of H_2O_2 addition (Figures 5-2A and 5-10). These data further show that AQP3 increases the permeability of mammalian cells to exogenous H_2O_2, and validates the use of HyPer as an alternative methodology for the detection of H_2O_2 uptake.

AQP3-Mediated H_2O_2 Uptake Influences Intracellular Signaling Cascades. After establishing that AQP3 can facilitate the uptake of H_2O_2 by two independent imaging methods, we sought to determine whether AQP3-mediated H_2O_2 accumulation could affect downstream intracellular processes. For these experiments we utilized HeLa cells, owing to their high number of signaling proteins and lack of endogenous AQP3 expression, to provide a clean reconstituted mammalian cell model. First we confirmed that AQP3 could also mediate H_2O_2 uptake in this cell line. Control HeLa cells exposed to 10 μM H_2O_2 show no statistically significant fluorescence enhancements as determined by HyPer fluorescence (Figure 5-2 B and C). In

contrast, AQP3-overexpressing HeLa cells exhibit a 50 ± 4% fluorescence increase within 2 min of H_2O_2 addition (Figure 5-2 B and C). We then sought to probe whether these differences in H_2O_2 uptake obtained by the overexpression of AQP3 could affect downstream cell signaling pathways that rely on this ROS as a physiological effector molecule. In this context, a compelling relationship has emerged between H_2O_2 signaling and the phosphorylation status of the serine/threonine kinase AKT/PKB, a major node in cellular signal transduction [50]. ROS signals can amplify AKT signaling cascades in the forward direction through transient oxidative inactivation of the phosphatase and tensin homolog (PTEN) and other phosphatases that oppose AKT phosphorylation.[21] Accordingly, we utilized the phosphorylation status of AKT as a central marker for signal transduction that can be modulated by H_2O_2. Initial experiments tested the direct effects of H_2O_2 on AKT phosphorylation. Serum-starved control HeLa cells do not exhibit increases in pAKT/AKT ratios upon addition of H_2O_2 (Figure 5-2D). However, AQP3-overexpressing, serum-starved HeLa cells treated with H_2O_2 for 20 min triggers a marked enhancement in AKT phosphorylation (Figure 5-2D). When correlated with the imaging data this result shows that AQP3 can enhance permeability of cells to H_2O_2 and amplify downstream signaling that relies on this ROS as an intracellular messenger.

Endogenous AQP3 Levels Regulate H_2O_2 Uptake. We next tested whether endogenously expressed AQP3 could also facilitate H_2O_2 uptake and downstream intracellular signaling. For these experiments we turned our attention to HT29 human colon cancer adenocarcinoma cells, as this model naturally expresses both AQP3 [45] and Nox proteins[46] and possesses the requisite AKT signaling hub. We utilized an shRNA construct targeted against AQP3 and validated in HEK 293 cells (Figure 5-6D) to knock down the expression of endogenous AQP3 in HT29 cells (Figure 5-3B). When control HT29 cells transfected with an shRNA construct targeting AQP4, an AQP isoform not found in this cell line, were treated with H_2O_2, we observed a ca. 20% increase in fluorescence intensity measured by HyPer (Figure 5-3 A, C, and D). In contrast, AQP3-knockdown cells showed no significant fluorescence increase when exposed to an equivalent amount of H_2O_2 (Figure 5-3 A, C, and D), establishing that natural levels of AQP3 can affect H_2O_2 uptake.

AQP3 Regulates Endogenous H_2O_2 Uptake and Downstream Cell Signaling Upon Growth Factor Stimulation. We then sought to determine whether AQP3-mediated uptake of naturally generated H_2O_2 could also mediate intracellular redox signaling. In this context, previous work has shown that epidermal growth factor (EGF) stimulation causes the activation of membrane-bound Nox proteins to produce H_2O_2, which in turn regulates intracellular signaling.[51] In agreement with experiments in HEK 293 and HeLa cells, addition of 100 μM H_2O_2 causes a marked increase intracellular fluorescence in both natural and AQP3-overexpressing HT29 cells, with a greater relative increase in the AQP3-elevated samples (Figures 5-11 and 5-12). Moreover, HT29 cells overexpressing AQP3 and stimulated with EGF exhibit a ca. 10% increase in intracellular fluorescence (Figure 5-4 A and B). We were unable to directly image Nox-generated H_2O_2 upon EGF stimulation of basal HT29 cells under similar conditions, which is presumably due to the low levels of H_2O_2 produced for signaling purposes that are under the detection limit of HyPer. These experiments do, however, establish that AQP3 can also enhance the uptake of endogenous H_2O_2.

As a more sensitive method for probing extracellular H_2O_2 generation and its subsequent effects on intracellular processes, we then assayed the effects of endogenous AQP3 on Nox-derived H_2O_2 uptake and signaling by western blot analysis of AKT phosphorylation status. As

expected, stimulation of HT29 cells with EGF causes a patent increase in AKT phosphorylation (Figure 5-4D). In contrast, stimulation with EGF in the presence of extracellular catalase, which will destroy any extracellular H_2O_2 produced by Nox, abrogates AKT phosphorylation, demonstrating that extracellular H_2O_2 production is linked to intracellular signaling processes. Similarly, EGF stimulation in the presence of diphenyleneiodonium (DPI), a general Nox/flavin inhibitor, also diminishes H_2O_2 signaling through AKT. Finally, cells that have endogenous AQP3 levels knocked down by shRNA also show small but significant decreases in EGF-induced AKT phosphorylation when compared to control cells transfected with an AQP4 targeting shRNA (Figure 5-4 E and F), as shown by quantification of the Western data. Taken together, these data establish that endogenous extracellular H_2O_2 produced by Nox at the cell surface is important for EGF signaling, and AQP3 plays a role in the transduction of that signal from the extracellular space to intracellular targets (Fig 4*C*). By showing that membrane regulation of H_2O_2 in this manner can occur and is essential for intracellular signaling, these results provide a key piece of the puzzle for use of the reactive metabolite H_2O_2 as a physiological effector while avoiding oxidative stress pathways but open the door to many new and interesting questions. In particular, the observation that RNAi knockdown of AQP3 does not abolish AKT signaling as much as the addition of extracellular catalase suggests that other H_2O_2 membrane transport mechanisms may be at play, potentially either some passive membrane diffusion or regulation by alternative aquaporins or other proteins. In addition, other membrane and non-membrane sources of H_2O_2 could also be implicated in these types of signaling pathways, a hypothesis that is supported by that fact that DPI abolishes AKT signaling to a greater extent compared to addition of extracellular catalase.

Conclusions

In summary, our findings challenge the commonly held view that H_2O_2 is freely diffusible across biological membranes and define a connection between its membrane regulation and downstream intracellular signaling. By utilizing PY1-ME, a new H_2O_2-specific synthetic small-molecule dye, in conjunction with protein reporters to directly visualize differences in H_2O_2 uptake in various cell lines as a function of AQP levels, we have established that specific types of AQP channels can regulate the uptake of H_2O_2 in mammalian cells. In particular, canonical members of the aquaglyceroporin (AQP3) and unorthodox (AQP8) family of these channels mediate H_2O_2 uptake through mammalian cell membranes, where a member of the classical type of aquaporin (AQP1) does not. Furthermore, AQP-mediated H_2O_2 accumulation can amplify or diminish downstream signaling cascades that rely on this ROS as a physiological messenger. Interestingly, in this context, membrane H_2O_2 regulation bears more resemblance to metal Ca^{2+} signals that require channel entry rather than the related small-molecule signal NO that can freely diffuse through membranes.

The evidence presented in this report indicates that some, but not all, AQPs can facilitate the uptake of H_2O_2 in mammalian systems, and that the ability to mediate H_2O_2 transport may correspond to specific AQP classes (classical, aquaglyceroporin, unorthodox). This selectivity suggests that the expression profiles of AQPs could dictate the susceptibility of a particular cell or tissue to external H_2O_2 signaling. Moreover, the notion that H_2O_2 uptake is controlled at biological barriers has broad implications for AQP channels as regulators of redox signaling, with particularly tantalizing connections in the areas of cell migration and wound healing. For example, AQP3 facilitates cell migration through an EGF/EGFr dependent pathway[52] and can

mediate wound healing in the epidermis via cell migration and proliferation through p38 MAPK-dependent pathways.[43] In addition, several reports have suggested a relationship between ROS fluxes and cell migration, based on imaging studies using non-specific ROS indicators at the leading edge of migrating endothelial cells.[53,54] Finally, an exciting discovery establishing the involvement of H_2O_2 signaling in wound repair has been reported recently, in which H_2O_2 generated by the Duox class of Nox proteins acts as a signaling molecule to attract leukocytes to the site of injury.[44] The involvement of both H_2O_2 fluxes and AQP channels in cell migration and wound healing raises the possibility that AQPs may modulate H_2O_2 permeability as a general way to modulate its downstream effects, where regulation of AQP channels through various mechanisms, including differential expression, trafficking, or posttranslational modification may allow for discrimination between extracellularly generated ROS molecules such as H_2O_2 or superoxide (O_2^-). We are actively exploring these possibilities in a wide variety of model systems.

Materials and Methods

Synthetic Materials and Methods. Silica gel P60 (SiliCycle) was used for column chromatography. Analytical thin layer chromatography was performed using SiliCycle 60 F254 silica gel (precoated sheets, 0.25 mm thick). Fmoc-piperazine rhodol boronate was synthesized according to literature procedures.[36] ^{1}H NMR spectra were collected in $CDCl_3$ or CD_3OD (Cambridge Isotope Laboratories, Cambridge, MA) at 25 ºC on a Bruker AV-300 spectrometer at the College of Chemistry NMR Facility at the University of California, Berkeley. Chemical shifts are reported in the standard δ notation of parts per million using the peak of residual proton signals of $CDCl_3$ or CD_3OD as an internal reference. Mass spectral analyses were carried out at the College of Chemistry Mass Spectrometry Facility at the University of California, Berkeley.

Peroxy Yellow-1 Methyl Ester, PY1-ME. Fmoc-piperazine rhodol boronate (15 mg, 0.02 mmol) was added to a vial and dissolved in 1.5 mL of acetonitrile. Two drops of piperidine were added to the solution and the mixture was stirred at room temperature for 30 min, after which the contents were evaporated under reduced pressure. Methyl N-succinimidyl adipate (Pierce, 10 mg, 0.04 mmol) and sodium bicarbonate (46 mg, 0.54 mmol) was added to the dry vial and the contents were dissolved in a mixture of 1.5 mL of acetonitrile and 2 mL of dichloromethane and stirred at room temperature for 6 hours. The reaction mixture was then dried under reduced pressure. Purification by column chromatography (3:1 ethyl acetate/hexanes) furnished **PY1-ME** as an orange solid (5 mg, 35%). ^{1}H NMR ($CDCl_3$/5% CD_3OD, 300 MHz): δ 8.03 (1H, d, *J* = 6.3 Hz), 7.72 (1H, s), 7.64 (1H, t, *J* = 6.6 Hz), 7.60 (1H, t, *J* = 6.6 Hz), 7.41 (1H, d, *J* = 7.8 Hz), 7.11 (1H, d, *J* = 6.3 Hz), 6.79 (1H, d, *J* = 7.8 Hz), 6.70 (1H, s), 6.68 (1H, d, *J* = 6.3 Hz), 6.60 (1H, dd, *J* = 2.1, 8.7 Hz), 3.72-3.82 (2H, m), 3.67 (3H, s), 3.58-3.64 (2H, m), 3.19-3.29 (4H, m), 2.32-2.43 (4H, m), 1.66-1.75 (4H, m), 1.34 (12H, s). HR-FABMS: calculated for [M^+] 653.3034, found 653.3026.

Spectrophotometric Characterization of PY1-ME. PY1-ME features two major visible region absorptions (λ_{abs} = 489 nm, ε = 18100 $M^{-1}cm^{-1}$; λ_{abs} = 510 nm, ε = 18700 $M^{-1}cm^{-1}$) and a weak emission (λ_{em} = 548 nm, (Φ = 0.040) in 20 mM HEPES, pH 7.0. The deprotected, phenol form of PYME has one major visible region absorption (λ_{abs} = 515 nm, ε = 79900 $M^{-1}cm^{-1}$) and enhanced emission (λ_{em} = 540 nm, (Φ = 0.402).

Antibodies. Rabbit anti-AQP3 polyclonal antibody was from Chemicon/Millipore. Goat anti-AQP3, rabbit anti-pAKT1/2/3, rabbit anti-AKT1/2/3, rabbit anti-AQP1, mouse anti-AQP8, goat anti-mouse IgG-HRP, and goat anti-rabbit IgG-HRP were from Santa Cruz Biotechnology. Bovine anti-goat IgG-Cy3 was from Jackson Immuno Labs. Mouse anti-actin was from Sigma.

Cell Culture and Transfection. Cell lines HEK293T and HeLa (ATCC) were maintained in DMEM (Invitrogen) supplemented with 10% FBS, 1% Non-essential amino acids, and 1% Gluta-MAX (Invitrogen). The HT-29 cell line (ATCC) was maintained in DMEM supplemented with 10% FBS. HEK293T cells were transfected with Lipofectamine 2000 (Invitrogen) according to the manufacturer's protocol. HeLa cells were transfected with either Lipofectamine LTX (Invitrogen) or DreamFect Gold (OZ Biosciences) according to the manufacturer's instructions. HT-29 cells were transfected using the Nucleofector II device (Lonza), using the high efficiency program W-017. Human AQP3 cDNA was obtained from ATCC (clone ID: BC013566) in the vector pCMV-SPORT6. The AQP3 gene was sub-cloned into the mammalian expression vector pNice under control of the CMV promotor using *NotI* and *EcoRI*. Human AQP1 was obtained from Origene (clone ID: M77829) in the vector pCMV6-XL4. Human AQP8 was obtained from Origene (clone ID: AB013456) in the vector pCMV6-XL4. shRNA constructs were designed against human AQP3 (NM_004925.3) using OligoEngine design tools. Three sequences were selected based on specificity and predicted strength of knockdown and incorporated into a pSUPER.retro.neo vector according to the manufacturer's instructions:

241: 5' ACCTGAACCCTGCCGTGAC 3'

243: 5' CTGAACCCTGCCGTGACCT 3'

824: 5' CAACGAGGAAGAGAATGTG 3'

Efficacy of the constructs was determined by co-transfection of the pSUPER construct along with AQP3 into HEK 293 cells (3:1 ratio of pSUPER:AQP3 DNA), followed by analysis of AQP3 levels by Western blot, 24 48 hours post-transfection. The construct targeted against 241 was selected for use in knock down studies.

Preparation of Cell Extracts and Immunoblotting. Following transfection, cells were grown to sub-confluency of 60-90% and then serum-starved in DMEM without supplements overnight (HeLa) or for 1 hour (HT-29). Appropriate stimulants were added and the cells incubated at 37 °C. After stimulation, cells were cooled on ice, washed with ice-cold DPBS, scraped into RIPA buffer (50 mM Tris, pH 7.4, 150 mM NaCl, 1% Triton X-100, 0.5% sodium deoxycholate, and 0.1% SDS) supplemented with protease inhibitors (Roche Complete MiniTab), and 1 mM Na_3VO_4, lysed for 30 minutes on ice, and clarified by centrifugation at 13.2 x 10^3 rpm for 10 minutes at 4 °C. Protein concentration was determined by BCA assay (Pierce), 4x Laemmli buffer (0.25 mM Tris, 2% SDS, 40% glycerol, 20% beta-mercaptoethanol, 0.04% bromophenol blue) was added, the samples denatured at 37°C for 20 minutes (for AQP8 blots), 70°C for 10 minutes (for AQP3 and AQP1 blots), or 95 °C for 5 minutes (pAKT/AKT blots), and equal amounts of total protein were loaded onto 12% SDS-PAGE gels. Proteins were transferred to PVDF membranes (Immobilon, Millipore), blocked for 1 hour in 5% non-fat dry milk in wash buffer (10 mM Tris, pH 7.5, 100 mM NaCl, 0.1% Tween-20), and incubated overnight at 4 °C in primary antibody (1:1000, x pAKT1/2/3, x AKT1/2/3; 1:500 x AQP3; 1:5000 x actin). Membranes were washed 5 times for 5 minutes in wash buffer, incubated 1 hour at room temperature with 1:1000 secondary antibody, washed 5 times for 5 minutes in wash buffer, and then visualized using enhanced chemiluminescence (Western Lightning, Perkin-Elmer) recorded

on a BioRad GelDoc imaging station. Densitometic analysis was performed using QuantityOne software (BioRad). Blots were stripped using Restore stripping buffer (Fisher) or 50 mM Tris pH 6.8, 2% SDS, 100 mM BME at 55 °C for 17 min.

Immunocytochemistry. Cells plated on 15 mm coverslips were fixed in 4% paraformaldehyde, permeabilized in PBST (PBS + 0.3% Triton X-100), blocked in 2% FBS in PBST, incubated with 1:1000 goat anti-AQP3 followed by bovine anti-goat IgG-Cy3, and mounted before imaging using an epifluorescence microscope.

Cell Sorting. HEK293T cells were plated at 2.5 x 10^5 well in a 24-well tray. One day after plating, cells were transfected with equal amounts (250 ng) of AQP expression vector or control vector and mRFP using Lipofectamine LTX. 48 hours after transfection, cells were washed once with DPBS and incubated with 5 μM PYME in DPBS for 15 minutes at 37 °C. Cells were then treated with 50 μM H_2O_2 or buffer and incubated for 30 minutes at 37 °C. After treatment, cells were typsinized, resuspended in DPBS, and sorted by mRFP fluorescence. The mean PYME fluorescence of mRFP-positives in the AQP and control cells was measured.

Confocal Microscopy. Sub-confluent HEK293T cells were plated on polylysine-coated 15 mm coverslips and transfected with mRFP and AQP3 or control vector. 24 - 48 hours post transfection, cells were washed with DPBS, and incubated with 5 μM PYME in DPBS for 15 minutes at 37 °C. Following incubation, H_2O_2 was added to give a final concentration of 50 μM and incubated for another 30 minutes at 37 °C. Cells were then washed with DPBS and imaged with a Zeiss 510 Axioplan equipped with a META detector and an Achroplan 40x/0.8 NA water immersion lens. Excitation for PYME was provided at 514 nm, with emission collected from 516-569 nm. Excitation for mRFP was provided at 543 nm, with emission collected from 601-676 nm. Regions of interest were generated within mRFP+ cells and the mean PYME fluorescence from these ROIs were measured using ImageJ.

HyPer Imaging. Sub-confluent HEK293T or HeLa cells plated on polylysine-coated 15 mm coverslips were transfected with equal amounts of AQP3 or control vector and HyPer and allowed to grow to approximately 80-90% confluency. Prior to imaging, the coverslips were transferred to 2 mL of DPBS (no Ca^{2+} or Mg^{2+}) in a 35 mm petri dish with a 14 mm glass microwell (MatTek). Images were acquired every 20 seconds to establish baseline fluorescence and then 1 mL of 3x H_2O_2 was added to the dish. The mean fluorescence intensity of HyPer-expressing cells was monitored over time using an Axiovert 200M equipped with an AxioCam MRm. The fluorescence intensity immediately before H_2O_2 addition was set to 1.00 and quantified using ImageJ. Excitation was provided by an X-Cite series 120 lamp using a filter cube containing a bandpass excitation filter at 470 / 40, a beamsplitter at 495, and a bandpass emission filter at 525 / 50. HT-29 imaging was done in a similar manner except that Hank's Balanced Salt Solution (HBSS) with Ca^{2+} and Mg^{2+} was used instead of DPBS and a final concentration of 100 μM H_2O_2 was used instead of 10 μM H_2O_2. For EGF imaging, HT-29 cells were starved in DMEM for 1 hour prior to imaging. As with H_2O_2 imaging experiments, 3x EGF (Upstate/Millipore) was added to give a final concentration of 100 ng/mL.

Figures and Schemes

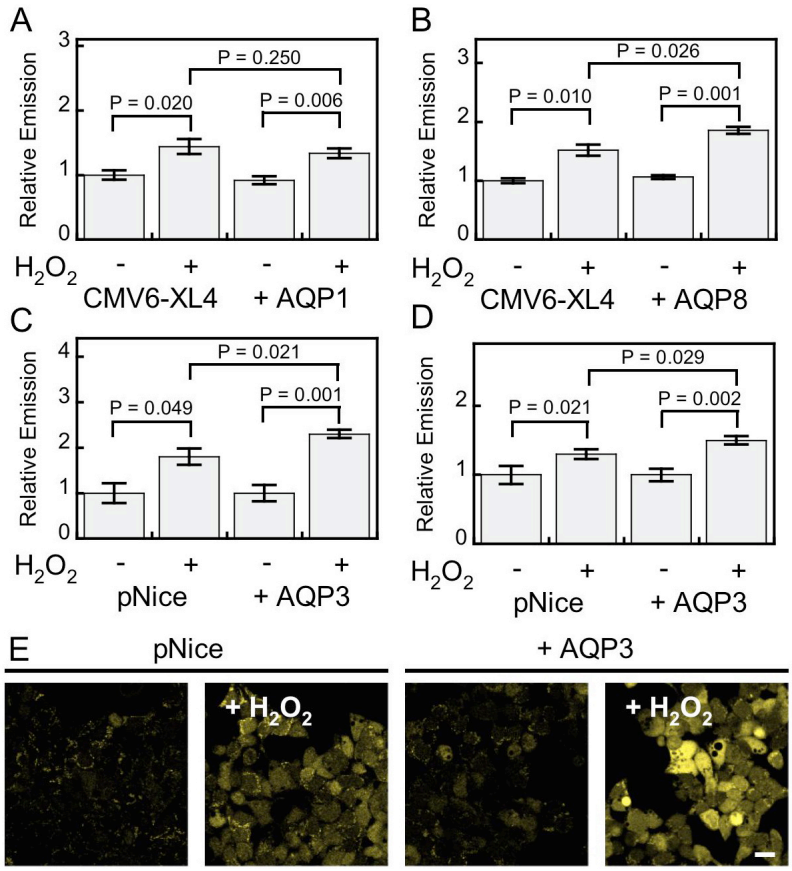

Figure 5-1. Application of PY1-ME to show some aquaporins can increase the uptake of H_2O_2 in mammalian cells. HEK 293 cells transfected with either a control vector or AQP1 (*A*), AQP8 (*B*), or AQP3 (*C*) expression vectors, loaded with PY1-ME, treated with 0 or 50 μM H_2O_2 for 30 min, and analyzed by flow cytometry (n = 3). (*D*) HEK 293 cells transfected with either a control vector or AQP3 and mRFP as a transfection marker and measured by confocal microscopy (n = 8). (*E*) Representative images of experiment represented in *D*. Scale bar = 20 μm. For all panels data were normalized to controls and statistical analyses were performed with a one-tailed Student's t-test. Error bars are ± s.e.m.

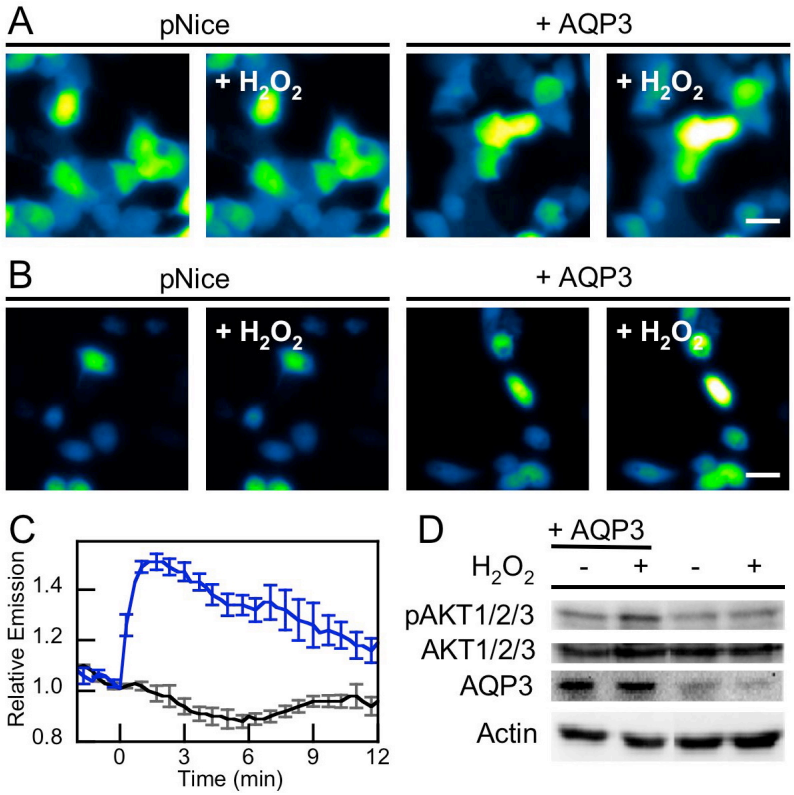

Figure 5-2. AQP3 mediated exogenous H_2O_2 uptake can effect intracellular signaling. (*A*) Live-cell imaging of changes in HyPer fluorescence upon treatment of HEK 293 cells with 10 μM H_2O_2. "pNice," HEK 293 cells expressing HyPer and transfected with pNice as a control vector before addition of H_2O_2. "+ AQP3," HEK 293 cells expressing HyPer and AQP3 before addition of H_2O_2. "+ H_2O_2," cells 2 min after addition of 10 μM H_2O_2. 20 μm scale bar. (*B*) Live-cell imaging of changes in HyPer fluorescence upon treatment of HeLa cells with 10 μM H_2O_2. "pNice," HeLa cells expressing HyPer and transfected with pNice as a control vector before addition of H_2O_2. "+ AQP3," HeLa cells expressing HyPer and AQP3 before addition of H_2O_2. "+ H_2O_2," cells 2 min after addition of 10 μM H_2O_2. 20 μm scale bar. (*C*) Time-course and quantification of *B*. HeLa cells expressing HyPer and transfected with pNice (black line) or AQP3 (blue line) were stimulated with 10 μM H_2O_2 at t = 0 and the changes in HyPer fluorescence monitored over time. Error bars are +/- s.e.m. (n = 3). (*D*) Western blot showing changes in pAKT1/2/3 levels in HeLa cells treated with H_2O_2. HeLa cells expressing AQP3 or control vector were serum-starved and then treated with 200 μM H_2O_2 for 20 minutes at 37 °C and then lysed. Phospho-AKT and AQP3 levels were measured by western blot analysis of whole cell extracts, followed by stripping and reprobing for total AKT or Actin, respectively.

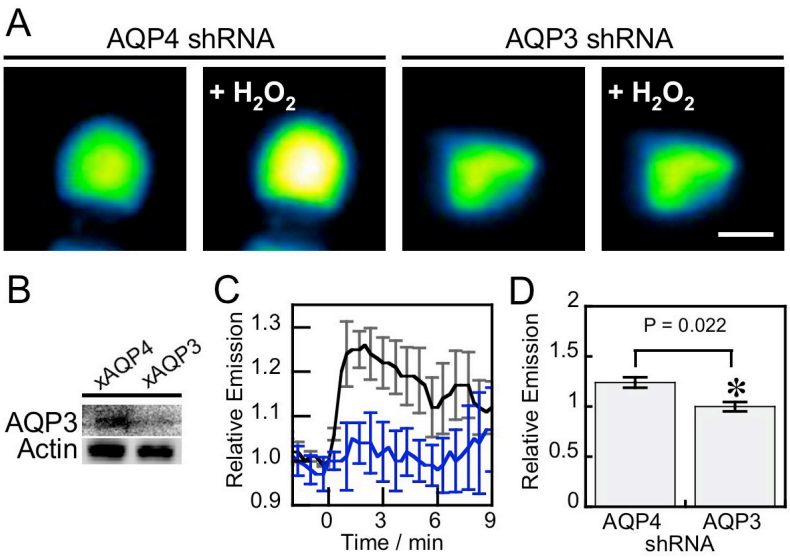

Figure 5-3. Natural levels of AQP3 can mediate exogenous H_2O_2 uptake. (*A*) HT29s transfected with either HyPer and shRNA targeted against AQP3(241) or AQP4(801) as a control with 100 μM H_2O_2 at t = 0 and the changes in HyPer fluorescence monitored over time. Images show cells at t = 0 and t = 2 min ("+ H_2O_2"). 10 μm scale bar. (*B*) Knockdown of endogenous AQP3 in HT29 cells. HT29 cells were transfected with either shRNA targeted against AQP3(241), or AQP4(801) as a control, then lysed and probed for AQP3 levels by western blot analysis of whole cell extracts, followed by stripping and reprobing for Actin. (*C*) Endogenous AQP3 can mediate H_2O_2 uptake. HT29 cells expressing HyPer and transfected with AQP4 shRNA as a control (black line) or AQP3 shRNA (blue line) were stimulated with 100 μM H_2O_2 at t = 0 and the changes in HyPer fluorescence monitored over time. Error bars are +/- S.E.M. (n = 3). (*D*) Quantification of C at t = 2. (n = 3). Data were normalized to controls and statistical analyses were performed with a one-tailed Student's t-test. Error bars are ± s.e.m.

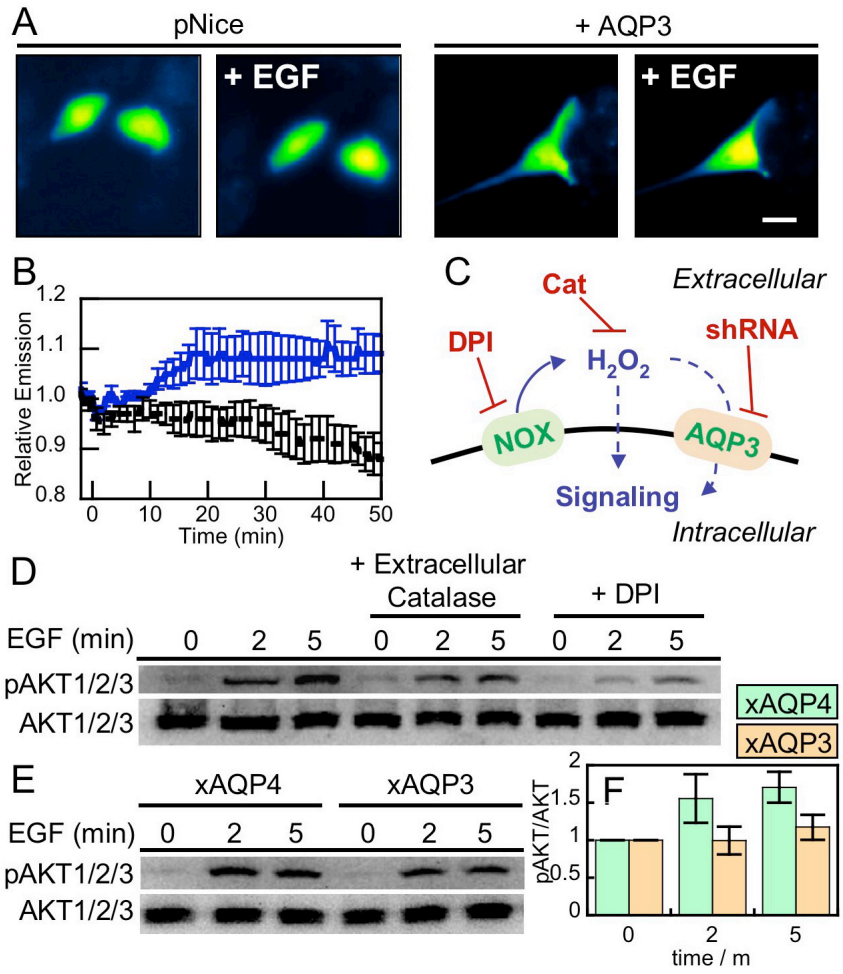

Figure 5-4. Natural levels of AQP3 can mediate uptake of Nox-generated H_2O_2 and effect intracellular signaling. (*A*) Live-cell imaging of changes in HyPer fluorescence upon treatment of HT29 cells with 100 ng/mL EGF. HT29 cells expressing HyPer and transfected with pNice as a control ("pNice") or AQP3 ("+ AQP3") before addition of EGF. Cells images at t = 0 and then again at t = 20 min ("+ EGF"). 20 μm scale bar. (*B*) Time-course and quantification of *A*. HT29 cells expressing HyPer and transfected with pNice (black line) or AQP3 (blue line) stimulated with 100 ng/mL EGF at t = 0 and the changes in HyPer fluorescence monitored over time. Error bars are +/- s.e.m. (n = 3). (*C*) Schematic illustrating where the H_2O_2 redox signal can by intercepted. EGF stimulation can activate a membrane-bound NADPH oxidase (Nox), which will then produce extracellular H_2O_2, which can then pass into the cell and modulate intracellular redox signaling. Diphenylene iodonium (DPI) will block the Nox production of H_2O_2 and extracellular catalase (Cat) will destroy any H_2O_2 produced outside of the cell. The genetic manipulation of AQP3 using shRNA will block any potential factilitated uptake of extracellular H_2O_2 by this protein. (*D*) Extracellular catalase and DPI abrogate EGF signaling in HT29 cells. Serum-starved HT29 cells were either preincubated with 5 μM DPI or DMSO as a carrier control for 30 min. 5 mg/mL catalase or water as a carrier control was then added while the cells were simulataneously stimulated with 100 ng/mL EGF. Phospho-AKT was measured by western blot analysis of whole cell extracts, followed by stripping and reprobing for total AKT. (*E*) HT29 cells were transfected with either AQP3 shRNA or AQP4 shRNA as a control, serum starved, stimulated with 100 ng/mL EGF, and lysed at the various time points. Phospho-AKT was measured by western blot analysis of whole cell extracts, followed by stripping and reprobing for total AKT. (*F*) Quantification of experiment as represented in *E* by analyzing 4 separate trials. pAKT normalized to total AKT and each experiment normalized to the t = 0 pAKT/AKT ratio. Error bars are ± s.e.m.

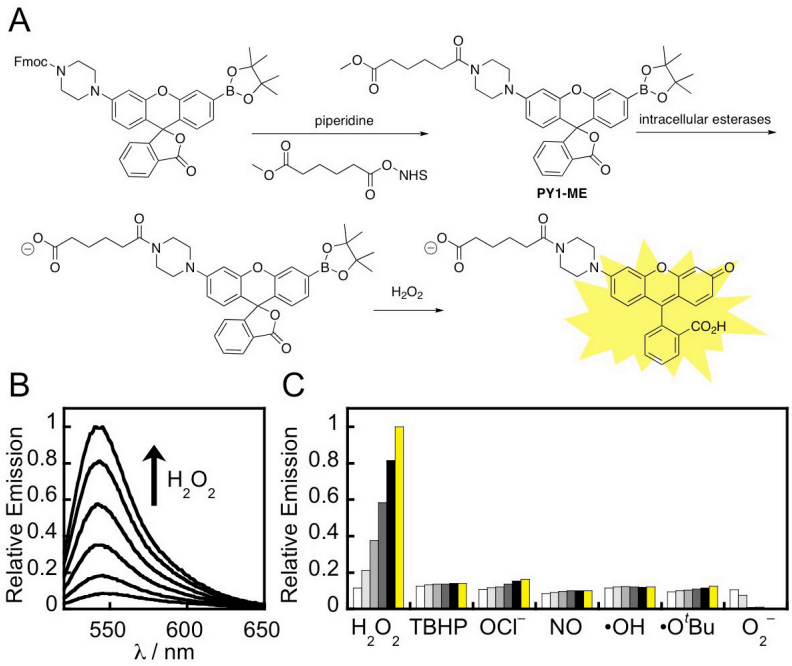

Figure 5-5. Design and characterization of PY1-ME. (*A*) Design and synthesis of PY1-ME, a new fluorescent probe for the selective detection of H_2O_2. (*B*) Fluorescence turn-on response of 5 μM PY1-ME at 0, 5, 15, 30, 45, and 60 min after the addition of 100 μM H_2O_2. (*C*) Fluorescence responses of 5 μM PY1-ME to various reactive oxygen species (ROS). Bars represent relative responses at 0, 5, 15, 30, 45, and 60 min after addition of each ROS. Data shown are for 10 mM O_2^- (with 10 μM Catalase), 200 μM NO, and 100 μM for all other ROS.

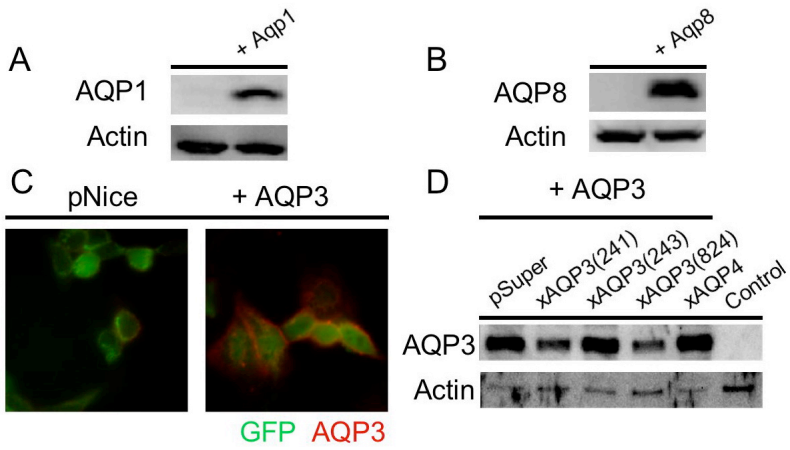

Figure 5-6. Verification of AQP overexpression. (*A*) Western blot showing the overexpression of AQP1 in HEK 293 cells. HEK 293 cells were transfected with either control (pCMV6-XL4) or AQP1 expression vector ("+ AQP1") and analyzed by western blot. (*B*) Western blot showing the overexpression of AQP8 in HEK 293 cells. HEK 293 cells were transfected with either control (pCMV6-XL4) or AQP8 expression vector ("+ AQP8") and analyzed by western blot. (*C*) Immunocytochemistry of HEK 293 cells transfected with HyPer and AQP3 or a control vector. (*D*) Western blot showing overexpression and knockdown of AQP3 in HEK 293 cells. Lane 1: HEK 293 cells transfected with AQP3 and pSUPER. Lane 2: HEK 293 cells transfected with AQP3 and xAQP3 241 shRNA. Lane 3: HEK 293 cells transfected with AQP3 and xAQP3 243 shRNA. Lane 4: HEK 293 cells transfected with AQP3 and xAQP3 824 shRNA. Lane 5: HEK 293 cells transfected with AQP3 and xAQP4 801 shRNA. Lane 6: Untransfected control HEK 293 cells. Blots were stripped and reprobed for actin as a loading control.

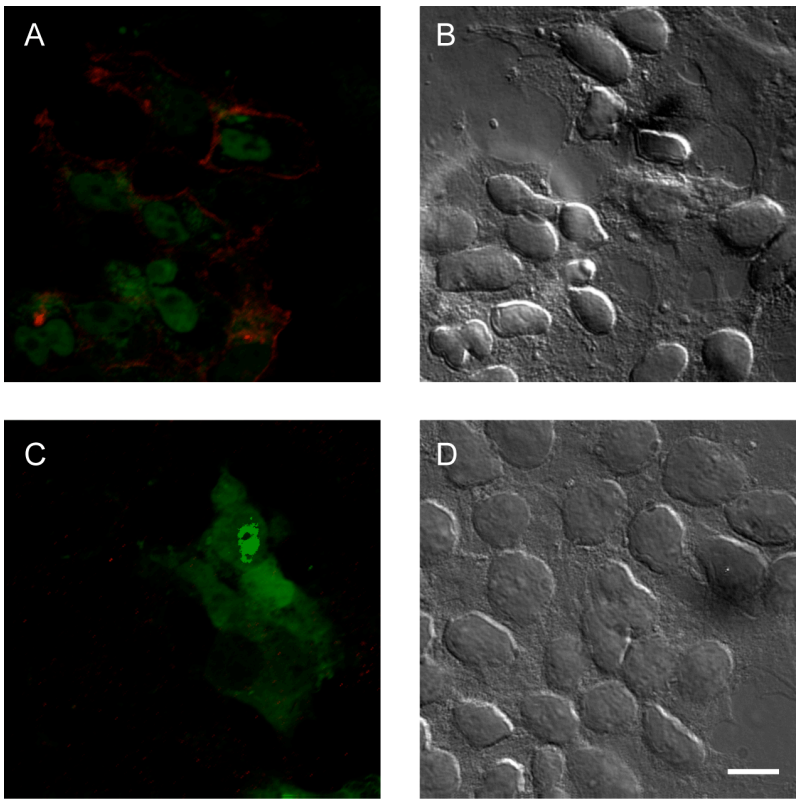

Figure 5-7. Immunocytochemistry of HEK 293 cells transfected with HyPer and AQP3 or control vector. After transfection, cells were fixed, permeablized, and treated with anti-AQP3 antibody. AQP3 localization was visualized by addition of Cy-3 conjugated secondary antibody (red channel); YFP fluorescence from the HyPer chromophore, as a marker of transfection, is visualized in green. A) HEK 293 cells expressing HyPer and AQP3. B) DIC image of cells in A. C) HEK 293 cells expressing HyPer and control vector. D) DIC image of cells in D. Scale bar = 10 μm.

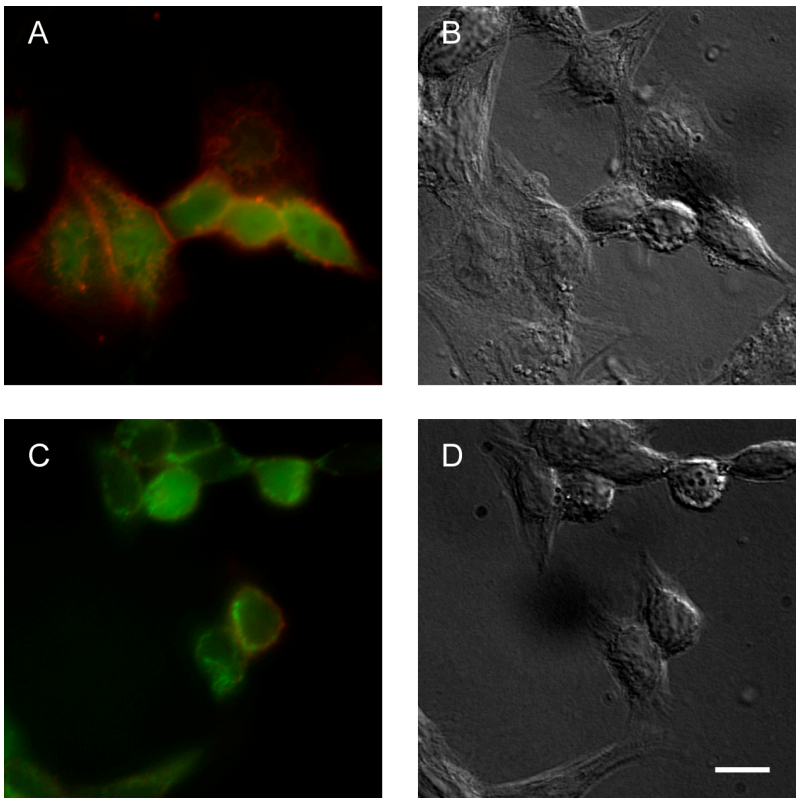

Figure 5-8. Immunocytochemistry of HeLa cells transfected with HyPer and AQP3 or control vector. After transfection, cells were fixed, permeablized, and treated with anti-AQP3 antibody. AQP3 localization was visualized by addition of Cy-3 conjugated secondary antibody (red channel); YFP fluorescence from the HyPer chromophore, as a marker of transfection, is visualized in green. A) HeLa cells expressing HyPer and AQP3. B) DIC image of cells in A. C) HeLa cells expressing HyPer and control vector. D) DIC image of cells in D. Scale bar = 10 μm.

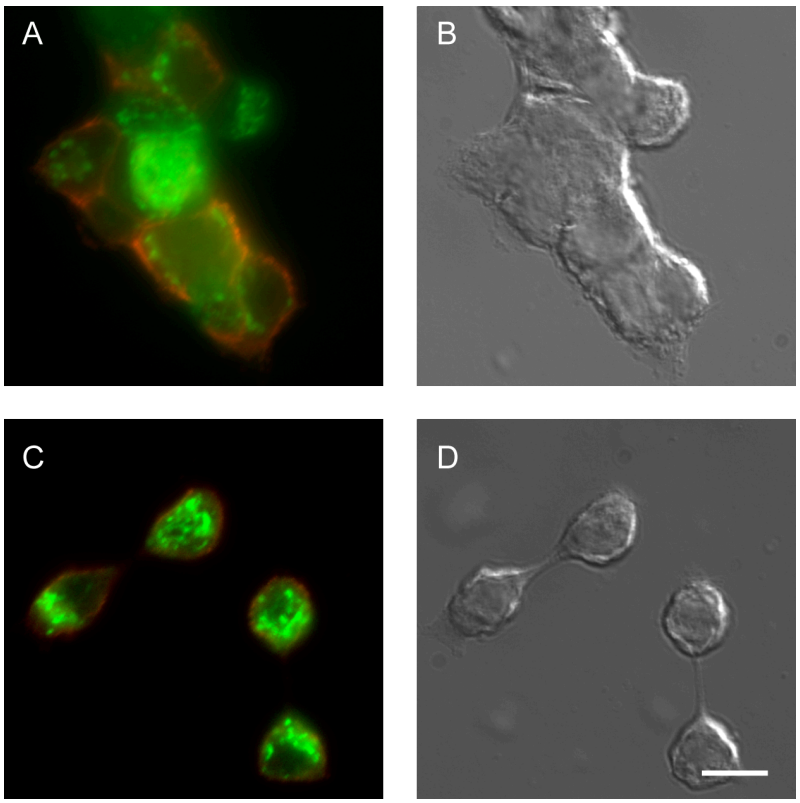

Figure 5-9. Immunocytochemistry of HT-29 cells transfected with HyPer and AQP3 or control vector. After transfection, cells were fixed, permeablized, and treated with anti-AQP3 antibody. AQP3 localization was visualized by addition of Cy-3 conjugated secondary antibody (red channel); YFP fluorescence from the HyPer chromophore, as a marker of transfection, is visualized in green. A) HT-29 cells expressing HyPer and AQP3. B) DIC image of cells in A. C) HT-29 cells expressing HyPer and control vector. D) DIC image of cells in D. Scale bar = 10 μm.

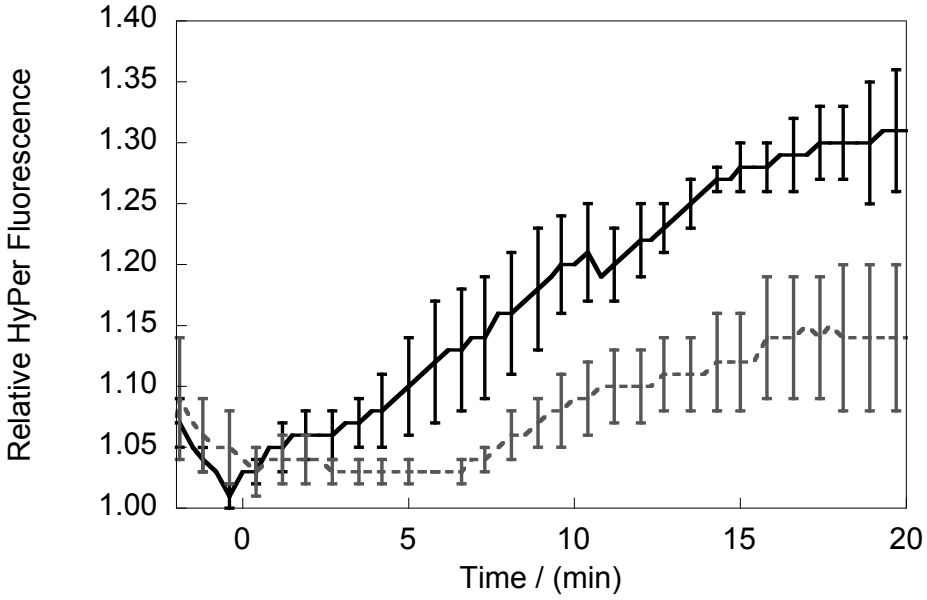

Figure 5-10. Live-cell imaging of changes in HyPer fluorescence upon treatment of HEK 293 cells with 10 μM H_2O_2. HEK 293 cells transfected with HyPer and AQP3 (solid line) or control vector (dashed line) were treated with 10 μM H_2O_2 and the changes in HyPer fluorescence were monitored over time. Error bars are ± s.e.m. (n = 3).

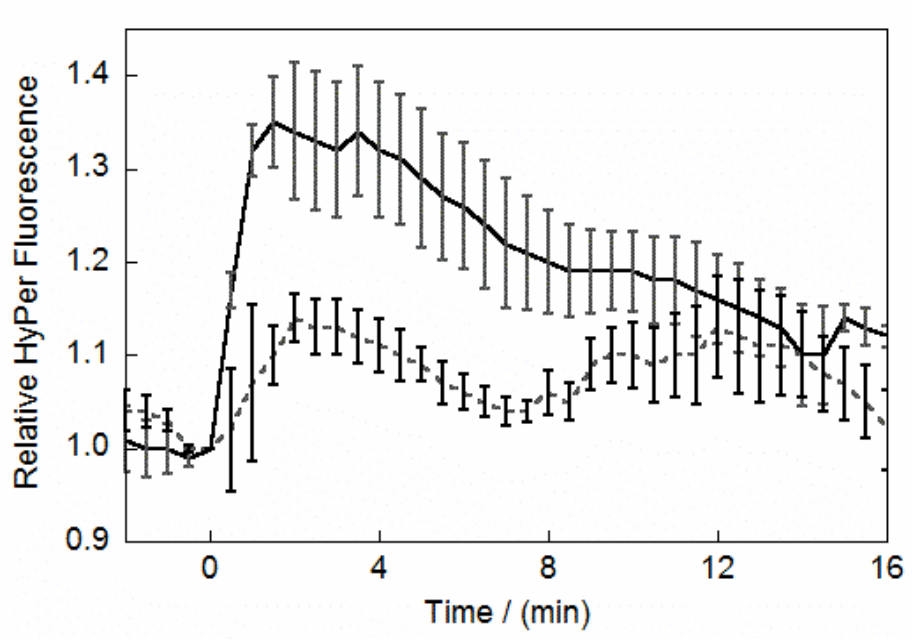

Figure 5-11. Live-cell imaging of changes in HyPer fluorescence upon treatment of HT-29 cells with 100 μM H_2O_2. HT-29 cells transfected with HyPer and AQP3 (solid line) or pNice vector (dashed line) were treated with 100 μM H_2O_2 and the changes in HyPer fluorescence were monitored over time. Error bars are ± s.e.m. (n = 3).

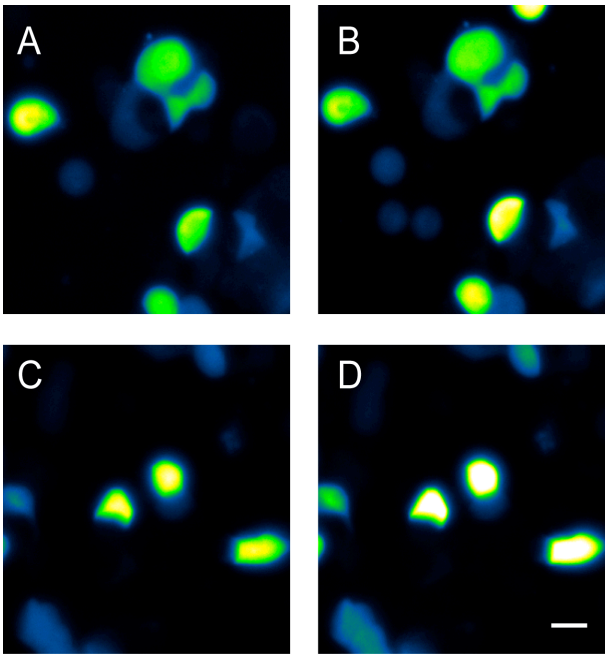

Figure 5-12. Live-cell imaging of changes in HyPer fluorescence upon treatment of HT-29 cells with 100 μM H_2O_2. A) HT-29 cells expressing HyPer and transfected with pNice as a control vector before addition of H_2O_2. B) Cells from A, 4 minutes after addition of 100 μM H_2O_2. C) HT-29 cells expressing HyPer and AQP3 before addition of H_2O_2. D) Cells from C, 4 minutes after addition of 100 μM H_2O_2. Scale bar = 20 μm.

References

1. Poole, L. B.; Karplus, P. A.; Claiborne, A. Protein sulfenic acids in redox signaling. *Annu. Rev. Pharmacol. Toxicol.* **2004**, *44*, 325-47.
2. Rhee, S. G. Cell signaling. H2O2, a necessary evil for cell signaling. *Science* **2006**, *312*, 1882-3.
3. D'Autreaux, B.; Toledano, M. B. ROS as signalling molecules: mechanisms that generate specificity in ROS homeostasis. *Nat. Rev. Mol. Cell. Biol.* **2007**, *8*, 813-24.
4. Winterbourn, C. C. Reconciling the chemistry and biology of reactive oxygen species. *Nat. Chem. Biol.* **2008**, *4*, 278-86.
5. Paulsen, C. E.; Carroll, K. S. Orchestrating Redox Signaling Networks through Regulatory Cysteine Switches. *ACS Chem. Biol.* **2010**, *5*, 47-62.
6. May, J. M.; de Haen, C. Insulin-stimulated intracellular hydrogen peroxide production in rat epididymal fat cells. *J. Biol. Chem.* **1979**, *254*, 2214-20.
7. Sundaresan, M.; Yu, Z. X.; Ferrans, V. J.; Irani, K.; Finkel, T. Requirement for generation of H2O2 for platelet-derived growth factor signal transduction. *Science* **1995**, *270*, 296-9.
8. Bae, Y. S.; Kang, S. W.; Seo, M. S.; Baines, I. C.; Tekle, E.; Chock, P. B.; Rhee, S. G. Epidermal growth factor (EGF)-induced generation of hydrogen peroxide. Role in EGF receptor-mediated tyrosine phosphorylation. *J. Biol. Chem.* **1997**, *272*, 217-21.
9. Zafari, A. M.; Ushio-Fukai, M.; Akers, M.; Yin, Q.; Shah, A.; Harrison, D. G.; Taylor, W. R.; Griendling, K. K. Role of NADH/NADPH oxidase-derived H2O2 in angiotensin II-induced vascular hypertrophy. *Hypertension* **1998**, *32*, 488-95.
10. Miller, E. W.; Tulyathan, O.; Isacoff, E. Y.; Chang, C. J. Molecular imaging of hydrogen peroxide produced for cell signaling. *Nat. Chem. Biol.* **2007**, *3*, 263-267.
11. Suh, Y. A.; Arnold, R. S.; Lassegue, B.; Shi, J.; Xu, X.; Sorescu, D.; Chung, A. B.; Griendling, K. K.; Lambeth, J. D. Cell transformation by the superoxide-generating oxidase Mox1. *Nature* **1999**, *401*, 79-82.
12. Geiszt, M.; Kopp, J. B.; Varnai, P.; Leto, T. L. Identification of renox, an NAD(P)H oxidase in kidney. *Proc. Natl. Acad. Sci. U.S.A.* **2000**, *97*, 8010-4.
13. Bao, L.; Avshalumov, M. V.; Patel, J. C.; Lee, C. R.; Miller, E. W.; Chang, C. J.; Rice, M. E. Mitochondria are the source of hydrogen peroxide for dynamic brain-cell signaling. *J. Neurosci.* **2009**, *29*, 9002.
14. Lee, S. R.; Kwon, K. S.; Kim, S. R.; Rhee, S. G. Reversible inactivation of protein-tyrosine phosphatase 1B in A431 cells stimulated with epidermal growth factor. *J. Biol. Chem.* **1998**, *273*, 15366-72.
15. Lee, S. R.; Yang, K. S.; Kwon, J.; Lee, C.; Jeong, W.; Rhee, S. G. Reversible inactivation of the tumor suppressor PTEN by H2O2. *J. Biol. Chem.* **2002**, *277*, 20336-42.
16. Wood, Z. A.; Poole, L. B.; Karplus, P. A. Peroxiredoxin evolution and the regulation of hydrogen peroxide signaling. *Science* **2003**, *300*, 650-653.
17. Woo, H. A.; Chae, H. Z.; Hwang, S. C.; Yang, K. S.; Kang, S. W.; Kim, K.; Rhee, S. G. Reversing the inactivation of peroxiredoxins caused by cysteine sulfinic acid formation. *Science* **2003**, *300*, 653-656.
18. van Montfort, R. L.; Congreve, M.; Tisi, D.; Carr, R.; Jhoti, H. Oxidation state of the active-site cysteine in protein tyrosine phosphatase 1B. *Nature* **2003**, *423*, 773-7.

19. Salmeen, A.; Andersen, J. N.; Myers, M. P.; Meng, T. C.; Hinks, J. A.; Tonks, N. K.; Barford, D. Redox regulation of protein tyrosine phosphatase 1B involves a sulphenyl-amide intermediate. *Nature* **2003**, *423*, 769-773.
20. Avshalumov, M. V.; Rice, M. E. Activation of ATP-sensitive K+ (K(ATP)) channels by H2O2 underlies glutamate-dependent inhibition of striatal dopamine release. *Proc. Natl. Acad. Sci. U.S.A.* **2003**, *100*, 11729-34.
21. Kwon, J.; Lee, S. R.; Yang, K. S.; Ahn, Y.; Kim, Y.; Stadtman, E. R.; Rhee, S. G. Reversible oxidation and inactivation of the tumor suppressor PTEN in cells stimulated with peptide growth factors. *Proc. Natl. Acad. Sci. U.S.A.* **2004**, *101*, 16419-24.
22. Budanov, A. V.; Sablina, A. A.; Feinstein, E.; Koonin, E. V.; Chumakov, P. M. Regeneration of peroxiredoxins by p53-regulated sestrins, homologs of bacterial AhpD. *Science* **2004**, *304*, 596-600.
23. Leonard, S. E.; Reddie, K. G.; Carroll, K. S. Mining the Thiol Proteome for Sulfenic Acid Modifications Reveals New Targets for Oxidation in Cells. *ACS Chem. Biol.* **2009**, *4*, 783-799.
24. Woo, H. A.; Yim, S. H.; Shin, D. H.; Kang, D.; Yu, D. Y.; Rhee, S. G. Inactivation of Peroxiredoxin I by phosphorylation allows localized H2O2 accumulation for cell signaling. *Cell* **2010**, *140*, 517-528.
25. Lancaster, J. R. Simulation of the diffusion and reaction of endogenously produced nitric oxide. *Proc. Natl. Acad. Sci. U.S.A.* **1994**, *91*, 8137-8137.
26. King, L. S.; Kozono, D.; Agre, P. From structure to disease: the evolving tale of aquaporin biology. *Nat. Rev. Mol. Cell. Biol.* **2004**, *5*, 687-698.
27. Stroud, R.; Harries, W.; Lee, J.; Khademi, S.; Savage, D. *Structural Biology of Membrane Proteins*; Royal Society of Chemistry: Great Britain, 2006.
28. Ho, J. D.; Yeh, R.; Sandstrom, A.; Chorny, I.; Harries, W. E. C.; Robbins, R. A.; Miercke, L. J. W.; Stroud, R. M. Crystal structure of human aquaporin 4 at 1.8 Å and its mechanism of conductance. *Proc. Natl. Acad. Sci. U.S.A.* **2009**, *106*, 7437-7442.
29. Bienert, G. P.; Møller, A. L.; Kristiansen, K. A.; Schulz, A.; Møller, I. M.; Schjoerring, J. K.; Jahn, T. P. Specific aquaporins facilitate the diffusion of hydrogen peroxide across membranes. *J. Biol. Chem.* **2007**, *282*, 1183-92.
30. Dynowski, M.; Schaaf, G.; Loque, D.; Moran, O.; Ludewig, U. Plant plasma membrane water channels conduct the signalling molecule H2O2. *Biochem. J.* **2008**, *414*, 53-61.
31. Rojek, A.; Praetorius, J.; Frøkiaer, J.; Nielsen, S.; Fenton, R. A. A current view of the mammalian aquaglyceroporins. *Annu. Rev. Physiol.* **2008**, *70*, 301-327.
32. Hempel, S. L.; Buettner, G. R.; O'Malley, Y. Q.; Wessels, D. A.; Flaherty, D. M. Dihydrofluorescein diacetate is superior for detecting intracellular oxidants: comparison with 2', 7'-dichlorodihydrofluorescein diacetate, 5 (and 6)-carboxy-2', 7'-dichlorodihydrofluorescein diacetate, and dihydrorhodamine 123-implications for intracellular measurement of reactive nitrogen species. *Free Radic. Biol. Med.* **1999**, *27*, 146-159.
33. Chang, M. C. Y.; Pralle, A.; Isacoff, E. Y.; Chang, C. J. A selective, cell-permeable optical probe for hydrogen peroxide in living cells. *J. Am. Chem. Soc.* **2004**, *126*, 15392-15393.
34. Miller, E. W.; Albers, A. E.; Pralle, A.; Isacoff, E. Y.; Chang, C. J. Boronate-based fluorescent probes for imaging cellular hydrogen peroxide. *J. Am. Chem. Soc.* **2005**, *127*, 16652-16659.

35. Srikun, D.; Miller, E. W.; Domaille, D. W.; Chang, C. J. An ICT-based approach to ratiometric fluorescence imaging of hydrogen peroxide produced in living cells. *J. Am. Chem. Soc.* **2008**, *130*, 4596-4597.
36. Dickinson, B. C.; Chang, C. J. A targetable fluorescent probe for imaging hydrogen peroxide in the mitochondria of living cells. *J. Am. Chem. Soc.* **2008**, *130*, 9638-9.
37. Dickinson, B. C.; Srikun, D.; Chang, C. J. Mitochondrial-targeted fluorescent probes for reactive oxygen species. *Curr. Opin. Chem. Biol.* **2010**, *14*, 50-56.
38. Srikun, D.; Albers, A. E.; Nam, C. I.; Ivarone, A. T.; Chang, C. J. Organelle-Targetable Fluorescent Probes for Imaging Hydrogen Peroxide in Living Cells via SNAP-Tag Protein Labeling. *J. Am. Chem. Soc.* **2010**, *132*, 4455-4465.
39. Dickinson, B. C.; Huynh, C.; Chang, C. J. A Palette of Fluorescent Probes with Varying Emission Colors for Imaging Hydrogen Peroxide Signaling in Living Cells. *J. Am. Chem. Soc.* **2010**, *132*, 5906.
40. Ma, T.; Song, Y.; Yang, B.; Gillespie, A.; Carlson, E. J.; Epstein, C. J.; Verkman, A. S. Nephrogenic diabetes insipidus in mice lacking aquaporin-3 water channels. *Proc. Natl. Acad. Sci. U.S.A.* **2000**, *97*, 4386-4391.
41. Hara, M.; Ma, T.; Verkman, A. S. Selectively Reduced Glycerol in Skin of Aquaporin-3-deficient Mice May Account for Impaired Skin Hydration, Elasticity, and Barrier Recovery. *J. Biol. Chem.* **2002**, *277:*, 46616-46621.
42. Thiagarajah, J. R.; Zhao, D.; Verkman, A. S. Impaired enterocyte proliferation in aquaporin-3 deficiency in mouse models of colitis. *Gut* **2007**, *56:*, 1529-1535.
43. Hara-Chikuma, M.; Verkman, A. Aquaporin-3 facilitates epidermal cell migration and proliferation during wound healing. *J. Mol. Med.* **2008**, *86*, 221-231.
44. Niethammer, P.; Grabher, C.; Look, A. T.; Mitchison, T. J. A tissue-scale gradient of hydrogen peroxide mediates rapid wound detection in zebrafish. *Nature* **2009**, *459*, 996-999.
45. Itoh, A.; Tsujikawa, T.; Fujiyama, Y.; Bamba, T. Enhancement of aquaporin-3 by vasoactive intestinal polypeptide in a human colonic epithelial cell line. *J. Gastroenterol. Hepatol.* **2003**, *18*, 203-210.
46. Perner, A.; Andresen, L.; Pedersen, G.; Rask-Madsen, J. Superoxide production and expression of NAD (P) H oxidases by transformed and primary human colonic epithelial cells. *Gut* **2003**, *52*, 231.
47. Hara-Chikuma, M.; Verkman, A. S. Roles of Aquaporin-3 in the Epidermis. *J. Invest. Dermatol.* **2008**, *128*, 2145-2151.
48. Rygiel, T. P.; Mertens, A. E.; Strumane, K.; van der Kammen, R.; Collard, J. G. The Rac activator Tiam1 prevents keratinocyte apoptosis by controlling ROS-mediated ERK phosphorylation. *J. Cell. Sci.* **2008**, *121*, 1183-1192.
49. Belousov, V. V.; Fradkov, A. F.; Lukyanov, K. A.; Staroverov, D. B.; Shakhbazov, K. S.; Terskikh, A. V.; Lukyanov, S. Genetically encoded fluorescent indicator for intracellular hydrogen peroxide. *Nat. Methods* **2006**, *3*, 281-6.
50. Manning, B. D.; Cantley, L. C. AKT/PKB Signaling: Navigating Downstream. *Cell* **2007**, *129*, 1261-1274.
51. Rhee, S. G.; Bae, Y. S.; Lee, S.-R.; Kwon, J. Hydrogen Peroxide: A Key Messenger That Modulates Protein Phosphorylation Through Cysteine Oxidation. *Sci. STKE* **2000**, *2000*, pe1.

52. Cao, C.; Sun, Y.; Healey, S.; Bi, Z.; Hu, G.; Wan, S.; Kouttab, N.; Chu, W.; Wan, Y. EGFR-mediated expression of aquaporin-3 is involved in human skin fibroblast migration. *Biochem. J.* **2006**, *400*, 225-34.
53. Ikeda, S.; Yamaoka-Tojo, M.; Hilenski, L.; Patrushev, N.; Anwar, G.; Quinn, M.; Ushio-Fukai, M. IQGAP1 regulates reactive oxygen species-dependent endothelial cell migration through interacting with Nox2. *Arterioscler. Thromb. Vasc. Biol.* **2005**, *25*, 2295-300.
54. Moldovan, L.; Moldovan, N. I.; Sohn, R. H.; Parikh, S. A.; Goldschmidt-Clermont, P. J. Redox changes of cultured endothelial cells and actin dynamics. *Circ. Res.* **2000**, *86*, 549-57.

Appendix 1:

A Targeted Fluorescent Sensor for Imaging Reversible Redox Cycles in the Mitochondria of Living Cells

As the site of cellular respiration, the mitochondria are a potentially potent source of damaging reactive oxygen species (ROS).[1,2] Therefore, monitoring the accumulation and maintenance of ROS within this specific microenvironment is critical to discerning the effect of mitochondrial redox status on both cellular pathology and physiology. There are currently an assortment of mitochondrial fluorescent indicators for a variety of ROS,[3] including hydrogen peroxide,[4] superoxide,[5] and highly reactive oxygen species.[6] However, all of these fluorescent probes irreversibly respond to a given ROS, making them inadequate for studying the recovery from oxidative stress within mitochondria. Several protein and peptide approaches have been developed,[7-12] some of which can potentially be targeted to subcellular locales with targeting sequences. However, these tools require transfection and are difficult to apply to tissue samples or *in vivo* imaging. Therefore, we sought to develop a small molecule based reversible redox sensor that is targeted to the mitochondria.

Previously we developed RF1, a naphthalene disulfide probe capable of monitoring reversible redox changes in the cytosol.[13] We sought to utilize this novel naphthalene-disulfide switch to create a mitochondrial-targeted form of this compound. As lipophilic cations tend to accumulate in the mitochodria due to the proton gradient,[3] we hypothesized that a rhodamine derivative of RF1, which would be cationic, would accumulate in the mitochondria without the need for additional targeting groups. To that end, the condensation of naphthalene-1,8-disulfide-4-carboxaldehyde with 3-dimethylaminophenol using microwave irradiation affords Mitochondrial Redox-Sensor 1 (MRS1, Scheme A1-1).

MRS1 (5 μM in DPBS, pH 7.4) has an excitation maximum around 540 nm and an emission around 590 nm, as expected for a rhodamine-type dye of this structure. The addition of one equivalent of TCEP causes a fast and robust decrease in fluorescent intensity, with maximal turn-off after about 4 minutes (Figure A1-1). As seen in Figure A1-2, the addition of 100 μM H_2O_2 causes a recovery of fluorescent signal after about 30 min. The addition of a second equivalent of TCEP causes another drop in fluorescent output, and after another 30 min incubation the fluorescent signal again recovers. These data indicate that MRS1 is capable of measuring reversible redox cycles.

We next turned our attention to the cellular distribution and validation of MRS1. To that end, HeLa cells loaded with MRS1 show low but measurable fluorescent signal corresponding to discrete subcellular regions (Figure A1-3a). The addition of 100 μM H_2O_2 to the cells results in enhanced fluorescent intensity after 15 min (Figure A1-3b). After removal of the H_2O_2 and a 25 min recovery period, the fluorescent output is similar to that of the starting conditions (Figure A1-3c). The addition of 100 μM H_2O_2 a second time causes an enhanced turn-on response compared to the first stimulation (Figure A1-3d, and A1-4), potentially due to the cells' weakened redox defense system after the initial redox insult. The cells were simultaneously loaded with Mitotracker Deep Red to stain mitochondria. These experiments confirm that the fluorescent signal from MRS1 is indeed arising from cellular mitochondria (Figure A1-3, d,e,f,g,h, and i). Additionally, this recovery response is opposite of that observed within the cytosol using RF1, possibly suggesting a differential redox recovery after insult within different compartments of the cell.

The aforementioned experiments demonstrate that MRS1 is capable of targeting the mitochondria of live cells, where it can then respond reversibly to redox changes. This molecule should prove useful in unraveling some of the complexities of mitochondrial redox homeostasis.

Experimental Section

Synthetic Materials and Methods. All reactions were carried out under a dry nitrogen atmosphere. Naphthalene-1,8-disulfide-4-carboxaldehyde[14] was synthesized according to literature procedures. Silica gel P60 (SiliCycle) was used for column chromatography. Analytical thin layer chromatography was performed using SiliCycle 60 F254 silica gel (precoated sheets, 0.25 mm thick). All chemicals were purchased from Sigma-Aldrich (St. Louis, MO) and used as received. MitoTracker Deep Red and LysoTracker Red were purchased from Invitrogen (Carlsbad, CA). ^{1}H NMR spectra was collected in $CO(CD_3)_2$/5% CD_3OD (Cambridge Isotope Laboratories, Cambridge, MA) at 25 ºC on a Bruker AVQ-400 spectrometer at the College of Chemistry NMR Facility at the University of California, Berkeley. All chemical shifts are reported in the standard δ notation of parts per million using the peak of residual proton signals of $CHCl_3$ as an internal reference. Mass spectral analyses were carried out at the College of Chemistry Mass Spectrometry Facility at the University of California, Berkeley. Microwave reactions were performed using a CEM Intelligent Explorer/Discover (Matthews, NC).

Mitochondrial Redox-Sensor-1 (MRS1). Napthalene-aldehyde (120 mg, 0.89 mmol) and 3-dimethylaminophenol (220 mg, 0.35 mmol) were dissolved in MeOH in a pressure flask and stirred at room temperature for 10 min. The contents were then dried under reduced pressure. The flask was then sealed and microwaved, solvent-free, at 155 ºC for 30 min. After cooling, the solid contents were then dissolved in MeOH and chloranil (100 mg, 0.41 mmol) was added. After stirring at room temperature for 30 min, the contents were dried under reduced pressure. Purification by flash chromatography (9:1:0.05 dichloromethane/methanol/water) yielded MRS1 (5.3 mg, 3%). ^{1}H NMR ($(CO(CD_3)_2$/5% CD_3OD 400 MHz): δ 7.61 (1H, d, J = 7.6 Hz), 7.46 (1H, s), 7.44 (1H, d, J = 2.0 Hz), 7.34 (1H, s), 7.32 (1H, s), 7.27 (1H, t, J = 8.0 Hz), 7.10 (1H, d, J = 2.4 Hz), 7.04 (1H, d, J = 2.4 Hz), 6.96-7.01 (3H, m), 3.37 (12H, s).

Preparation and Staining of Cell Cultures. HeLa cells were cultured in DMEM with high glucose, GlutaMAX, and 10% FBS. Two days before imaging, cells were passaged and plated on 18-mm glass coverslips. For all experiments, solutions of dyes (from 5 mM stocks in DMSO) were made in DBPS with calcium chloride and magnesium chloride (Sigma). H_2O_2 was added by bath application to the medium from a 100 mM aqueous stock. For paraquat treatment, HeLa cells were cultured as described above. One day prior to imaging, 1 mM paraquat was added to cells from a 0.5 M stock solution in water. An equal amount of water was added to control cells at the same time. Cells were then incubated at 37 °C, 5% CO_2. After 24 h, the media was exchanged for DPBS with 1 μM dye and incubated for 20 min.

Fluorescence Imaging Experiments. Confocal fluorescence imaging studies were performed with a Zeiss LSM510 NLO Axiovert 200 laser scanning microscope and a 40x Achroplan IR water-immersion objective lens. Excitation of MRS1-loaded cells was carried out with a 543 nm laser and emission was collected using a META detector between 554-587 nm. MitoTracker Deep Red was excited with a 633-nm laser and emission was collected between 672-704 nm. Excitation of Hoechst 33342 was carried out using a MaiTai two-photon laser at 780-nm pulses (mode-locked Ti:sapphire laser, Tsunami Spectra Physics) and emission was collected between 436-522 nm. Image analysis was performed in ImageJ.

Figures and Schemes

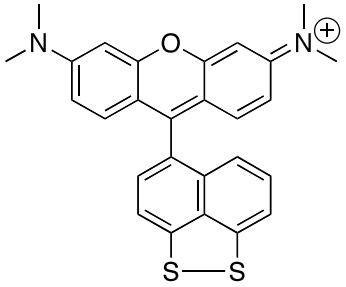

Scheme A1-1. *Structure of MRS1*.

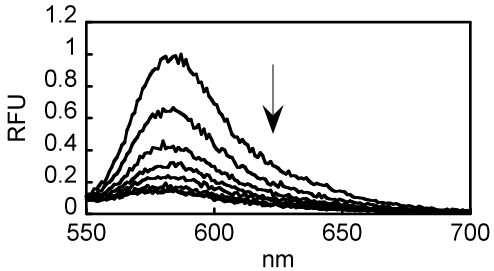

Figure A1-1. Time-course fluorescence spectra of MRS1 treated with TCEP. 5 μM MRS1 in DPBS scanned (ex 543 nm, scanned from 550-750 nm). Added 1 eq of TCEP after the first scan, then scanned after 20, 45, 80, 110, 170, 260 and 440 seconds.

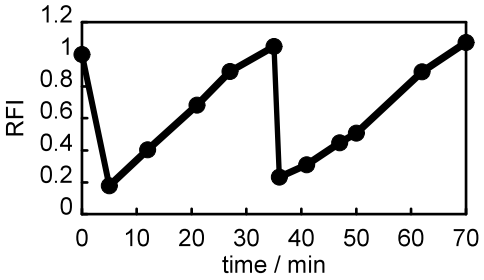

Figure A1-2. Sensing reversible redox changes with MRS1 *in vitro.* 5 μM MRS1 in DPBS scanned (ex 543 nm, integrated from 550-750 nm). Added 1 eq of TCEP after the first scan, 100 μM H_2O_2 at t = 5 min, and 10 eq. of TCEP at t = 32 min. Finally, added 100 μM H_2O_2 at t = 35 min. RFI = relative fluorecence intensity.

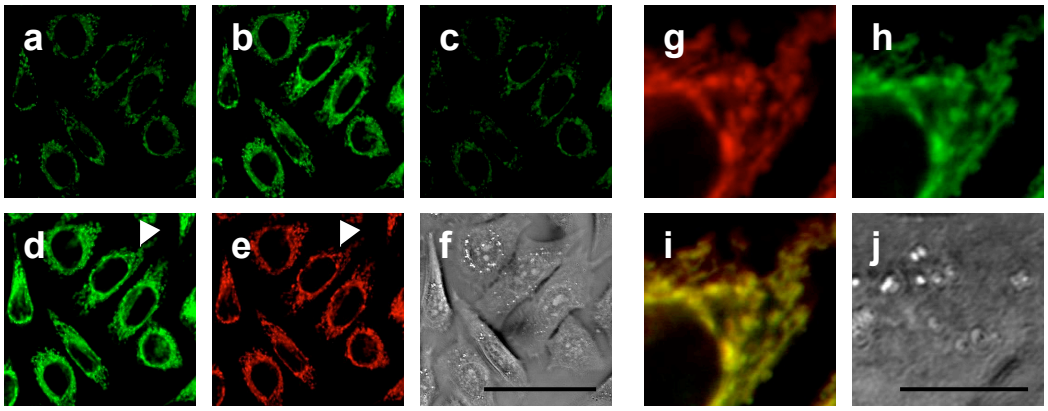

Figure A1-3. Confocal fluorescence images of live HeLa cells with varying mitochondrial redox states visualized with MRS1. Images displayed represent emission intensities collected in optical windows between 565 nm and 615 nm upon excitation at 543 nm for MRS1 and between 650 nm and 700 nm upon excitation at 633 nm for Mitotracker Deep Red. HeLa cells incubated with 5 μM MRS1 for 15 min, then swapped for fresh DPBS and imaged with MRS1 (a). The cells were then treated with 100 μM H_2O_2 for 20 min and imaged with MRS1 (b). The cells were then washed twice with DPBS, incubated for 25 min, and imaged with MRS1 (c). The cells were then treated with 100 μM H_2O_2 again for 15 min and imaged with MRS1 (d), Mitotracker Deep Red (e) and a brightfield (overlay, f) with a 50 μm scale bar. The cell identified with an arrow in d and e is shown enlarged with the fluorescent signal from Mitotracker Deep Red (g), MRS1 (h), and an overlay (i) with a 10 μm scale bar.

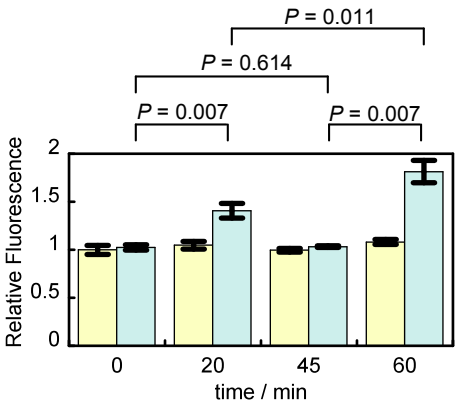

Figure A1-4. Quantification of fluorescence from live HeLa cells with varying mitochondrial redox states visualized with MRS1. The experiment as conducted in Figure A1-3 was quantified (k, blue bars) with 3 images counted for each time point, along with a simultaneous control experiment with cells treated and imaged identically without any H_2O_2 added at any stage (k, yellow bars).

References

1. Turrens, J. F. Mitochondrial Formation of Reactive Oxygen Species. *The Journal of Physiology* **2003**, *552*, 335-344.
2. Addabbo, F.; Montagnani, M.; Goligorsky, M. S. Mitochondria and Reactive Oxygen Species. *Hypertension* **2009**, *53*, 885-892.
3. Dickinson, B. C.; Srikun, D.; Chang, C. J. Mitochondrial-targeted fluorescent probes for reactive oxygen species. *Current Opinion in Chemical Biology* **2010**, *14*, 50-56.
4. Dickinson, B. C.; Chang, C. J. A Targetable Fluorescent Probe for Imaging Hydrogen Peroxide in the Mitochondria of Living Cells. *J. Am. Chem. Soc.* **2008**, *130*, 11561-11561.
5. Robinson, K. M.; Janes, M. S.; Pehar, M.; Monette, J. S.; Ross, M. F.; Hagen, T. M.; Murphy, M. P.; Beckman, J. S. Selective fluorescent imaging of superoxide in vivo using ethidium-based probes. *Proceedings of the National Academy of Sciences, USA* **2006**, *103*, 15038.
6. Koide, Y.; Urano, Y.; Kenmoku, S.; Kojima, H.; Nagano, T. Design and Synthesis of Fluorescent Probes for Selective Detection of Highly Reactive Oxygen Species in Mitochondria of Living Cells. *Journal of the American Chemical Society* **2007**, *129*, 10324-10325.
7. Østergaard, H.; Henriksen, A.; Hansen, F. G.; Winther, J. R. Shedding light on disulfide bond formation: engineering a redox switch in green fluorescent protein. *The EMBO Journal* **2001**, *20*, 5853-5862.
8. Lee, K.; Dzubeck, V.; Latshaw, L.; Schneider, J. P. De novo designed peptidic redox potential probe: Linking sensitized emission to disulfide bond formation. *J. Am. Chem. Soc* **2004**, *126*, 13616-13617.
9. Hanson, G. T.; Aggeler, R.; Oglesbee, D.; Cannon, M.; Capaldi, R. A.; Tsien, R. Y.; Remington, S. J. Investigating mitochondrial redox potential with redox-sensitive green fluorescent protein indicators. *Journal of Biological Chemistry* **2004**, *279*, 13044.
10. Cline, D. J.; Thorpe, C.; Schneider, J. P. Structure-based design of a fluorimetric redox active peptide probe. *Analytical biochemistry* **2004**, *325*, 144-150.
11. Belousov, V. V.; Fradkov, A. F.; Lukyanov, K. A.; Staroverov, D. B.; Shakhbazov, K. S.; Terskikh, A. V.; Lukyanov, S. Genetically encoded fluorescent indicator for intracellular hydrogen peroxide. *Nature Methods* **2006**, *3*, 281-286.
12. Wang, W.; Fang, H.; Groom, L.; Cheng, A.; Zhang, W.; Liu, J.; Wang, X.; Li, K.; Han, P.; Zheng, M. Superoxide flashes in single mitochondria. *Cell* **2008**, *134*, 279-290.
13. Miller, E. W.; Bian, S. X.; Chang, C. J. A fluorescent sensor for imaging reversible redox cycles in living cells. *J. Am. Chem. Soc* **2007**, *129*, 3458-3459.
14. Miller, E. W.; Bian, S. X.; Chang, C. J. A Fluorescent Sensor for Imaging Reversible Redox Cycles in Living Cells. *J. Am. Chem. Soc.* **2007**, *129*, 3458-3459.

Appendix 2:

Synthesis of Derivatives of the Peroxy Yellow and Peroxyfluor Classes of Mono-Boronate Hydrogen Peroxide Sensors

Synopsis

This appendix describes the synthesis of various derivatives of targeted hydrogen peroxide (H_2O_2) sensors based on the asymmetric piperazine-rhodol scaffold utilized for MitoPY1 in Chapter 3. Peroxy Yellow Methyl Bromide (PYMBr) is a probe containing a reactive electrophile designed for either cellular uptake by reaction with intracellular glutathione or for bioconjugation reactions with cysteine-containing polypeptides. Peroxy Yellow Acetoxymethyl Ester (PYAM) is a first-generation trappable probe with an acetoxymethyl ester protected carboxylic acid for enhanced intracellular uptake and retention. This molecule was later replaced by PF6-AM (Chapter 4) as multiple anionic groups were found to be required for efficient trapping. Peroxy Yellow Palmitic Acid (PYPal) is a first-generation membrane-targeted probe featuring a lipophilic carbon tail. However, PYPal tracked to not only the outer membrane, but also the inner membranes of cells, rendering it inappropriate for detection of H_2O_2 at the outer membrane. Therefore, a second-generation membrane targeted probe, Membrane-targeted Peroxy Yellow 1 (MembrPY1) was synthesized featuring a lipohilic palmitic acid tail for membrane targeting and an anionic aspartic acid residue to hold the probe on the outer membrane. As seen in figures A2-1 and A2-2, MembrPY1 can track to the cell membrane and respond to both endogenous and exogenous H_2O_2. Finally, the synthesis and characterization of PF5 (the other isomer of PF6, the carboxyfluorescein derivative of the probe used in Chapter 4) is described. As seen in figures A2-3 and A2-4, PF5 has a turn-on response to H_2O_2 and is selective over other biologically relevant reactive oxygen species (ROS).

Results and Experimental Details

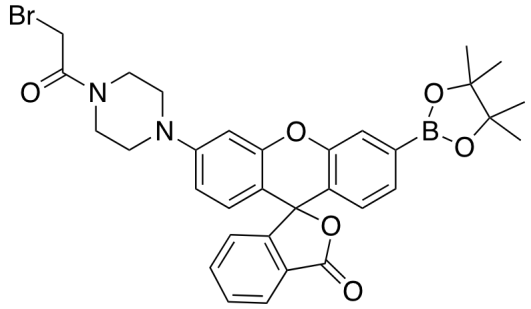

Peroxy Yellow Methyl Bromide, "PYMBr". Fmoc-piperazine boronate (12 mg, 0.02 mmol) was added to a vial and dissolved in 1.5 mL of acetonitrile. Two drops of piperidine were added to the solution and the mixture was stirred at room temperature for 30 min, after which the contents were evaporated under reduced pressure. The vial was then brought into an inert atmosphere box, where bromoacetic acid NHS-ester (10 mg, 0.04 mmol), sodium bicarbonate (20 mg, 0.24 mmol), and 1.5 mL of acetonitrile were added to the vial and the reaction was stirred at room temperature for 24 hours. The vial was then brought out of the box and the crude reaction was filtered through a celite plug. The reaction contents were then dried under reduced pressure. Purification by column chromatography (1:4 hexanes/ethyl acetate) yielded **PYMBr** as an orange solid (4.3 mg, 34%). ^{1}H NMR ($CDCl_3$/5% CD_3OD, 300 MHz): δ 7.91 (1H, d, J = 6.9 Hz), 7.60 (1H, s), 7.55 (2H, quintet, J = 6.6 Hz), 7.29 (1H, d, J = 7.8 Hz), 7.02 (1H, d, J = 6.9 Hz), 6.66 (1H, d, J = 8.1 Hz), 6.63 (1H, s), 6.49-6.60 (2H, m), 3.81 (2H, s), 3.38-3.45 (4H, m), 3.32-3.38 (4H, m), 1.23 (12H, s). HR-FABMS: calculated for [M^+] 631.1615, found 631.1607.

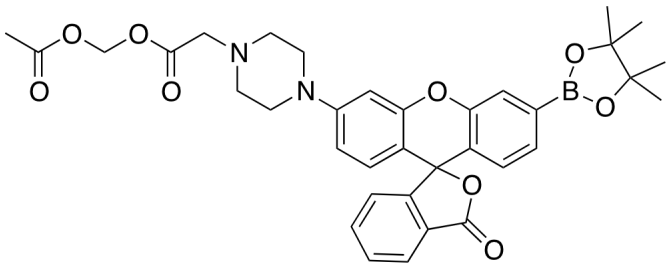

Peroxy Yellow Acetoxymethyl Ester, "PYAM". Fmoc-piperazine boronate (21 mg, 0.03 mmol) was added to a vial and dissolved in 2 mL of dichloromethane. Two drops of piperidine were added to the solution and the mixture was stirred at room temperature for 30 min, after which the contents were evaporated under reduced pressure. Bromoacetic acid (11 mg, 0.08 mmol), sodium bicarbonate (23 mg, 0.27 mmol), and 3 mL of acetonitrile were added to the vial and the contents stirred at room temperature overnight. The contents were evaporated under reduced pressure and put on a high-vac to dry. The crude reaction mixture was then dissolved in 3 mL of DMF, and 100 μL of diisopropylethylamine and 3 drops of bromomethyl acetate were added to the reaction. After 24 hours of stirring at room temperature, the product was extracted into ethyl acetate, washed three times with water, and dried under reduced pressure. Purification by column chromatography (4:1 ethyl acetate/hexanes) furnished **PYAM** as an orange solid (8 mg, 47%). ^{1}H NMR ($CDCl_3$ /10% CD_3OD, 500 MHz): δ 7.96 (1H, d, *J* = 7.5 Hz), 7.65 (1H, s), 7.61 (1H, t, *J* = 7.5 Hz), 7.57 (1H, t, *J* = 7.5 Hz), 7.35 (1H, d, *J* = 8.0 Hz), 7.07 (1H, d, *J* = 7.5 Hz), 6.72 (1H, d, *J* = 8.0 Hz), 6.67 (1H, d, *J* = 2.5 Hz), 6.60 (1H, d, *J* = 9.0 Hz), 6.56 (1H, dd, *J* = 2.5, 9.0 Hz), 5.74 (2H, s), 3.38 (2H, bs), 3.30 (4H, bs), 2.79 (4H, bs), 2.07 (3H, s), 1.29 (12H, s). ^{13}C NMR ($CDCl_3$ /10% CD_3OD, 125 MHz): δ 170.0, 169.7, 153.3, 152.3, 150.8, 135.1, 129.7, 129.1, 128.6, 127.1, 126.2, 124.9, 123.8, 123.3, 121.41, 112.0, 102.3, 84.2, 79.3, 52.3, 20.5. HR-FABMS: calculated for [M^+] 641.2665, found 641.2672.

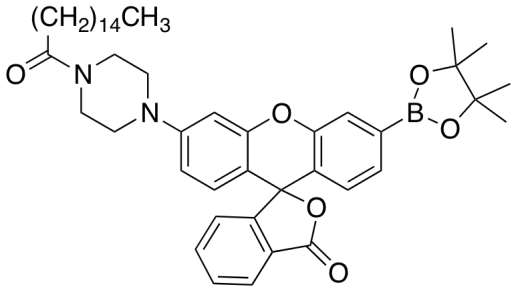

Peroxy Yellow Palmitic Acid, "PYPal". Fmoc-piperazine boronate (12 mg, 0.02 mmol) was added to a vial and dissolved in 1.5 mL of acetonitrile. Two drops of piperidine were added to the solution and the mixture was stirred at room temperature for 30 min, after which the contents were evaporated under reduced pressure. Palmitic acid NHS-ester (14 mg, 0.04 mmol), cesium carbonate (13 mg, 0.04 mmol), and 1.5 mL of acetonitrile were added to the vial and the reaction was stirred at room temperature overnight. The reaction contents were then dried under reduced pressure. Purification by column chromatography (1:1 hexanes/ethyl acetate) yielded **PYPal** as an orange solid (6.4 mg, 43%). ^{1}H NMR ($CDCl_3$, 400 MHz): δ 8.04 (1H, d, *J* = 6.4 Jz), 7.73 (1H, s), 7.63 (2H, quintet, 6.8 Hz), 7.42 (1H, d, *J* = 8.0 Hz), 7.12 (1H, d, *J* = 7.6 Hz), 6.80 (1H, d, *J* = 7.6 Hz), 6.67-6.74 (2H, m), 6.12 (1H, d, *J* = 8.8 Hz), 3.74-3.84 (2H, m), 3.59-3.66 (2H, m), 3.19-

3.29 (4H, m), 1.56-1.70 (7H, m), 1.35 (12H, s), 1.19-1.31 (24H, m). HR-FABMS: calculated for [M^+] 749.4701, found 749.4706.

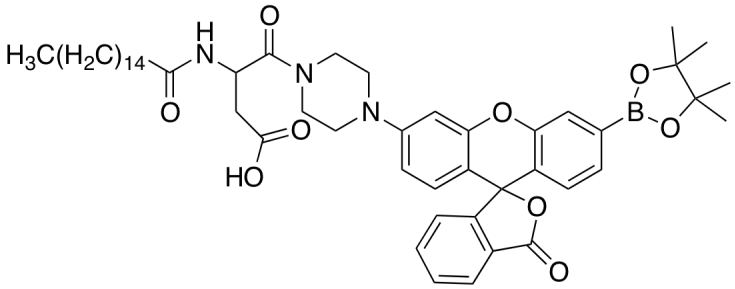

Membrane-targeted Peroxy Yellow 1, "MembrPY1" (25). Fmoc-piperazine boronate (214 mg, 0.33 mmol) was added to a vial and dissolved in 3.0 mL of acetonitrile. Five drops of piperidine were added to the solution and the mixture was stirred at room temperature for 30 min, after which the contents were evaporated under reduced pressure. Fmoc-Asp(OtBu)-NHS ester and 200 mg of sodium bicarbonate were added to the vial and the reaction contents were dissolved in 5 mL of acetonitrile and stirred at room temperature for 2 hours. The reaction contents were dried under reduced pressure and semi-purified via column chromatography (40:1 dichloromethane/methanol). 90 mg of the crude intermediate was dissolved in 4 mL of acetonitrile. Five drops of piperidine were added and the contents stirred at room temperature for 30 min. After drying the reaction contents under reduced pressure, palmitic acid NHS-ester (100 mg), sodium bicarbonate (100 mg), and 4 mL of acetonitrile were added to the vial and the reaction stirred for 2 hours. More palmitic acid NHS-ester (50 mg) was added to the mixture and the stirring was continued for another 20 minutes. The crude reaction mixture was dried under reduced pressure. Column chromatography (gradient from 4.5:4.5:0.25 dichloromethane/ethyl acetate/ethanol to 8:2:1 dichloromethane/methanol/acetone) yielded a mixture of the pinnacol protected and deprotected tert-butyl protected product. After dissolving the crude product in 1 mL of dichloromethane, 1 mL of trifluoroacetic acid was added and the solution was stirred for 2 hours. The mixture was then dried under reduced pressure. Purification by column chromatography (225:225:25:2 dichloromethane/ethyl acetate/methanol/trifluoroacetic acid) yielded **MembrPY1** as a reddish solid (23 mg, 9%). ^{1}H NMR ($CDCl_3$/5% CD_3OD, 400 MHz): δ 8.00 (1H, bs), 7.76 (1H, d, *J* = 6.4 Hz), 7.56-7.69 (2H, m), 7.39-7.46 (1H, m), 7.30-7.39 (1H, m), 7.10 (1H, d, *J* = 6.4 Hz), 6.76 (1H, d, *J* = 6.4 Hz), 6.63-6.74 (1H, m), 6.55-6.63 (1H, m), 4.09 (2H, d, *J* = 6.8 Hz), 3.69-3.88 (4H. m), 2.24-3.55 (16H, m), 2.18 (1H, s), 1.10-1.30 (19H, m). HR-FABMS: calculated for [M^+] 780.4049, found 780.4037.

5-Carboxyfluorescein monotriflate. 5-Carboxyfluorescein (5.24 g, 13.9 mmol) was added to a vial and dissolved in 70 mL of acetonitrile. Diisopropylethylamine (25 mL, 248 mmol) was then added and the reaction stirred for 10 min. *N*-Phenyl-bis(trifluoromethanesulfonimide) (5.0 g, 14.0 mmol) and 50 mL of DMF were then added, the vessel was sonicated for 5 minutes, and the reaction was stirred 72 hours at room temperature. The reaction mixture was then dried under reduced pressure. Purification by column chromatography (19:1 CH_2Cl_2/MeOH) afforded compound **5-Carboxyfluorescein monotriflate** as a yellow oil (412 mg, 60% yield). ^{1}H NMR ($(CD_3)_2CO$, 400 MHz): δ 8.64 (1H, s), 8.43 (1H, d, *J* = 8.0 Hz), 7.42-7.54 (2H, m), 7.22 (1H, dd, *J* = 2.4, 8.8 Hz), 7.16 (1H, d, *J* = 8.8 Hz), 6.86 (1H, s), 6.77 (1H, d, *J* = 8.8 Hz), 6.71 (1H, d, *J* =

8.8 Hz). ^{13}C NMR ($(CH_3)_2CO$, 100 MHz): δ 168.3, 167.9, 160.4, 155.4, 152.4, 152.2, 150.6, 136.7, 135.5, 131.0, 129.7, 127.2, 124.8, 124.7, 120.3, 117.4, 113.9, 111.0, 109.7, 103.1, 82.1. ^{19}F NMR ($(CH_3)_2CO$, 376.5 MHz): δ -73.02. Low-resolution MS: 508.1.

PF5. 5-Carboxyfluorescein monotriflate (478 mg, 0.94 mmol), $Pd(OAc)_2$ (345 mg, 1.54 mmol), Bis(pinacolato)diboron (365 mg, 1.42 mmol), Cyclohexyl JohnPhos (203 mg, 0.58 mmol), diisopropylethylamine (742 mg, 5.74 mmol), and 5 mL of dioxane were added to a vial in an inert atmosphere glove box and the reaction was stirred overnight at room temperature. The vial was then brought out of the glove box and the contents were evaporated to dryness. Purification by column chromatography (19:1 dichloromethane/methanol) furnished **PF5** as a yellow solid (157 mg, 34% yield). ^{1}H NMR ($CDCl_3$, 300 MHz): δ 8.56 (1H, s), 8.19 (1H, d, J = 8.1 Hz), 7.65 (1H, s), 7.33 (1H, d, J = 7.8 Hz), 7.13 (1H, d, J = 8.1 Hz), 6.64-6.76 (2H, m), 6.44-6.55 (2H, m), 1.27 (12H, s). ^{13}C NMR ($(CD_3)_2CO$, 75 MHz): δ 168.95, 167.49, 160.71, 156.45, 153.18, 151.59, 137.42, 135.69, 130.27, 128.43, 127.72, 125.13, 124.76, 123.89, 122.62, 113.69, 110.69, 103.58, 85.10, 25.21.

PF5 features two visible region absorptions (λ_{abs} = 370 nm, ε = 10,000 $^{-1}$cm^{-1}; 460 nm, ε = 14,000 M^{-1}cm^{-1}) and a weak emission (λ_{em} = 527 nm, Φ = 0.07). Kinetics measurements of the H_2O_2-mediated boronate deprotection were performed under pseudo-first-order conditions (5 μM dye, 10 mM H_2O_2), giving an observed rate constant of $k = 5.5(1) \times 10^{-3}$ s^{-1}.

Figures

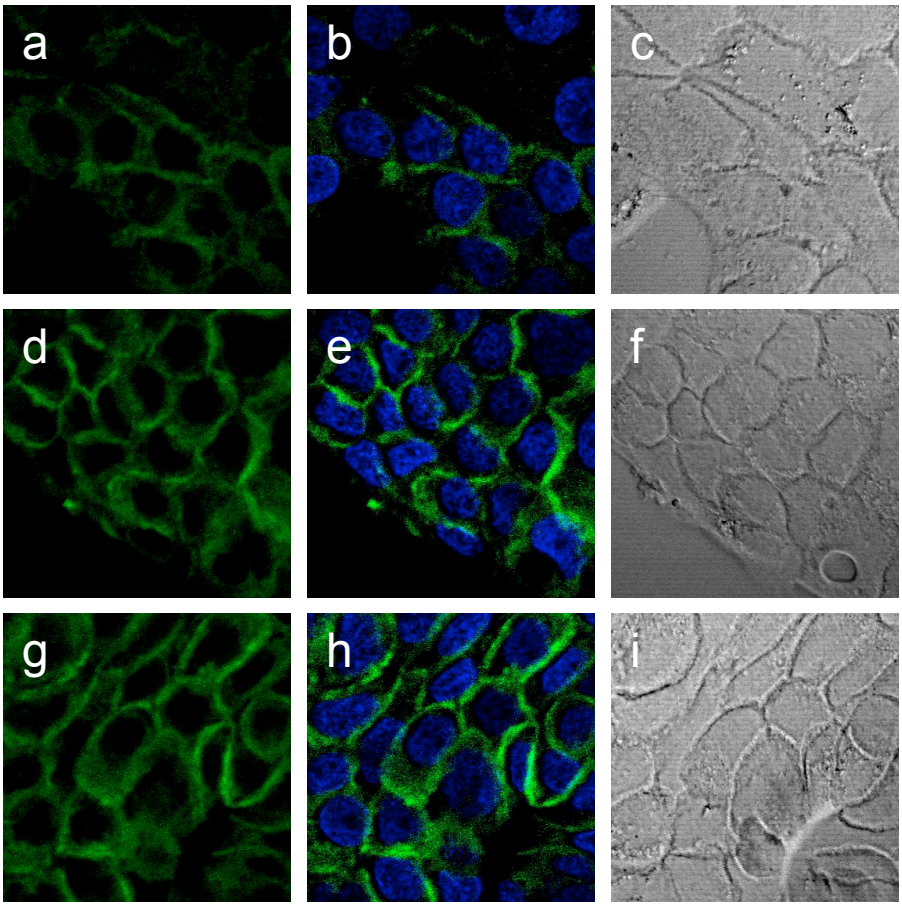

Figure A2-1. Imaging of membrane H_2O_2 in live A431 cells. A431 cells loaded with 5 μM MembrPY1 in DPBS with 1 μM Hoechst 33342 at 37 °C for 10 min. Cells then stimulated with either water carrier, 100 μM H_2O_2, or 500 ng/mL EGF for 30 minutes at 37 °C. Cells then analyzed by confocal microscopy. Shown are control cells stained with MembrPY1 (a), MembrPY1 with Hoechst 33342 overlay (b), brightfield (c), EGF-treated cells stained for MembrPY1 (d), MembrPY1 with Hoechst 33342 overlay (e), brightfield (f), and H_2O_2-treated cells stained for MembrPY1 (g), MembrPY1 with Hoechst 33342 overlay (h), brightfield (i).

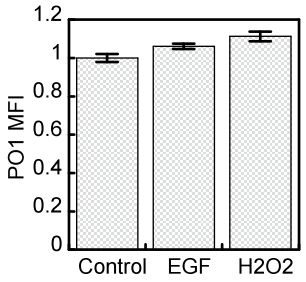

Figure A2-2. Quantification of membrane H_2O_2 in live A431 cells. Quantification of experiment from Figure A2-1 with 4 images counted per condition and error bars as S.E.M. MFI = mean fluorescent intensity.

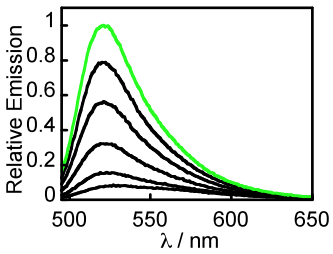

Figure A2-3. Fluorescence response of PF5 to H_2O_2. Fluorescence turn-on response of 5 μM PF6 at 0, 5, 15, 30, 45, and 60 minutes after the addition of 100 μM H_2O_2.

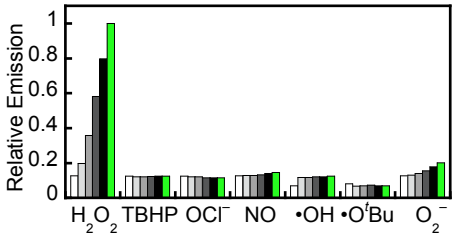

Figure A2-4. Fluorescence responses of 5 μM PF5 to various reactive oxygen species (ROS). Bars represent relative responses at 0, 5, 15, 30, 45, and 60 min after addition of each ROS. Data shown are for 10 mM O_2^- (with 10 μM Catalase), 200 μM NO, and 100 μM for all other ROS.

Appendix 3:

Protocol for Aliquoting Boronate Probes

.Introduction

The boronate probes are best stored as dry stocks free of water and oxygen at -20 °C. Additionally, the dyes keep best if the solid stocks are dissolved and utilized the day of experimentation. This protocol describes how to aliquot probes in a manner that keeps volumes minimal but allows for optimal storage of the dyes. See Figure A3-1 for a picture of the entire setup.

Protocol

1. Weigh out an appropriate amount of dye in a clean, glass vial.
2. Calculate the volume of solvent to add to make the stock concentration of dye that is appropriate.
    a. In general, the boronate dyes are made as 5 mM stocks.
    b. For example, if you weighed out 50 mg of a dye that had a molecular weight of 500 g/mol, you would calculate: 0.05 / 500 / 0.005 = 0.02. This means that dissolving the dye in 20 mL will make a 5 mM stock.
3. Dissolve the dye in the calculated volume of solvent. Select a solvent that is easily evaporated but that can also be pipetted. Ethyl acetate is optimal, followed by acetone, dichloromethane and methanol. Dichloromethane is very difficult to pipette accurately and methanol can cause decomposition of the boronate. Mixtures of solvents also work, as long as the volume is accurately measured.
4. Allign PCR tubes with lids attached along an empty pipette tip box. It is generally best to use every-other row, as the lids will get in the way of the previous row.
5. Use the lid of a pipette tip box to serve as a reservoir for the dye solution.
    a. Make sure you test the lid for chemical reactivity prior to adding the dye stock. To test the lid, add some solvent into the box and ensure that it does not dissolve it.
6. Pour the dye stock into the box, keeping it propped up at an angle so the solution forms a basin along one of the edges.
7. Use a multichannel pipette to add the dye to the PCR tubes. This should be done quickly, as the solution of dye will evaporate and continue to become more concentrated over time.
    a. Generally, stocks between 10 and 100 μL are made.
8. Put the tubes into a dessicator with a vacuum attachement and completely dry between 24 and 48 hours.
9. Remove the tubes, seal the lids, and put into 50 mL conical tubes. Add about 3 mL of Drierite to each tube, seal them, and store them in the freezer.
10. Mark the tubes with the name of the compound, the date, the volume aliquoted out per tube, and the final concentration that volume would provide.
    a. For example, “Dye X, dissolve in 50 μL for a 5 mM stock.”

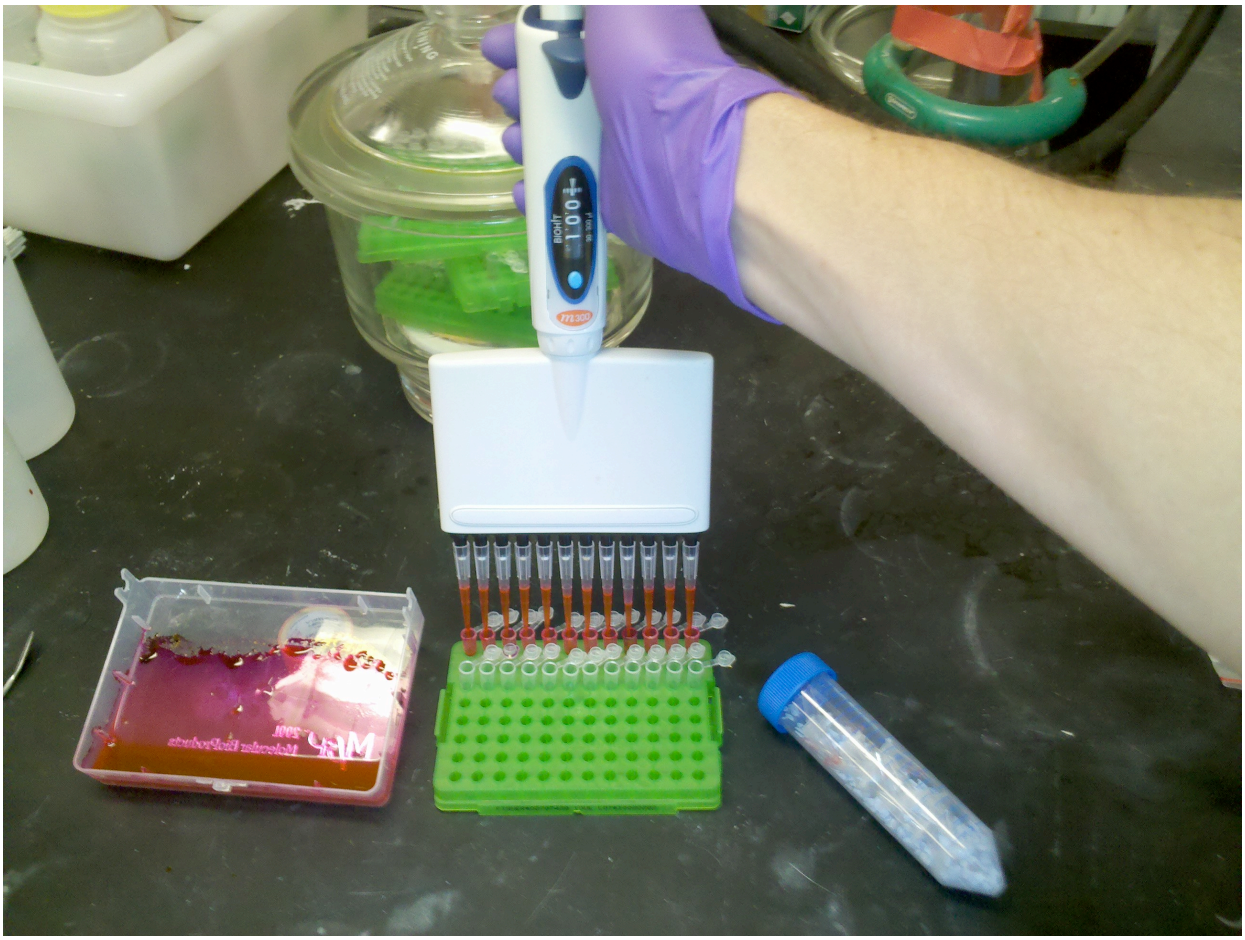

Figure A3-1: Picture demonstrating the protocol for aliquoting out boronate probes. Note the plastic tip lid being used as a basin for the organic dye stock, the PCR tubes aligned in a tip rack, the tubes drying in a dessicator under vacuum, and the conical tube of tubes of dye with Drierite.

Appendix 4:
Adult Hippocampal Stem/Progenitor Cell Culture and Analysis Protocols

Portions of this work were adapted from the following source:

Peltier, J.; Agrawal, S.; Robertson, M. J.; Schaffer, D. V. In *Protocols for Adult Stem Cells* 2009; Vol. 621, p 65-87.

Introduction

This appendix describes some experimental protocols for cell culture of adult hippocampal progenitor/stem cells (AHPs) including Poly-L-Ornithine/Laminin plate coating, AHP cell thawing, AHP cell passing, AHP proliferation assay, and AHP differentiation.

Poly-L-Ornithine/Laminin Plate Coating

Reagents:

1. Sterile H_2O
2. Sterile Gibco PBS, pH 7.4
3. Poly-ornithine, 30-40 kDa (Sigma Cat. No. P-3655)
    a. Dilute entire container in H_2O.
    b. Syringe Filter Sterilize.
    c. Aliquot and store at -20 °C.
4. Purified Mouse Laminin (Gibco Cat. No. 680-30171V)
    a. Store unopened stocks at –80 °C.
    b. Avoid repeated freeze/thaws (Opened laminin can be stored at –20 °C and should be used within 2 weeks.

Methods:

1. Based on the number and type of plates required, calculate required volumes of pOrn and Laminin working solutions (10 cm plate: 7 mL, 6 cm plate: 3 mL, 3.5 cm plate: 2 mL, 6/12/24-well plate: 12 mL, 96-well plate: 10 mL).
2. Based on the volume of solutions needed for coating, calculate the required amount of laminin for a 5 μg/mL working solution. Thaw laminin concentrate overnight at 4 °C.
3. Dilute pOrn in sterile water to generate a 10 μg/mL working solution.
4. Add pOrn working solution to each plate according to the table above. Incubate overnight at room temperature in tissue culture hood with the blower off, the sash closed, and the UV light off.
5. Rinse plates 2X with sterile water using the same volumes for each rinse as used for adding working solutions. Take care not to allow plates to dry out during this process. This step is best done with two people; one person to aspirate and the next to immediately add the next solution.
6. Dilute laminin in Gibco PBS pH 7.4 to a final concentration of 5 μg/ml.
7. Add laminin working solution to each plate. Incubate overnight at 37 °C.
8. Wrap complete plates in Saran Wrap and store at –20 °C. Plates last approximately 6 months when stored frozen.

9. *Optional:* To check and make sure coating process was sterile, use a single 10 cm coated dish, fill with sterile media (i.e. DMEM/F12), and incubate at 37 °C. Check for the next 2 days and make sure nothing grows on the plate by microscopy.

AHP Cell Thawing

Methods

1. Warm DMEM/F-12 + N-2 to 37°C and thaw a 6 cm poly-L-ornithine/laminin coated plate at room temperature.
2. Remove the vial from cryopreservation and immediately thaw in a 37 °C water bath with gentle swirling for about 2-3 min.
3. Gently pipette 1 mL DMEM/F-12 + N-2 into the vial, then pipette the entire contents of the vial to a 15 mL centrifuge tube, taking care to avoid bubbles.
4. Slowly and with gentle mixing, add 5 mL warm DMEM/F-12 + N-2 to the cell suspension. Steps 1-4 should be completed as quickly as possible (while avoiding contamination).
5. Pellet cells at 1000 rpm (200 x *g*) for 2.5 min.
6. Aspirate supernatant and add 2 mL DMEM/F-12 + N-2 to the cell pellet.
7. Use a flame-polished pipette to gently triturate the cell pellet.
8. Aspirate PBS from the freshly thawed poly-L-ornithine/laminin coated plate and immediately add 2 mL warm DMEM/F-12 + N-2.
9. Add the entire 2 mL of cell suspension to the plate. Immediately after adding the inoculum, gently rock the plate back and forth several times to mix.
10. Supplement the culture with 20 ng/mL FGF-2 (0.2 μL FGF-2 stock per mL of culture) and again rock the plate to mix.
11. Incubate overnight at 37 °C in 5% CO_2 atmosphere.
12. To remove residual DMSO, aspirate and replace the medium with fresh, warm DMEM/F-12 + N-2 the day after inoculation. Re-supplement with 20 ng/mL FGF-2.
13. Incubate at 37 °C in 5% CO_2 atmosphere and monitor daily to determine when to pass the culture, which is generally the next day. Cells are ready for experimentation after one passage.

AHP Cell Passing

Reagents:

1. Accutase
2. Poly-ornithine/laminin coated culture dishes
3. DMEM/F-12 Media + N-2 supplement
    a. Thaw 5 mL N2 solution at 4 °C overnight.

b. Add entire 5 mL N-2 solution to DMEM/F12.

4. 100 µg/mL FGF-2
    a. Dilute lyophilized FGF-2 in DMEM/F12 + N-2.
    b. Pipette up and down several times to dissolve.
    c. Aliquot out into microcentrifuge tubes and store at –20 °C (thawed aliquots can be stored at 4 °C for up to 2 weeks).

Methods:

1. Warm DMEM/F12 + N2 in 37°C water bath.
2. Thaw poly-ornithine/laminin coated plates. Add sterile, room temperature PBS to plates in order to for them to thaw faster and ensure they do not have dry spots during the thawing process. It is best to thaw them at room temperature, but can also be done at 37 °C if need be.
3. Aspirate media from culture dish, leaving ~0.5 mL behind to hydrate the cells
4. Add cold Accutase directly from the 4 °C storage to the plate (10 cm: 2.5 mL, 6 cm: 1.5 mL, 3.5 cm: 1.0 mL) and then incubate the plate at 37 °C for 2-3 min to detach the cells. Immediately put the Accutase back in storage. Gently tilt and shake the plate to dislodge cells. Check under a microscope to make sure cells have detached.
5. Add 5 mL DMEM/F12 + N2 to the plate to put the cells in suspension. Pipette the suspension into a 15 mL centrifuge tube and spin at 1000 rpm (200 x *g*) for 2.5 min.
6. Aspirate media to remove Accutase and add fresh media to the pellet. Generally cells should be resuspended in about 2.0 mL media. However, if you need a more or less concentrated solution of cells, this number can be modified.
7. Flame polish a cotton plugged Pasteur pipette to remove sharp edges and narrow the bore. Using the flame polished pipette, gently dissociate the cell pellet by pipetteting up and down several times.
8. Aspirate PBS from pOrn/Lam coated plates and immediately add fresh media (10 cm: 8 mL, 6 cm: 4 mL, 3.5 cm: 2 mL), ensuring that the plates do not dry out.
9. Add dissociated cells to plate and immediately mix by rocking plate back and forth. Do not swirl or all of the cells will be forced to the edge of the plate.
10. Add FGF-2 to final concentration of 20 μg/mL and mix again by rocking plate back and forth.

13. Incubate cells at 37°C.

AHP Proliferation Assay

Reagents:

1. Hemacytometer
2. Cell Proliferation Reagent WST-1 (Roche, Indianapolis, IN). Upon receipt, thoroughly thaw at 37 °C and swirl/pipette to ensure all aggregates dissolve. Then aliquot and store

at -20°C. Protect from light. Aliquots can be freeze/thawed if necessary. Before use, warm again to 37°C to dissolve aggregates.

Methods:

Day 0: Inoculation

1. Thaw 96-well poly-L-ornithine/laminin coated plate. This can be done at room temperature or 37°C.
2. Prepare all media solutions at 2X working concentration. For instance, prepare DMEM/F-12 + N-2 with 40 ng/mL FGF-2 if the experiment calls for 20 ng/mL FGF-2.
3. Fill the wells along the outer edge of the plate completely (~300 μL) with sterile PBS. These wells should not be used for the assay as they are prone to evaporation and changes in concentration during the course of the experiment.
4. Aspirate PBS from the other wells and immediately add 50 μL of the 2X media. Do not allow the wells to dry out. Place plate in 37 °C incubator to warm the media.
5. Prepare cells. Determine the cell concentration of the cell suspension by hemacytometer. This solution is generally quite concentrated, so a 1:10 dilution in DMEM/F-12 + N-2 prior to counting is usually necessary. Keep cell suspensions well mixed throughout the counting and diluting process.
6. Dilute the 1:10 solution used to quantify cell concentration to 20,000 cells/mL in DMEM/F-12 + N-2.
7. Using a multi-channel pipette, add 50 μL of 20,000 cell/mL suspension to each well. To ensure that cells are evenly plated from one row to the next, the cell suspension in the pipette basin should be well mixed between each row. This can be achieved by pipeting up/down with the multi-channel pipette multiple times.
8. Continue culturing the leftover cells, as they will be used on day 5 to generate a standard curve.
9. Incubate cells at 37 °C in 5% CO_2 atmosphere. After 30 minutes visually confirm under the microscope that cells are evenly plated across all wells.

Days 1-4: Media changes

10. Perform daily 50% media changes on all wells. Using a multi-channel pipette as appropriate, remove 50 μL of media and replace it with 50 μL fresh 1X media.
11. Continue passaging the leftover cells in parallel to give an ~80% confluent 10 cm dish on day 5.

Day 5: Plate standard curve and quantify cell number by WST-1

12. Dissociate, dilute, and count the leftover cells maintained in parallel.
13. Prepare standard curve and plate 100 μL per well of each cell concentration. Quadruplicate is best, but triplicate is sufficient. Plate out cells at 100,000, 50,000, 25,000, 12,500, 6,250, 3,125, and 0 (DMEM/F-12 + N-2 only) cells per well. There is no need to wait for cells to attach.

14. Thaw WST-1 at 37°C for at least 5 minutes. Briefly vortex to ensure all aggregates dissolve.
15. Using a multi-channel pipette, add 10 μL WST-1 to each well. Gently rock plate to mix.
16. Incubate at 37 °C for 2 hours.
17. Measure samples against blank (media only) on microplate reader. Measure absorbance at 440 and 700 nm. Subtract A_{700} from A_{440}. This is the experimental readout.
18. Plates can then be returned to the incubator and re-analyzed up to 4 hours after WST-1 addition. Use the standard curve to determine the best read. This will depend on the cell concentrations of the standard curve, but generally 2-3 hours post WST-1 addition provides the best results.
19. Use the standard curve to interpolate cell numbers and perform statistical analyses as necessary.

AHP Differentiation

1. Dissociate, count, and seed cells at 20,000 cells/cm^2. If, after differentiation, the culture will be analyzed by immunostaining, use either 8-well CultureSlides or poly-L-lysine/Laminin coated coverslips. If, after differentiation, the culture will be analyzed by Western blot analysis, use 6-well culture plates.
2. Supplement the culture with 20 ng/mL FGF-2 and incubate overnight at 37 °C in 5% CO_2 atmosphere.
3. Remove FGF-2 medium and replace with differentiation medium of your choice:
    a. Mixed population: 1 μM retinoic acid + 1% (v/v) FBS in DMEM/F-12 + N-2
    b. Neuronal: 1 μM retinoic acid + 5 μM forskolin in DMEM/F-12 + N-2
4. Incubate at 37°C in 5% CO_2 atmosphere for two days.
5. Day 3: Replace media.
6. Day 5: Cultures are now ready for analysis. Alternatively, another media swap can be performed and the cells can be allowed an extra 24-48 h to differentiate.

Appendix 5:
Protocol for *In Vitro* Hydrogen Peroxide Quantification Using PF2 and PF3

This work was performed in collaboration with Dr. Alexander Michels.

Introduction

This appendix describes as experimental protocol for analyzing hydrogen peroxide (H_2O_2) *in vitro* utilizing a microplate reader.

Protocol

1. Prepare PF2 or PF3 stock solution by dissolving the appropriate amount of dye in DMSO to make a 1 mM (PF2) or 5 mM (PF3) stock. Keep the stock away from light but at room temperature until use.
2. Use a black, flat-bottom 96-well plate (i.e. Costar 9017) for the fluorescence assay. Turn on the fluorescence plate reader to warm up before starting to prepare the plate.
3. Dilute H_2O_2 stock solution in Chelex-treated PBS. The working range of the dyes in this format is between 1-100 μM. Since all wells will have an equal volume of dye added at the end, all standards should be prepared at a higher concentration (2-200 μM before dilution). Place the appropriate amount of H_2O_2 standard in each well needed for a standard curve, in a final volume of 100 μL. Make sure to prepare each standard in triplicate, at least (quadruplicates are even better).
4. Before assembling reactions, attention must be paid to the nature of the H_2O_2-generating system. Enzymes involved in the reaction should be pre-incubated in the buffers before substrates are added (this includes SOD or Catalase as well). Inhibitors should also be present before reactions are started. The working volume of the reaction is 100 μM, while the final volume will be 200 μM (with dye) and these concentrations will have to be determined during this assembly.
5. Prepare solutions to be tested in Chelex-treated PBS (If solutions are to be tested other than PBS, these will need to be compared to solutions and standards in PBS). Again, triplicate or quadruplicate samples on the wells are needed. Incubate solutions if needed before preparing and adding dye (steps 6 and 7).
6. After reactions are assembled, dilute the stock dye to a working concentration in 10 mL of Chelex-treated PBS (or enough dye add 100 μL to each well of the plate). The final concentration of PF2 should be between 1-2.5 μM, while PF3 operates best at a 5 μM concentration. Thus, the diluted stocks should be 2-5 μM or 10 μM, respectively to account for the dilution. Limit dye exposure to light.
7. Add 100 μL of working solution of dye to each well. Agitate briefly and place in fluorescence plate reader. Set the excitation wavelength for 488 nm, emission at 515 nm. Read the fluorescence immediately, and every 2 minutes for at least 20-30 minutes to establish the rate of dye reaction with H_2O_2.
8. Using the linear rate of product formation from the fluorescence data, generate a standard curve and compare test compounds to that curve. Make sure to exclude any replicate samples that do not show linear rates of increase in fluorescence.

Notes

- For 96-well plates, 200 μL final volume seems essential. PF2, for instance, worked poorly at volumes below 200 μL.

- Concentration of dye is important for establishing sensitivity range. The less dye used, the less sensitive the reaction. However, use of too much dye results in well saturation at higher concentrations of H_2O_2 standards. PF2 seems particularly sensitive to dye concentration.
- Cell-culture media causes unpredictable results in this system. This can be due to several factors:
    - Many FBS preparations contain Catalase, which interferes with H_2O_2 production.
    - Media sometimes contains Pyruvate, which can react with H_2O_2.
    - Vitamins added to media (like MEM Vitamin Solution, which consists primarily of B vitamins) seem to enhance, while amino acids may inhibit, the reaction of dye with H_2O_2. In combination, or when added individually, they seem to produce stable results.
    - Redox-active transition metals might react with H_2O_2 and limit its reaction with the dye.
- Final concentrations of dye and working solutions are suggestions. Using more concentrated working dye solution (followed by further dilution upon addition to the well) can also work. The important parameters are total volume (min. 200 μM) and final concentration of dye in well (as stated above).

Appendix 6:
Protocol for *In Vitro* Reactive Oxygen Species Selectivity

This work was written in collaboration with Dr. Evan Miller.

Introduction

This appendix describes the *in vitro* preparation of various reactive oxygen species (ROS) for use in selectivity measurements for ROS probes.

General Notes:

- Generally, ROS will be at tested at a final concentration of 100-200 μM.
- The dye or other probe being tested is usually at a concentration of around 5 μM.
- HEPES pH 7.0 or DPBS pH 7.4 are usually used as the buffer for experiments.
- If possible, it's best to do all of the selectivity measurements on the same day, so that they can be calibrated to the "on" form (often the 100 μM H_2O_2 sample) and the "off" form (the blank).
- If all of the tests aren't done on the same day, make sure to do a H_2O_2 (or whatever the ROS the probe responds to) and blank sample for each day so that the results of that day can be bracketed between the "on" and "off" readings for that day and compared to the rest of the selectivity measurements.
- For each condition (i.e. blank, H_2O_2, *tert*-butylhydroperoxide (TBHP), hypochlorite, etc), take the following time points: 0, 5, 15, 30, 45, and 60 minutes.
- To compile the results, plot the integrated emission for each result versus time, setting the 60 min H_2O_2 response as 1.00. Everything else then becomes a fraction of the H_2O_2 response.

Recipes:

- *Blank:*
    - 5 μM dye in buffer solution; take scans at appropriate time points.
- *Hydrogen peroxide:*
    - Make a 100 mM H_2O_2 stock (1:100 dilution from 30% H_2O_2).
    - Dilute 100 mM stock of H_2O_2 1:1000 for a final concentration of 100 μM.
- *Tert-butylhydroperoxide (TBHP):*
    - Make a 100 mM TBHP stock (12.9 μL of 70% TBHP in 1 mL buffer).
    - Dilute 100 mM stock of TBHP 1:1000 for a final concentration of 100 μM.
- *Hypochlorite (NaOCl):*
    - Make a 100 mM NaOCl stock (120 μL of 6.15% NaOCl in 1 mL buffer)
    - Dilute 100 mM stock of NaOCl 1:1000 for a final concentration of 100 μM.
- *Hydroxyl and* tert-*butoxyl radical:*
    - The procedures for generating these radicals are identical, differing only in the addition of either H_2O_2 or TBHP to generate the corresponding radicals.

- Buffered solutions must be degassed prior to generating these radicals.
- Radicals are generated by use of the Fenton reaction.
- Screw-cap cuvettes with septa should be used for these ROS so that an oxygen-free environment can be maintained.
- Make a 100 mM solution of Fe(II) in a 1.5 mL eppendorf tube (25 mg of Fe(II) perchlorate heptahydrate in 1 mL of 0.1 N HCl).
- Degas this solution for 5 min by sticking a needle through the top of the eppendorf tube and bubbling N_2 through the solution.
- Add 100 μL of this solution to 10 mL of a degassed dye/buffer solution and degas an additional 5 min or so
- Take a blank spectrum using 1 mL.
- Add 1 μL of 100 mM H_2O_2 or 1 μL 100 mM TBHP.
- Seal cuvette and take spectra at appropriate time points.

- *Ozone:*
  - Use the screw cap cuvettes, since O_3 will be added as a gas.
  - Assuming O_3 is an ideal gas and that PV = nRT, ~2.5 μL O_3/mL is required to give a 100 μM solution.
  - Use the ozonolysis machine in the Toste group, draw 2.5 μL of ozone per mL of dye/buffer solution into a gas/liquid syringe by inserting the syringe into the ozone line (be sure to follow all of the Toste group procedures for using the ozonator).
  - Quickly add the ozone to the septum-sealed cuvette.
- *Nitric oxide:*
  - Nitric oxide readily forms reactive oxides in the presence of oxygen, which can complicate the results of this analysis; therefore, the dye/buffer solutions must be exhaustively degassed and maintained under a nitrogen atmosphere throughout the testing.
  - Make a 1 mM stock solution of Noc-5 in 0.1 M NaOH.
  - Use stock solution to make a 280 μM solution of Noc-5 in dye solution. The degradation of 280 μM Noc-5 in aqueous solution will generate 200 μM NO after 60 min.
- *Singlet oxygen:*
  - Irradiation of a polymer-bound RoseBengal (pbRB), a triplet sensitizer, generates singlet oxygen.
  - Add 1 mg of pbRB in 1 mL of dye/buffer in a quartz cuvette (so UV irradiation can pass through).
  - Add 1 mL of dye/buffer in a second quartz cuvette (this will be the blank).

- Irradiate for 5 min in the Sarpong light box.
- Filter off the pbRB and then take spectra of both the blank and the sensitized sample over the course of an hour.

- *Superoxide:*
  - Add a small chunk of KO_2 to 10 mL of dye/buffer solution and then take spectra (this results in ~10 mM superoxide concentration)
  - If background is high, Catalase can be added to the solution to sop up H_2O_2 generated by spontaneous dismutation.
- *Peroxynitrite*
  - Prepare peroxynitrite by first mixing 18 mL of 0.55 N NaOH with 20 mL of isopropanol. Sequentially add 0.93 mL 30% H_2O_2 and 0.07 mL isoamyl nitrite (7.51 M). Stir the contents during the additions and for an additional 10 min at room temperature.
  - Extract peroxynitrite reaction into 4 × 2 volumes of dichloromethane. Add about 5 g of MnO_2 and stir for 5 min. Filter off MnO_2 and purge solution with N_2 for 10 min.
  - Measure the concentration of the final solution by measuring the absorbance at 302 nm ($\varepsilon = 1670\ M^{-1}\ cm^{-1}$).
  - Add in whatever concentration of peroxynitrite from this stock to probe solutions.